

NOTE TO USERS

This reproduction is the best copy available.

UMI[®]

**REDOX SHUTTLES AND THEIR USE AS OVERCHARGE
PROTECTION IN LITHIUM-ION CELLS**

by

Lee Moshurchak

Submitted in partial fulfillment of the requirements
for the degree of Doctor of Philosophy

at

Dalhousie University
Halifax, Nova Scotia

~~September 2009~~

MAY 2010

© Copyright by Lee Moshurchak, 2009



Library and Archives
Canada

Published Heritage
Branch

395 Wellington Street
Ottawa ON K1A 0N4
Canada

Bibliothèque et
Archives Canada

Direction du
Patrimoine de l'édition

395, rue Wellington
Ottawa ON K1A 0N4
Canada

Your file *Votre référence*
ISBN: 978-0-494-56427-1
Our file *Notre référence*
ISBN: 978-0-494-56427-1

NOTICE:

The author has granted a non-exclusive license allowing Library and Archives Canada to reproduce, publish, archive, preserve, conserve, communicate to the public by telecommunication or on the Internet, loan, distribute and sell theses worldwide, for commercial or non-commercial purposes, in microform, paper, electronic and/or any other formats.

The author retains copyright ownership and moral rights in this thesis. Neither the thesis nor substantial extracts from it may be printed or otherwise reproduced without the author's permission.

AVIS:

L'auteur a accordé une licence non exclusive permettant à la Bibliothèque et Archives Canada de reproduire, publier, archiver, sauvegarder, conserver, transmettre au public par télécommunication ou par l'Internet, prêter, distribuer et vendre des thèses partout dans le monde, à des fins commerciales ou autres, sur support microforme, papier, électronique et/ou autres formats.

L'auteur conserve la propriété du droit d'auteur et des droits moraux qui protègent cette thèse. Ni la thèse ni des extraits substantiels de celle-ci ne doivent être imprimés ou autrement reproduits sans son autorisation.

In compliance with the Canadian Privacy Act some supporting forms may have been removed from this thesis.

While these forms may be included in the document page count, their removal does not represent any loss of content from the thesis.

Conformément à la loi canadienne sur la protection de la vie privée, quelques formulaires secondaires ont été enlevés de cette thèse.

Bien que ces formulaires aient inclus dans la pagination, il n'y aura aucun contenu manquant.


Canada

DALHOUSIE UNIVERSITY

To comply with the Canadian Privacy Act the National Library of Canada has requested that the following pages be removed from this copy of the thesis:

Preliminary Pages

Examiners Signature Page (pii)

Dalhousie Library Copyright Agreement (piii)

Appendices

Copyright Releases (if applicable)

TABLE OF CONTENTS

List of Tables	vii
List of Figures	viii
Abstract	xiv
List of Abbreviations and Symbols Used	xv
Acknowledgements.....	xix
Chapter 1. Introduction	1
1.1. Motivation for the Research Project.....	1
1.2. What is a Battery	2
1.3. Lithium-Ion Batteries	3
1.3.1. Electrochemistry of Lithium-Ion Batteries	4
1.3.2. Solid-Electrolyte Interphase.....	8
1.3.3. Current Lithium-Ion Battery Technology	10
1.3.3.1. Negative Electrode.....	10
1.3.3.2. Positive Electrode	12
1.3.3.3. Electrolyte	13
1.3.3.3.1. Salt.....	13
1.3.3.3.2. Solvent.....	15
1.3.3.3.3. Additives	16
1.3.3.4. Polymer Binders and Separators	17
1.4. Safety.....	18
1.4.1. Redox Additives.....	19
1.4.1.1. Shuttles.....	20
1.4.1.2. Polymers.....	24
1.5. Scope of this Thesis.....	26

Chapter 2.	Experimental Techniques.....	28
2.1.	Electrochemical Testing.....	28
2.1.1.	Coin Cells.....	28
2.1.1.1.	Two-Electrode Cells	29
2.1.1.2.	Three-Electrode Cells	32
2.1.2.	Solution-Based Electrochemistry.....	33
2.1.2.1.	Spectroelectrochemistry.....	33
2.1.2.2.	Cyclic Voltammetry.....	35
2.2.	Summary	41
Chapter 3.	Properties of Redox Shuttles.....	43
3.1.	Overcharge Current.....	46
3.2.	Effect of Redox Potential	48
3.3.	Heat Generation.....	50
3.4.	Death of the Shuttle.....	53
3.5.	Summary	61
Chapter 4.	Low V Shuttles.....	62
4.1.	Substituted Benzenes.....	62
4.2.	2,2,6,6-Tetramethylpiperidine-1-oxyl.....	82
4.3.	Phenothiazines.....	91
4.4.	Triphenylamines.....	103
4.5.	Direct Comparison of Select Shuttles	112
Chapter 5.	High Potential Shuttles.....	125
5.1.	Fluorinated Naphthalenes.....	125
5.2.	Substituted Benzenes.....	129
Chapter 6.	Computational Studies	137
6.1.	Method	140
6.2.	Motivation.....	142
6.3.	Nomenclature	143

6.4.	Results	145
6.5.	Discussion	148
6.6.	Experimental	152
6.7.	Conclusions	156
Chapter 7.	Conclusions	157
7.1.	Conclusions	157
7.2.	Future Work	165
References	169
Appendix A - List of Shuttle Molecules Sorted by Oxidation Potential	176
Appendix B - List of Shuttle Molecules Sorted by Length of Overcharge Protection...		189

LIST OF TABLES

Table 4-1	List of tested substituted benzene molecules, their shuttle potentials and number of cycles of 100% overcharge protection measured in LiFePO ₄ -based coin cells.	68
Table 4-2	Effect of substituent groups on the redox potential of substituted benzene shuttle molecules.....	76
Table 4-3	List of TEMPO molecules tested in coin cells and their measured shuttle potentials and number of cycles of 100% overcharge protection.	84
Table 4-4	List of tested phenothiazine molecules, their coin cell measured shuttle potentials and number of cycles of 100% overcharge protection. Molecules that prevented cells from charging are shown as ---.	97
Table 4-5	Summary of coin cell results for a variety of phenothiazine molecules.	100
Table 4-6	Summary of coin cell results for the shuttles DDB, TEMPO and MPT with either Li _{4/3} Ti _{5/3} O ₄ or graphite negative electrodes and either LiBOB or LiPF ₆ based electrolytes.....	122
Table 5-1	Summary of coin cell results for the molecule DBFB.....	134
Table 6-1	Calculated properties of 43 molecules as redox shuttles: E _{ox} - the oxidation potential vs Li/Li ⁺ ; E _b (ER) - the maximum binding energy of the molecule with the ethyl radical, which is a reactivity index.....	143
Table 6-2	Comparison of calculated and experimental results for the six molecules that were tested. Calculated results include the oxidation potential (E _{ox}) and the ethyl radical binding energy (E _b (ER)). Experimental results include the oxidation potential (E _{ox}) and the number of cycles of 100% overcharge protection provided by the shuttle molecule in graphite/LiFePO ₄ and Li _{4/3} Ti _{5/3} O ₄ /LiFePO ₄ coin cells.	153

LIST OF FIGURES

Figure 1.1	Schematic of electrode potentials within a lithium-ion cell. At any point in time, the cell potential is the difference between the positive electrode potential and the negative electrode potential.....	5
Figure 1.2	Binding energy of lithium in various lithium compounds vs lithium metal.....	6
Figure 1.3	A schematic diagram of a redox shuttle operating within a cell.	21
Figure 1.4	Schematic of electrode potentials allowing shuttling during charge and discharge.	23
Figure 1.5	Redox polymer bilayer during normal charge (A), initial stage of overcharge (B), sustained overcharge (C), initial stage of discharge (D) and normal discharge (E).	25
Figure 2.1	Exploded view of the hardware in a 2325 coin cell.	31
Figure 2.2	Exploded view of 3-electrode coin cell hardware.	32
Figure 2.3	Schematic of cells used for spectroelectrochemical measurements.....	34
Figure 2.4	Schematic of CV cells using three electrodes.	36
Figure 2.5	Schematic of CV cells using four electrodes, wired as two three-electrode cells using common counter and reference electrodes.	38
Figure 2.6	Schematic representation of an experiment utilizing the four-electrode CV cell to determine if a shuttle molecule can function through the formation of the SEI layer. The top panel shows the potential of the working electrode and the oxidation potential of the shuttle. The bottom panel shows the potential of the second working electrode and the potentials where SEI formation occurs begins in LiBOB and LiPF ₆ containing electrolytes.	40
Figure 2.7	CV of the molecule 2,5-di- <i>t</i> -butyl-1,4-dimethoxybenzene in battery electrolyte vs Li/Li ⁺ and vs Ag/AgCl.	41
Figure 3.1	Data from a UV-vis experiment of the molecule 2,5-di- <i>t</i> -butyl-1,4-dimethoxybenzene. The left panel shows the controlled potential and the current response of the experiment. The right panel shows the UV-vis spectra at select times from 300 nm to 1100 nm. The middle panel shows a contour plot of how the intensity of the peaks in the UV-vis spectra change with time.....	43
Figure 3.2	Three-electrode coin cell data for a LiFePO ₄ /Li _{4/3} Ti _{5/3} O ₄ cell containing 2,5-di- <i>t</i> -butyl-1,4-dimethoxybenzene. The cell potential and the individual electrode potentials are shown.	45

Figure 3.3:	Shuttle current as a function of cell potential.	49
Figure 3.4:	Shuttle current on a log scale as a function of cell potential.	49
Figure 3.5:	Calculated 18650 cell temperature during shuttle-protected overcharge at various rates of charge.	52
Figure 3.6:	Calculated 18650 cell temperature during shuttle-protected overdischarge at various rates of discharge.	53
Figure 3.7:	Histogram summarizing the duration of protection provided by shuttles found and reported as a function of the number cycles with 100% overcharge per cycle. Classes of molecules of special interest are shown in for molecules similar to 2,5-di- <i>t</i> -butyl-1,4-dimethoxybenzene, for various substituted TEMPO molecules and for various substituted phenothiazines.	54
Figure 3.8	Concentration of S, S ⁺ and S ⁺⁺ at the positive electrode as a function of the positive electrode potential with a variety of second oxidation potentials.	57
Figure 3.9:	Calculated voltage profile of a shuttle during a constant overcharge period and experimental results for a cell in continuous overcharge with 2,5-ditertbutyl-1,4-dimethoxybenzene as the redox shuttle.....	58
Figure 3.10	Positive electrode potential as a function of the overcharge current.	59
Figure 3.11	Concentration of S, S ⁺ and S ⁺⁺ at the positive electrode as a function of the overcharge current shown with the second oxidation potential 0.2 V above the first oxidation potential.....	60
Figure 3.12	Concentration of S, S ⁺ and S ⁺⁺ on a log ₁₀ scale at the positive electrode as a function of the overcharge current shown with the second oxidation potential 0.2 V above the first oxidation potential.	60
Figure 4.1	First 2 cycles for LiFePO ₄ /Li and Li _{4/3} Ti _{5/3} O ₄ /Li half cells.	65
Figure 4.2	First cycle for LiFePO ₄ /Li _{4/3} Ti _{5/3} O ₄ and LiFePO ₄ /MCMB coin cells containing the shuttle 2,5-di- <i>t</i> -butyl-1,4-dimethoxybenzene.....	67
Figure 4.3	CV's of a) 2,5-di- <i>t</i> -butyl-1,4-dimethoxybenzene and b) 1,4-dimethoxybenzene.	74
Figure 4.4	Potential vs number of a) substituted alkyl groups and b) substituted halogens for a variety of molecules.	75
Figure 4.5	Cycling data for a LiFePO ₄ /Li _{4/3} Ti _{5/3} O ₄ coin cell containing 0.1 M anisole. Cycle numbers are shown.....	77
Figure 4.6	Cycling data for a LiFePO ₄ /Li _{4/3} Ti _{5/3} O ₄ coin cell containing 0.1 M 2-bromoanisole. Cycle numbers are shown.	77
Figure 4.7	Cycling data for a LiFePO ₄ /MCMB coin cell containing 0.1 M 2,5-di- <i>t</i> -butyl-1,4-dimethoxybenzene. Cycle numbers are shown.....	79

Figure 4.8	Structure and regions of electron density for the molecules a) 2,5-di- <i>t</i> -butyl-1,4-dimethoxybenzene and b)1,3,5-tri- <i>t</i> -butyl-2-methoxybenzene.	80
Figure 4.9	Calculated regions of electron density for the LUMO(S ⁺) for the molecule TEMPO. The electron density is localized to the nitrogen and oxygen.	83
Figure 4.10	CVs of TEMPO a) and b) between 1.4 V and 4.5 V vs Li/Li ⁺ and c) and d) between 0.2 V and 4.5 V vs Li/Li ⁺ in electrolytes a) and c) containing 0.5 M LiBOB and b) and d) containing 0.5 M LiPF ₆	86
Figure 4.11	Cycling data for a LiFePO ₄ /Li _{4/3} Ti _{5/3} O ₄ coin cell containing 0.3 M TEMPO with cycle numbers shown.	87
Figure 4.12	Charge and discharge capacities for a LiFePO ₄ /Li _{4/3} Ti _{5/3} O ₄ coin cell containing 0.3 M TEMPO.	88
Figure 4.13	Cycling data for 4-methoxy-TEMPO, 4-cyano-TEMPO and 3-cyano-PROXYL with cycle numbers shown.	90
Figure 4.14	CV of MPT between 2.7 V and 4.9 V vs Li/Li ⁺	92
Figure 4.15	CVs of MPT a) and b) between 1.4 V and 4.5 V vs Li/Li ⁺ and c) and d) between 0.2 V and 4.5 V vs Li/Li ⁺ in electrolytes a) and c) containing 0.5 M LiBOB and b) and d) containing 0.5 M LiPF ₆	93
Figure 4.16	Cycling data for a LiFePO ₄ /Li _{4/3} Ti _{5/3} O ₄ coin cell containing 0.1 M MPT with cycle numbers shown.	94
Figure 4.17	Charge and discharge capacities for a LiFePO ₄ /Li _{4/3} Ti _{5/3} O ₄ coin cell containing 0.1 M MPT.	95
Figure 4.18	Cycling data for LiFePO ₄ /MCMB coin cells containing 0.1 M MPT in electrolytes containing 0.5 M LiBOB, and 0.5M LiPF ₆ . Cycle numbers are shown.	96
Figure 4.19	Calculated electron densities for the LUMO(S ⁺) for the molecules a) 10-methylphenothiazine and 10-ethyl-3-chlorophenothiazine. The electron density is highest on the nitrogen and sulfur. Substitution on the carbons has little effect on the electron density.	98
Figure 4.20	Cycling data for 10-ethylphenothiazine, 3-chloro-10-ethylphenothiazine, and 10-isopropylphenothiazine with cycle numbers shown.	99
Figure 4.21	Cycling data for a LiFePO ₄ /Li _{4/3} Ti _{5/3} O ₄ cell containing 10-acetylphenothiazine with cycle numbers shown.	101
Figure 4.22	Cycling data for a coin cell containing 0.1M MPT. The two shuttle plateaus correspond to the potentials at which the first and second oxidation of MPT occur.	102
Figure 4.23	¹ H NMR spectrum of a sample of the molecule tris(2,4-dibromophenyl)amine synthesized for testing.	104

Figure 4.24	Expanded view of the aromatic region of the NMR spectrum for tris(2,4-dibromophenyl)amine.	105
Figure 4.25	Assignment of protons to their corresponding peaks in the ^1H spectrum.	105
Figure 4.26	CVs of triphenylamine, tris(4-bromophenyl)amine, and tris(2,4-dibromophenyl)amine.	106
Figure 4.27	Literature and measured oxidation potentials for several brominated triphenylamines.	107
Figure 4.28	Cycling data for a $\text{LiFePO}_4/\text{Li}_{4/3}\text{Ti}_{5/3}\text{O}_4$ cell containing triphenylamine with cycle numbers shown.	108
Figure 4.29	Cycling data for a $\text{LiFePO}_4/\text{Li}_{4/3}\text{Ti}_{5/3}\text{O}_4$ cell containing tris(4-bromophenyl)amine with cycle numbers shown.	109
Figure 4.30	Reaction mechanism showing the dimerization of triphenylamine to tetraphenylbenzidine.	110
Figure 4.31	Calculated electron density of the LUMO(S^+) for triphenylamine. The electron density is heaviest on the central nitrogen, but can also be seen on the aromatic rings at the ortho and para positions.	111
Figure 4.32	Figure 2. Cyclic voltammograms for a) 2,5-di- <i>tert</i> -butyl-1,4-dimethoxybenzene (DDB) b) 2,2,6,6-tetramethylpiperidine-1-oxyl (TEMPO) and c) 10-methylphenothiazine (MPT) in both LiPF_6 and LiBOB-based electrolytes.	113
Figure 4.33	Figure 3. Determination of diffusion constants for the molecules 2,5-di- <i>tert</i> -butyl-1,4-dimethoxybenzene (left), 2,2,6,6-tetramethylpiperidine-1-oxyl (centre), and 10-methylphenothiazine (right).	114
Figure 4.34	Figure 4. Cyclic voltammograms of 10-methylphenothiazine in LiBOB and LiPF_6 -containing electrolytes to a variety of lower cutoff potentials.	117
Figure 4.35	Figure 5. Electrode setup for 4-electrode cyclic voltammetry experiments.	118
Figure 4.36	Figure 7. Results from a series of 4-electrode cyclic voltammetry experiments with the molecules 2,5-di- <i>t</i> -butyl-1,4-dimethoxybenzene, 2,2,6,6-tetramethylpiperidine-1-oxyl, and 10-methylphenothiazine, in both LiBOB (left) and LiPF_6 (right) based electrolytes.	120
Figure 5.1	Coin cell data for a cell containing 0.1 M OFN in an electrolyte composed of 0.5 M LiBOB in PC:DMC:EC:DEC. The cell was charged at C/10 rate for 20 hours then discharged at C/10 rate.	126
Figure 5.2	Coin cell data for a cell containing 0.1 M OFN in an electrolyte composed of 0.5 M LiBOB in PC:DMC:EC:DEC. The cell was charged at C/10 rate for 12 hours then discharged at C/10 rate.	127

Figure 5.3	Charge and discharge capacities for a cell containing 0.1 M OFN in an electrolyte composed of 0.5 M LiBOB in PC:DMC:EC:DEC. The cell was charged at C/10 rate for 12 hours then discharged at C/10 rate.....	127
Figure 5.4	Coin cell data for cells containing 0.1 M HFN in an electrolyte composed of 0.5 M LiBOB in PC:DMC:EC:DEC. The cell was charged at C/10 rate for 12 hours then discharged at C/10 rate.....	128
Figure 5.5	Charge and discharge capacities for a cell containing 0.1 M HFN in an electrolyte composed of 0.5 M LiBOB in PC:DMC:EC:DEC. The cell was charged at C/10 rate for 12 hours then discharged at C/10 rate.....	128
Figure 5.6:	Structure and electron density of the LUMO(S ⁺) of a) 2,5-di- <i>t</i> -butyl-1,4-dimethoxybenzene (DDB) and b) 2,5-di- <i>t</i> -butyl-1,4-bis(2,2,2-trifluoroethoxy)benzene (DBFB).....	131
Figure 5.7:	Cyclic voltammetry data for DDB and DBFB at a concentration of 0.1 M in a electrolyte composed of 0.5 M LiPF ₆ in PC:DMC:EC:DEC. A sweep rate of 100 mV/sec was used. The upper cutoffs used were 4.6 V vs Li/Li ⁺ for DDB and 4.9 V for DBFB. The lower cutoffs used were 2.9 V vs Li/Li ⁺ in a) and 0.2 V in b). The insert shows an expanded view of the low potential region.....	132
Figure 5.8:	Coin cell data for cells containing 0.1 M DBFB in an electrolyte composed of 0.5 M LiPF ₆ in PC:DMC:EC:DEC. The cells are; LiFePO ₄ /Li, LiFePO ₄ /MCMB and LiFePO ₄ /Li _{4/3} Ti _{5/3} O ₄ . Cells were charged at C/10 rate for 20 hours then discharged at C/10 rate.....	133
Figure 5.9:	Coin cell data for cells containing 0.1 M DBFB in an electrolyte composed of 0.5 M LiPF ₆ in PC:DMC:EC:DEC. The cells are LiCoO ₂ /Li and Li[Ni _{1/3} Mn _{1/3} Co _{1/3}]O ₂ /Li. Cells were charged at C/10 rate for 20 hours then discharged at C/10 rate.....	133
Figure 5.10:	Discharge capacities for coin cells containing 0.1 M DBFB in an electrolyte composed of 0.5 M LiPF ₆ in PC:DMC:EC:DEC. The cells are; Li/LiFePO ₄ , MCMB/LiFePO ₄ and Li _{4/3} Ti _{5/3} O ₄ /LiFePO ₄ . Cells were cycled at C/10 rate. A MCMB/LiFePO ₄ coin cell that contained no shuttle is also included for comparison sake.....	135
Figure 6.1	Potential energy curve showing the energy as a function of internuclear distance.....	138
Figure 6.2	Explanation of the naming scheme used to describe the molecules in this paper. The symbol TM--M- represents this molecule, where 'T', 'M' and '-' stand for <i>t</i> -butyl, methoxy and hydrogen bonded on a ring carbon atom, respectively. The name for this molecule would be 2- <i>t</i> -butyl-1,4-dimethoxybenzene.....	144

Figure 6.3	The effects of single <i>t</i> -butyl or methoxy substituent on oxidation potentials and reactivity. A. Benzene with $E_{ox} = 5.24V$; B. T----- with $E_{ox} = 4.99V$; C. M----- with a methoxy in the plane of the aromatic ring with $E_{ox} = 4.44V$ and D. M----- with a methoxy out of plane with the aromatic ring with $E_{ox} = 4.98V$. For B, C and D, their LUMO(S^+) are drawn at an isovalue of 0.08. The numbers by the atoms are the $E_b(ER)$ values, in eV, at the corresponding site.	146
Figure 6.4	$E_b(ER)$ in eV vs E_{ox} in V for all 43 molecules with the number of methoxy groups indicated in the upper panel, or the number of <i>t</i> -butyl groups in the lower panel. Circles represent molecules that were also experimentally tested.	149
Figure 6.5	$E_b(ER)$ in eV vs E_{ox} in V for the molecules containing exactly two methoxy groups. The symbols O, M and P represent the substitution pattern of the methoxy groups as <i>ortho</i> , <i>meta</i> and <i>para</i> , respectively.	150
Figure 6.6	100 hours of cycling data for the following molecules: a) #4, T--M--; b) #7, TM--M--; c) #9, T-MM--; d) #27, T-TMM--; e) #36, TM-TM--; f) #41, TMT-T-. The cells were MCMB/LiFePO ₄ Li-ion cells with 0.1M shuttle in the electrolyte. The numbers over the shuttling plateaus indicate the cycle number.	154
Figure 6.7	Number of cycles of 100% overcharge on a log scale as a function of $E_b(ER)$ for the six molecules tested in coin cells. Both MCMB/LiFePO ₄ and Li _{4/3} Ti _{5/3} O ₄ /LiFePO ₄ cell data are shown. The grey data points are for molecule #9.	155
Figure 7.1	Cycling data for an LiFePO ₄ /graphite 18650 cell containing the shuttle DDB.	160
Figure 7.2	Charge and discharge capacities for an 18650 cell containing DDB. The cell was cycled for 600 cycles with no overcharging, then for another 120 cycles with 20% overcharging per cycle.	161
Figure 7.3	Cycling data with charge and discharge capacities for a 3 cell pack of 18650 cells in a series string. The three cells were of a similar capacity, so no overcharging occurs.	162
Figure 7.4	Cycling data with charge and discharge capacities for a 3 cell pack of 18650 cells in a series string. One of the cells was continually being discharged by a 330 Ω resistor.	163
Figure 7.5	Solubility limits for DDB in electrolytes containing various concentrations of LiPF ₆ or LiBOB in a variety of solvents.	164

ABSTRACT

Lithium-ion batteries are currently used to power most portable electronic devices. They also have use in electric and hybrid electric vehicles and as a storage device for clean, non-constant energy sources, such as solar and wind power. A lot of effort and money is currently being expended on lithium-ion battery research. Much of this research goes towards increasing the power or energy density of the batteries, but there is also significant interest in making these batteries safer and more user friendly. One way of doing this is to use a redox shuttle electrolyte additive to protect cells against overcharge.

As more and more cells are placed together in series strings, it becomes more and more important to ensure that the cells are properly balanced in the pack. If the capacities are not properly balanced, or if they become unbalanced during use, individual cells can experience overcharge, which can further degrade cells or pose a safety risk. Redox shuttles can be used to prevent overcharge conditions and they can also be used to periodically rebalance the individual cells in a pack, which would increase the overall lifetime of the pack.

Many molecules, as well as the properties that make some molecules better shuttles than others, are discussed in this thesis. Molecules that make good redox shuttles must have an oxidation potential that is suitable for use with the electrodes used in the cell and they must provide overcharge protection for a large number of cycles. The molecule 2,5-di-*t*-butyl-1,4-dimethoxybenzene, several substituted analogues of 2,2,6,6-tetramethylpiperidine-1-oxyl and several substituted phenothiazines are shown here to be excellent for use in cells that contain a LiFePO₄ positive electrode. For higher potential positive electrodes, fluorinated naphthalenes or 2,5-di-*t*-butyl-1,4-bis(2,2,2-trifluoroethoxy)benzene are shown to be useful shuttles.

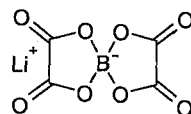
LIST OF ABBREVIATIONS AND SYMBOLS USED

2325	coin cell battery, 23 mm in diameter and 2.5 mm tall
18650	cylindrical battery, 18 mm in diameter and 65.0 mm tall
6-31G(d,p)	basis set describing core orbitals with 6 primitive gaussians and valence orbitals with 3 and 1 primitive gaussians, also including d-type basis functions and a set of p-type polarization functions
a	rate constant
α	spin up electron
A	area
AA	standard battery size 13.5-14.5 mm in diameter and 51 mm in length
AAA	standard battery size 10.5 mm in diameter and 44.5 mm in length
α -H	hydrogen bonded to the to the first carbon of a substituent group
APT	10-acetylphenothiazine
ARC	accelerated rate calorimetry
β	spin down electron
B3LYP	a hybrid model of density functional theory with the Becke three-parameter functional for electron exchange and the Lee-Yang-Parr electron correlation functional
C	initial shuttle concentration
C	Coulomb
C_{cell}	heat capacity of a cell
C rate	rate of charging a battery to full capacity in one hour
CV	cyclic voltammetry
D	diffusion constant
d	interelectrode spacing
DBFB	1,4-di-t-butyl-2,5-bis(2,2,2-trifluoroethoxy)benzene
DDB	2,5-di-t-butyl-1,4-dimethoxybenzene
DEC	diethyl carbonate
DMC	dimethyl carbonate
DME	dimethoxyethane
e	elementary charge - 1.602176×10^{-19} Coulombs

e^-	electron
E_b	binding energy
$E_b(ER)$	maximum binding energy between a molecule and an ethyl radical
EC	ethylene carbonate
ECE	electrochemical-chemical-electrochemical reaction mechanism
E°	standard oxidation potential
EPT	10-ethylphenothiazine
ER	ethyl radical
η	viscosity
F	Faraday's constant - 96485 C mol^{-1}
ϕ	separator porosity
FEC	fluoroethylene carbonate
GC/MS	gas chromatograph with a mass spectrometer
GC-FID	gas chromatograph with a flame ionization detector
G°	standard free energy of formation
h	surface heat transfer coefficient
HFN	2-methoxyheptafluoronaphthalene
HOMO	highest occupied molecular orbital
I	current
-I	inductive effect from an electron withdrawing group
I_{\max}	maximum current capable of being carried by the shuttle
I_p	peak anodic current
IPT	10-isopropylphenothiazine
k	Boltzmann constant - $1.38065 \times 10^{-23} \text{ J K}^{-1}$

LiBOB

lithium bis(oxalato)borate



Λ_m

molar conductivity

LUMO

lowest unoccupied molecular orbital

μ

chemical potential

+M

mesomeric effect from an electron donating group

M	transition metal
MPT	10-methylphenothiazine
n	number of electrons involved in a reaction
v	linear potential sweep rate
NHE	normal hydrogen electrode
NMP	N-methyl-2-pyrrolidinone
NMR	nuclear magnetic resonance
OC	overcharge
OD	overdischarge
OFN	octafluoronaphthalene
π	the ratio of the circumference of a circle to its diameter, 3.1415926...
P	power
P3BT	poly 3-butylthiophene
PC	propylene carbonate
PCM	polarizable continuum model
PROXYL	2,2,5,5-tetramethylpyrrolidiny-1-oxyl
PVDF	polyvinylidene fluoride
r	radius
R	unspecified chemical group
R	ideal gas constant - $8.3145 \text{ J K}^{-1} \text{ mol}^{-1}$
R-X	unspecified halogenated molecule
S	neutral shuttle molecule species
S ⁺	singly oxidized shuttle species
S ⁺⁺	double oxidized shuttle species
[S]	concentration of neutral shuttle
[S ⁺]	concentration of singly oxidized shuttle
[S ⁺⁺]	concentration of doubly oxidized shuttle
SCE	saturated calomel electrode
SEI	solid-electrolyte interphase
t	time
T	temperature

TEMPO	2,2,6,6-tetramethylpiperidiny-1-oxyl
TPA	triphenylamine
TPB	tetraphenylbenzidine
UV-Vis	ultraviolet-visible
V	potential
V	volume
V ₊	first oxidation potential
V ₊₊	second oxidation potential
VC	vinylene carbonate
X	halogen

ACKNOWLEDGEMENTS

I would like to acknowledge the considerable work from a variety of people that contributed to this research project. In chronological order, Jun Chen, Claudia Buhrmester, Junwei Jiang and Rita Garsuch have all contributed immensely to this field of research, making numerous coin cells while being members of the Dahn lab. Richard Wang has been instrumental in figuring out and performing the calculations that have come to guide much of our search for new molecules. William Lamanna and Mike Bulinski, both employees of 3M, have also contributed to the project by synthesizing molecules in their labs that we did not have the resources to attempt to create ourselves.

In addition to those people who directly contributed to the shuttle project, I would like to acknowledge all the members of the Dahn lab throughout the years that I have been here. Many of these people have made the years of work more enjoyable. You know who you all are.

Chapter 1. Introduction

1.1. Motivation for the Research Project

Today's modern world continues to demand more and more energy with each passing year. This increasing demand requires technology to keep up, and energy storage is a key concern. There are many technologies that currently exist that store electrochemical energy. Two important criteria in evaluating these technologies are energy density and power density. Energy density is reported either in terms of specific energy density (Wh g^{-1}) or as volumetric energy density (Wh L^{-1}). Power density is a measure of the rate of energy use from a device, and can also be described per unit mass (W g^{-1}) or per unit volume (W L^{-1}). The choice of using specific or volumetric density is often determined by the use of the device. Some applications require small power sources, for compact designs, while some applications require lightweight power sources.

Three common devices for electrochemical energy storage and conversion are, supercapacitors, fuel cells and batteries. Supercapacitors are known to have very high power densities but low energy density and they currently operate with an efficiency of around 90%. Fuel cells are known to provide large energy densities, and can have high power density, but only operate with an efficiency of around 50%. Batteries are capable of providing a mix of both reasonably high power and energy density, as well as an efficiency of over 90%, which makes them desirable for energy storage.

Of the various battery chemistries, lithium-ion batteries are known for having the highest energy density. Despite this, in North America it is not currently possible to find rechargeable lithium-ion batteries of standard sizes (AA or AAA for example) for

everyday use in portable devices. This is because of the inherent safety concerns associated with the technology. Lithium-ion batteries can currently only be found in specially designed packs where each cell can be carefully controlled. Americans alone purchase around 3 billion batteries a year, many of which are quickly thrown away. If all disposable batteries could be replaced by safe and efficient rechargeable lithium-ion batteries, around 180,000 tons of material could be kept out of landfills.

One method for improving the safety of lithium-ion batteries for use by consumers would be to add a redox shuttle to the electrolyte that would prevent the cell from entering dangerous overcharge conditions. If the right redox shuttles could be found, this is one method that could lead to the development of a drugstore lithium-ion battery that could replace many of the single use batteries currently being produced.

1.2. What is a Battery

A battery is a device that contains one or more electrochemical cells that convert chemical potential energy into electrical energy by passing ions from one electrode to another through an electrolyte. As the ions move through the electrolyte, electrons move through an external circuit and can be used to power devices. Primary batteries are ones that can be used only once and are then thrown away. Examples of primary battery chemistries include alkaline or zinc-carbon. Secondary batteries are also known as rechargeable batteries and utilize electrochemistry that is reversible, so they can be charged and discharged many times. Examples of rechargeable battery chemistries include nickel-cadmium, nickel-metal hydride, lead acid, and lithium-ion batteries.

1.3. Lithium-Ion Batteries

Rechargeable batteries containing lithium were introduced into the market in the mid 1980's [1]. Initially, these batteries used lithium metal as the negative electrode and a transition metal sulfide as the positive electrode. At the negative electrode, the lithium atoms separate into an ion and an electron. The lithium ions diffuse across the interelectrode gap through the ionically conducting electrolyte, while the electron travels through the external circuit where it can be used to perform electrical work. The ion then recombines with an electron at the positive electrode and intercalates into the host structure of the positive electrode. During charge, work is then performed on the electrochemical cell to remove lithium from the transition metal sulfide electrode and deposit it back on the lithium electrode.

These rechargeable batteries based on lithium metal negative electrodes are no longer commercially available due to safety concerns. These problems have been attributed to the lithium electrode after continual cycling [2]. This lithium consists of high surface area dendrites [3] that are reactive with the electrolyte solutions [4] and can pierce the separator and cause an internal short circuit. As these batteries are cycled, these dendrites grow and become more and more reactive. Thus, rechargeable cells based on lithium metal negative electrodes were only safe during early cycles, after which they could produce serious safety hazards. There have been reports that some cells vent with flames [5].

Because these batteries were determined to be unsafe due to the lithium metal inside them, the lithium metal was replaced with an intercalation compound. Cells of this type became known as lithium-ion batteries.

Lithium-ion batteries were first brought to market in 1991 by the Sony Corporation of Japan [6]. Since then, lithium-ion batteries have been used in many portable consumer products. Lithium-ion batteries have played a leading role in the portable secondary battery market because of their large energy density, higher voltage and longer lifetime compared to conventional battery systems.

One of the common cell configurations produced by battery manufacturers is the 18650 cell. These cells get their name from their dimensions. They are 18 mm in diameter and 65 mm in length. Typically they can deliver about 2.4 Ah of charge [7].

1.3.1. Electrochemistry of Lithium-Ion Batteries

The voltage of an electrochemical cell depends on the difference in the chemical potential of the lithium atoms in the two host materials

$$V = \frac{-(\mu_{pos} - \mu_{neg})}{e}, \quad (1-1)$$

where μ_{pos} and μ_{neg} are the chemical potential of lithium atoms in the positive and negative electrode materials respectively, and e is the magnitude of the electron charge [8]. In the case of lithium batteries, the chemical potential of lithium metal, μ_{neg} , is constant because it is composed of a single, fixed composition phase, but the chemical potential of lithium within intercalation compounds can vary with the lithium content of the lattice. Thus, the change in the cell potential is a direct measurement of the change in chemical potential of lithium within the transition metal oxide electrode. When both electrodes are intercalation compounds, as is the case with lithium-ion batteries, the cell potential varies with respect to the state of lithiation of both electrodes. Figure 1.1 shows a schematic representation of the electrode potentials within a lithium-ion cell.

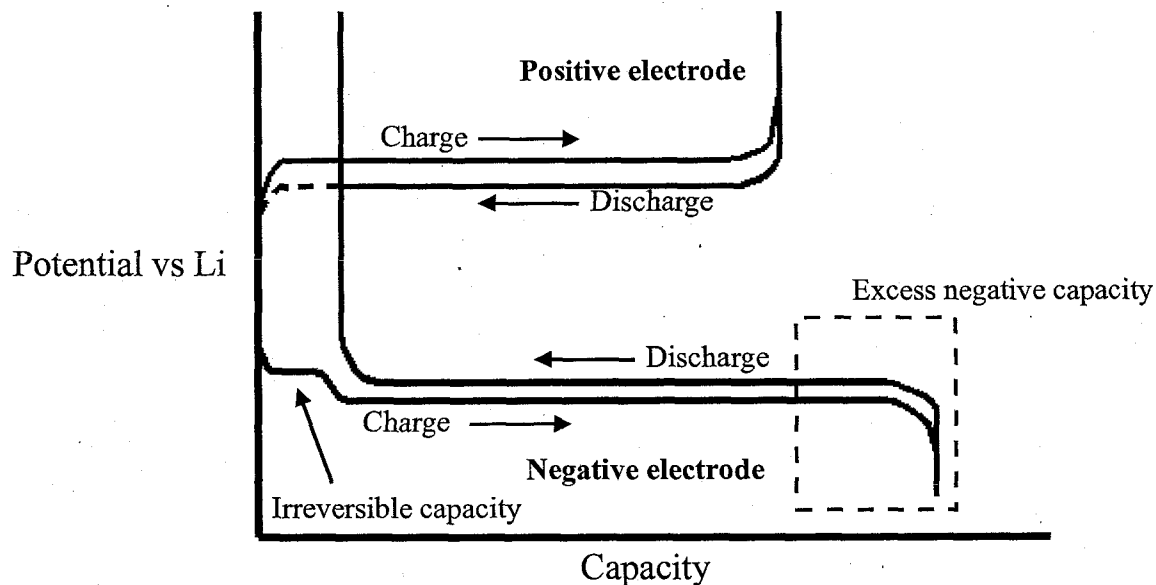


Figure 1.1 Schematic of electrode potentials within a lithium-ion cell. At any point in time, the cell potential is the difference between the positive electrode potential and the negative electrode potential.

In order to produce a large potential from lithium-ion cells, (equation 1-1), the difference between the chemical potential of lithium within the electrodes must be maximized. Figure 1.2 depicts the binding energy of lithium atoms in various intercalation hosts [9]. Positive electrode materials with a low chemical potential for lithium and thus high binding energy for lithium, such as the lithium transition metal oxides, LiCoO_2 or LiMn_2O_4 , are preferred. The negative electrode material should be chosen such that the lithium associated with this electrode has a binding energy similar to that of the pure metal in order to maximize the cell potential. In addition, the negative electrode material must have a large specific capacity and show good charge/discharge characteristics. Commonly used choices are a variety of carbon materials, $\text{Li}_{4/3}\text{Ti}_{5/3}\text{O}_4$ or

more recently, Sn-Co-C alloys [10]. In these rechargeable cells, the reactions at both negative and positive electrodes have to be highly reversible.

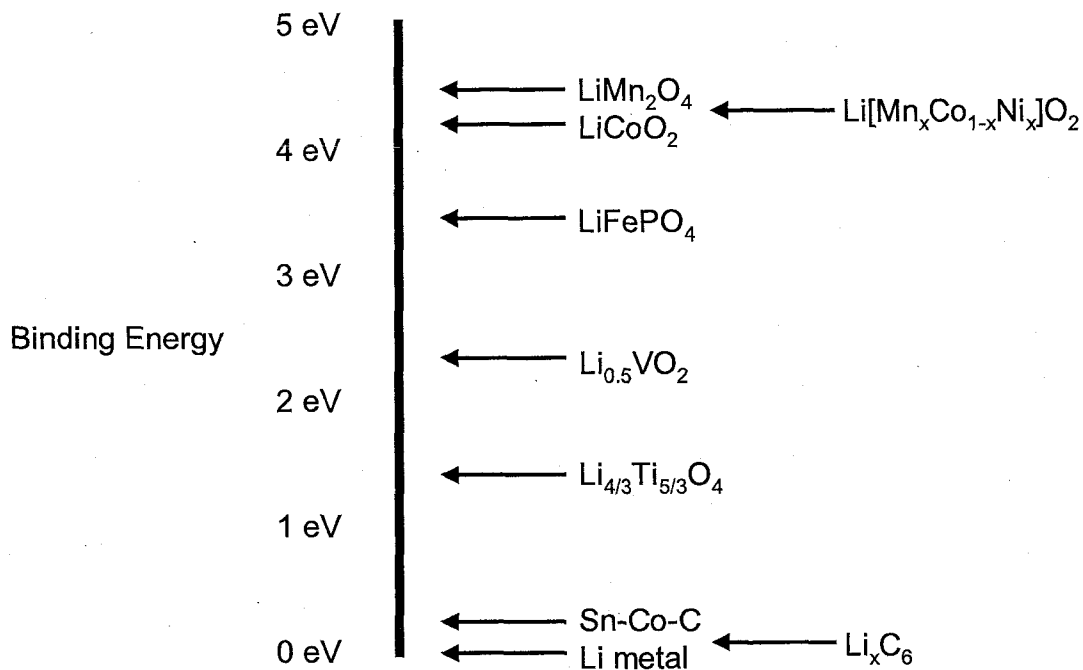


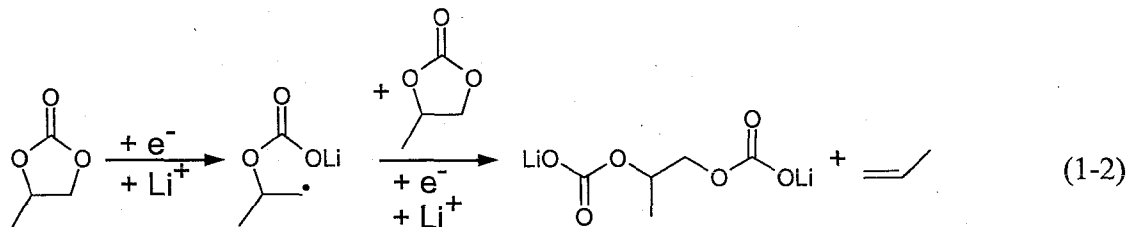
Figure 1.2 Binding energy of lithium in various lithium compounds vs lithium metal.

Traditionally, in newly constructed cells, the lithium atoms in a lithium-ion cell are stored in the positive electrode. This is the fully discharged state, where the lithium in the battery is in its most stable form. Cells with lithiated positive electrodes must be charged prior to use. During charge, work is performed to remove an amount of lithium from the transition metal oxide electrode (LiMO_2 , where $\text{M} = \text{Ni}, \text{Co}$) and add it to the negative electrode.

Not all of the lithium removed from the positive electrode intercalates into the negative electrode. This loss of lithium in the first cycle is the irreversible capacity within the cell. Before intercalation into the negative electrode can occur, the lithium atoms that form at the negative electrode react with the organic solvent and salt in the

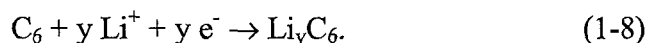
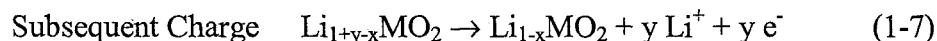
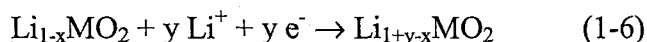
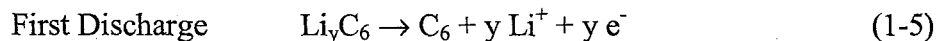
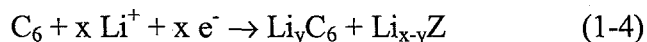
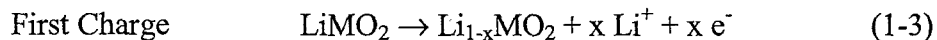
electrolyte. For example, a possible reaction of lithium with propylene carbonate (PC) is:

[11,12]



The solid products of such reactions are normally insoluble in the organic electrolyte and deposit on the surface of the negative electrode forming an interphase between the electrode and the electrolyte. This layer is known as the solid electrolyte interphase (SEI) [13]. This interfacial layer is ionically conductive, which means that it allows the passage of lithium ions, but is electronically insulating. Therefore, once the surface of the anode is fully coated with this insulator, a process called passivation, the reaction of lithium with the solvent stops and its intercalation into the negative electrode can proceed. The net result of this is that fewer lithium atoms intercalate into the negative electrode than were initially stored within the positive electrode. During the subsequent discharge, the lithium intercalated into the negative electrode is returned to the positive electrode, but the lithium that was spent forming the SEI is unrecoverable. This capacity that is lost is known as the irreversible capacity, while the capacity that remains during cycling is known as the reversible capacity. Ideally, less irreversible capacity is better than more.

The half reactions during the charge/discharge process for a lithium-ion cell containing a transition metal oxide positive and a graphite negative electrode can be written as follows:



In equations 1-3 to 1-8, Li_{x-y}Z is a representation of the various products from the reaction of lithium with electrolyte, and M is a transition metal (for example, Co, Ni). Equation 1-3 represents the delithiation of the positive electrode material. This delithiation is not necessarily always complete, hence the $\text{Li}_{1-x}\text{MO}_2$ species.

1.3.2. Solid-Electrolyte Interphase

The term solid electrolyte interface (or interphase), was first coined by Peled in the late 1970's [13]. It was used to describe the surface layer that instantly forms on lithium metal on contact with the electrolyte solution. In lithium-ion batteries, there is no direct use of lithium metal, but the potential of charged graphite approaches that of metallic lithium, therefore there is a reaction between the non-aqueous solvents and the lithium atoms [14,15]. This layer acts as an interphase between the electrode and the solution, through which electrons cannot pass, with the properties of a solid electrolyte. The SEI, once produced to a limiting thickness, suppresses further decomposition of the solvent, thus, after the first cycle there is never a direct contact between the carbon electrode and the electrolyte solution. The features that an SEI must possess are: very low electronic conductivity to prevent further growth; high Li^+ conductivity to allow the

intercalation of the lithium; and low solubility in the electrolyte. It is very fortunate that the SEI formed in lithium-ion batteries has all of these properties. Comparing the result of putting lithium metal in electrolyte to the result of putting lithium metal in water, reveals the beneficial properties of the SEI. The composition of the SEI is determined by the composition of the electrolyte. Reduction products of the carbonate solvents, namely lithium alkyl carbonates or lithium carbonate, and reduction products of the salt anion, namely LiF in the case of LiPF_6 [16] or three-coordinate borates for the case of lithium bis(oxolato)borate (LiBOB), make up the bulk of the SEI [17]. The SEI formation reactions are undesirable because the lithium is irreversibly consumed and must be balanced by including additional cathode material, which increases costs and more importantly, decreases the energy density of the cell.

It is widely accepted that SEI formation occurs on the negative electrode during the first charge of a lithium-ion cell, but the exact compositions of the SEI depends on several factors including solvents, the electrolyte salt, the temperature and even the type of electrode surface.

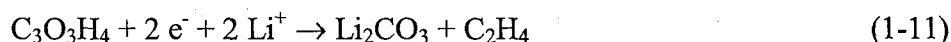
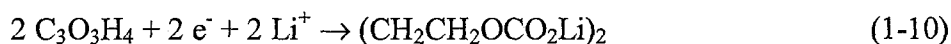
Major contributors to the formation of the SEI are the solvents when they are reduced to semicarbonates. For example, EC is reduced to form the semicarbonate $(\text{CH}_2\text{OCO}_2\text{Li})_2$ (see equation 1-9) [18]. Similar reactions occur for PC and the linear carbonates DEC and DMC [11,19,20,21,22,23]. Lithium carbonate (Li_2CO_3) can also be formed when the semicarbonates react with trace water in the cell.

Analysis has shown that the SEI in an LiPF_6 based electrolyte is composed of lithium carbonate and various lithium alkylcarbonate components (ROCO_2Li), in addition to a small amount of lithium halides (LiF) from the reduction of the electrolyte salt (see

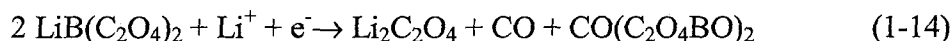
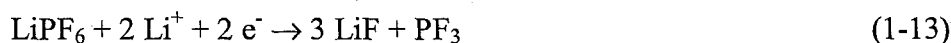
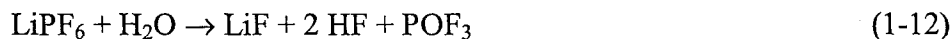
equations 1-12 and 1-13) [24]. When LiBOB is used as the salt, the SEI also contains lithium oxalate and a tri-coordinated borate species [22,25].

The proposed reactions to form these products are as follows:

Solvent (ethylene carbonate) reduction



Salt reduction



The SEI layer, which is an electronic insulator, must have some effect on the ability of redox shuttles to work. One of the major concerns regarding the electrochemical shuttle is whether it would even work in the presence of the SEI layer. As the results will show, some molecules are able to shuttle for long periods of time, which works out to be thousands of oxidations and reductions for each molecule of shuttle added to the electrolyte. It seems unlikely that the process of shuttling would degrade the SEI, rather, the shuttle must function through the SEI.

1.3.3. Current Lithium-Ion Battery Technology

1.3.3.1. Negative Electrode

Graphite is one of the most commonly used negative electrodes. The early attempts at using graphite as an intercalation compound for lithium failed due to its

strong reactivity with the electrolyte and the co-intercalation of solvent molecules into the host structure [26,27]. This so-called “solvated intercalation” results in extreme expansion of the graphite matrix and frequently leads to exfoliation of the graphite, which results in a decrease in the capacity of the cell [28]. When the electrolyte solution contains ethylene carbonate (EC), the SEI that is formed protects the graphite from exfoliation, allowing it to be used as a negative electrode material.

Graphite has a low binding energy for lithium so that the combination of a graphite negative electrode with a high binding energy positive electrode, such as LiCoO_2 , produces a cell having a high voltage. In addition, graphitic materials show a high degree of structural tolerance for reversible intercalation, which leads to good charge/discharge cycling performance [29,30].

An alternative negative electrode material is $\text{Li}_{4/3}\text{Ti}_{5/3}\text{O}_4$. The theoretical specific capacity of this material is 175 mAh/g, and the discharge potential for lithium insertion is 1.55 V [31]. $\text{Li}_{4/3}\text{Ti}_{5/3}\text{O}_4$ is known as a “zero-strain” insertion material because during lithium insertion into $\text{Li}_{4/3}\text{Ti}_{5/3}\text{O}_4$, there is no expansion of the material, making it an ideal electrode material [32]. However, the lower cell potential of cells made with $\text{Li}_{4/3}\text{Ti}_{5/3}\text{O}_4$ has prevented it from being widely used by manufacturers.

Recently, many efforts have been made to search for new negative electrode materials with high capacities. Amorphous silicon has been investigated by several groups [33,34] because of its high capacity, which can be up to 3580 mAh/g. A silicon thin film electrode of thickness 150 nm was shown to cycle more than 1000 times while still retaining 90 % of its initial capacity [35]. Tin is another attractive negative electrode material because of its high theoretical capacity of 980 mAh/g [36,37,38]. Sony has

released what it calls the “next generation lithium ion secondary battery” which they name their Nexelion battery. The Nexelion battery was the first commercialized lithium-ion battery to use a tin-based negative electrode [39].

1.3.3.2. Positive Electrode

The structures that have been found to be the most successful center around the LiMO_2 structure, where M can be Mn, Co, or Ni [40,41]. LiCoO_2 was first suggested as a positive electrode material in 1980 [42]. Although practically all the lithium in LiCoO_2 can be removed electrochemically, there is a limited composition range that will allow for reversible cycling [43]. This is due to the high oxidizing power of almost completely delithiated LiCoO_2 , which can cause oxidative decomposition of the electrolyte. Additionally, upon lithium removal, the structure becomes unstable as the +4 oxidation state is not common for cobalt. Because of this, LiCoO_2 must be restricted to cycling to only about two thirds of its theoretical capacity, that is it can only be delithiated to $\text{Li}_{0.33}\text{CoO}_2$, in order to maintain good reversibility during cycling [44]. There has been much effort in finding a suitable replacement for LiCoO_2 .

LiMn_2O_4 spinel has become an increasingly popular alternative to LiCoO_2 . This is because its delithiated structure (Mn_2O_4) is more thermally stable than $\text{Li}_{0.33}\text{CoO}_2$ [45]. The main disadvantage of spinel used to be its poor cyclability that was believed to be due largely to the dissolution of manganese from the compound into the electrolyte during cycling [46]. Another disadvantage of spinel is its relatively low capacity. The capacity of spinel is 120 mAh/g, which is about 20 mAh/g lower than LiCoO_2 that has been charged to 4.2 V vs lithium metal. What this means is that the energy density of cells made with spinel is lower than the energy density of cells made with LiCoO_2 . This

lower capacity has hindered the widespread introduction of LiMn_2O_4 as a positive electrode material for small commercial cells, however, its lower cost makes it desirable for larger applications, such as in electric vehicles.

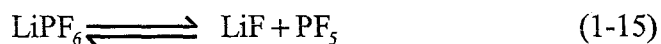
Another potential positive electrode material is LiFePO_4 [47,48,49]. Pure LiFePO_4 has a relatively low electrical conductivity of around $10^{-7} \sim 10^{-9} \text{ S cm}^{-1}$, compared to LiCoO_2 which has a conductivity of $10^{-3} \text{ S cm}^{-1}$ [50]. This means that the rate capability of LiFePO_4 is worse than that of LiCoO_2 . One way to solve this problem is to coat the LiFePO_4 with 0.2 wt. % of a conducting carbon [51]. Using this method, a conductivity of $10^{-4} \text{ S cm}^{-1}$ has been achieved. Previous reports have examined various methods of coating LiFePO_4 with carbon and have been able to achieve good cyclability and rate capability [52]. Other methods used to improve the conductivity of this material have included doping the material with trace amounts of elements such as Nb or Cr [53,54], substituting a fraction of the Fe in the material with Mn [55], and synthesizing the material as nanoparticles [56].

1.3.3.3. Electrolyte

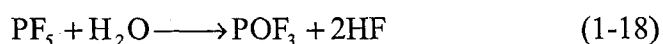
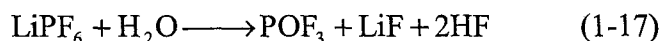
1.3.3.3.1. Salt

In lithium-ion batteries, the nature of the lithium-containing salt is also important. A good salt should have the following characteristics, high solubility and conductivity in a variety of nonaqueous electrolyte systems; a wide range of electrochemical stability; the ability to form a stable SEI; and good cycling behaviour.

In lithium-ion batteries, lithium salts can be classified into two categories, fluorinated salts and non-fluorinated salts. Examples of fluorinated salts include LiPF_6 [57] and LiAsF_6 [58]. At elevated temperatures, these salts can decompose as follows:



The product, PF_5 , is a strong Lewis acid that can react easily with organic solvents present in the electrolyte such as ethylene carbonate, driving the equilibrium towards the products. Additionally, the P-F bond in PF_5 is highly susceptible to hydrolysis by trace amounts of water, resulting in the release of HF and capacity fade for these cells [59].



In recent years, the salt lithium bis(oxalato)borate (LiBOB) has been proposed as a potential replacement for LiPF_6 [59,60,61,62]. It meets the requirements for a salt to be used in lithium-ion cells, as outlined earlier. One of the biggest advantages of LiBOB is the SEI that is formed. The SEI formed with LiBOB components is more stable than that formed with LiPF_6 . The LiBOB SEI is so stabilizing that it has been shown to prevent solvent intercalation of neat propylene carbonate into graphite electrodes [17]. Furthermore, LiBOB gives better thermal stability to the negative electrode than LiPF_6 in

organic solvents [59]. The decomposition products of LiBOB are also much less toxic than those of LiPF₆ (B₂O₃ and CO₂ compared to POF₃ and HF).

1.3.3.2. Solvent

Interest in graphitic negative electrodes increased in 1990 when it was demonstrated that lithium-containing graphitic negative electrodes could cycle in electrolyte systems based on ethylene carbonate (EC) [14,63]. The decomposition products of EC form an effective protective coating on external graphite surfaces that permits lithium insertion and prevents solvent co-intercalation [14,63]. Ethylene carbonate, which is a solid at room temperature, must be mixed with other low viscosity solvents, such as ethers (e.g., 1,2-dimethoxyethane (DME) [63,64]) and alkyl carbonates (e.g., dimethyl carbonate (DMC) [64,65], and diethyl carbonate (DEC) [66,67]) in order to be useable as an electrolyte solvent. The goal of this solvent mixing is not only to produce a lower melting point, but to also lower the viscosity of the solvent, which increases the ionic conductivity. A simple way to see the connection between conductivity and viscosity is to first look at the Stokes-Einstein equation (1-19) which relates the diffusion constant, D , of a spherical particle with radius r , in a solvent of viscosity η at a temperature T . This is making a broad assumption that the ions in solution behave similarly to macroscopic balls in solution.

$$D = \frac{kT}{6\pi\eta r} \quad (1-19)$$

The Nernst-Einstein equation directly relates the molar conductivity (Λ_m) to the diffusion constant of the ions in the electrolyte

$$\Lambda_m \propto D. \quad (1-20)$$

Thus it is predicted that,

$$\Lambda_m \propto \frac{1}{\eta}. \quad (1-21)$$

We therefore assume that when solvent viscosity is decreased, ionic conductivity of ions will be increased [68].

Commercial lithium-ion battery manufacturers do not divulge their electrolyte compositions, but they are most likely LiPF_6 dissolved in a variety of organic solvents, typically containing a significant amount of EC. Some manufacturers also place additives in the electrolyte that are believed to promote the formation of a more compact and protective inorganic film on the carbon anode [69].

1.3.3.3. Additives

Additives are added to electrolytes for a variety of purposes. Additives are used to help form a more stable SEI film, improve thermal stability and to improve safety, among other purposes.

When lithium-ion cells are stored at elevated temperatures, they exhibit capacity loss over time. The use of additives such as dimethyl acetamide [70], vinylene carbonate [70,71] or 1,3-benzodioxole [72] has been shown to reduce the capacity loss by preventing the degradation of the SEI layer.

As mentioned previously, the SEI layer is composed of many species formed from a variety of electrolyte components. Additives can be added in small amounts (less than 5%) to aid in the formation of more stable SEI layers. A good example of this is the use of fluorinated ethylene carbonate (FEC) to help form a stable SEI on the surface of

silicon-based electrodes [73]. Cells containing 3% FEC showed an improved cycling and capacity retention which was attributed to the formation of a more stable SEI.

Biphenyl [74] and some xylenes [75] have also been proposed as additives to protect a cell against overcharge. The way this is done is through electro-oxidative polymerization of the molecules to form a conductive polymer within the cell that covers the positive electrode and pierces the separator to short circuit the cell. At normal operating potentials, the molecules are inert within the cell, but when an electrode potential rises sufficiently high, the molecules polymerize and shut the cell down. Unlike redox shuttle additives, however, this procedure is irreversible and once activated, the cell can no longer be cycled normally.

1.3.3.4. Polymer Binders and Separators

In a battery, a polymer binder is used to hold the electrode particles together and to adhere them to the current collector. The choice of binder affects the interface between the electrode and the electrolyte so that the choice of binder may affect the characteristics of lithium-ion batteries [76,77]. This is of primary interest in cells that experience a large volume change during charge/discharge cycles. The most commonly used polymer is poly-vinylidene difluoride (PVDF), however, there has recently been some work reported looking for suitable non-fluorinated binders. The reason for switching to non-fluorinated polymers is because fluorinated polymers react with lithium metal and lithiated graphite to form LiF and C=CF, in an exothermic reaction that can help lead to thermal runaway [78]. Also, water soluble binders can be used, which drastically reduce the environmental impact of the electrode manufacturing process.

One final component within lithium-ion cells is the separator. The separator is a thin sheet, typically composed of polypropylene or polyethylene or a mixture of the two. The separator is porous, allowing ions in solution to pass, but prevents electrical contact between the electrodes, which could short out the cell. The main difference between types of separator is the temperature at which they melt, 150°C for polypropylene, 130°C for polyethylene. Once the polymer begins to melt, the pores within it seal shut. This permanently stops the transfer of ions within the cell.

1.4. Safety

One of the criteria of manufactured batteries is that they should be safe and easy to use under a variety of conditions. The cells should not produce dangerous conditions when they are abused. Safety is a key consideration for any technology that is destined for consumer use.

Lithium-ion batteries have a very high energy density mainly due to their high working voltage. This high working voltage is caused by the inherent reactivity of the materials in the cell. This reactivity means that for lithium-ion cells, safety is a key concern. Many companies perform tests on constructed cells that look at mechanical failure of the cell, such as a nail penetration test or a crush test. In both of these tests, localized short circuits are created, forming hot spots within the cells that can lead to thermal runaway and then to combustion. These tests are very subjective since it is very difficult to get two batteries to fail in the exact same way in a reproducible manner.

It is also possible to test the thermal stability of materials alone, using accelerating rate calorimetry (ARC) [79]. During ARC testing, electrode materials are placed in a

sealed stainless steel tube with electrolyte and then heated in a calorimeter while monitoring for heat being produced within the sample. Materials with a high self heating rate and a lower onset temperature are considered to be less safe than materials with a slower self-heating rate or a high onset temperature.

Another dangerous condition for lithium-ion cells are the conditions of overcharge, or overdischarge [80]. Commercial cells have an equal amount of capacity in the positive and negative electrodes. In practicality, this is very difficult to achieve. In cases where there is excess negative capacity, during overcharge, the positive electrode is fully delithiated, so any further current drawn results in the polarization of the electrode. The potential of the positive electrode rises sharply results in the formation of decomposition products, which will eventually destroy the cell. In the case where there is excess positive capacity, the excess current will result in the deposition of metallic lithium on the surface of the negative electrode. Lithium deposition results in the formation of dendrites which grow towards the positive electrode and can result in an internal short circuit. Overdischarge is generally less of a concern since the electrode materials are in their most stable forms. However, in a severely overdischarged cell, oxidation will produce decomposition products at the negative electrode. These conditions could eventually lead to venting of the cell and even fire.

1.4.1. Redox Additives

Lithium-ion cells are charged until they reach a specific potential. Taking a cell beyond this potential can be detrimental to the cell. As mentioned previously, LiCoO_2 can only be reversibly delithiated to $\text{Li}_{0.33}\text{CoO}_2$, which occurs at a potential of about 4.5 V. Also, at high potentials the electrolyte can decompose, evolving gas and causing the

cell to rupture and fail. Overcharging is easily avoided for individual cells by simply charging the cell only to a specified potential. However, for a battery containing multiple cells that are in a series string, the entire battery pack is charged, and therefore each individual cell needs to be protected against overcharge. In such a situation, the standard method of overcharge protection is to employ overcharge protection circuitry. This is circuitry that is capable of shunting the current around individual cells as they become fully charged, but will still allow the other cells in the pack to continue charging. This type of circuitry currently adds cost, bulk and complexity to battery pack [81]. There are currently several alternative approaches for protecting against overcharge and overdischarge being investigated.

1.4.1.1. Shuttles

Redox shuttle additives are organic molecules, which are added in small amounts to the electrolyte. During overcharge, these shuttle molecules continuously cycle between oxidized and reduced forms while providing an internal shunt for overcharge current. Figure 1.3 shows a schematic representation of the shuttling process.

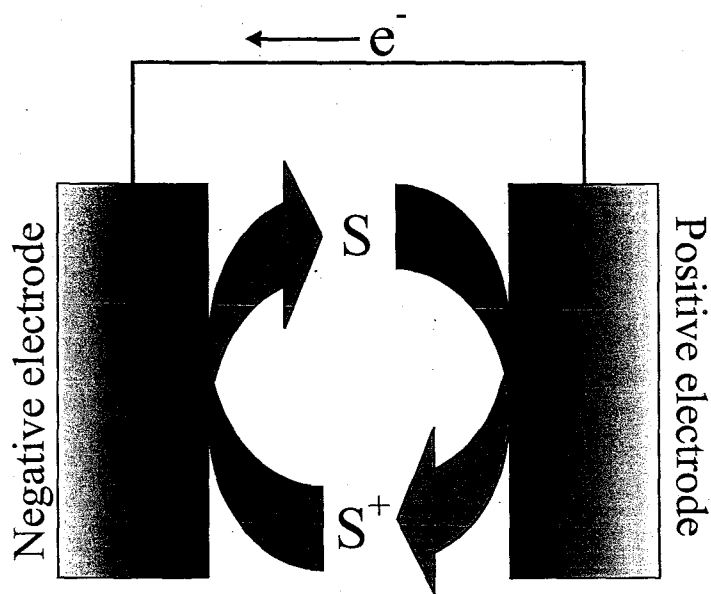
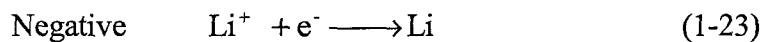
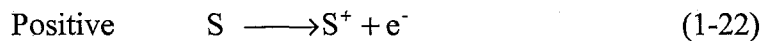
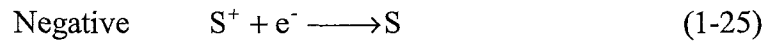
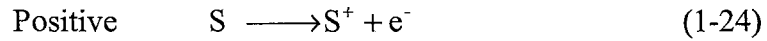


Figure 1.3 A schematic diagram of a redox shuttle operating within a cell.

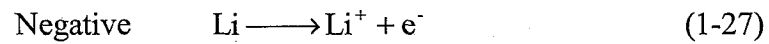
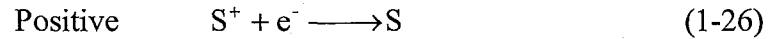
When the cell is operating in normal charge/discharge cycles, the shuttle molecules are inert. Once the potential of the positive electrode reaches the oxidation potential of the shuttle, the shuttling process begins. The reactions within the cell at each electrode are as follows:



Equations 1-22 and 1-23 represent the reactions that occur at the positive and negative electrode at the beginning of the shuttling process. As molecules of neutral shuttle are initially oxidized at the positive electrode, lithium is plated onto, or intercalated into, the negative electrode in order to maintain charge neutrality. Then, once the oxidized shuttle reaches the negative electrode, it will be reduced instead of the lithium ions, as shown in equations 1-24 and 1-25:



Then, during the initial steps of discharge or open circuit, the oxidized shuttle within the cell is reduced back to its neutral state, as shown in equations 1-26 and 1-27:



It can be seen that the shuttling process results in an amount of lithium being removed from the negative electrode. This amount of lithium is equal to the amount of lithium that would be deposited at the onset of the shuttling process. It should be noted that the shuttle works both in overcharge and in overdischarge. During stable overdischarge, the reactions at the electrodes are as follows:

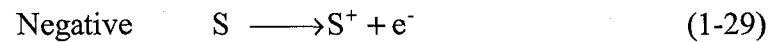
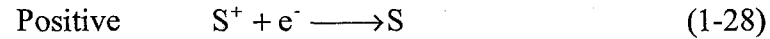


Figure 1.4 depicts how the shuttle protects in both overcharge and overdischarge.

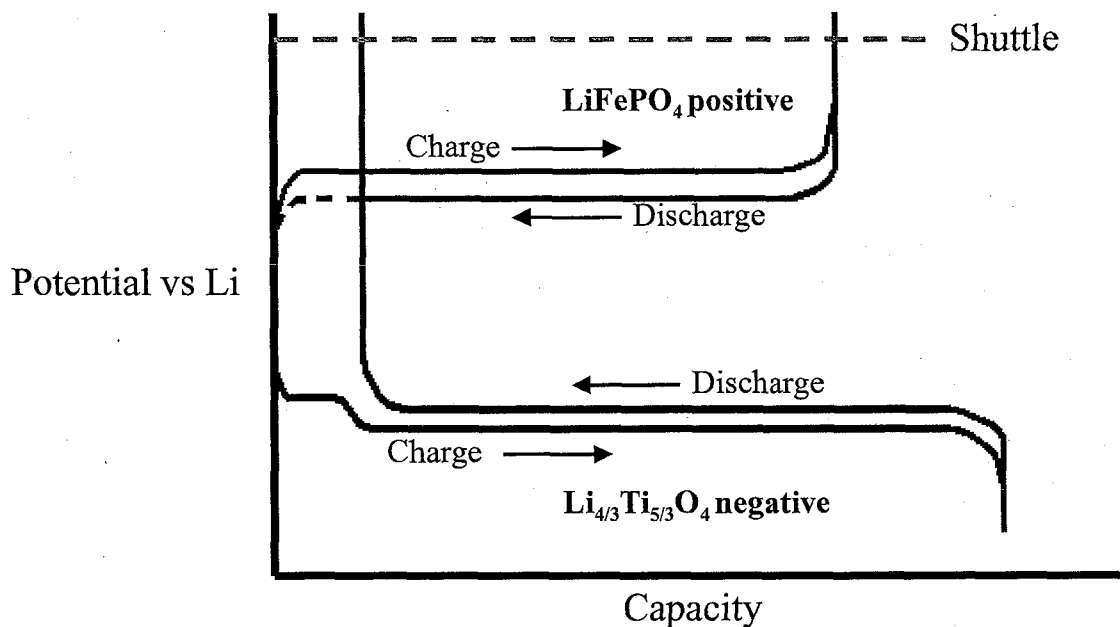


Figure 1.4 Schematic of electrode potentials allowing shuttling during charge and discharge.

Figure 1.4 shows that the result of the excess negative electrode capacity is that at the end of charge, the positive electrode is emptied of lithium before the negative electrode is filled. This results in the potential of the positive electrode rising sharply and activating the shuttle on overcharge. Then, during discharge, because of the irreversible capacity within the cell, the negative electrode empties of lithium before the positive fills, so the potential of the negative electrode rises sharply and will activate the shuttle during overdischarge.

Work on shuttles began in the late 1980's when metallocenes were patented as a desirable class of shuttles in lithium batteries [82]. These molecules were low in

potential, around 3.0 to 3.5 V vs lithium, so they had little use in cells with positive electrodes that contained LiCoO_2 , LiMnO_4 , or LiFePO_4 .

Later, in 1998, Sony filed a patent on halogen-containing dimethoxybenzenes [83,84]. These molecules showed redox potentials around 4.0 V vs lithium. This means that they are suitable for use within LiFePO_4 cells. This work did not present any long-term cycling results which would have shown that these molecules, while at the right potential, were not capable of providing protection for more than a handful of cycles [85]. These molecules were then tested in our lab and results showed the limited shuttling capability of these molecules.

1.4.1.2. Polymers

An overcharge protection method similar to that of the redox shuttle is the use of redox active polymers. To protect cells, the porous separator is impregnated with the polymer by soaking in a solution containing the polymer, followed by drying. The result of impregnating the separator with the redox polymer is that a percentage of the pores become filled with polymer which connects the two electrodes. The morphology and porosity of the separator after impregnation is dependent on the solvent used [86]. When the electrode potential is below the oxidation potential of the polymer, the polymer is insulating. The polymer will become conducting when it is p-doped, which occurs when the positive electrode potential rises high enough during overcharge. The conductivity of the polymer can change by several orders of magnitude, depending on the level of doping. The polymer poly(3-butylthiophene) (P3BT) changes from 10^{-9} S/cm in the neutral state to 0.1 S/cm at its maximum stable doping level of 0.28 electrons per formula

unit [87,88]. It should also be noted that in order to maintain charge neutrality, after the polymer is oxidized, an anion diffuses into the polymer.

One limitation of electroactive polymers is their electrochemical stability window. Typically, polymers that have high oxidation potentials also have high reduction potentials. This means that in order to have a polymer that will become conducting at high potentials, as with LiCoO_2 or LiMnO_2 electrodes, the polymer will not be reductively stable at lithium potential or at the potential of lithiated graphite electrodes. Figure 1.5 depicts a polymer double layer, which is one way of overcoming this problem [86].

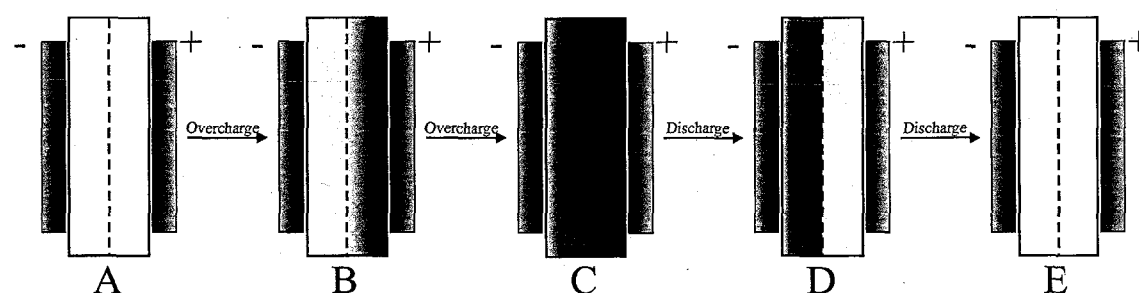


Figure 1.5 Redox polymer bilayer during normal charge (A), initial stage of overcharge (B), sustained overcharge (C), initial stage of discharge (D) and normal discharge (E).

In this double layer, two polymers are used that have different oxidation potentials. The polymer touching the positive electrode should have a high oxidation potential, but will probably degrade at the low potential of the negative electrode, so between it and the negative electrode is a polymer that has a lower oxidation potential. This second polymer will be stable at the low potential electrode and is protected from the high potential of the positive electrode by the first polymer as long as the first polymer is insulating. Only

when the first polymer becomes conducting (B) does the second polymer also become conducting (C) and the overcharge current is shunted through the polymer. Then, after the overcharge is finished, the first polymer becomes insulating (D), which prevents additional self discharge within the cell.

1.5. Scope of this Thesis

The work presented in this thesis is multidisciplinary in its scope and as such, many different people have contributed to different parts of this project. Chapter 1 of this thesis discusses background information regarding lithium-ion batteries. Chapter 2 covers the experimental techniques used throughout this work. Chapter 3 provides a more in depth look at various aspects of redox shuttles. Chapters 4 and 5 contain experimental results from a variety of redox shuttle molecules, specifically those with low redox potentials and those with high redox potentials. Much of this work was begun by Dr. Jun Chen and Dr. Claudia Buhrmester while Dr. William Lamanna, a Division Scientist at 3M Co., has used his knowledge of synthetic chemistry to create a number of molecules presented here that would otherwise not have been available. Chapter 6 shows how computational chemistry can be of use in this field. The theoretical work was performed by Dr. Richard Wang, a research associate in the Department of Physics at Dalhousie University, and is presented with accompanying experimental results to show the excellent correlation between theory and experiment. Lastly, Chapter 7 offers conclusions drawn from this work as well as suggesting future work.

Much of this work has been published in journals including the Journal of the Electrochemical Society. Parts of these of published works are reproduced here with the permission of the Electrochemical Society.

Chapter 2. Experimental Techniques

2.1. Electrochemical Testing

A variety of electrochemical testing methods were employed to test various aspects of shuttle performance. Coin cells were used to show the length of overcharge protection in lithium-ion cells as well as the shuttling potential of each molecule. The length of overcharge protection is defined here to be the number of cycles of 100% overcharge per cycle that a shuttle will operate for. Solution-based electrochemistry can provide information about the potential window that a molecule is stable within, as well as the diffusion constant and the redox potential of the molecule.

2.1.1. Coin Cells

The electrodes for coin cells were prepared by combining the electrode active material powder with 10%, by mass, each of Super S carbon black (MMM Carbon, Belgium) and polyvinylidene difluoride (PVDF) binder (9% PVDF Kynar 301F solution in N-methyl-2-pyrrolidinone (NMP) obtained from the NRC, Canada). The LiFePO_4 was supplied by Phostech Lithium (Montréal, PQ, Canada) and the $\text{Li}_{4/3}\text{Ti}_{5/3}\text{O}_4$ was obtained from NEI Corp. (Piscataway, NJ, USA). The carbon black ensures electrical contact between all the grains in the electrode while the binder is used to ensure that the electrode holds together and to the current collector. The solvent, NMP, was then added in excess to make a slurry with a suitable consistency to make electrodes. After shaking in a jar with zirconia beads for 30 minutes, the mixture was poured onto either aluminum or copper foil. Aluminum was used as the current collector for LiFePO_4 positive

electrodes as well as for $\text{Li}_{4/3}\text{Ti}_{5/3}\text{O}_4$ negative electrodes. Copper was used as the current collector for graphite negative electrodes. The reason for the different choices of current collector material is because copper will dissolve at potentials around 3.4 V vs Li/Li^+ so electrodes that will go to higher potentials need to be spread on aluminum. Aluminum, on the other hand, will alloy with lithium below about 0.3 V vs Li/Li^+ so it is not suitable for use with graphite, which has its capacity just above lithium potential. The slurries were then spread to a thickness of 0.016", 0.011" or 0.006" before being dried overnight in an oven set at 110°C. Once dry, 1.3 cm diameter circular electrodes were punched and then weighed to determine the amount of active material on each disk.

Redox shuttles were tested in a variety of coin cells, containing LiFePO_4 positive electrode, MCMB or $\text{Li}_{4/3}\text{Ti}_{5/3}\text{O}_4$ negative electrodes and either LiBOB or LiPF_6 as the electrolyte salt, unless otherwise stated. Of the cells that were made for each shuttle molecule, only the result for the cell with the largest number of cycles is reported. This is considered acceptable to do in the battery industry because it would be assumed that under ideal conditions, each cell would be expected to perform at least as well as the best cell. Minute deviations in cell construction can have a significant impact on the cycling of a cell, so the quality of a shuttle molecule is best judged by the best cell, not an average value. In cases where repeat cells of the same chemistry were prepared, the number of shuttle-protected overcharge cycles obtained was generally within 30%

2.1.1.1. Two-Electrode Cells

Figure 2.1 shows the components of a coin cell, which was assembled in an argon-filled glove box. The typical 2325 coin cell hardware (23 mm diameter, 2.5 mm thickness) is composed of a stainless steel top and bottom casing. The positive electrode

was placed in the center of the bottom casing and electrolyte was added on top of the electrode. The electrolyte was composed of either 0.5 M or 0.7 M salt, either LiPF_6 (obtained from Stella Chemifa Corp., Japan) or LiBOB (obtained from Chemetal, Germany), in propylene carbonate (PC): dimethyl carbonate (DMC):ethylene carbonate (EC): diethyl carbonate (DEC) in the ratio 1:2:1:2 by volume. The solvents were obtained from Ferro Corp. (Grant Chemical Division, USA). A single layer of a 25 μm polypropylene separator (Celgard, USA) was then placed above the electrode after which the negative electrode was added. Finally, a stainless steel spacer and spring (purchased from the NRC, Canada) were added to maintain good electrical contact between the electrodes. The cell top had a polypropylene gasket around the edge which made an air tight seal when the cell was crimped shut. Coin cells destined for shuttle testing were designed to have at least 30% excess capacity in the negative electrode to ensure that shuttling would occur during overcharge without plating lithium. Cells were tested using a computer-controlled constant-current charger system obtained from Moli Energy (1990) Ltd.

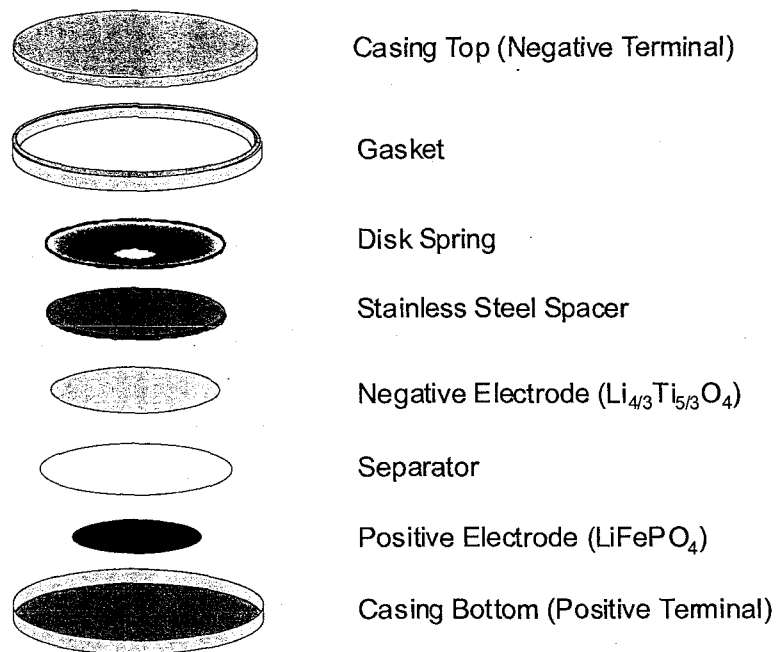


Figure 2.1 Exploded view of the hardware in a 2325 coin cell.

The coin cells were charged with a constant current and the potentials were measured every few minutes. Standard coin cell testing procedures are to charge a cell, that is remove lithium from the positive electrode and insert it into the negative electrode, until the cell reached a specified upper cutoff potential. In cells that contained redox shuttles that prevented the potential from rising above the oxidation potential, it was also necessary to set a maximum time limit for each cycle. This time limit was typically chosen to be twice the normal charging time of the cell, in other words, each cycle experienced 100% overcharge. Cells with shuttles would then be charged until either the upper cutoff potential was reached or the maximum charge time was reached, whichever occurred first.

2.1.1.2. Three-Electrode Cells

The standard cell design can be changed to include the insertion of a third electrode, a reference electrode, within the cell. The reference electrode was a thin strip of 25 μm stainless steel foil with a small amount of lithium metal attached at the end. To prevent contact between the reference electrode and either electrode, two separators were used. To prevent contact between the reference electrode and the can, the steel foil was laminated with thin sheets of polypropylene. Figure 2.2 shows a schematic of a 3-electrode coin cell.

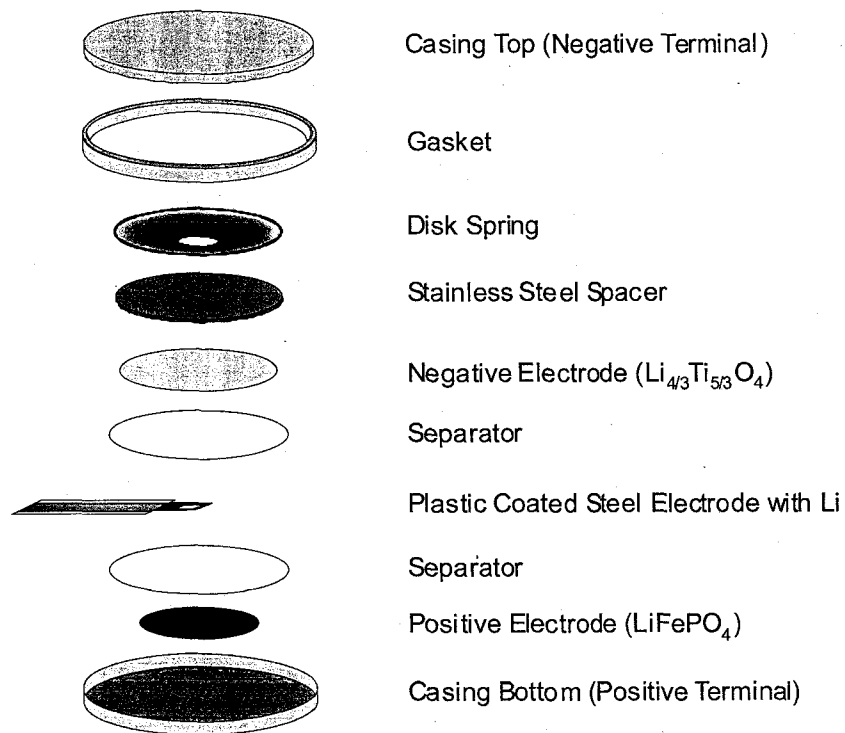


Figure 2.2 Exploded view of 3-electrode coin cell hardware.

The purpose of 3-electrode coin cells was to allow for the direct measurement of the potential of the electrodes within the lithium-ion cell. In 2-electrode cells, only the difference in potential between the electrodes could be measured. With a 3-electrode

cell, it was possible to measure the potential of one of the electrodes vs the inserted lithium reference electrode. It was arbitrarily decided to measure the potential of the negative electrode and then calculate the potential of the positive electrode as the sum of the cell potential and the negative electrode potential.

Experiments using 3-electrode coin cells were run in a similar manner to those involving standard coin cells except that a second charger channel was required. This second channel was connected to the reference electrode and the negative electrode and was run as a slave to the first channel so that it would record data but not pass any current.

2.1.2. Solution-Based Electrochemistry

2.1.2.1. Spectroelectrochemistry

Voltammetric experiments were performed with an Arbin Instruments BT4+ potentiostat, run with MITS Pro software. UV-vis spectra were taken using an Agilent 8453 UV-visible spectroscopy system and run with the accompanying software. Figure 2.3 shows a schematic of the modified cell used to carry out all measurements.

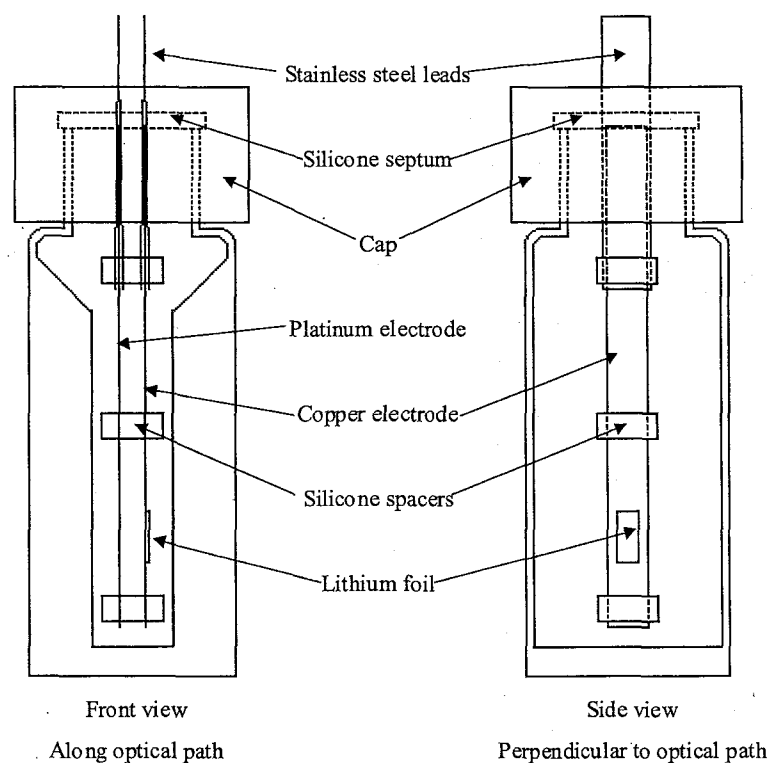


Figure 2.3 Schematic of cells used for spectroelectrochemical measurements.

These electrochemical cells were constructed inside quartz UV-Vis cuvettes. These cuvettes have wells that are 4 mm wide and 10 mm deep. Cells with narrow wells were chosen in an effort to minimize the volume of electrolyte required to run each experiment. Cells have a screw top cap with a silicone rubber septum. The septa were cut to allow stainless steel leads to be passed through to connect the electrodes to the Arbin Instruments BT4+ potentiostat, run with MITS Pro software and were then sealed with silicone sealer. The positive electrode was a strip of 20 μm thick platinum foil and the negative electrode is a strip of copper foil with a small (2 mm x 5 mm) piece of 125 μm thick lithium foil attached. The purpose of the lithium foil was to hold the potential of the negative electrode fixed at Li/Li^+ potential so that it could act as both a counter

electrode and a reference electrode. Both electrodes were cut to be approximately 4 mm x 20 mm and were separated by a distance of about 2 mm. The foil electrodes were kept apart using small pieces of silicone rubber as separators placed at various lengths along the electrode. The electrodes were aligned in the cell to match the path of light from the spectrophotometer.

The electrolyte used in the spectroelectrochemical cell was a mixture of PC:DMC:EC:DEC in the ratio 1:2:1:2 by volume with 0.5 M LiBOB as the electrolyte salt. LiPF_6 was not used for two reasons: it degraded all silicone pieces and trace HF could harm the cell. Shuttle molecules were added in mM concentrations to keep the absorbance within the detection limit of the instrument. The potential sweep experiments were run with very slow sweep rates to allow more time for diffusion of oxidized/reduced species within the cell.

2.1.2.2. Cyclic Voltammetry

Larger volume cells, on the order of 1-2 mL were designed and machined from polypropylene for the purpose of running more careful potential sweep experiments. Polypropylene was chosen over glass for two main reasons, the presence of HF in LiPF_6 based electrolytes is detrimental to glass, and the robustness of the material, which includes the ease of machining. The electrodes used were as follows: the reference electrode was a 'no leak' Ag/AgCl reference electrode from ESA Inc., the counter electrode was a copper rod, the working electrode could be either a 1 mm diameter Pt disc or a 1 mm diameter glassy carbon disk, both also from ESA Inc. Cells are constructed inside an argon glove box to prevent exposure to air and moisture. These cells have a threaded top and an o-ring seal making them air tight. In our non-aqueous

electrolyte solution, the reference electrode was calibrated against the ferrocene/ferrocenium redox pair and was found to have a potential that is 2.93 V above Li/Li^+ . All results are therefore reported against Li/Li^+ . Figure 2.4 shows a schematic representation of the cell geometry

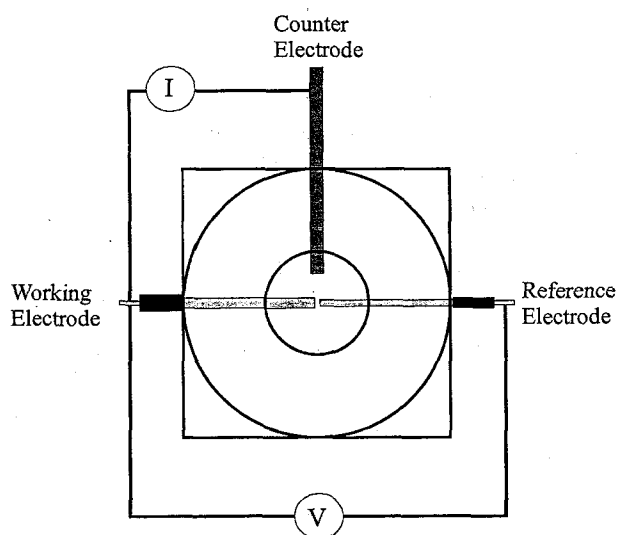


Figure 2.4 Schematic of CV cells using three electrodes.

The working electrode and the reference electrode were placed as closely together as possible while the counter electrode was placed farther away. These cells operate within semi-infinite boundary conditions, namely, that the cell is large compared to the length of diffusion, d . This means that for tests conducted within a reasonable amount of time, we assume:

$$\lim_{x \rightarrow \infty} [S](x, t) = C \quad (2-1)$$

$$\lim_{x \rightarrow \infty} [S^+](x, t) = 0 \quad (2-2)$$

for all values of t , where C is the initial concentration of the shuttle in the electrolyte, $[S](x, t)$ is the concentration of the neutral shuttle species at a distance x from the working

electrode at a time t and $[S^+](x,t)$ is the concentration of the oxidized shuttle species at a distance x from the working electrode at a time t .

These three-electrode cells allowed for cyclic voltammograms (CV's) of molecules to be taken by sweeping the potential up and down. This allowed the determination of the redox potential of various shuttle molecules. Also, it is possible to vary the sweep rates of subsequent sweeps and use the data to determine the diffusion constant of shuttle molecules using the Randles-Sevcik equation [89]:

$$I_p = 0.4463(F^3/RT)^{1/2} n^{3/2} A D^{1/2} C \nu^{1/2} \quad (2-3)$$

where I_p is the peak anodic current, F is the Faraday constant, R is the gas constant, T is the absolute temperature, n is the number of electrons involved in the redox reaction, A is the working electrode surface area, D is the diffusion coefficient, C is the concentration of the shuttle molecule in mol/cm^3 , and ν is the linear potential sweep rate. By plotting I_p against $\nu^{1/2}$ it is possible to extract the diffusion coefficient from the slope, assuming that the electron transfer step is much faster than the rate of diffusion.

Figure 2.5 shows the configuration of four-electrode cells designed to make results more representative of those from coin cells, which include a second working electrode.

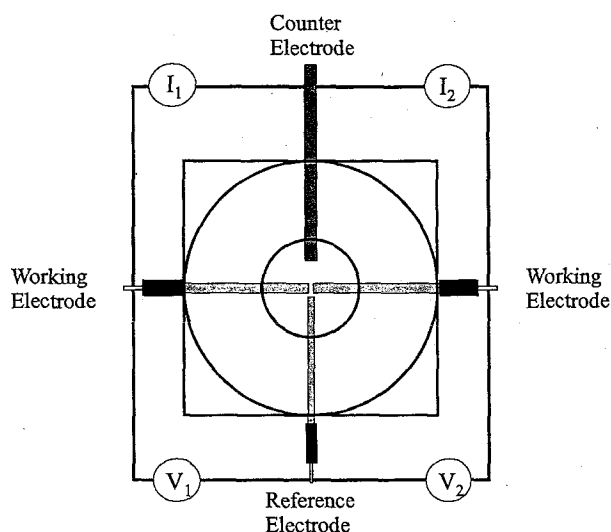


Figure 2.5 Schematic of CV cells using four electrodes, wired as two three-electrode cells using common counter and reference electrodes.

The fourth electrode is a second working electrode. Both working electrodes share a common reference and counter electrode, but are run on separate potentiostat channels. With this setup, it is possible to use one electrode as the “positive electrode” and the other as the “negative electrode”. The distance between the electrodes is difficult to measure inside a constructed cell because the well is narrow and deep. Also, because the electrodes are placed by hand, the electrode spacing varies from cell to cell. The electrode spacing is approximated by using the calculated diffusion constant of the molecule being tested and the delay in signal response between the time the positive electrode is placed above the redox potential of the shuttle and oxidation begins and the time the negative electrode begins to register a reductive current. The interelectrode distance is then approximated as:

$$d = (D \times t)^{1/2}, \quad (2-4)$$

where d is the interelectrode distance, D is the diffusion constant and t is the time required for diffusion across the gap. Typically, the electrode spacing ends up being in the range of 25 to 50 μm , which is on the same order as a coin cell.

The main advantage of the four-electrode design is that the potential of the “negative electrode” remains low, below the oxidation potential of the molecule being examined, while the potential of the “positive electrode” can remain high, well above the potential where an SEI layer will begin to form. In standard CV experiments, a single electrode is swept through a wide range of potentials. Actual battery experiments are more closely approximated by the four-electrode design.

Figure 2.6 shows the potentials of the two electrodes in one experiment using a four-electrode cell. This experiment was designed to try and determine if shuttle molecules could shuttle through an SEI layer. The top panel shows the potential of the “positive electrode”, which was held slightly above the shuttling potential of the molecule of interest. Since it was held at this potential, it was constantly generating a supply of oxidized shuttle that could diffuse to the “negative electrode”. The bottom panel shows the potential of the “negative electrode” as it was swept during the experiment. The potential of the “negative electrode” was always well below the oxidation potential of the shuttle molecule of interest, so any oxidized shuttle reaching the surface would be immediately reduced. Any changes in the current during the scans must therefore be due to other reactions on the negative electrode, such as the formation of an SEI layer.

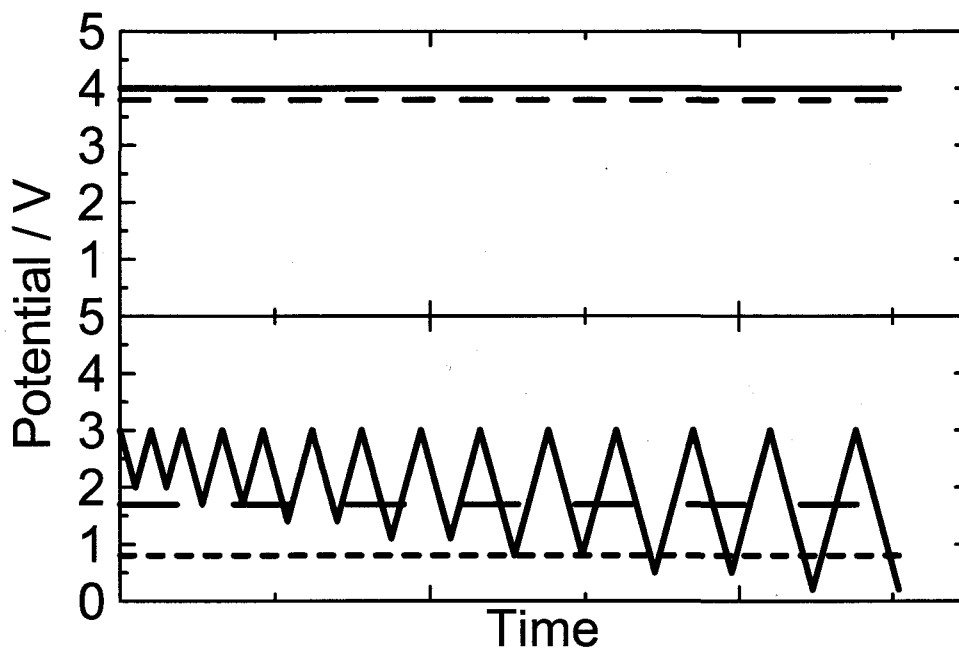


Figure 2.6 Schematic representation of an experiment utilizing the four-electrode CV cell to determine if a shuttle molecule can function through the formation of the SEI layer. The top panel shows the potential of the working electrode (—) and the oxidation potential of the shuttle (---). The bottom panel shows the potential of the second working electrode (—) and the potentials where SEI formation occurs begins in LiBOB (---) and LiPF₆ (---) containing electrolytes.

Additionally, the four-electrode design allows for easy calibration of the Ag/AgCl reference electrodes used in all CV experiments. Published oxidation potentials in the solvents used in these experiments are extremely rare, so it was necessary to know where the potential of the reference was with respect to other potentials of interest, namely Li/Li⁺. To do this, the four-electrode cell was assembled with one working electrode, one counter electrode and two reference electrodes. One of the reference electrodes was the commercial Ag/AgCl reference electrode, and the other was a piece of stainless steel rod that had one end coated in lithium metal. The cell was then assembled in the argon-filled glovebox and filled with the electrolyte of interest containing a molecule with a

reversible oxidation, such as the molecule 2,5-di-*t*-butyl-1,4-dimethoxybenzene. CVs were then run in a standard fashion for a 3-electrode cell, and the connection to the reference electrode was moved to the other reference electrode between runs. Figure 2.7 shows the results of one such calibration. It can be seen that with respect to Li/Li^+ , the oxidation potential is at 3.95 V and with respect to Ag/AgCl , the oxidation potential is 0.95 V. The commercial Ag/AgCl reference electrode is therefore 3.00 V above the Li/Li^+ couple.

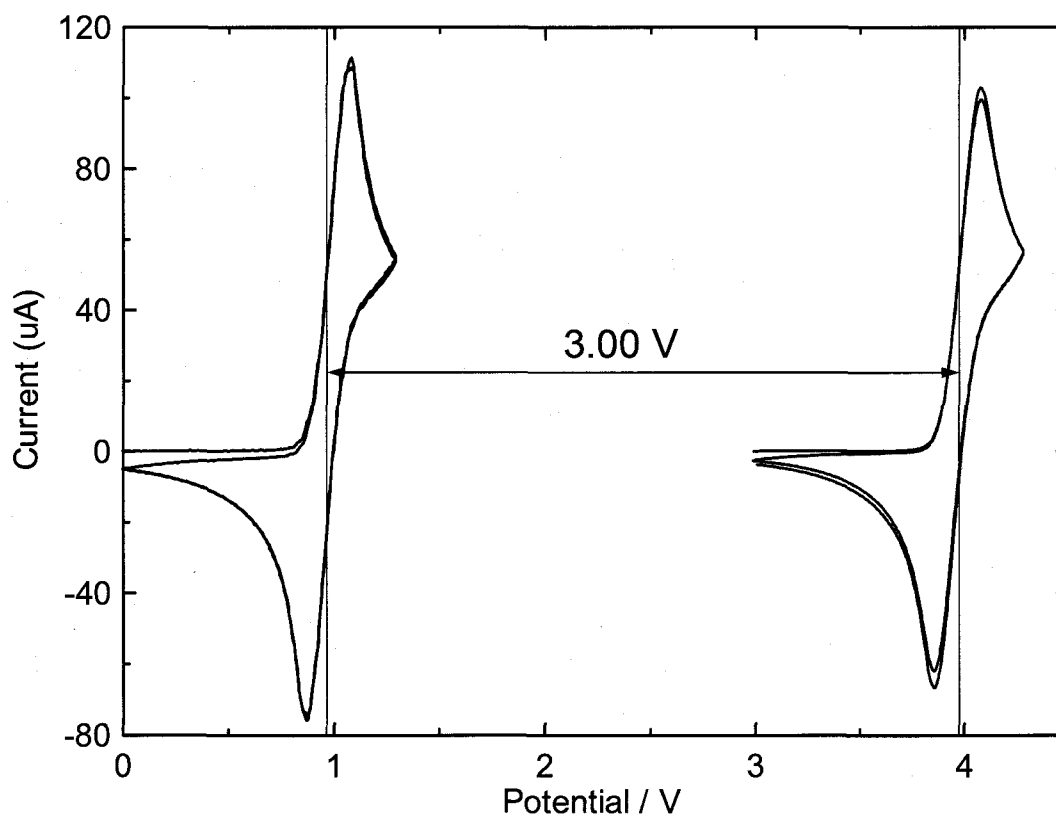


Figure 2.7 CV of the molecule 2,5-di-*t*-butyl-1,4-dimethoxybenzene in battery electrolyte vs Li/Li^+ (—) and vs Ag/AgCl (---).

2.2. Summary

The techniques discussed in this chapter have all been useful in studying redox shuttles and their use in batteries. Coin cells in particular give good information about

the use of redox shuttle molecules in lithium-ion batteries, but other techniques, such as CV can be useful to explore a variety of properties of redox shuttles. These properties and how they can affect the usefulness of specific molecules are the focus of the next chapter of this thesis.

Chapter 3. Properties of Redox Shuttles

One of the first questions to be answered should be, how can we be sure that shuttles will operate as expected in cells? Figure 3.1 shows the results from a UV-vis experiment where the absorbance was measured as the potential of the electrode was swept above and below the oxidation potential of the molecule, which in this case is the molecule 2,5-di-*t*-butyl-1,4-dimethoxybenzene (DDB) [90].

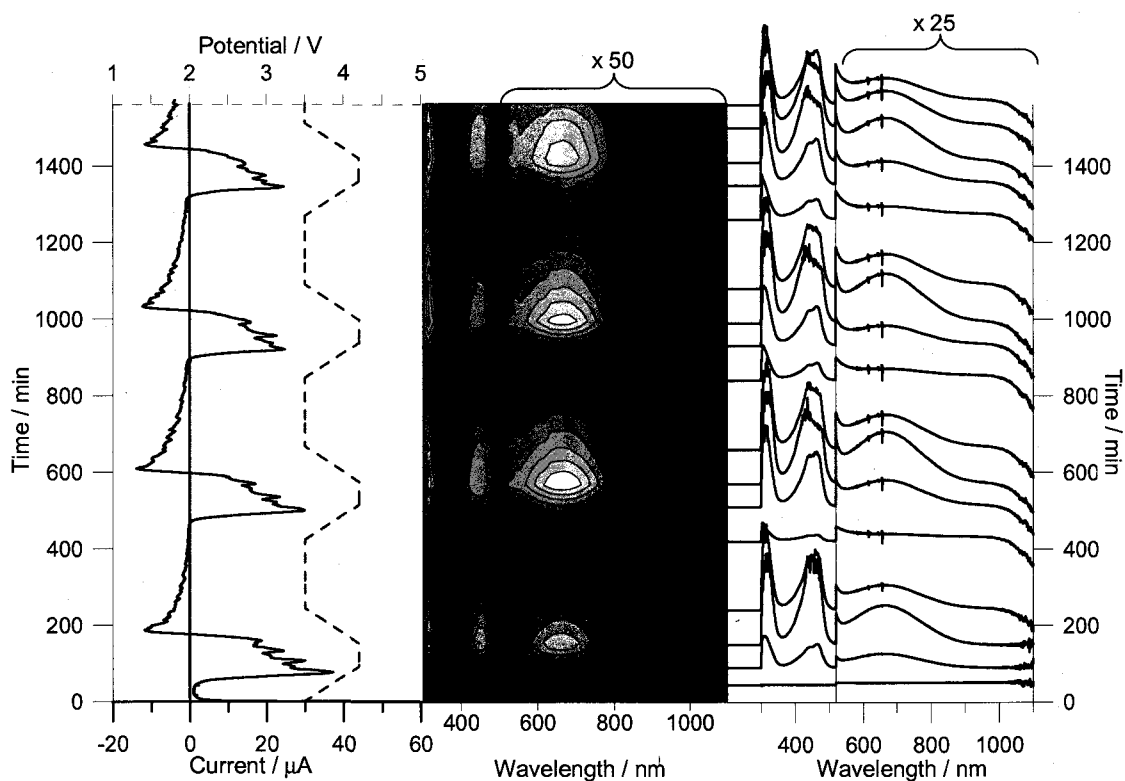


Figure 3.1 Data from a UV-vis experiment of the molecule 2,5-di-*t*-butyl-1,4-dimethoxybenzene. The left panel shows the controlled potential and the current response of the experiment. The right panel shows the UV-vis spectra at select times from 300 nm to 1100 nm. The middle panel shows a contour plot of how the intensity of the peaks in the UV-vis spectra changes with time.

The left panel of Figure 3.1 shows the current response as the cell potential was swept as shown. When the potential went above the oxidation potential of the shuttle, there was a positive current flowing, indicating that the molecule was being oxidized, and when the potential was swept down, there was a negative current, indicating that the oxidized shuttle was being reduced. The right panel shows the UV-vis spectra at selected times from 300 nm to 1100 nm and the middle panel shows a contour plot of the UV-vis data in an easier to follow form. It can be seen that before the oxidation occurs, there were no peaks, but once the potential was increased above the oxidation potential of the molecule, several peaks formed in the spectrum. Then, when the potential was swept down again, the peaks shrunk. This pattern repeats for several times. The peaks never fully disappear because of the large volume of the cell and large diffusion distances in the cell compared to those that would be seen inside a coin cell. On the timescale of these experiments, there was not enough time allowed for all of the oxidized shuttle to be reduced before the next cycle began. It should be noted that initially, the electrolyte was a clear colourless solution, and upon oxidation, the solution turned yellow-green.

So it appears that indeed, the shuttle is capable of being oxidized and reduced in an electrochemical cell, but what about inside a coin cell? One of the problems with standard coin cells is that only the potential difference between the two electrodes is measured. Three-electrode coin cells allow for the direct measurement of the potential of one of the electrodes to make sure that the shuttling is occurring as expected in a cell. Figure 3.2 shows the results from a three-electrode coin cell containing DDB.

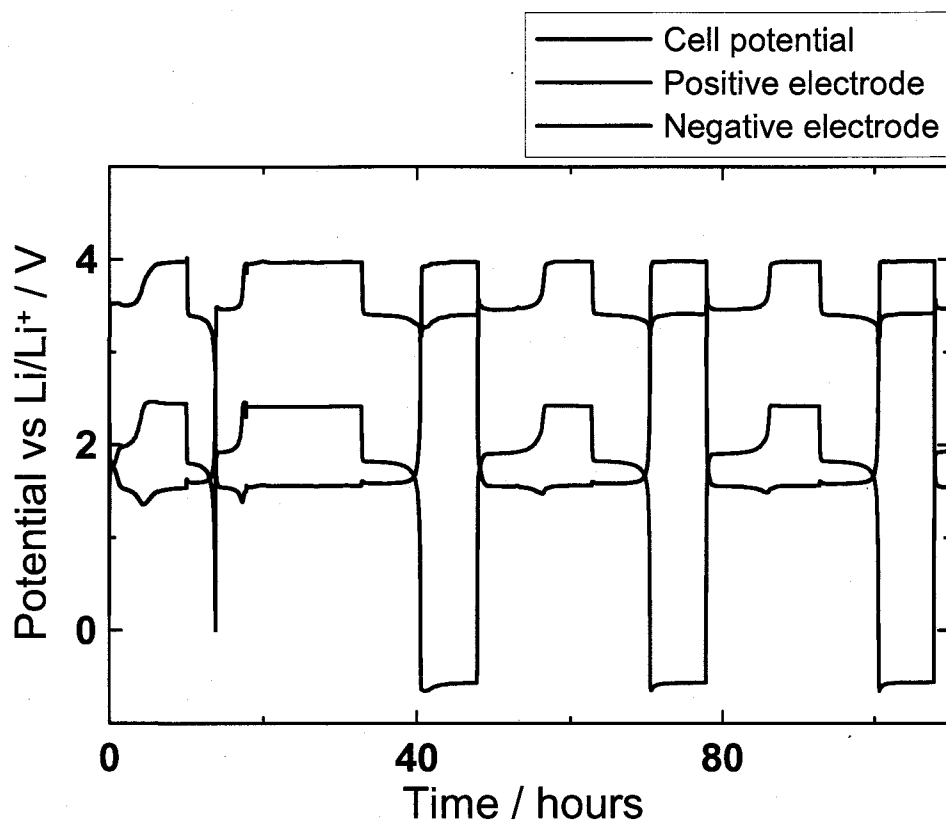


Figure 3.2 Three-electrode coin cell data for a $\text{LiFePO}_4/\text{Li}_{4/3}\text{Ti}_{5/3}\text{O}_4$ cell containing 2,5-di-*t*-butyl-1,4-dimethoxybenzene. The cell potential and the individual electrode potentials are shown.

The cell shown in Figure 3.2 consisted of a LiFePO_4 positive electrode and $\text{Li}_{4/3}\text{Ti}_{5/3}\text{O}_4$ negative electrode, making the cell potential during charging nominally 2 V, as shown by the blue line. The potential of the negative electrode, in black, was then measured against the reference electrode and the potential of the positive electrode, in red, was the sum of the negative electrode potential and the cell potential. It can be seen that during shuttling, the potential of the positive electrode increases and is held constant at just below 4 V, as would be expected. During overcharge, there is very little change in the potential of the negative electrode. If the cell is exposed to overdischarge conditions, the potential of the negative electrode goes positive and is held at just below 4 V, which is the same potential

that the positive electrode is held at during overcharge. This is, of course, due to the fact that the oxidation of the shuttle is occurring at this potential. So, indeed, the shuttle is operating at both electrodes as would be expected in both overcharge and overdischarge.

Once redox shuttles had been shown to work both in electrochemical tests and in coin cells, it was of interest to determine certain properties of the molecules themselves. Key characteristics of shuttle molecules are: electrochemical stability over the whole potential range of cell operation and an extremely reversible redox reaction. These characteristics are required for the shuttle molecules to provide protection for extended periods of time. Other qualities of interest are a high diffusion coefficient and a high solubility in the electrolyte. These characteristics are important because they are directly related to the maximum current that can be carried by the shuttle.

3.1. Overcharge Current

During shuttle-protected overcharge, all of the electrons in the overcharge current are drawn from the shuttle molecules in the electrolyte. The current carried by the shuttle molecules can be calculated if certain other parameters are known [91]. If $[S^+]_x$ and $[S]_x$ are the concentrations of the oxidized and neutral forms of the shuttle at a distance x from the positive electrode, and the diffusion constants of the two species are assumed to be equal, during overcharge:

$$C = [S^+]_x + [S]_x \quad (3-1)$$

where C is the initial concentration of shuttle in the electrolyte and x is the distance from the positive electrode such that $0 < x < d$, where d is the interelectrode spacing.

Using Fick's Law of diffusion [92], eventually, the rate of oxidation of S at the positive electrode will equal the rate of reduction of S⁺ at the negative electrode, which is being supplied to the negative electrode by diffusion. At this point, a steady state is attained where the overcharge current is given by:

$$I = \frac{FAD([S^+]_0 - [S^+]_d)}{d} \quad (3-2)$$

Since the electron transport is fast compared to diffusion, the limiting conditions for the current exist at the negative electrode. In other words, it is assumed that [S⁺]_d is zero, so equation 3-2 becomes:

$$I = \frac{FAD([S^+]_0 - 0)}{d} \quad (3-3)$$

At the positive electrode, the electrode potential is governed by the Nerst equation:

$$V = V_+ + \frac{kT}{e} \ln \frac{[S^+]_0}{[S]_0} \quad (3-4)$$

where V is the electrode potential and V₊ is the first oxidation potential of the shuttle molecule. Using equation 3-1, the Nerst equation can be rewritten as:

$$V = V_+ + \frac{kt}{e} \ln \frac{[S^+]_0}{C - [S^+]_0} \quad (3-5)$$

and solving for [S⁺]₀ yields:

$$[S^+]_0 = C \frac{\left(\exp \left(\frac{V - V_+}{\frac{kT}{e}} \right) \right)}{\left(1 + \exp \left(\frac{V - V_+}{\frac{kT}{e}} \right) \right)} \quad (3-6)$$

so the current is then:

$$I = \left(\frac{FACD}{d} \right) \frac{\exp\left(\frac{V - V_+}{\frac{kT}{e}}\right)}{1 + \exp\left(\frac{V - V_+}{\frac{kT}{e}}\right)} \quad (3-7)$$

Equation 3-7 shows the relationship that exists between the overcharge current and the cell potential and that can be used to calculate the maximum current that can be carried by the shuttle molecules. This would occur at electrode potentials higher than the redox potential of the molecule where $(V - V_+) \gg (kT/e)$ and the maximum current the shuttle could carry (I_{\max}) would be defined as:

$$I_{\max} = \frac{FACD}{d} \quad (3-8)$$

3.2. Effect of Redox Potential

The choice of shuttles based on their redox potential is an important one. The redox potential should not be too high so that the shuttling process begins before any damage is caused to the cell, but should not be too low so that any self-discharge from the shuttle is minimized. This is important because even below the redox potential of the shuttle, there is a small amount of shuttle being oxidized and causing self discharge. The amount of oxidized shuttle present can be determined from the Nernst equation and the self-discharge current from the shuttle can be found from equation 3-7. Figure 3.3 shows a plot of I/I_{\max} as a function of cell potential.

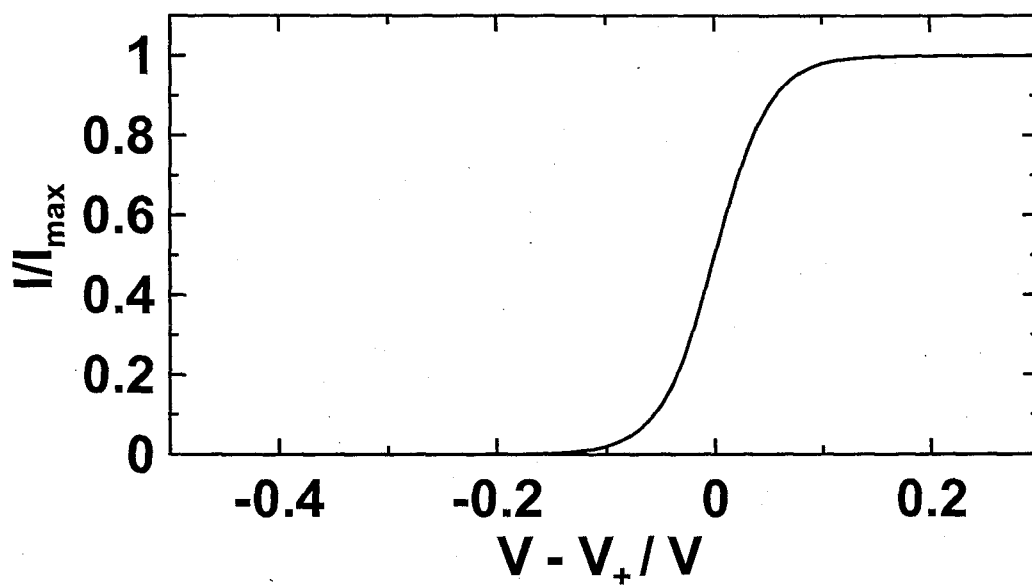


Figure 3.3: Shuttle current as a function of cell potential.

Figure 3.3 suggests that at potentials 0.2 V below the shuttle potential that there is no current associated with the shuttle. Figure 3.4 shows the function from Figure 3.3 plotted on a log scale.

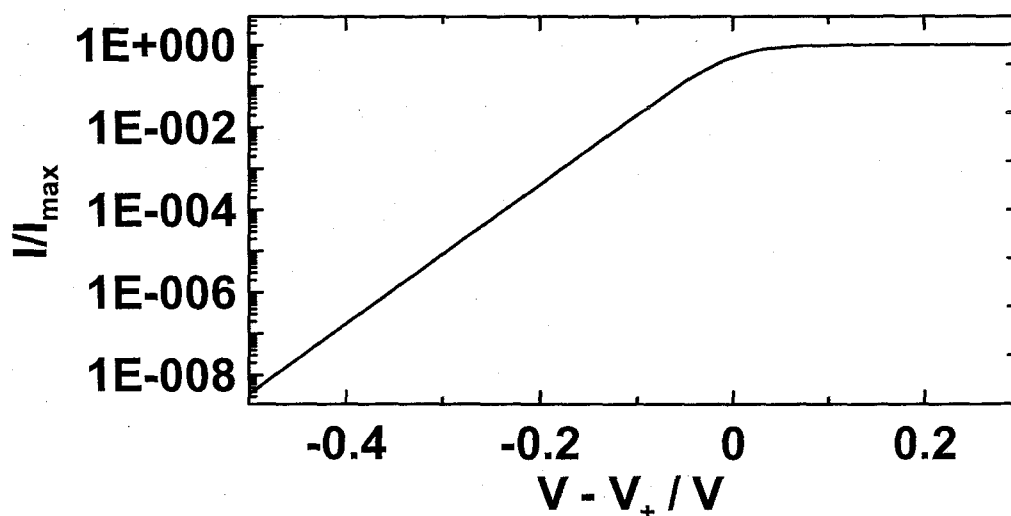


Figure 3.4: Shuttle current on a log scale as a function of cell potential.

Figure 3.4 shows that at -0.2 V there would be a self discharge current around $I/I_{\max} = 0.001$. If the maximum current corresponds to C rate (full charge in a time of one hour), then the shuttle would cause a cell whose positive electrode was 0.2 V below the shuttle's redox potential to completely discharge in 1000 hours. At potentials 0.3 V below the shuttle potential, a current of approximately $I/I_{\max} = 0.00001$ will flow within the cell, causing self-discharge. Again, if the maximum current is approximately C rate, then the self discharge from the shuttle will be $C/100000$, which would be much more acceptable. For this reason, the redox potentials of shuttles should be about 0.3 V above the potential of the positive electrode at the end of its charge.

3.3. Heat Generation

One underappreciated, but very important property involving redox shuttles inside cells, is the generation of heat. A first assumption is that the thermal conductivity within the cell is high enough that the temperature within the cell is uniform. During normal charging, the current passed through the cell is used to do work, namely increasing the electric potential energy of the cell. The temperature of the cell does not rise appreciably during normal charging. However, when the shuttle is carrying the current in the cell, the situation is very different. Heat is generated within the cell by the current carried by the shuttle during overcharge or overdischarge. All of the power passing through the cell generates heat [93]. This power is calculated as:

$$P = I \times V \quad (3-9)$$

In cells utilizing a lithium metal or graphite negative electrode, we can assume that V is very close to the shuttling potential V_+ . The heat within the cell will then be dissipated to the environment approximately according to Newton's law of cooling [92]:

$$P_{\text{out}} = A h (T_{\text{cell}} - 20^\circ\text{C}). \quad (3-10)$$

The thermal parameters of 18650 cells manufactured by E-One Moli Energy have been previously determined [94]. Parameters of interest are:

1. h - The surface heat transfer coefficient.

For a Moli 18650 cell, $h = 0.001354 \text{ W}/(\text{cm}^2 \text{ K})$

2. C_{cell} - The heat capacity of the cell.

For a Moli 18650 cell, $C_{\text{cell}} = 36.54 \text{ J}/(\text{K})$.

3. A - The surface area of the cell.

For a Moli 18650 cell, $A = 42 \text{ cm}^2$.

The rate of change of temperature with time is as follows:

$$dT/dt = [IV_+ - A h (T_{\text{cell}} - T_{\text{environ}})]/C_{\text{cell}}. \quad (3-11)$$

This can be solved numerically to predict the temperature of an 18650 cell in 20°C air during shuttle-protected overcharge. Figure 3.5 shows the temperature-time profiles during shuttling, assuming a 3.9V shuttle in an 18650 cell with a capacity of 2.4 Ah being charged at various C rates.

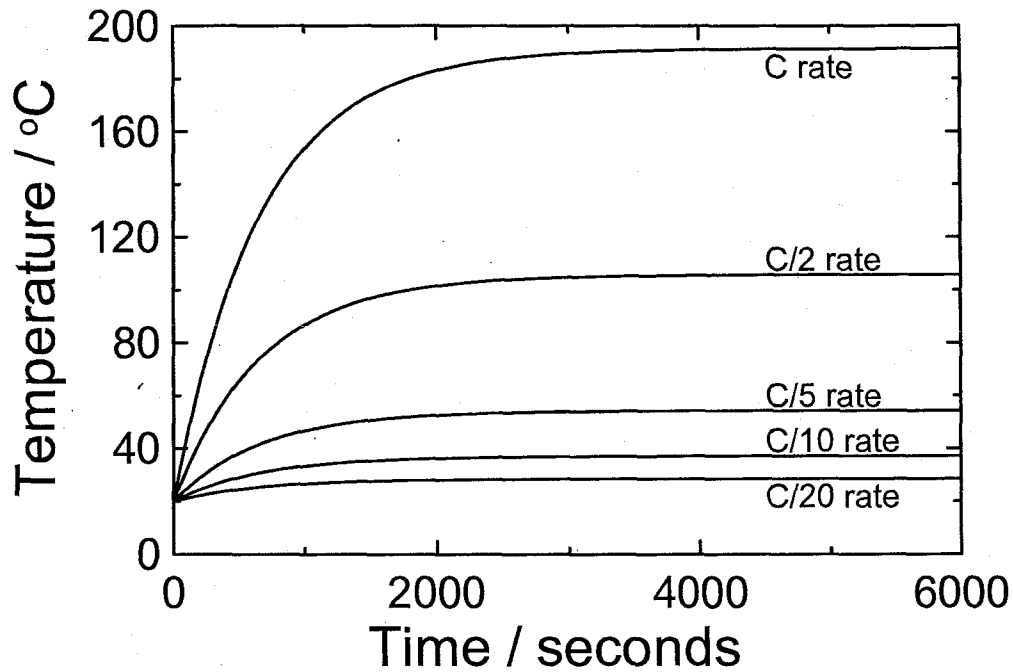


Figure 3.5: Calculated 18650 cell temperature during shuttle-protected overcharge at various rates of charge.

As shown, during shuttle-protected overcharge at C rate, the temperature of the cell increases to above 160 °C. This is one of the fundamental limitations of redox shuttles that will surely limit their use for extended periods of shuttle-protected overcharge at high rates. During overdischarge, the story is a little different. The potential difference between the positive electrode and the negative electrode during overdischarge is only about 0.4 V, assuming a LiFePO_4 positive and a 3.9 V shuttle. Figure 3.6 shows the temperature of a cell during shuttle-protected overdischarge.

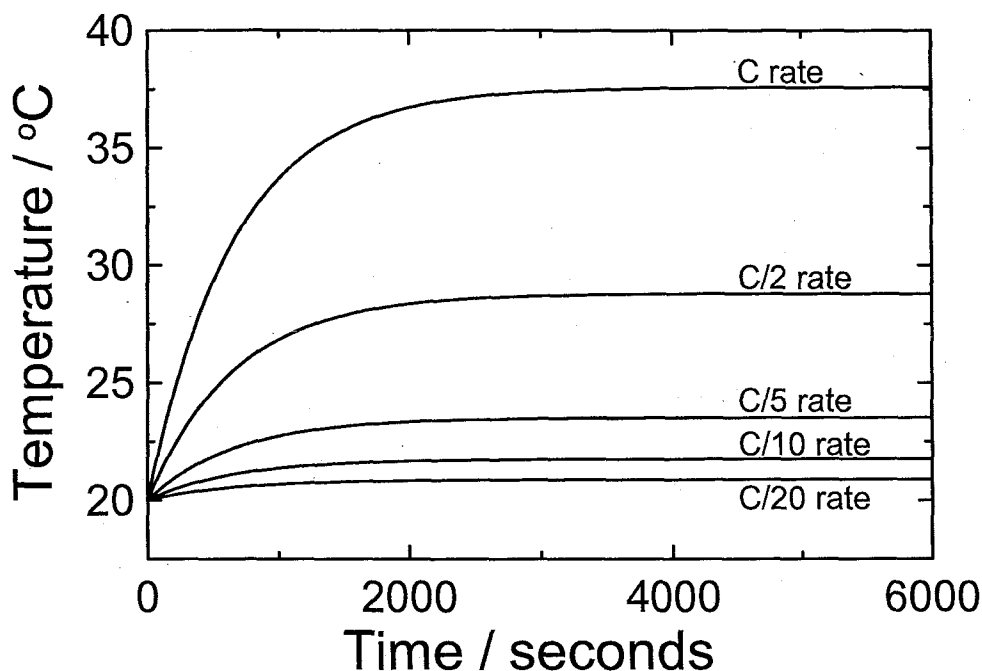


Figure 3.6: Calculated 18650 cell temperature during shuttle-protected overdischarge at various rates of discharge.

Even at C rate, the temperature of the cell stays below 40°C. This means that the shuttle would be an excellent method of overdischarge protection with cells that require moderate discharge rates.

It should also be mentioned that redox polymers also produce heat in a similar manner during overcharge, so this is not a significant advantage for one technology over the other.

3.4. Death of the Shuttle

Redox shuttles do not provide overcharge protection forever. Over time the protection from the shuttles disappears and the cell is no longer protected. The quality of shuttle molecules is directly related to the duration of protection they can provide. Better

shuttles give protection for a longer period of time. Figure 3.7 shows a brief overview of known shuttle overcharge protection longevity.

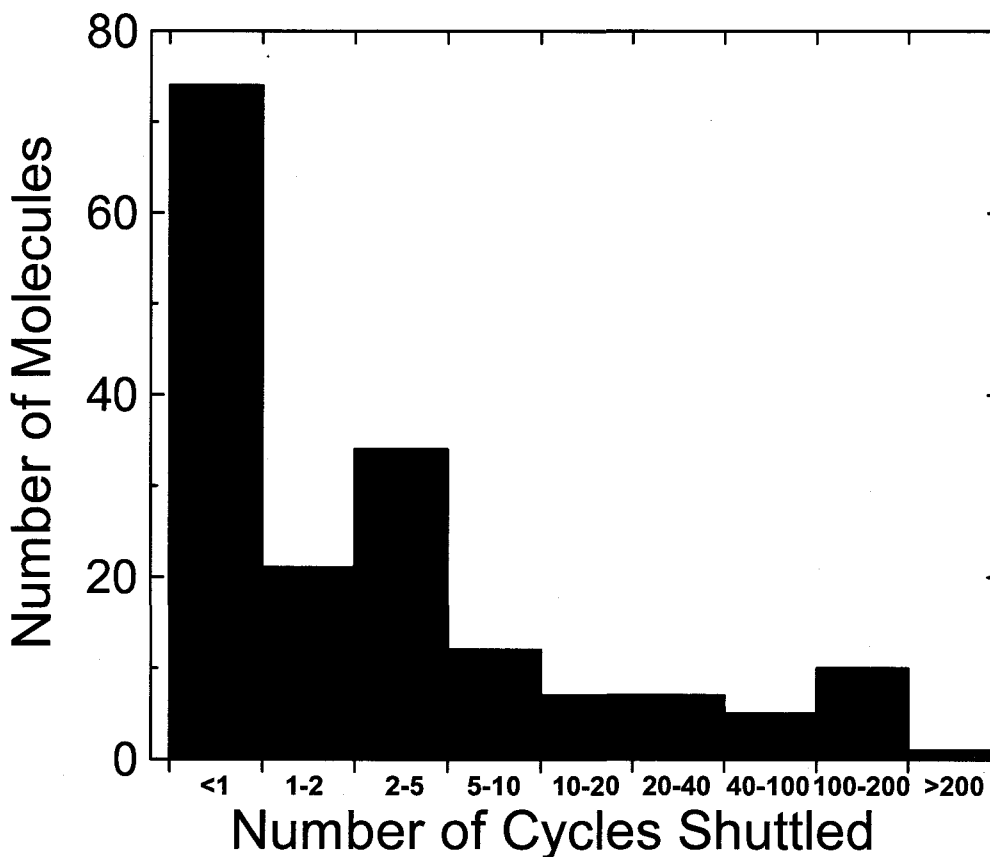


Figure 3.7: Histogram summarizing the duration of protection provided by shuttles found and reported as a function of the number cycles with 100% overcharge per cycle. Classes of molecules of special interest are shown in (■) for molecules similar to 2,5-di-*t*-butyl-1,4-dimethoxybenzene, (■) for various substituted TEMPO molecules and (■) for various substituted phenothiazines.

Figure 3.7 shows that there are very few known shuttles that are capable of providing substantial protection [95]. The three classes of molecules that provide overcharge protection for more than 100 cycles will be examined in the following chapters. The lifetime of the shuttle additive appears to be related to the stability of the radical cation formed upon oxidation. In the case of most shuttle candidate molecules, the protection

from the shuttle is quickly lost within the first cycle or two. In the case of many of the methoxybenzenes, this is reported to be due to irreversible polymerization of the radical cation [96]. The shuttle 2,5-ditertbutyl-1,4-dimethoxybenzene (DDB) apparently yields a stable radical cation upon oxidation. It is believed that when it is doubly oxidized, however, that it is irreversibly converted into the corresponding quinone [97]. This means that the loss of protection offered by DDB is directly related to the formation of the doubly oxidized species, S^{++} .

If one then assumes that the initial concentration of neutral shuttle C is the sum of the neutral shuttle, $[S]$, the singly oxidized shuttle, $[S^+]$, and the doubly oxidized shuttle, $[S^{++}]$, $[S]$ can be replaced in the Nernst equation to yield:

$$V = V_+ + \frac{kT}{e} \ln \frac{[S^+]}{C - [S^+] - [S^{++}]} \quad (3-12)$$

and $[S^+]$ can be solved for:

$$[S^+] = (C - [S^{++}]) \frac{\exp\left(\frac{V - V_+}{\frac{kT}{e}}\right)}{1 + \exp\left(\frac{V - V_+}{\frac{kT}{e}}\right)} \quad (3-13)$$

Similarly, the concentration of the doubly oxidized species $[S^{++}]$ can be calculated as a function of the starting shuttle concentration, C , the cell potential, V_{cell} , the first oxidation potential of the shuttle, V_+ , and the second oxidation potential of the shuttle, V_{++} by starting with the following form of the Nernst equation:

$$V = V_{++} + \frac{kT}{e} \ln \frac{[S^{++}]}{[S^+]} \quad (3-14)$$

Substituting $[S^+]$ as calculated from 3-13 yields $[S^{++}]$ in terms of the first and second oxidation potentials and the initial shuttle concentration in the cell.

$$[S^{++}] = C \frac{\left(\frac{\exp\left(\frac{V-V_+}{e}\right)}{1 + \exp\left(\frac{V-V_+}{e}\right)} \right) \exp\left(\frac{V-V_{++}}{e}\right)}{1 + \left(\frac{\exp\left(\frac{V-V_+}{e}\right)}{1 + \exp\left(\frac{V-V_+}{e}\right)} \right) \exp\left(\frac{V-V_{++}}{e}\right)} \quad (3-15)$$

Figure 3.8 shows the concentrations of $[S]$, $[S^+]$ and $[S^{++}]$ at various potentials with a variety of second oxidation potentials.

It is possible to calculate what the voltage profile should look like during continual constant-current shuttle-protected overcharge during the life of the shuttle. A constant current should indicate a constant $[S^+]$ at the surface of the positive electrode. The next assumption made is that the formation of the doubly oxidized shuttle is irreversible, that is:

$$\frac{dC}{dt} = -a[S^{++}] \quad (3-16)$$

where 'a' is an unknown rate constant.

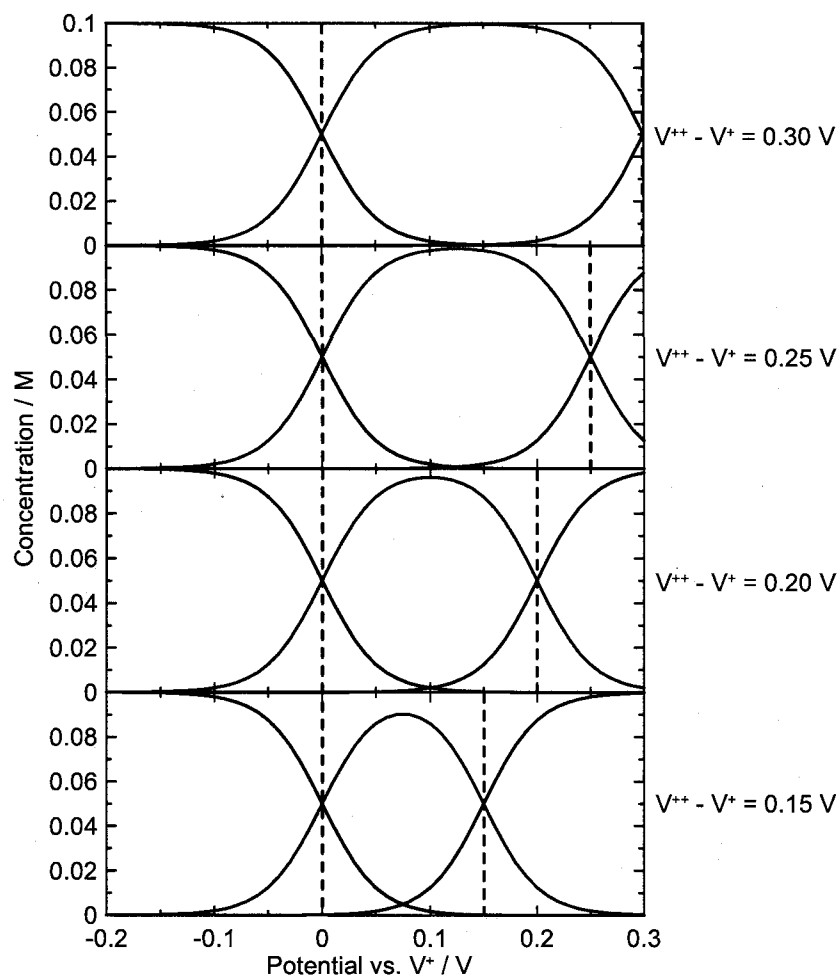


Figure 3.8 Concentration of S (—), S^+ (---) and S^{++} (···) at the positive electrode as a function of the positive electrode potential with a variety of second oxidation potentials.

This can be solved numerically in small increments of dt to get a new value for C which then yields a new value for $[S]$ and then a new potential. The equation can be solved iteratively to predict the voltage profile of a cell during continuous overcharge. Figure 3.9 shows the experimental results from a cell with LiFePO_4 and $\text{Li}_{4/3}\text{Ti}_5/3\text{O}_4$ electrodes, 0.2 M 2,5-di-*t*-butyl-1,4-dimethoxybenzene as the shuttle and 0.5 M LiPF_6 in PC:DEC as the electrolyte being continually overcharged at a $C/2$ rate. Figure 3.9 also shows the calculated voltage with time for a cell in shuttle-protected overcharge with $I/I_{\text{max}} = 0.5$

and the second oxidation potential being 0.2 V above the first oxidation potential. The experimental results appear to match the calculated results pretty well for the case of 2,5-di-*t*-butyl-1,4-dimethoxybenzene, as would be expected if the double oxidation is the cause of the shuttle death.

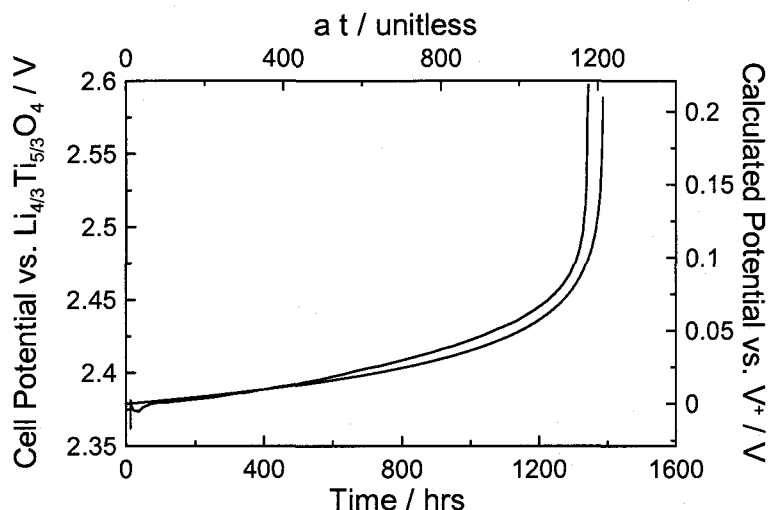


Figure 3.9: Calculated voltage profile (—) of a shuttle during a constant overcharge period and experimental results (---) for a cell in continuous overcharge with 2,5-ditertbutyl-1,4-dimethoxybenzene as the redox shuttle.

If the value of V_{++} were to be changed to be more than 0.2 V above V_+ , the overall shape of the curve remains unchanged, but the x-axis would be extended. That means that the increase in potential would occur more slowly. If V_{++} were to be closer to V_+ , the rise in potential would occur faster. This only serves to change the scale shown on the graph. Since the x-axis for the calculated value is scaled by an unknown rate constant, the effect of changing the separation between the first and second oxidation potential is only a matter of scaling the data to more closely match the experimental curve.

While it may be clear that the rate of the decay of the shuttle will increase with an increased potential, what might not be clear is the effect of the overcharge current on the death of the shuttle. Substituting equation 3-8 into equation 3-7 and solving for $V - V_+$ can reveal how the electrode potential is affected by the overcharge current:

$$V - V_+ = \frac{kT}{e} \ln \left(\frac{\frac{I}{I_{\max}}}{1 - \frac{I}{I_{\max}}} \right) \quad (3-17)$$

Equation 3-17 shows the dependence of the electrode potential during overcharge on the overcharge current applied. Figure 3.10 shows the effect of current on the electrode potential during overcharge. It shows that as the overcharge current is increased, the electrode potential is increased. This has an effect on the species present within the cell.

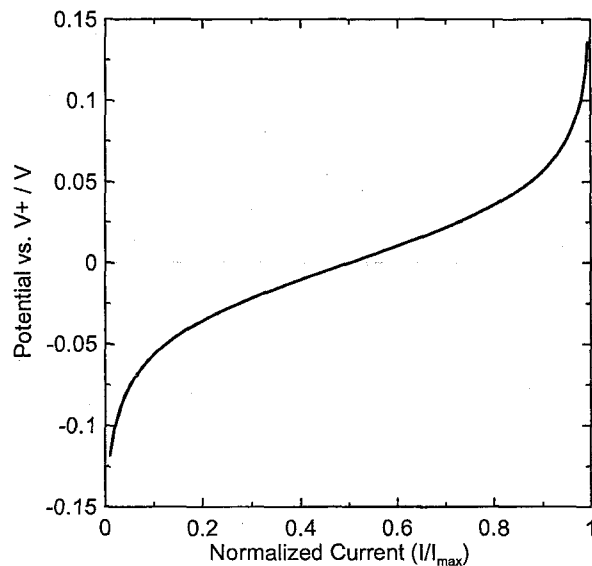


Figure 3.10 Positive electrode potential as a function of the overcharge current.

Figure 3.11 shows the effect of current on the formation of the doubly oxidized species. Figure 3.12 shows a \log_{10} plot of the curves shown in Figure 3.11 to make it easier to see how the line corresponding to $[S^{++}]$ behaves. While the concentration of

$[S^{++}]$ is much lower than $[S]$ or $[S^+]$, $[S^{++}]$ increases exponentially with the current. Since the rate of the shuttle decay is directly related to the formation of S^{++} , the lifetime of the shuttle depends strongly on the overcharge current.

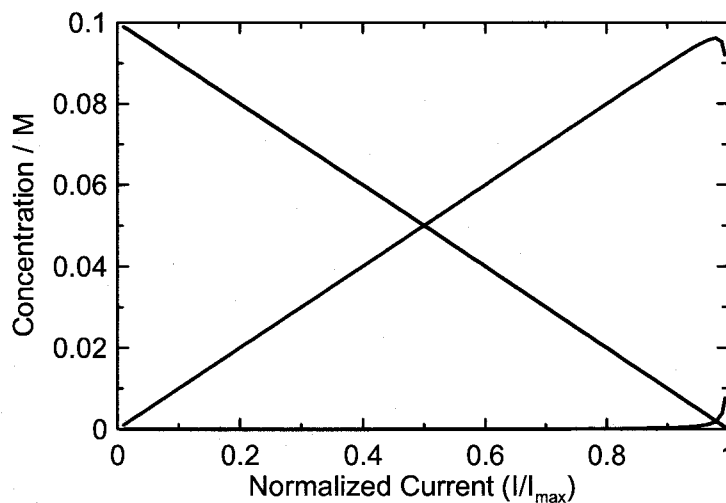


Figure 3.11 Concentration of S (—), S^+ (—) and S^{++} (—) at the positive electrode as a function of the overcharge current shown with the second oxidation potential 0.2 V above the first oxidation potential.

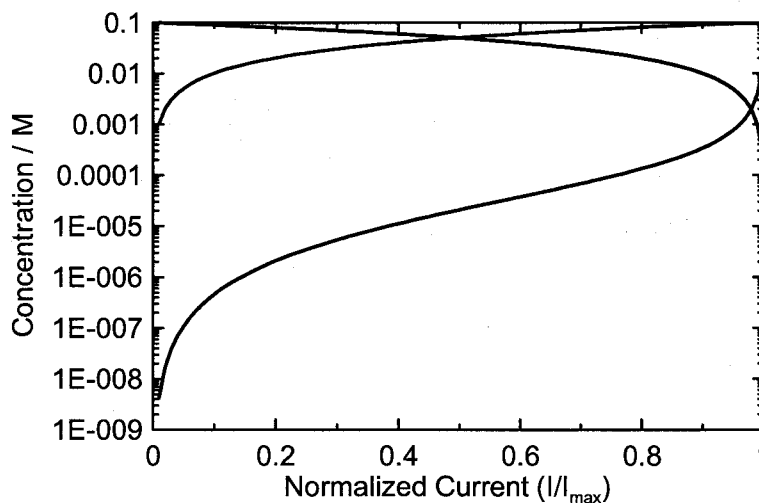


Figure 3.12 Concentration of S (—), S^+ (—) and S^{++} (—) on a \log_{10} scale at the positive electrode as a function of the overcharge current shown with the second oxidation potential 0.2 V above the first oxidation potential.

3.5. Summary

Now that the properties of redox shuttles have been discussed, it is possible to study the shuttle molecules themselves. The next two chapters will show results from a variety of shuttle molecules, with special interest given to the molecules that provide the longest duration of overcharge protection.

Chapter 4. Low V Shuttles

4.1. Substituted Benzenes

Several classes of molecules have been tested for chemical overcharge protection of lithium and lithium-ion batteries. In the 1980s and 1990s ferrocene and its derivatives were extensively examined because these molecules were known to have very reversible oxidations [82,98,99]. However, these molecules were unsuitable to be used as redox shuttles in lithium-ion batteries due to their low redox potentials. Halogenated aromatic molecules were examined by researchers at Sony as possible redox shuttles starting in the early 1990's [83,84,100]. Originally, it was claimed that aromatic molecules must contain at least one halogen to be successful as a shuttle [83]. To help understand the characteristics that make a good shuttle molecule, a set of aromatic molecules was studied with a variety of substituent groups to determine if any trends were apparent.

Screening procedures involved the testing of the each molecule directly in lithium-ion coin cells, not by cyclic voltammetry (CV) or other methods. The advantages of testing in lithium-ion coin cells are numerous. First, coin cells are hermetically sealed and suited for long-term testing. Second, the interelectrode spacing in a coin cell is about 25 μm , the thickness of a separator, so the shuttle molecule does not need to diffuse long distances. Third, the amount of electrolyte and hence redox shuttle in the cell is relatively small, and during a standard overcharge period (100% overcharge each cycle) each shuttle molecule must make the journey between electrodes many times. The number of oxidations per molecule of shuttle can be approximated by comparing the moles of

electrons during the overcharge to the moles of shuttle molecules present in the electrolyte between the electrodes.

$$\text{Moles of } S = C \times V = 1.3 \times 10^{-7} \text{ mol} \quad (4-1)$$

Where C is the initial shuttle concentration in the cell, 0.1 M, and V is the volume of electrolyte between the electrodes assuming that the volume of electrolyte is a cylinder with the cross sectional area equal to the area of a punched disc electrode, A , and a height equal to the separator thickness, d , and also factoring in the separator porosity, ϕ . The volume is then:

$$V = A \times d \times \phi = (1.3 \text{ cm}^2)(25\mu\text{m})(0.4) = 1.3 \times 10^{-6} \text{ L} \quad (4-2)$$

The moles of charge passed during overcharge can be calculated by:

$$\text{Moles of Charge} = \text{Capacity} / F = 3.7 \times 10^{-5} \text{ mol} \quad (4-3)$$

where the nominal capacity of a coin cell is 1 mA hr and F is Faraday's constant. During a single cycle of 100% overcharge, there is nearly 300 times more current flowing than there are shuttle molecules to carry the current, so on average, each shuttle molecule must be oxidized and reduced 300 times during each overcharge cycle.

This brings up the answer to another commonly asked question, is it really shuttling that is carrying the current or simply electrolyte decomposition? First, the solvent is assumed to be pure EC. EC was chosen since it has the lowest molecular weight of the solvents used so the number of moles of solvent present will be maximized. EC has a molecular weight of 88.06 g/mol and a density of 1.321 g/mL. Using the volume calculated from equation 4-2, the number of moles of EC present between the

electrodes is 2.4×10^{-8} mol. This value is almost 1000 times less than the number of electrons passed in a single cycle of 100% overcharge, so any shuttle molecule that shows more than a single cycle of overcharge protection must be demonstrating shuttling, and not simply decomposing electrolyte.

There are disadvantages to using coin cells instead of three-electrode cells. First, there is no reference electrode in the coin cell. This is a minor problem since the potentials of the electrodes used are well known, so the redox potential of the shuttle can still be estimated to ± 0.1 V. Figure 4.1 shows the potential vs specific capacity for the first two cycles of $\text{Li}_{4/3}\text{Ti}_{5/3}\text{O}_4/\text{Li}$ and $\text{LiFePO}_4/\text{Li}$ coin cells. In these cells, lithium foil acts as a counter and reference electrode. The potentials of the plateaus for $\text{Li}_{4/3}\text{Ti}_{5/3}\text{O}_4$ and LiFePO_4 are near 1.55 and 3.45 V, respectively. Using these electrodes in a lithium-ion coin cell leads to an open-circuit plateau potential of about 1.90 V. By contrast, if graphite is used as the negative electrode, then the LiFePO_4 -based Li-ion coin cell has a plateau potential near 3.35 V since graphite has the bulk of its capacity near 0.1 V. It is also important that the effects of cell polarization be minimized during such measurements so charging and discharging occurred at a relatively slow C/10 rate. CV would allow the exact determination of the redox potential in cases where the shuttle molecule is stable, but the redox potential need not be determined so accurately for practical applications. Second, CV under controlled conditions allows the determination of the diffusion coefficient of the shuttle molecule. Although this is a useful parameter to know, the stability of the shuttle is far more important for determining whether or not a molecule would be useful as a shuttle.

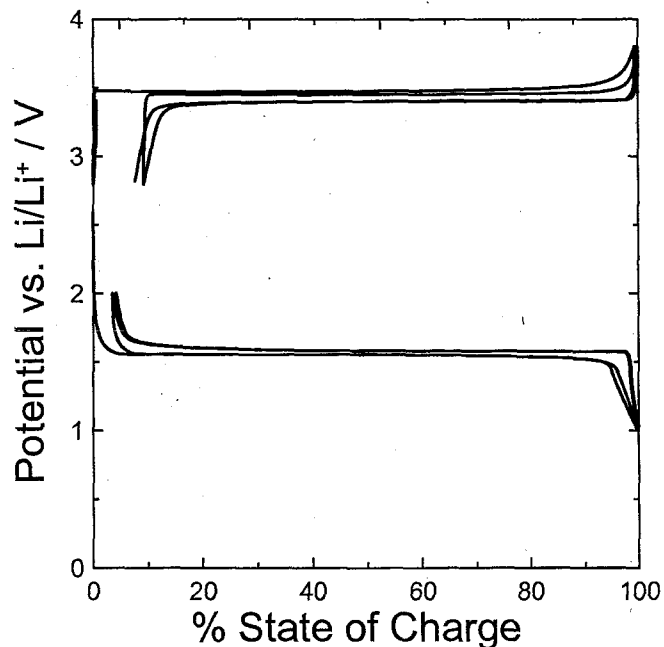


Figure 4.1 First 2 cycles for $\text{LiFePO}_4/\text{Li}$ and $\text{Li}_{4/3}\text{Ti}_{5/3}\text{O}_4/\text{Li}$ half cells.

The shuttle molecules were obtained from Aldrich Chemical Co., Fluka, Fisher Scientific, and SALOR, among others and were used without further purification. Possible impurities in the shuttle molecules may be a cause for concern because it is possible that redox behaviour might come from an impurity rather than the molecule of interest or that the impurities may have detrimental effects on the electrode materials or on the shuttle lifetime. Any impurities present at less than 1% would have concentrations of 0.001 M or less in the electrolyte, if these had diffusion coefficients similar to the shuttle molecules, then they could support a maximum shuttle current density in a coin cell of 0.02 mA/cm^2 [93]. The current densities in experiments were near 0.1 mA/cm^2 so it is unlikely that observed shuttle redox potentials could be due to any impurity molecules. Second, although lithium-ion cells are intolerant to some impurities like HF, they are remarkably tolerant to other impurities like benzene and toluene [101,102].

There is no reason to believe that a small amount of an aromatic impurity would be detrimental to the performance of our test cells. Finally, when the shuttle molecules "die" and the shuttle effect is no longer observed, the LiFePO_4 -based lithium-ion cells generally continue to charge and discharge normally, simply without the shuttle-protected overcharge. Therefore, although it would be preferable to use highly purified reagents, the results of this work using "as-received" reagents are still valuable and most likely reliable. Cells were charged using currents corresponding to a normal recharge in 10 h ($C/10$ rate), and cells were charged to 200% of their normal charge capacity (100% overcharge) or until a specified upper cutoff potential (normally 4.9 V vs Li/Li^+) was reached, whichever occurred first.

Figure 4.2 shows the results of typical shuttle screening tests. Figure 4.2 shows the cell potential vs time as a $\text{LiFePO}_4/\text{Li}_{4/3}\text{Ti}_{5/3}\text{O}_4$ and a $\text{LiFePO}_4/\text{MCMB}$ coin cell is charged and discharged. The cell contains a shuttle additive that operates near 3.90 V vs Li/Li^+ . This can be inferred by adding 1.55 V (the potential of the $\text{Li}_{4/3}\text{Ti}_{5/3}\text{O}_4$ negative electrode with respect to Li/Li^+) to the 2.35 V plateau measured while the shuttle is active in the $\text{LiFePO}_4/\text{Li}_{4/3}\text{Ti}_{5/3}\text{O}_4$ cell or by reading the potential of the plateau in the $\text{LiFePO}_4/\text{MCMB}$ cell. The shuttle plateau potential can be measured directly from this graph, because the graphite electrode nears 0 V vs Li/Li^+ when the cell is fully charged. Estimates for the redox potential of the shuttle molecule could be made using either type of coin cell and these can be compared for consistency. The addition and operation of the shuttle molecule does not normally affect the normal charge and discharge capacity of the cells, and this is a quality a useful shuttle molecule must have.

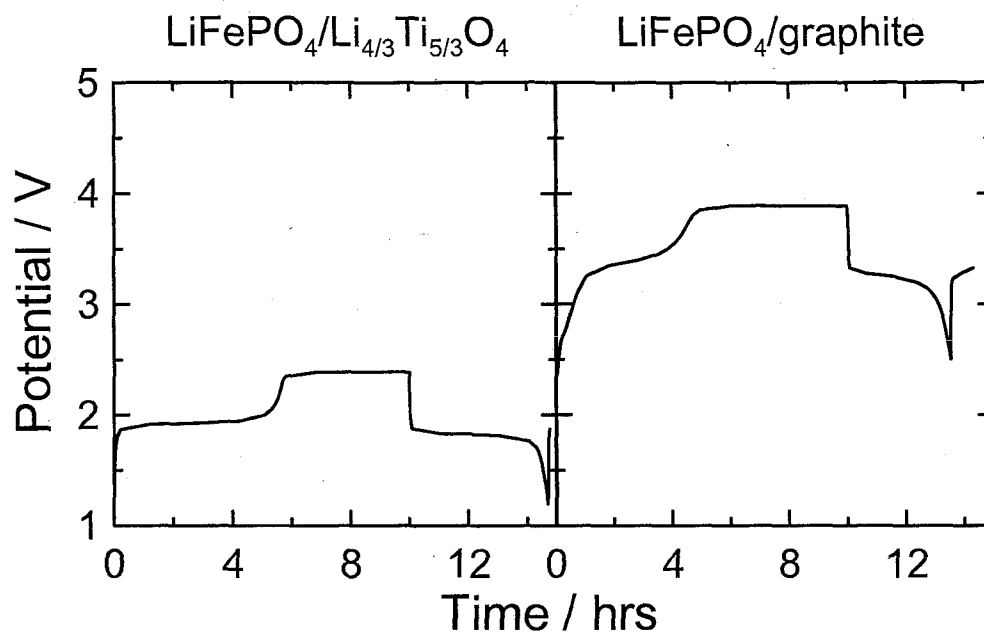


Figure 4.2 First cycle for $\text{LiFePO}_4/\text{Li}_{4/3}\text{Ti}_{5/3}\text{O}_4$ and $\text{LiFePO}_4/\text{MCMB}$ coin cells containing the shuttle 2,5-di-*t*-butyl-1,4-dimethoxybenzene.

Table 4-1 lists results for a variety of substituted benzene molecules that were tested. The molecular name, the molecular structure, the redox potential measured in coin cell experiments, and the number of cycles of shuttle-protected overcharge are listed in the remaining columns, respectively. Some of the results collected suggest that second and third ionizations of shuttle molecules were observed. The analysis of the first cycle of coin cells containing 1,4- and 1,2-dimethoxybenzene and 1,3,5-trimethoxybenzene suggests the presence of a second oxidation and for 1,3,5-trimethoxybenzene, there is a third ionization step. The potentials of these higher oxidation steps are noted in Table 4-1. The number of cycles of overcharge protection represents the maximum number seen for each molecule in $\text{LiFePO}_4/\text{Li}_{4/3}\text{Ti}_{5/3}\text{O}_4$ or $\text{LiFePO}_4/\text{MCMB}$ coin cells.

Table 4-1 List of tested substituted benzene molecules, their shuttle potentials and number of cycles of 100% overcharge protection measured in LiFePO₄-based coin cells.

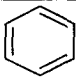
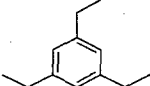
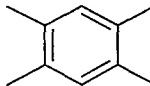
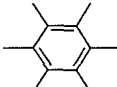
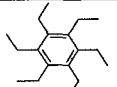
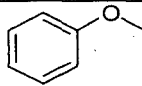
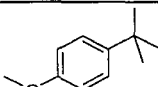
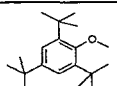
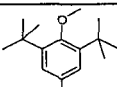
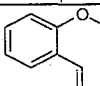
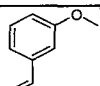
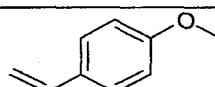
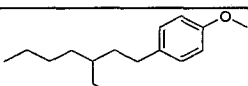
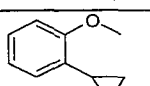
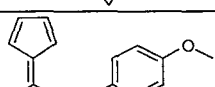
Name	Structure	Shuttle Potential vs Li/Li ⁺ / V	Cycles of Overcharge Protection
benzene		4.8	2
1,3,5-triethylbenzene		4.3	1
1,2,4,5-tetramethylbenzene		4.3	1
hexamethylbenzene		4.2	7
hexaethylbenzene		4.3	1
anisole		4.2	33
4-t-butyl-1-methoxybenzene		4.15	4
1,3,5-tri- <i>t</i> -butyl-2-methoxy-benzene		4.4	3
1,3-di- <i>t</i> -butyl-2-methoxy-5-methylbenzene		3.7, 4.2	3
2-ethynylanisole		4	2
3-ethynylanisole		4.2	1
4-ethynylanisole		4.0, 4.3	1
4-[(2-ethyl)hexyl]oxy]anisole		4	1
1-cyclopropyl-2-methoxybenzene		4.1	1
1-(3-(2,4-cyclopentadien-1-ylidene)-1-butenyl)-4-methoxybenzene		4	2

Table 4-1 continued from previous page.

Name	Structure	Shuttle Potential vs Li/Li ⁺ / V	Cycles of Overcharge Protection
2-bromoanisole		4.35	12
3-bromoanisole		4.2	2
4-bromoanisole		4.4	1
2,4,6-tribromoanisole		4.8	1
2,5-dichloroanisole		4.6	1
2,4,6-trichloroanisole		4.8	6
5- <i>t</i> -butyl-1,3-dinitro-2-methoxybenzene		4.9	2
2-bromo-4-fluoroanisole		4.7	1
3-methoxybenzylbromide		—	0
3-methoxycatechol		—	0
dimethyl-4-methoxyphthalate		4.7	6
1-(Ethoxycarbonyloxy)imino)methyl-4-methoxybenzene		4	1
2,4-di(<i>t</i> -pentyl)phenyl-L3-acetamido-4-methoxybenzene sulfonate		4.35	4
3-amino-N-dodecyl-4-methoxybenzulfonamide		4	1
2- <i>t</i> -butyl-4,6-dinitro-5-methylanisole		—	0

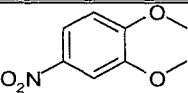
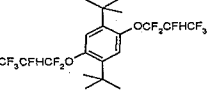
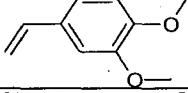
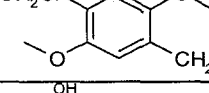
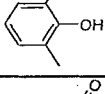
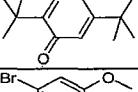
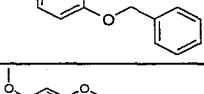
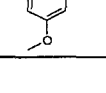
Table 4-1 continued from previous page.

Name	Structure	Shuttle Potential vs Li/Li ⁺ / V	Cycles of Overcharge Protection
3- <i>t</i> -butyl-4-methoxybenzonitrile		4.7	1
3- <i>t</i> -butyl-4-methoxybenzaldehyde		4.4	2
dimethyl-5-methoxy isophthalate		4.7	4
1,2-dimethoxybenzene		4	2
1,4-dimethoxybenzene		3.9, 4.1	1
1,4-diethoxybenzene		3.95	2
2,3-dimethoxytoluene		4.05	3
3,4-dimethoxytoluene		4.1	15
2,5-dimethyl-1,4-dimethoxybenzene		3.85	13
2-ethoxyanisole		4.0, 4.7	2
1,4-dimethoxy-2,3,5-trimethylbenzene		4	3
2,3,5,6-tetramethyl-1,4-dimethoxybenzene		4.1	16
2- <i>t</i> -butyl-1,4-dimethoxybenzene		4	30
4- <i>t</i> -butyl-1,2-dimethoxybenzene		4.2	9
2,5-di- <i>t</i> -butyl-1,4-dimethoxybenzene		3.92	363

Table 4-1 continued from previous page.

Name	Structure	Shuttle Potential vs Li/Li ⁺ / V	Cycles of Overcharge Protection
2,5-di- <i>t</i> -butyl-1,4-diethoxybenzene		3.9, 4.3	48
2,5-di- <i>t</i> -butyl-1,4-bis(trimethylsilyl)benzene		4.8	1
2,5-di- <i>t</i> -butyl-1,4-bis(2,2,2-trifluoroethoxy)benzene		4.3	170
2,5-di- <i>t</i> -butyl-1,4-di(tri- <i>i</i> -propylsiloxy)benzene		3.9	1
3,5-di- <i>t</i> -butyl-1,2-dimethoxybenzene		4.1	10
4-bromo-1,2-dimethoxybenzene		4.1	3
2-bromo-1,3-dimethoxybenzene		4.1	6
4-fluoro-1,2-dimethoxybenzene		4.1	18
2,4-dibromo-1,3-dimethoxybenzene		4.3	2
1,2,3,4-tetrabromo-5,6-dimethoxybenzene		4.7	1
1,2,4,5-tetrabromo-3,6-dimethoxybenzene		4.8	1
1,2,4,5-tetrafluoro-3,6-dimethoxybenzene		4.6	4
1,2,4,5-tetrafluoro-3,6-diethoxybenzene		4.6	25
1,2,4,5-tetrafluoro-3,6-di- <i>t</i> -butoxybenzene		4.3	8
hexadecyloxy-4-methoxybenzene		4.1	1

Table 4-1 continued from previous page.

Name	Structure	Shuttle Potential vs Li/Li ⁺ / V	Cycles of Overcharge Protection
1,2-dimethoxy-4-nitrobenzene		4.5	2
2,5-di- <i>t</i> -butyl-1,4-bis(hexafluoropropyl)benzene		4.8	6
4-allyl-1,2-dimethoxybenzene		3.9	2
2,5-bis(chloromethyl)-1,4-dimethoxybenzene		3.8, 4.2	1
3-methyl-1,2-benzenediol		3.9	1
2,6-di- <i>t</i> -butyl-1,4-benzoquinone		4.1	9
1-(benzyloxy)-4-bromo-2-methoxybenzene		4.2	5
1,3,5-trimethoxybenzene		3.8, 4.5, 4.8	1

Several of these molecules have oxidation potentials reported in the literature. In many cases, there are differences between reported oxidation potentials and those measured in coin cells. The differences, when observed, between the measured redox potentials observed in coin cells and literature values can be explained as follows. For a reversible redox system, such as the molecule 2,5-di-*t*-butyl-1,4-dimethoxybenzene (DDB), the difference between the onset potential and the half-wave potential in nonaqueous electrolyte is on the order of 0.1 V. Figure 4.3 shows a CV of the first oxidation of DDB. The half-wave potential is about 3.9 V in Figure 4.3(a), which agrees well with the potential obtained from the coin cell, 3.92 V listed in Table 4-1. In cases

where the oxidized shuttle molecule is not stable for long time periods, the onset potential, which is very close to that measured by the coin cell experiment, and the half-wave potential can be significantly different. Figure 4.3(b) shows the CV for the molecule 1,4-dimethoxybenzene. In this case, the coin cell experiment measures 3.9 V, which agrees well with the onset potential in Fig. 3(b), not with the half-wave potential. By contrast, the literature values in acetonitrile [103,104] agree closer with the half-wave potential we measure by CV than with the onset potential. The CV in Figure 4.3(b) is not characteristic of a reversible process (it is far too broad), and hence the half-wave potential cannot be taken reliably as a measure of the redox potential. Much of the literature reports half-wave potentials without showing the original CV data, and in cases where the molecules do not show significant stability, these values may be unreliable. Finally, much of the literature data has been collected in different solvents and with different supporting electrolytes, which would cause shifts in the measured potentials [105].

The influence of some substituent groups on the redox potential can be extracted from Table 4-1. Methoxy groups decrease the redox potential because they donate electron density to the ring and therefore stabilize the radical cation (+M effect). Groups with an electron-withdrawing effect (-I effect), such as halogens, increase the redox potential.

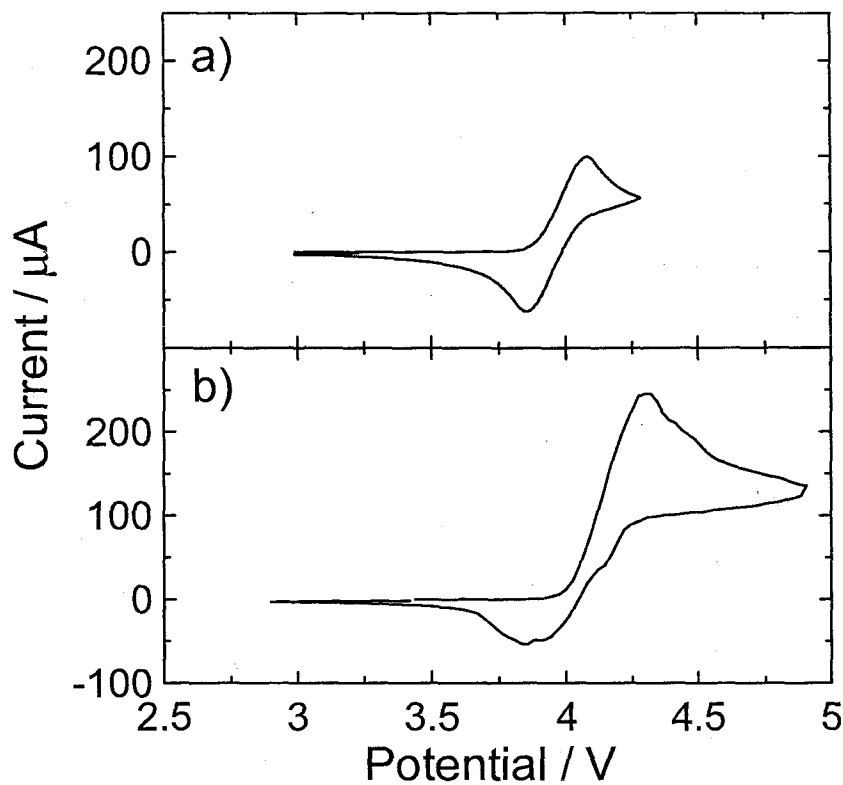


Figure 4.3 CV's of a) 2,5-di-*t*-butyl-1,4-dimethoxybenzene and b) 1,4-dimethoxybenzene.

Figure 4.4 summarizes the redox potentials of molecules containing alkyl groups and molecules containing halogens. The position of the group has not been specified in the Figure because it plays a minor role on the redox potential. The redox potential of benzene is high because of the lack of groups able to donate electron density to the aromatic ring. The introduction of an alkyl group decreases the redox potential by comparison to the bare benzene molecule.

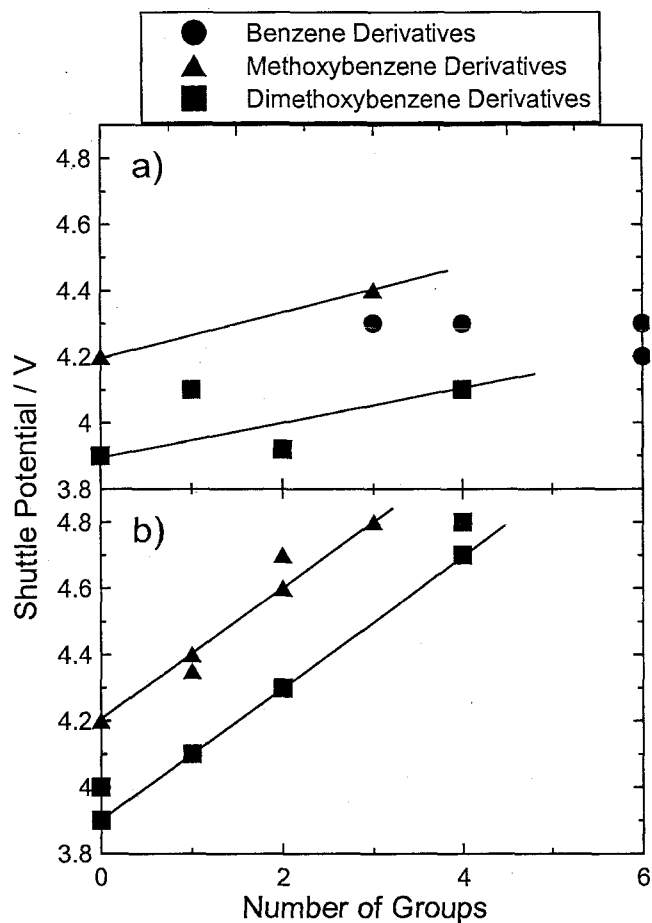


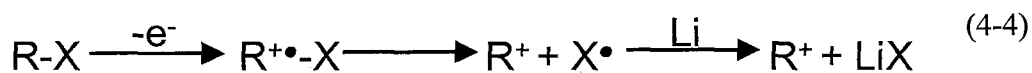
Figure 4.4 Potential vs number of a) substituted alkyl groups and b) substituted halogens for a variety of molecules.

Looking at the redox potentials of the halogenated molecules, it can easily be seen that there is an increase in the redox potential with the number of halogens, regardless of type (e.g., F, Cl, or Br) or substitution pattern. With each halogen attached to the benzene ring, the redox potential is raised by about 0.2 V. Table 4-2 shows the estimated influence of various substituent groups attached to the aromatic ring on the redox potential. Groups such as $-\text{NO}_2$, $-\text{COOCH}_3$, and halogens have a strong electron-withdrawing effect ($-\text{I}$ effect) and increase the overall redox potential. Groups with an electron-donating effect decrease the redox potential.

Table 4-2 Effect of substituent groups on the redox potential of substituted benzene shuttle molecules.

Δ per group / V		Δ per group / V	
Alkyl	0.05	-OCH ₂ CH ₃	-0.1
<i>t</i> -butyl	0.0 - 0.1	-OCH ₃	-0.2
Halogen	0.2	-OH	-0.2
-CH=CH ₂	0.1	-COOCH ₃	0.25
Conjugated π system	as much as -0.8	-CHO	0.1
		-COCH ₃	0.2

For most of the tested molecules, the cycling stability was poor and the shuttle effect lasted only a few cycles. However, there are a few molecules that showed better cycling stability. Figure 4.5 shows coin cell results for anisole, which is a simple molecule with no additional groups to protect the oxidized molecules from possible dimerization leading to polymerization [106]; however, it shows shuttle protected overcharge for 33 cycles. The introduction of 3 bulky *t*-butyl groups does not significantly increase the shuttle stability. 1,3,5-tri-*t*-butyl-2-methoxybenzene shows a shuttle effect for only three overcharge cycles. Another simple molecule, 2-bromoanisole, has a higher cycling stability (12 cycles) than all the other halogenated molecules tested. Figure 4.6 shows the 12 successful overcharge cycles for this molecule. This low stability shown by all tested halogenated molecules is likely due to reactions involving lithium at the negative electrode. For example:



where X is a halogen, and R-X is a halogenated aromatic shuttle molecule. The oxidation step would occur at the fully charged positive electrode, and the reaction with lithium

would occur at the surface of the fully charged negative electrode. The presence of such a reaction pathway may lead to the death of the shuttle.

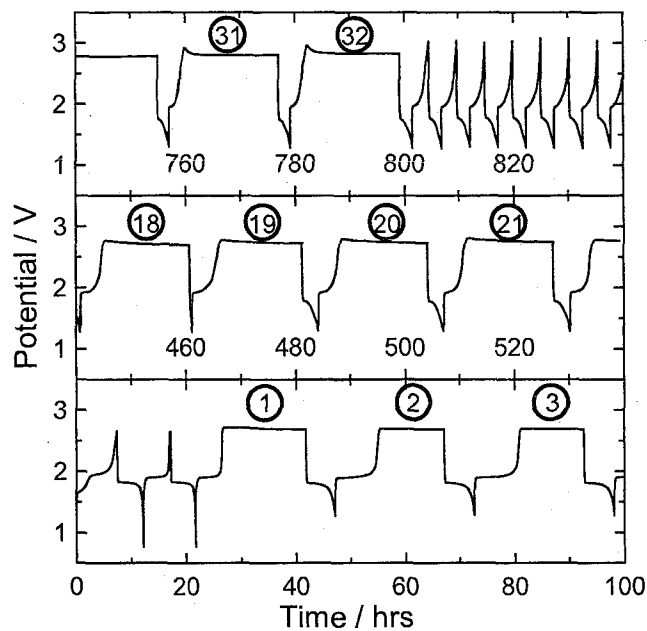


Figure 4.5 Cycling data for a $\text{LiFePO}_4/\text{Li}_{4/3}\text{Ti}_{5/3}\text{O}_4$ coin cell containing 0.1 M anisole. Cycle numbers are shown.

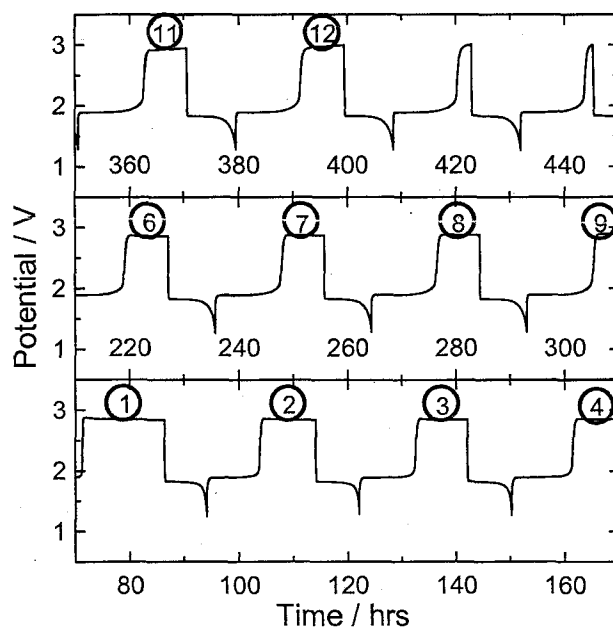


Figure 4.6 Cycling data for a $\text{LiFePO}_4/\text{Li}_{4/3}\text{Ti}_{5/3}\text{O}_4$ coin cell containing 0.1 M 2-bromoanisole. Cycle numbers are shown.

DDB shows excellent cycling stability. Over 300 overcharges at 100% overcharge each cycle have been achieved at C/10 rate. Figure 4.7 shows the excellent stability of the shuttle effect displayed by this molecule. The molecule has two *t*-butyl groups which provide steric bulk and serve to protect the aromatic ring from reactions with other molecules in the electrolyte. 2,3,5,6-tetramethyl-1,4-dimethoxybenzene has no free H-atoms attached to the aromatic ring and is therefore protected from reactions between the aromatic ring and other molecules, but it shows effective shuttle activity for only 16 cycles, so it is not only the presence of aromatic hydrogens that has an impact on the stability of a shuttle molecule. The presence of hydrogens bonded to the aromatic ring may reduce the stability of aromatic molecules as shuttles since protons are an excellent leaving group. Because of this, it is important to have no aromatic hydrogens or to protect the hydrogens with other neighboring groups.

The stability of a radical cation is decreased by the introduction of α -H atoms, that is hydrogens bonded to the carbon bonded to the aromatic ring, such as the hydrogens on a methyl group. For molecules with α -H's the radical cation can be stabilized by the cleavage of the C-H $^{\alpha}$ bond. The *t*-butyl group contains no α -hydrogens, which may be one reason why the *t*-butyl group affords more stability to a molecule than a methyl or an ethyl group would in the same position.

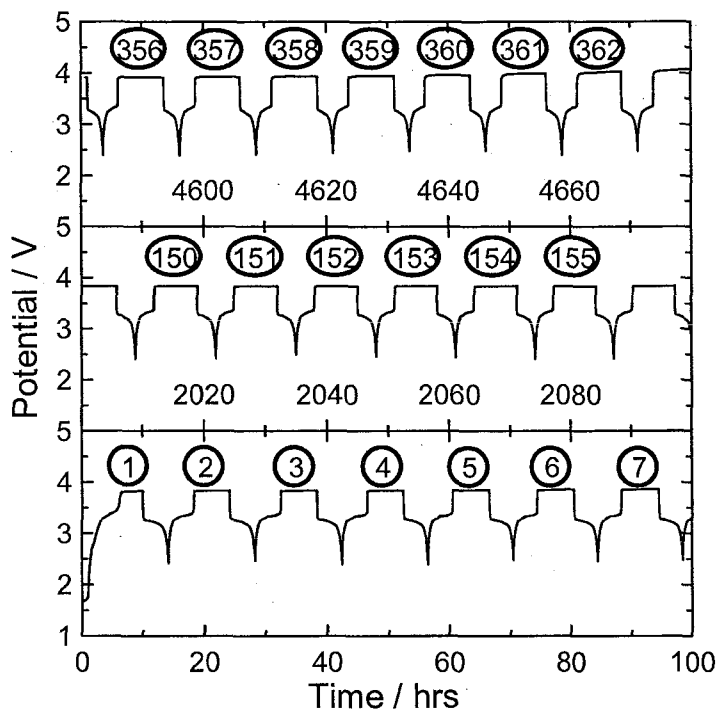


Figure 4.7 Cycling data for a $\text{LiFePO}_4/\text{MCMB}$ coin cell containing 0.1 M 2,5-di-*t*-butyl-1,4-dimethoxybenzene. Cycle numbers are shown.

The molecule 2,5-di-*t*-butyl-1,4-dimethoxybenzene is an excellent molecule for overcharge protection, while 1,3,5-tri-*t*-butyl-2-methoxybenzene, a very similar molecule, shows far fewer cycles of overcharge protection. Both molecules contain only *t*-butyl and methoxy groups and have no α -hydrogens. The main difference in these two molecules is their structure. The presence of an unsubstituted aromatic carbon next to the methoxy groups allows the methoxy groups in 2,5-di-*t*-butyl-1,4-dimethoxybenzene to be in plane with the aromatic ring, which is a more energetically favourable position compared to being out of plane since it allows for orbital overlap between the oxygen and the π -system of the ring [107]. The bulky *t*-butyl groups on both sides of the methoxy group of 1,3,5-tri-*tert*-butyl-2-methoxybenzene prevent the methoxy group from being in plane with the ring, destabilizing the molecule. Figure 4.8 shows the differences in

structure of these molecules as well as the calculated regions of electron density for the lowest unoccupied molecular orbital (LUMO) of the molecule in the oxidized form. Results from calculations are described in more detail in Chapter 6. The energetically preferred orientation of the methoxy and *t*-butyl groups in 2,5-di-*t*-butyl-1,4-dimethoxybenzene leads to protection of the adjacent position. In 1,3,5-tri-*t*-butyl-2-methoxybenzene, for example, the methoxy group is sterically forced into an out-of-plane configuration, which is energetically less preferred and so would be expected to be a less stable shuttle molecule, which is the case. The molecules 1,4-dimethoxybenzene and 1,2-dimethoxybenzene do not show good shuttle stability presumably because they are not sterically protected at all.

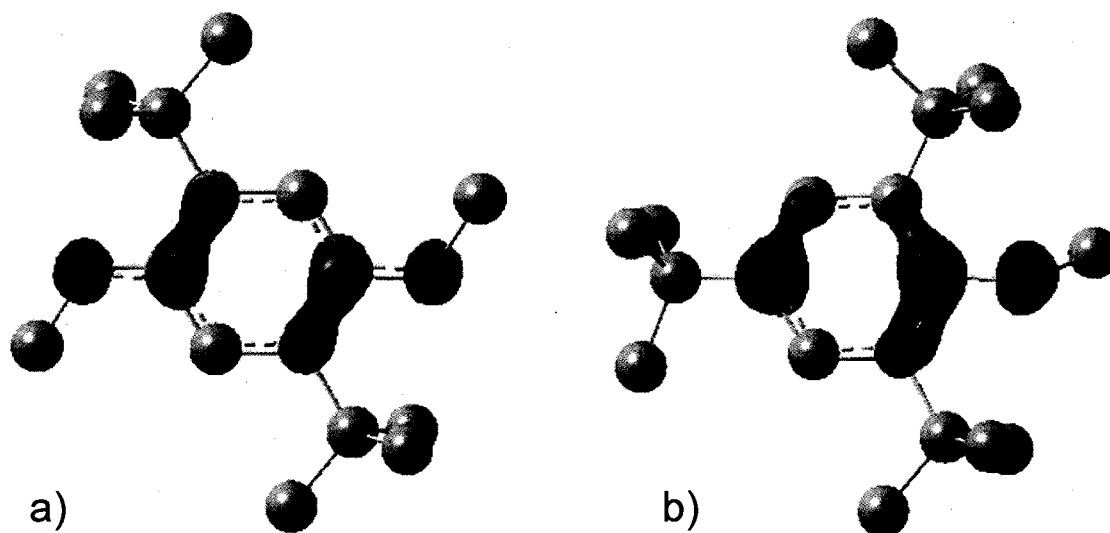


Figure 4.8 Structure and regions of electron density for the molecules a) 2,5-di-*t*-butyl-1,4-dimethoxybenzene and b) 1,3,5-tri-*t*-butyl-2-methoxybenzene.

The results give a good overview of the influence of substituent groups attached to the aromatic ring on the redox potential. Some understanding of why certain molecules behave as stable shuttles and why others do not was also obtained. DDB appears to show

uniquely high stability as a shuttle molecule because of the type of substituent groups on the molecule, their placement and the symmetry of the molecule.

The screening of a whole variety of aromatic molecules has led to some understanding of the qualities a stable shuttle molecule should have. These include a high solubility of the molecule and redox potential of the molecule as well as the stability of the shuttle. The solubility of the shuttle in the polar solvents used as electrolytes can be important to consider, more polar molecules should be soluble to higher concentrations. The redox potential of the shuttle molecules can be affected by the presence of a variety of substituent groups; electron donating groups lower the redox potential while electron withdrawing groups raise it.

When it comes to shuttle stability, a few trends can be observed. Aromatic molecules with hydrogens on the aromatic ring are susceptible to a variety of reactions so it is usually beneficial to shuttle stability to replace these hydrogens with other groups or to have sterically bulky groups nearby. Molecules with an alcohol group (-OH) do very poorly as alcohols tend to have reactions with lithium that are similar to those seen between water and lithium. Aromatic molecules containing halogens can undergo reactions which result in loss of the original shuttle molecule. Molecules with substituent groups that contain α -hydrogens also do not do well as shuttle molecules. This means that groups such as the methyl (-CH₃) or ethyl groups (-CH₂CH₃) are not expected to be as stable as molecules with a *t*-butyl group. Groups that seem to improve shuttle performance include those that help delocalize the radical cation and those that provide steric bulk to the other possible reaction sites. Examples of these groups are the alkoxy group (-OR) and the *t*-butyl group. One last factor worth noting about substituent groups

is that they all add to the bulk of the molecule and larger molecules are expected to diffuse more slowly through the electrolyte.

4.2. 2,2,6,6-Tetramethylpiperidine-1-oxyl

Since the year 2000, 2,2,6,6-tetramethylpiperidine-1-oxyl (TEMPO) and its derivatives have been proposed for use in secondary batteries, mainly to enhance cycling performance, as a fire retardant, or as an additive in lithium-sulfur batteries [108,109,110,111]. In the past years, functional groups based on TEMPO have been incorporated into a polymer that was then successfully used as the positive electrode in an organic radical battery [112,113,114]. This work has suggested that TEMPO and some derivatives of TEMPO could potentially be used as redox shuttles in lithium-ion batteries.

TEMPO and TEMPO-like molecules are neutral radicals that are fairly stable as solids and in solution. After oxidation, the formed cation has a closed-shell structure which is an electronically preferred state and may give the cation additional stability. When aromatic molecules are oxidized, there is delocalization of the positive charge and the unpaired electron throughout the aromatic ring, making these sites more reactive and in need of steric protection to prevent chemical reactions. It was this distribution of the charge, and the resulting enhanced stability of the radical cation, compared to that seen in aliphatic molecules, that was the reason that aromatic molecules were initially tested as shuttles. An oxidized TEMPO molecule does not exhibit significant delocalization of the positive charge, rather is localized to the nitrogen and oxygen atoms. This reduces the number of sites on the molecule that are likely to be sites for reactions to take place. Figure 4.9 shows that the charge is distributed between the nitrogen and oxygen of the

nitroxide group, which, for TEMPO, is sterically protected by four neighboring methyl groups.

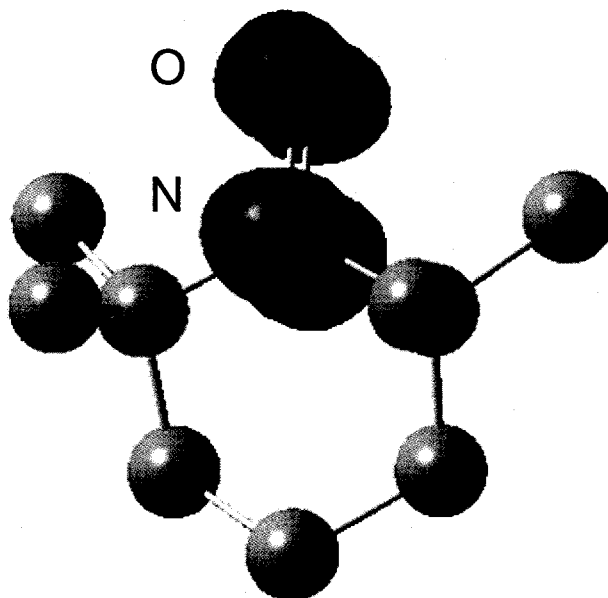


Figure 4.9 Calculated regions of electron density for the LUMO(S⁺) for the molecule TEMPO. The electron density is localized to the nitrogen and oxygen.

TEMPO and TEMPO-like molecules were therefore investigated as a promising class of molecules. Chabita and Mandal investigated a variety of TEMPO-like molecules and found the redox potential for these molecules to be between 0.85 and 1.0 V vs NHE (3.85 to 4.0 V vs Li/Li⁺) [115]. The diffusion coefficients were of the order 10⁻⁵ cm²s⁻¹ in aqueous solution. Both of these values are near those of the molecule 2,5-di-*t*-butyl-1,4-dimethoxybenzene [93], which has already been shown to be an excellent shuttle molecule. Additionally, the polarity of the TEMPO molecule results in a very high solubility in the solvents used. Solubility of TEMPO in the electrolyte used for coin cell testing was over 5 M, which is significantly higher than the aromatic molecules that were tested.

Table 4-3 List of TEMPO molecules tested in coin cells and their measured shuttle potentials and number of cycles of 100% overcharge protection.

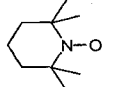
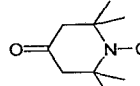
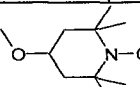
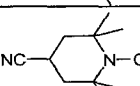
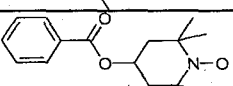
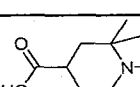
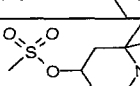
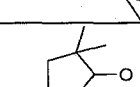
Name	Structure	Potential vs Li/Li ⁺ / V	Cycles of Overcharge Protection
TEMPO		3.45	124
4-oxo-TEMPO		3.67	33
4-methoxy-TEMPO		3.45	133
4-cyano-TEMPO		3.61	158
4-hydroxy-TEMPO benzoate		3.58	86
4-carboxy-TEMPO		3.66	5
4-methylsulfonyloxy-TEMPO		3.56	35
3-cyano-PROXYL		3.69	158

Figure 4.10 shows cyclic voltammograms of 0.1 M TEMPO in both 0.5 M LiBOB and 0.5 M LiPF₆ electrolyte solutions. Both experiments were initially conducted in a potential range between 1.4 and 4.55 V vs Li/Li⁺ and showed similar results, although the experiment in 0.5 M LiPF₆ solution exhibits a tail down at lower potentials (Figure 4.10(b)) that was not seen in the LiBOB solution (Figure 4.10(a)). This tail is most pronounced during the first few cycles and is presumably due to the lack of a passivating layer on the electrode. In LiPF₆ containing electrolytes, this passivating layer begins to form at a lower potential than in LiBOB containing electrolytes, so there is less resistance

to the possible reduction of shuttle molecules themselves. When the lower potential was set to 0.1 V, the 0.1 M TEMPO in 0.5 M LiBOB solution showed no signal from either oxidation or reduction (Figure 4.10(c)), but TEMPO in 0.5 M LiPF₆ solution exhibited a roughly normal behavior (Figure 4.10(d)). This difference in behaviour is likely due to the different properties of the SEIs formed in the different electrolytes. It appears that on the short timescale of the CV experiments, the SEI formed in LiBOB-containing electrolytes prevents the oxidation of TEMPO. A careful study of Figure 4.10(d) does show that the peak at 3.6 V measured during the anodic sweep is reduced slightly during each cycle, suggesting that some decomposition process leaves a film of reaction products on the electrode surface after each sweep to low potential. After the sweep up to 4.5 V, the reduction peak at 3.35 V appears normal, suggesting that the decomposition products are removed at high potentials. In any event, the features observed in Figure 4.10, panels (c) and (d), suggest that TEMPO may have problems acting as a shuttle at the graphite negative electrode, but that it should function effectively at the Li_{4/3}Ti_{5/3}O₄ electrode where the negative electrode potential is much higher. This is also an excellent example of the different characteristics that the SEI can have based on the salt composition of the electrolyte.

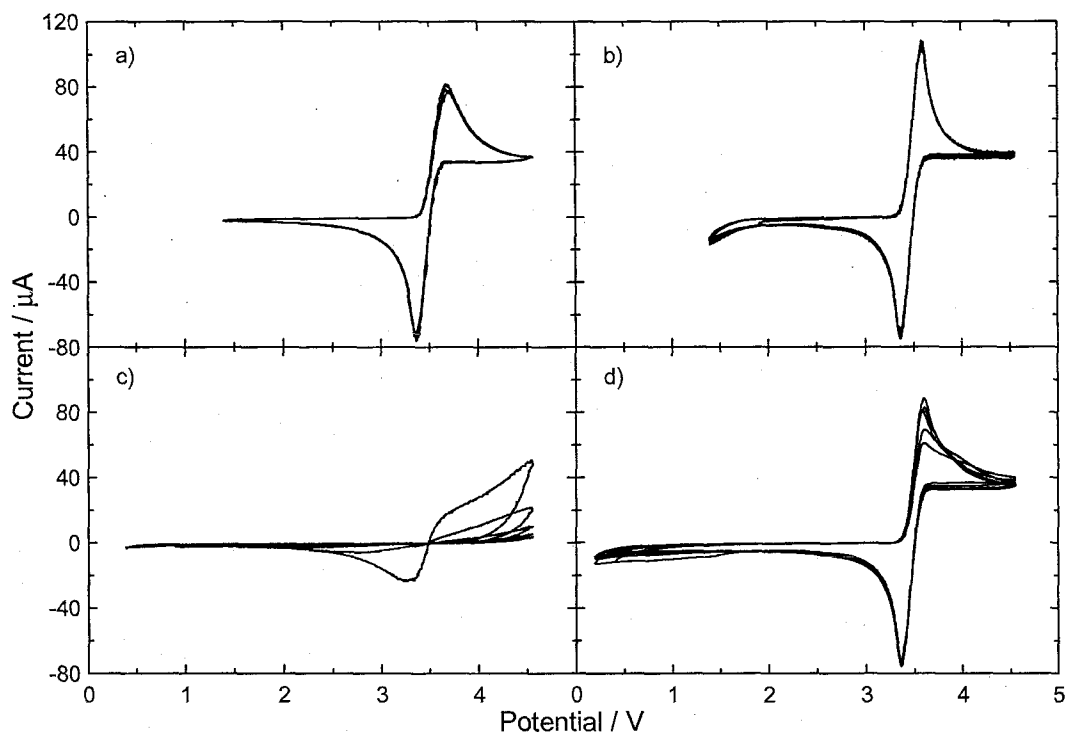


Figure 4.10 CVs of TEMPO a) and b) between 1.4 V and 4.5 V vs Li/Li⁺ and c) and d) between 0.2 V and 4.5 V vs Li/Li⁺ in electrolytes a) and c) containing 0.5 M LiBOB and b) and d) containing 0.5 M LiPF₆.

Figure 4.11 shows the long-term cycling behavior of a Li_{4/3}Ti_{5/3}O₄/LiFePO₄ cell with 0.3 M TEMPO in a 0.5 M LiBOB electrolyte solution at C/5 rate. The shorter of the two plateaus during charging (at about 1.9 V) corresponds to the removal of Li from LiFePO₄ and the longer plateau, initially near 2.0 V, corresponds to the shuttle-protected overcharge provided by TEMPO. After around 3000 h of testing, the flat plateaus indicative of shuttling become deformed. This indicates that the shuttling process is no longer the same reaction it was in the first cycles.

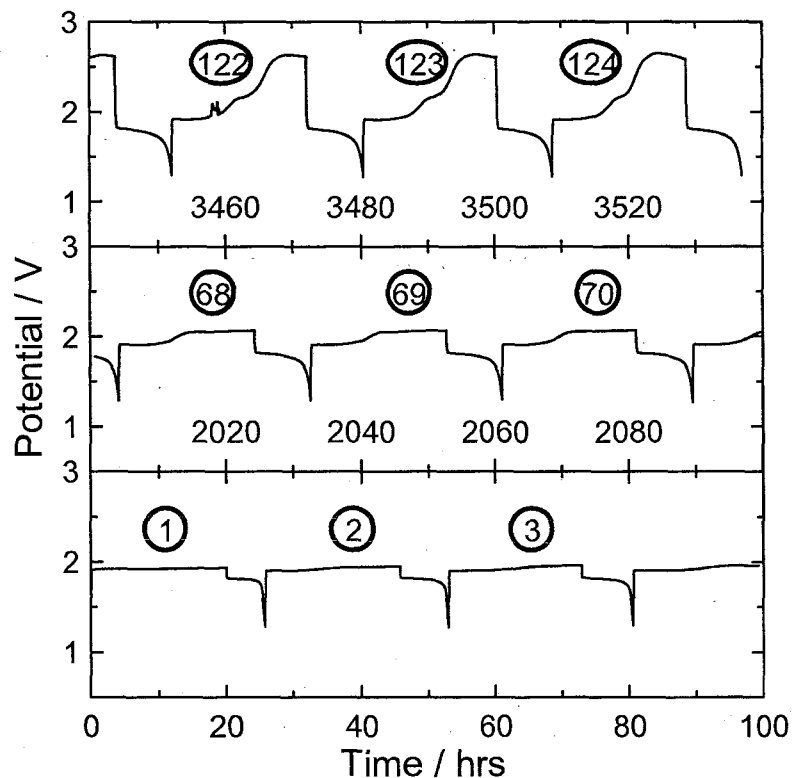


Figure 4.11 Cycling data for a $\text{LiFePO}_4/\text{Li}_{4/3}\text{Ti}_{5/3}\text{O}_4$ coin cell containing 0.3 M TEMPO with cycle numbers shown.

Figure 4.12 shows the capacity vs cycle number for the cell that was cycled for 120 cycles. Figure 4.12 shows that a discharge capacity of 130 mAh/g of LiFePO_4 was obtained and that this capacity was maintained for 120 cycles, even during operation of the shuttle. The capacity of the cell increases over the first few charge-discharge cycles. This was due to the proximity of the TEMPO redox potential to the LiFePO_4 charging potential, which caused some shuttling to occur during the charging of the cell. This self discharge reduces the apparent capacity of the cell. During the first cycles, surface films were formed. These surface films would impede electron transfer and therefore increase the potential at which shuttling occurs. Once these surface films were formed and stable, the increased shuttling potential allowed for the complete charging of the cell with

minimal self discharge and the cell capacity leveled off. This suggested that the redox potential of TEMPO was too close to that of LiFePO_4 and would need to be increased by adding electron withdrawing groups to make more useful molecules.

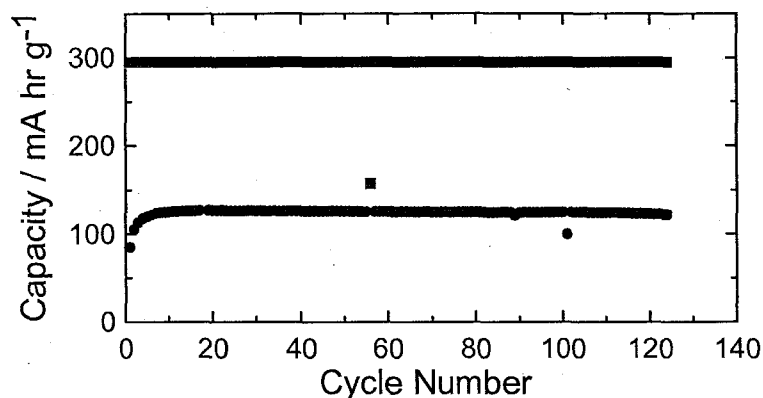


Figure 4.12 Charge (■) and discharge (●) capacities for a $\text{LiFePO}_4/\text{Li}_{4/3}\text{Ti}_{5/3}\text{O}_4$ coin cell containing 0.3 M TEMPO.

To investigate the influence of substituent groups on the redox potential and the cycling performance, a variety of TEMPO-like molecules with substituents on the 4-position were purchased for testing. Table 4-3 gives a complete list of the molecules tested along with the shuttling potential and the number of shuttle-protected overcharge cycles before the shuttle effect was no longer observed. Also listed are results measured for a commercially available, substituted five-membered analog of TEMPO named 3-cyano-2,2,5,5-tetramethylpyrrolidiny-1-oxyl (3-cyano-PROXYL), under the same conditions.

Table 4-3 shows that the introduction of an electron-withdrawing group raises the redox potential, although the influence is much weaker than in aromatic molecules. A group in the 3-position to the N-O group apparently has a larger impact than in the 4-position (compare 3-cyano-PROXYL with 4-cyano-TEMPO). Table 4-3 also shows that normally the group placed at the 4-position of TEMPO-like molecules does not strongly

influence the number of shuttle-protected overcharge cycles achieved. The exceptions to this may be explained by the reaction of the substituent group with the solvent molecules. A free OH group can react with molecules from the solution, and thus the shuttle molecule would undergo a transformation to another substance, as in the case of 4-carboxy-TEMPO. The investigation of the follow-up reaction is not the aim of this study and therefore was not studied. The molecule 4-hydroxy-TEMPO benzoate has an ester group and may undergo transesterification with the carbonate solvent molecules and possibly other subsequent reactions [116]. Due to this process, we believe that over time, the number of shuttle molecules in the solution is reduced, and after some time, overcharge protection is no longer possible. Presumably, the methylsulfonyloxy group can undergo similar reactions with an ester group when it is in the environment of the electrolyte solution.

Figure 4.13 shows the excellent overcharge protection afforded by 4-methoxy-TEMPO (solid line), 4-cyano-TEMPO (dotted line), and 3-cyano-PROXYL (dashed line) in a 0.5 M LiBOB electrolyte solution during over 3000 h of cycling with a 100% shuttle-protected overcharge applied during each cycle. The latter molecule has a redox potential that could be suitable for LiFePO_4 -based cells.

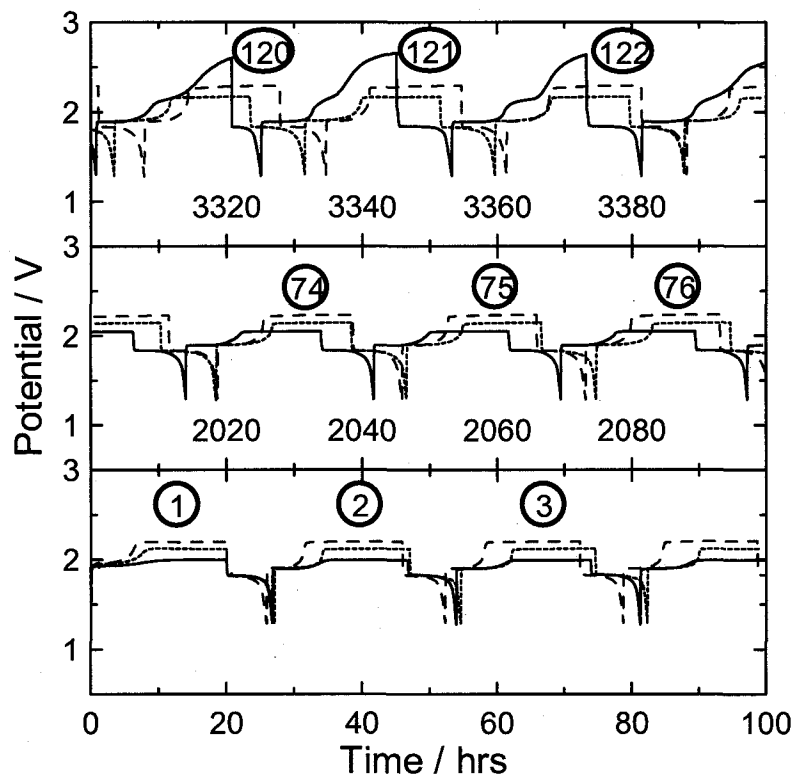


Figure 4.13 Cycling data for 4-methoxy-TEMPO (—), 4-cyano-TEMPO (---) and 3-cyano-PROXYL (-·-) with cycle numbers shown.

TEMPO and TEMPO-like molecules have potential as a promising class of shuttle molecules. The molecules, TEMPO, 4-methoxy-TEMPO, 4-cyano-TEMPO, and 3-cyano-PROXYL all can support more than 100 cycles of 100% shuttle-protected overcharge in $\text{Li}_{4/3}\text{Ti}_{5/3}\text{O}_4/\text{LiFePO}_4$ cells. One problem with these molecules is that their redox potentials are somewhat low, even for LiFePO_4 -based cells and this may result in unacceptably high rates of self discharge. Theoretically, the redox potentials could be adjusted by replacing hydrogen atoms in the methyl groups with fluorine atoms. Unfortunately, such molecules are not presently available commercially for testing.

4.3. Phenothiazines

One requirement for an effective redox shuttle additive is the stability of the formed radical cation. Tran-Van and co-workers examined two dihydrophenazine derivatives as possible molecules for overcharge protection of rechargeable lithium batteries [117]. The redox potentials of these two molecules were reported to be 3.0 and 3.5 V, which are too low for use in LiFePO₄-based Li-ion cells. As pointed out by Sun and co-workers [118], the radical cations of phenothiazine and 10-methylphenothiazine (MPT) show significant stability. The measured redox potential of phenothiazine in the literature was 0.61 V vs a saturated calomel reference electrode (SCE) (3.89 V vs Li/Li⁺), and the redox potential of MPT was reported as 0.79 V vs SCE (4.07 V vs Li/Li⁺) [118] or 0.43 V vs Ag/Ag⁺ (3.69 V vs Li/Li⁺) [119]. These potentials are promising for use in LiFePO₄-based lithium-ion cells.

MPT was used as an example molecule for a large number of tests due to its availability in relatively large quantity. The effect of varying the groups on the nitrogen atom and on the carbon atoms on the redox potential was examined by testing five different phenothiazine derivatives that were commercially available in small quantities.

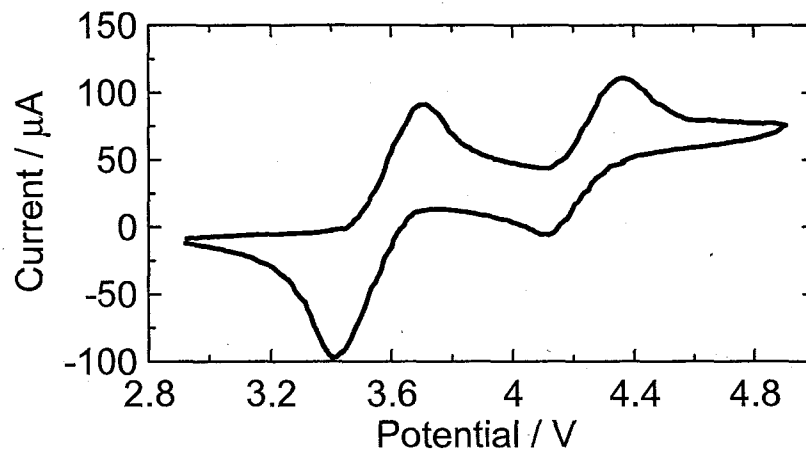


Figure 4.14 CV of MPT between 2.7 V and 4.9 V vs Li/Li⁺.

Figure 4.14 shows a typical CV of MPT over the range 2.9 to 4.9 V vs Li/Li⁺. Two redox potentials are revealed, as found by Sun and co-workers [118]. Both redox processes are reversible and are separated by about 0.7 V. Figure 4.15 shows the CVs of MPT in both LiBOB and LiPF₆-containing electrolytes. When the lower potential limit was reduced to 0.2 V, there appears to be a buildup of resistance on the working electrode in the LiBOB electrolyte, as evidenced by changes to the oxidation peaks. It is likely that this change is associated with the reduction products of LiBOB, which appear at about 1.7 V vs Li/Li⁺, which help form an SEI on the working electrode [17,59,62]. By contrast, no such change to the CV of MPT in LiPF₆ electrolyte is observed when the lower scan limit is reduced to 0.2 V, indicating that the SEI that contains components from LiPF₆ is more compatible with the shuttling of MPT than the SEI formed from LiBOB.

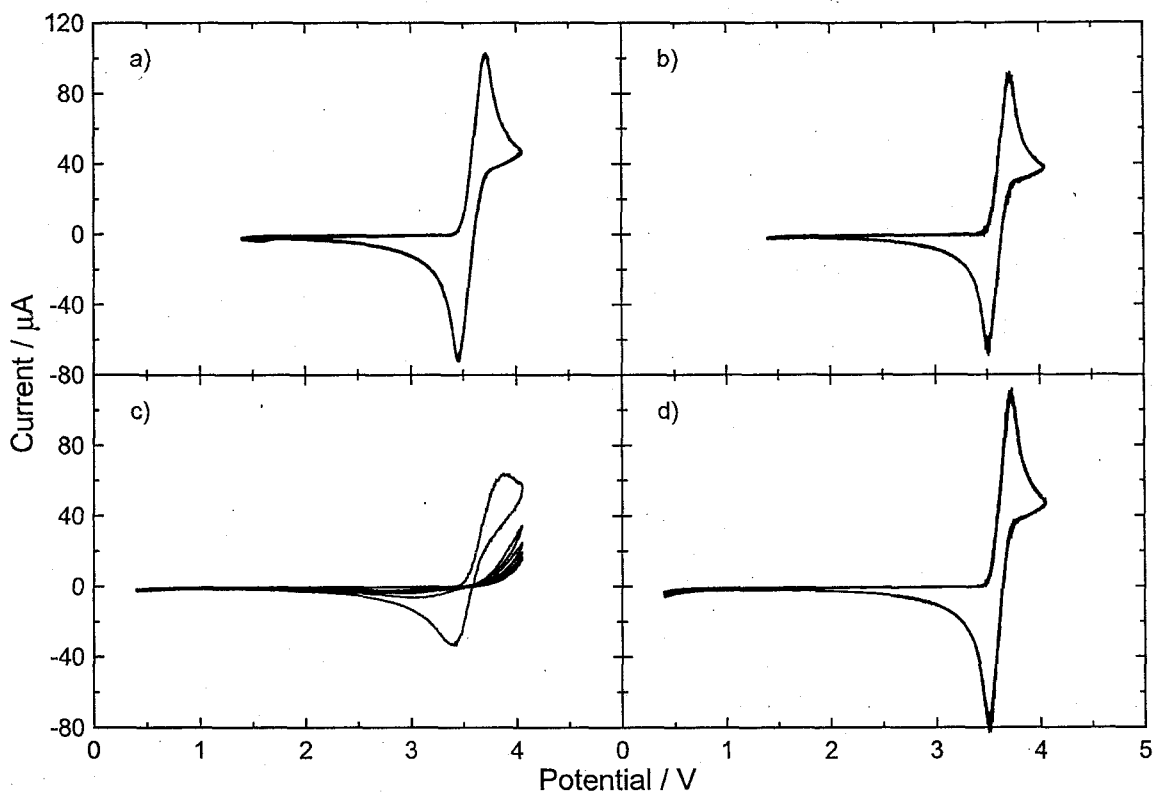


Figure 4.15 CVs of MPT a) and b) between 1.4 V and 4.1 V vs Li/Li^+ and c) and d) between 0.2 V and 4.1 V vs Li/Li^+ in electrolytes a) and c) containing 0.5 M LiBOB and b) and d) containing 0.5 M LiPF_6 .

Figure 4.16 shows the potential vs time for a coin cell using $\text{Li}_{4/3}\text{Ti}_{5/3}\text{O}_4/\text{LiFePO}_4$ electrodes and an electrolyte containing 0.1 M MPT and 0.5 M LiPF_6 . Figure 4.17 shows the cell's specific capacity plotted vs charge-discharge cycle number. The presence of the shuttle does not apparently cause degradation in the capacity with cycle number. Figure 4.16 shows the cycling of a coin cell containing MPT and Figure 4.17 shows the capacity for each cycle for the same cell. This demonstrates that MPT has excellent stability as a shuttle molecule. Unfortunately, the redox potential is too close to that of LiFePO_4 and there is overlap between the charging and the shuttling. This explains why the discharge capacity started low and increased over the first 20 cycles. As was the case with

TEMPO, a surface film likely formed during the first cycles. Presumably, this surface film resulted in an increased potential at which shuttling occurs. Once these surface films were formed and stable, the increased shuttling potential allowed for the complete charging of the cell with minimal self discharge and an increased apparent capacity. This suggested that the redox potential of MPT was too close to that of LiFePO_4 .

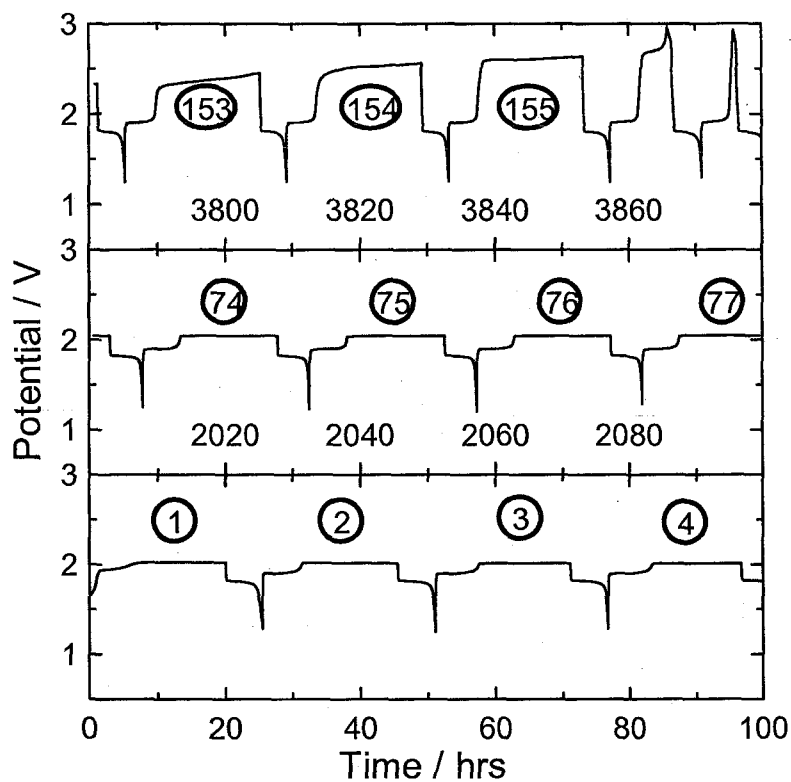


Figure 4.16 Cycling data for a $\text{LiFePO}_4/\text{Li}_{4/3}\text{Ti}_{5/3}\text{O}_4$ coin cell containing 0.1 M MPT with cycle numbers shown.

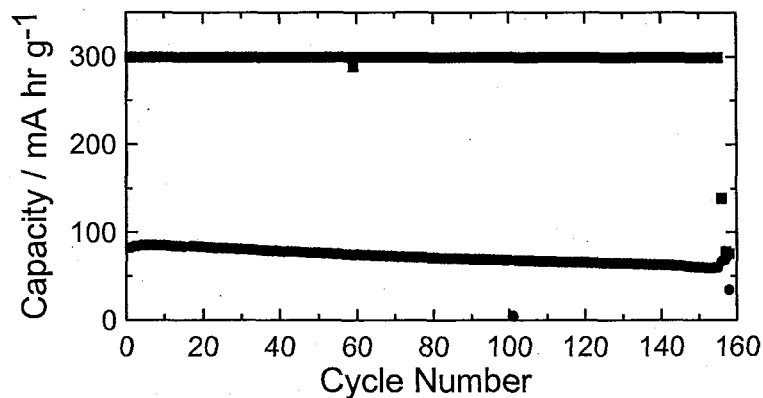


Figure 4.17 Charge (■) and discharge (●) capacities for a $\text{LiFePO}_4/\text{Li}_{4/3}\text{Ti}_{5/3}\text{O}_4$ coin cell containing 0.1 M MPT.

Figure 4.18 shows the potential vs time of two LiFePO_4 /graphite coin cells charged and discharged at nominal $C/10$ current. The cell corresponding to the solid line had an electrolyte containing 0.1 M MPT and 0.5 M LiBOB, while the cell corresponding to the dashed line used 0.1 M MPT and 0.5 M LiPF_6 . The cell using the LiBOB electrolyte only could support 13 shuttle-protected overcharges, while the cell with LiPF_6 electrolyte ran for 56 cycles. This observation (cells with graphite electrodes and LiPF_6 salt lasting longer than cells with LiBOB salt) may be related to the CV results shown in Figure 4.15. This was where it was shown that some decomposition process occurs on electrodes taken to low potentials in LiBOB containing electrolytes. Because the graphite electrode is always at about 0.1 V vs Li/Li^+ , in the presence of MPT and the MPT radical cation, this decomposition may consume the shuttle molecule over time, leading to the behavior in Figure 4.18.

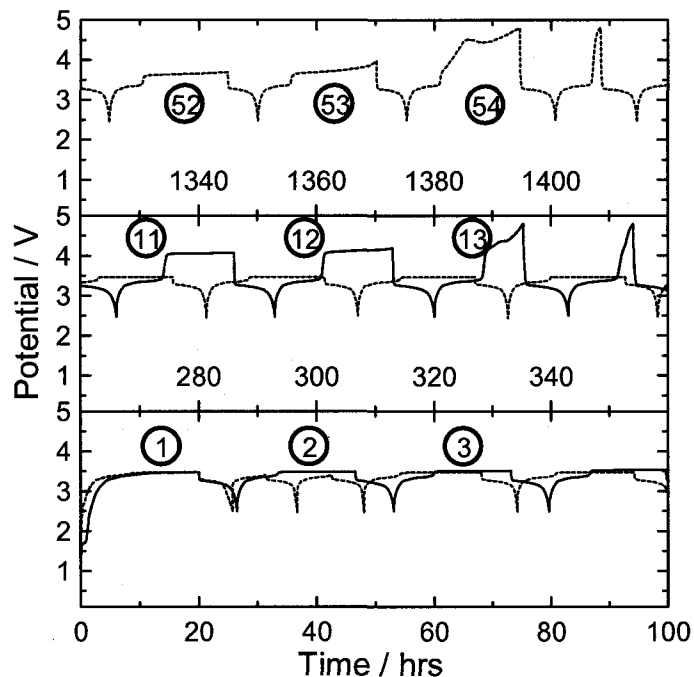


Figure 4.18 Cycling data for $\text{LiFePO}_4/\text{MCMB}$ coin cells containing 0.1 M MPT in electrolytes containing 0.5 M LiBOB (—), and 0.5M LiPF_6 (—). Cycle numbers are shown.

Based on the coin cell results, MPT, based on the phenothiazine core, is a relatively stable shuttle molecule. The problem with MPT for LiFePO_4 -based cells is that its redox potential is low, that is its oxidation potential is too close to that of LiFePO_4 to prevent significant self discharge. Therefore, other molecules based on the phenothiazine core were studied in LiFePO_4 -based lithium-ion coin cells.

Table 4-4 gives the experimentally determined redox potentials of five phenothiazine-based molecules. Group substitutions were made in two positions on the molecule, first on the N-atom and second on the outer sp^2 -carbon atoms. Table 4-4 shows that the variation of the redox potential for alkyl substitutions at the N atom in MPT, ethylphenothiazine (EPT), and isopropylphenothiazine (IPT), is negligible. The comparable electron-donating effect of the methyl, ethyl, and isopropyl groups on the

nitrogen atom does not lead to a significant change in the redox potential and is in agreement with the values given by Tran-Van and co-workers [117]. Due to the larger electron-withdrawing effect of the acetyl group ($-\text{COCH}_3$), electron density is withdrawn from the phenothiazine core; therefore, more energy must be employed to extract an electron and thus, the redox potential is raised in acetylphenothiazine (APT).

Table 4-4 List of tested phenothiazine molecules, their coin cell measured shuttle potentials and number of cycles of 100% overcharge protection. Molecules that prevented cells from charging are shown as ---.

Name	Structure	Shuttle Potential vs Li/Li ⁺ / V	Cycles of Overcharge Protection
phenothiazine		---	0
2-(trifluoromethyl) phenothiazine		---	0
10-ethylphenothiazine		3.47	150
3-chloro-10-ethylphenothiazine		3.53	146
10-isopropylphenothiazine		3.5	163
10-acetylphenothiazine		3.88	114
2-chloro-10-(cyanoethyl)-phenothiazine		3.71	1
10-methylphenothiazine		3.47	156
10-ethyl-3-nitrophenothiazine-5-oxide		4.21	1
10-ethylphenothiazine-5,5-dioxide		4.2	5
3-(trifluoromethylsulfonyl) phenothiazine		3.66	17
10-(trifluoroacetyl)phenothiazine		4.39	5

By comparing EPT and 3-chloro-EPT, the redox potential is raised by only about 0.1 V when a chlorine atom is added at the 3-position. This potential increase is smaller than was seen when halogen atoms were added to aromatic molecules. A possible explanation can be made by comparing the MPT radical cation's LUMO to the 3-chloro-EPT radical cation's LUMO, as is done in Figure 4.19. The electron density in the LUMO of the phenothiazine core is mainly on the S and N atoms and not distributed heavily over the outer sp^2 -carbon atoms as it is in a radical cation of a benzene-type molecule. Therefore, substitutions on the N atom have a much higher impact than substitutions on the outer C-atoms.

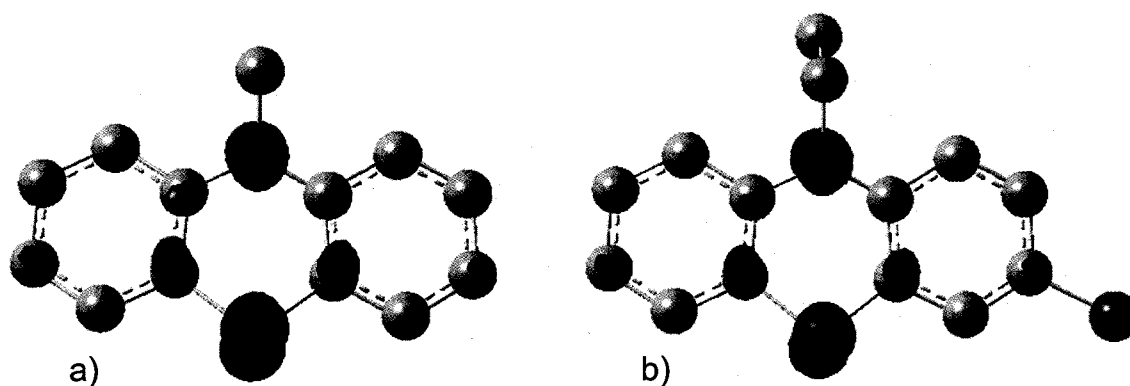


Figure 4.19 Calculated electron densities for the LUMO(S^+) for the molecules a) 10-methylphenothiazine and 10-ethyl-3-chlorophenothiazine. The electron density is highest on the nitrogen and sulfur. Substitution on the carbons has little effect on the electron density.

Figure 4.20 shows the potential vs time for three $\text{LiFePO}_4/\text{Li}_{4/3}\text{Ti}_5/3\text{O}_4$ coin cells containing 0.1 M EPT, 3-chloro-EPT and IPT, respectively, in 0.5 M LiBOB electrolyte. All shuttle molecules operate well for over 3500 h under these test conditions which were

charged at a C/10 rate for 20 h. A large number of tests of these molecules were not possible due to their limited availability and their high cost.

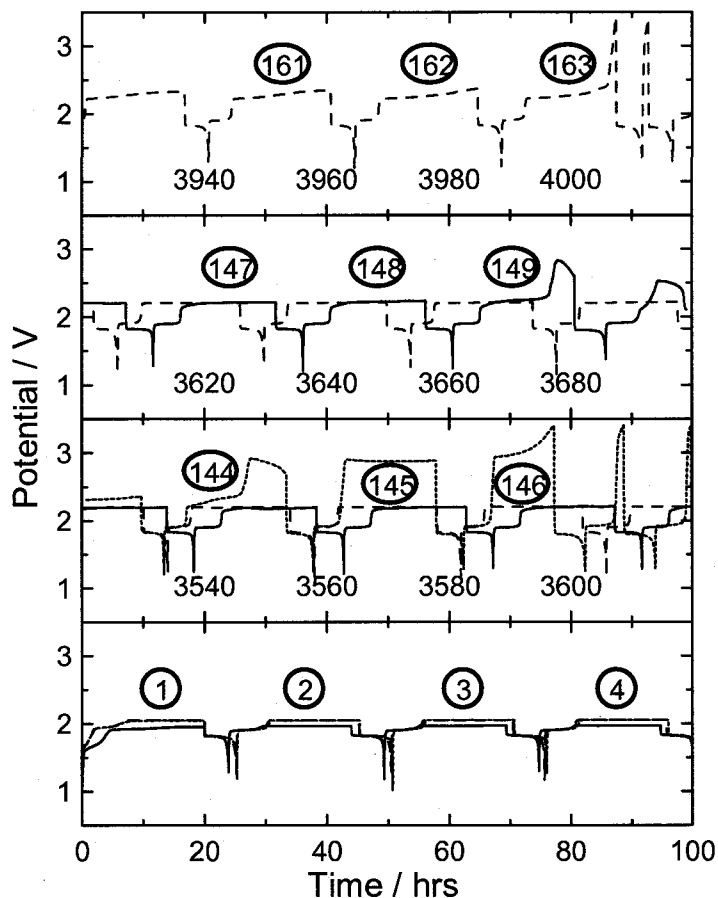


Figure 4.20 Cycling data for 10-ethylphenothiazine (—), 3-chloro-10-ethylphenothiazine (—), and 10-isopropylphenothiazine (—) with cycle numbers shown.

Table 4-5 summarizes the results of the tests that were carried out on these molecules. These shuttle molecules work well in $\text{LiFePO}_4/\text{Li}_{4/3}\text{Ti}_{5/3}\text{O}_4$ coin cells but show lower stability in $\text{LiFePO}_4/\text{graphite}$ coin cells.

Table 4-5 Summary of coin cell results for a variety of phenothiazine molecules.

Molecule	Negative electrode material	Cycles of overcharge protection
10-methyl-phenothiazine	$\text{Li}_{4/3}\text{Ti}_{5/3}\text{O}_4$ graphite	156 13
10-ethyl-phenothiazine	$\text{Li}_{4/3}\text{Ti}_{5/3}\text{O}_4$ graphite	150 18
3-chloro-10-ethyl-phenothiazine	$\text{Li}_{4/3}\text{Ti}_{5/3}\text{O}_4$ graphite	146 32
10-isopropyl-phenothiazine	$\text{Li}_{4/3}\text{Ti}_{5/3}\text{O}_4$ graphite	163 7
10-acetyl-phenothiazine	$\text{Li}_{4/3}\text{Ti}_{5/3}\text{O}_4$ graphite	114 1

Figure 4.21 shows the potential vs time for a $\text{LiFePO}_4/\text{Li}_{4/3}\text{Ti}_{5/3}\text{O}_4$ coin cell containing 0.1 M APT and 0.5 M LiBOB electrolyte. The cell was tested using a C/10 current and was charged for 20 h. Figure 4.21 shows that for the majority of the cycles, the potential decreased during each overcharge cycle. This is very atypical for shuttle molecules and was only observed in one other molecule that was tested, anisole. Nevertheless, the stability of APT is good in $\text{LiFePO}_4/\text{Li}_{4/3}\text{Ti}_{5/3}\text{O}_4$ coin cells which displayed 114 shuttle-protected overcharge cycles in LiBOB electrolyte.

Figure 4.22 shows the potential vs time for a $\text{LiFePO}_4/\text{MCMB}$ cell containing 0.1 M MPT and 0.5 M LiBOB. The "death" of a shuttle molecule is characterized by an increase in potential of the shuttle plateau.

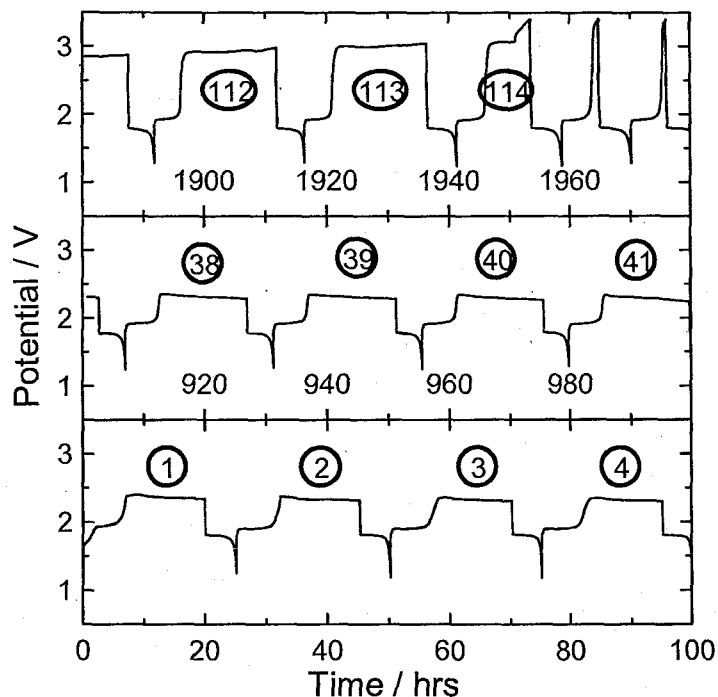


Figure 4.21 Cycling data for a $\text{LiFePO}_4/\text{Li}_{4/3}\text{Ti}_{5/3}\text{O}_4$ cell containing 10-acetylphenothiazine with cycle numbers shown.

As shown in Figure 4.22 after 220 hours there is a step in the potential where the second oxidation potential is reached. There could be many reasons for the "death" of the shuttle molecule. A general assumption is that the number of shuttle molecules decreases slowly with time for various reasons, such as decomposition, polymerization, and reaction with other molecules in the electrolyte. As the cycling proceeds, at some point the concentration is too low to carry the current and therefore the potential rises. Eventually the second oxidation plateau is reached and each remaining shuttle molecule can carry two charges, so the shuttling carries on for some cycles more before all shuttling capacity is lost.

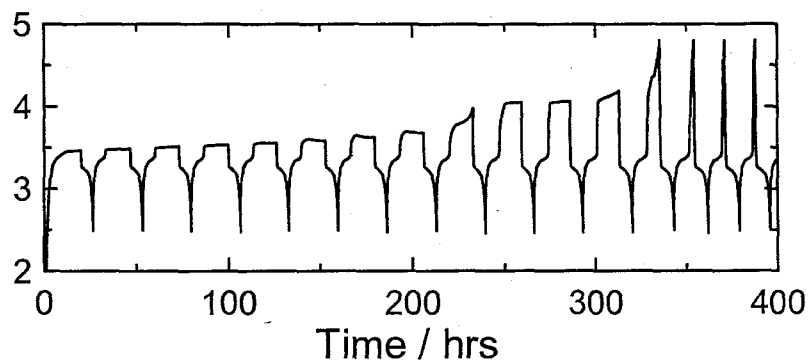


Figure 4.22 Cycling data for a coin cell containing 0.1M MPT. The two shuttle plateaus correspond to the potentials at which the first and second oxidation of MPT occur.

Phenothiazine-based molecules are a promising class of molecules as an electrolyte additive in Li-ion batteries for overcharge and overdischarge protection. Although the redox potential of MPT is too low for a commercial application, the redox potential can be modified by substituting the methyl group with a more electron-withdrawing group such as a carboxylic ester group or trifluoromethyl group, thus leading to a higher redox potential.

In accordance with CV measurements, LiFePO₄/graphite cells containing MPT, EPT, 3-chloro-EPT, IPT, and APT provide larger numbers of cycles of shuttle-protected overcharge at 30°C if LiPF₆ electrolyte is used compared to LiBOB electrolyte. In LiFePO₄/Li_{4/3}Ti_{5/3}O₄ cells, the choice of electrolyte salt is not so dramatic for cells operated at 30°C. At higher temperatures (e.g., 55°C), LiFePO₄/Li_{4/3}Ti_{5/3}O₄ cells show larger numbers of shuttle-protected overcharge cycles if a LiBOB-containing electrolyte is used instead of LiPF₆-based electrolyte. For a given cell type and a given electrolyte, the number of shuttle-protected overcharge or overdischarge cycles that can be sustained is less at 55°C than at 30°C.

4.4. Triphenylamines

Another class of molecules that provides better than average overcharge protection in lithium-ion coin cells is based on the molecule triphenylamine. With the charge spread throughout the three aromatic rings and the central nitrogen, these molecules are stable and have a tuneable oxidation potential, as shown when electron withdrawing bromine atoms are added to the rings.

The molecule triphenylamine (TPA) and several substituted triphenylamine molecules have been studied electrochemically [120,121]. The oxidation of TPA has been reported to be 0.98 V vs a normal hydrogen electrode (NHE) in acetonitrile solutions [120]. This would mean that triphenylamine and substituted triphenylamines could have a sufficiently high oxidation potential, vs Li/Li^+ , to be of interest as a redox shuttle in LiFePO_4 based Li-ion cells.

The shuttle molecules were added in a concentration of 0.1 M for triphenylamine, 0.04 M for tris(4-bromophenyl)amine and 0.01M for tris(2,4-dibromophenyl)amine, which were the maximum solubilities of the shuttle in the electrolyte in the cases of tris(4-bromophenyl)amine and tris(2,4-dibromophenyl)amine. The molecules tris(4-bromophenyl)amine and tris(2,4-dibromophenyl)amine were synthesized by the author according to the literature [122] and were characterized by ^1H and ^{13}C NMR spectroscopy. The chemical shifts of the molecules matched those found in the literature [122].

Figure 4.23 shows the proton NMR from a sample of tris(2,4-dibromophenyl)amine from 0 to 8 ppm. NMR samples were run at the Atlantic Regional

Magnetic Resonance Centre with assistance of Dr. Kathy Robertson. A very small signal is still present at 3.73 ppm (quartet) and 1.26 ppm (triplet) that is attributed to ethanol and a peak at 1.54 ppm (singlet) is attributed to residual water in the sample. These solvent impurities were later removed from the sample using heat and vacuum. The large signal at 7.27 ppm is due to the solvent CDCl_3 and there are small spinning side bands from this peak at 7.48 ppm and 7.06 ppm.

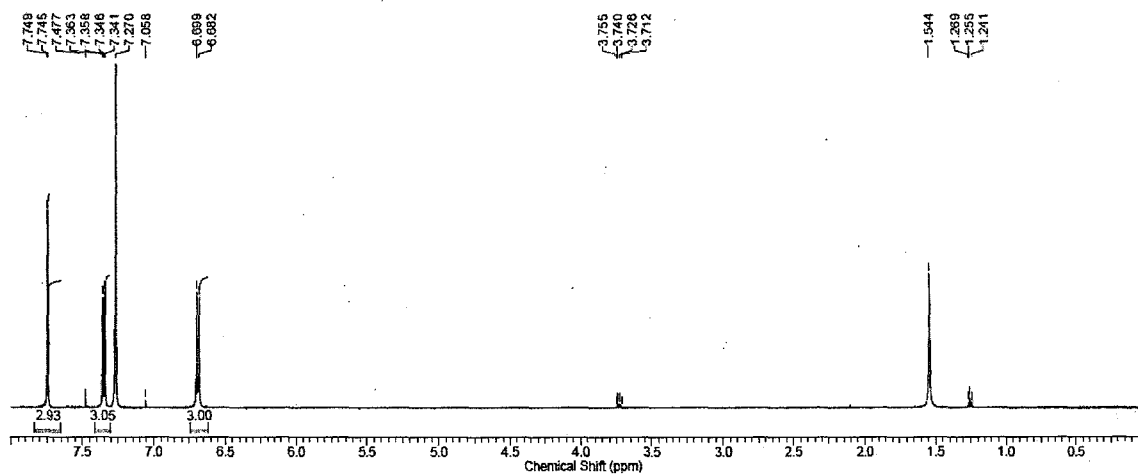


Figure 4.23 ^1H NMR spectrum in CDCl_3 of a sample of the molecule tris(2,4-dibromophenyl)amine synthesized for testing.

Figure 4.24 shows an expanded view of the signals in the range of 6.5 ppm to 7.9 ppm, which is where the signal from tris(2,4-dibromophenyl)amine is located.

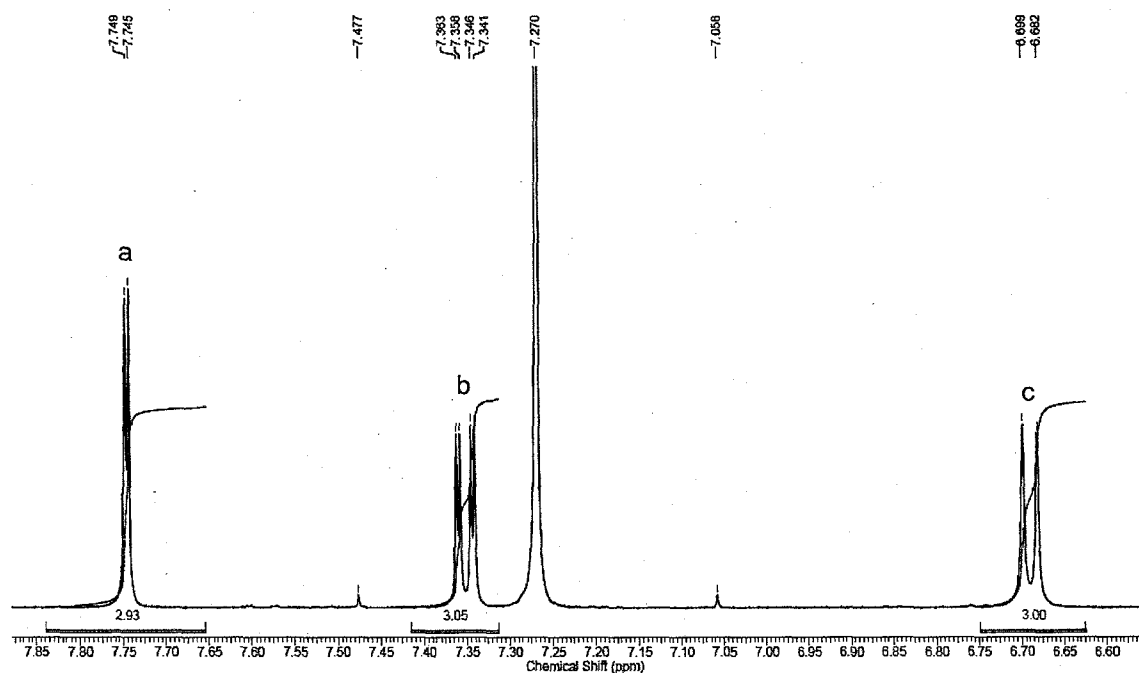


Figure 4.24 Expanded view of the aromatic region of the ^1H NMR spectrum for tris(2,4-dibromophenyl)amine.

The peaks are located at 7.747 ppm (doublet), 7.352 ppm (doublet of doublets) and 6.691 ppm (doublet) and have integrated areas of 0.98:1.02:1.00, respectively. The absence of other peaks in the spectrum indicates the purity of the sample. Figure 4.25 shows the assignment of these peaks to the protons in the molecule based on chemical shifts and coupling patterns.

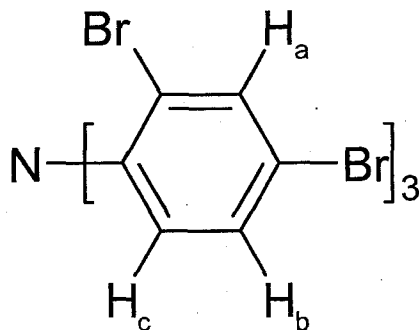


Figure 4.25 Assignment of protons to their corresponding peaks in the ^1H NMR spectrum.

Figure 4.26 shows the cyclic voltammograms for the three molecules; triphenylamine, tris(4-bromophenyl)amine and tris(2,4-dibromophenyl)amine. The oxidation potential of these can be seen to increase as the number of bromines increases on the triphenylamine molecule. The oxidation potentials for triphenylamine, tris(4-bromophenyl)amine and tris(2,4-dibromophenyl)amine are 3.76 V, 3.90 V and 4.30 V, respectively. The peak current is highest for triphenylamine and lowest for tris(2,4-dibromophenyl)amine. As the number of bromines is increased, the peak current is decreased. This is due in part to the decreased solubility of the molecules in the electrolyte as the molecular weight of the molecules increase. The increased molecular weight would also be expected to have a detrimental effect on the diffusion coefficient of the molecule, which would reduce the maximum current capable of being carried by the shuttle.

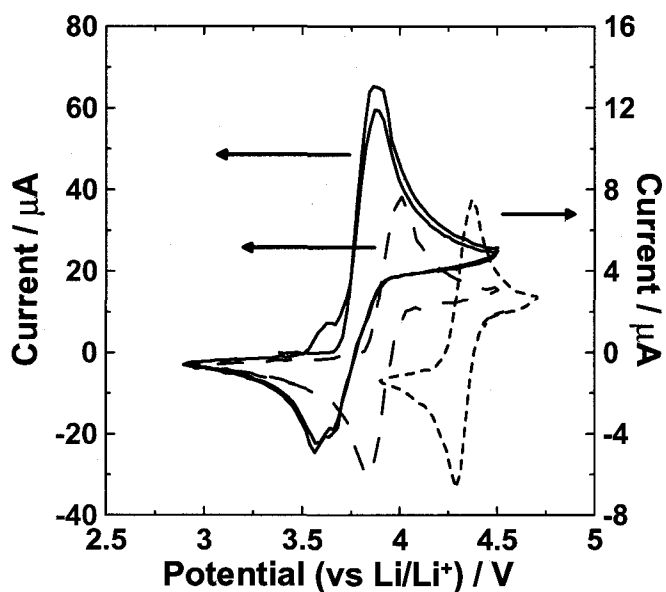


Figure 4.26 CVs of triphenylamine (—), tris(4-bromophenyl)amine (---), and tris(2,4-dibromophenyl)amine (-·-·-).

Figure 4.27 shows the measured values for the oxidation potential of a variety of brominated triphenylamine molecules, as stated by Schmidt and Steckhan [122], and the measured oxidation potential for the molecules triphenylamine, tris(4-bromophenyl)amine and tris(2,4-dibromophenyl)amine vs Li/Li^+ . Figure 4.27 shows that the first and second oxidation potentials of these triphenylamine molecules are linearly correlated with the number of bromines in the molecule. The first oxidation potential increases by 0.11 V per bromine and the second oxidation potential increases by 0.07 V per bromine. The left axis of Figure 4.27 corresponds to the literature values for the oxidation potential of various brominated triphenylamines as reported vs NHE potential, and the right hand axis corresponds to the data as measured in battery electrolyte, reported vs Li/Li^+ potential. The two scales were aligned such that the data points corresponding to tris(4-bromophenylamine) were overlapped.

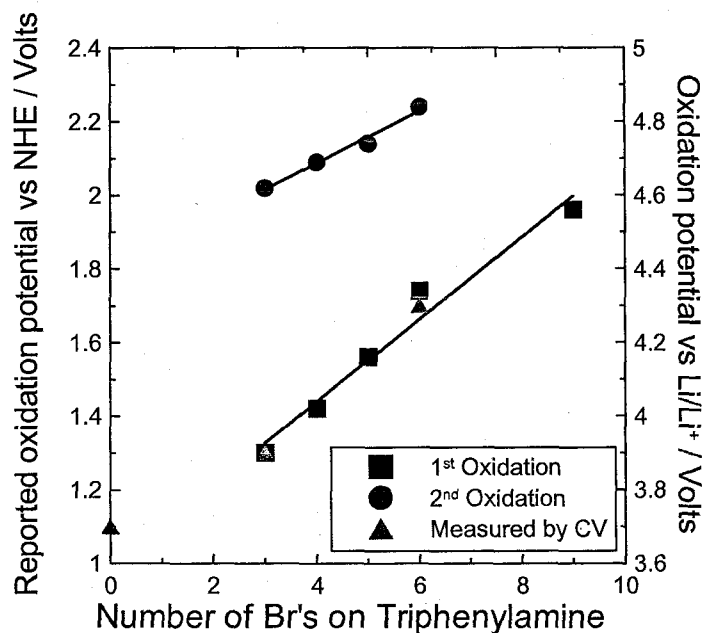


Figure 4.27 Literature and measured oxidation potentials for several brominated triphenylamines:

Figure 4.28 and Figure 4.29 show the charge/discharge data from coin cells containing the molecules triphenylamine and tris(4-bromophenyl)amine, respectively. Several cells were made and cycled, with graphite or $\text{Li}_{4/3}\text{Ti}_{5/3}\text{O}_4$ negatives and with LiPF_6 or LiBOB containing electrolytes and the data shown is from the longest cycling cell for each molecule. The cell containing triphenylamine shuttled for 22 cycles with 100% overcharge per cycle. The cell containing tris(4-bromophenyl)amine cycled for 41 cycles of 100% overcharge per cycle. This tells us that the brominated molecule is more stable as a redox shuttle than triphenylamine.

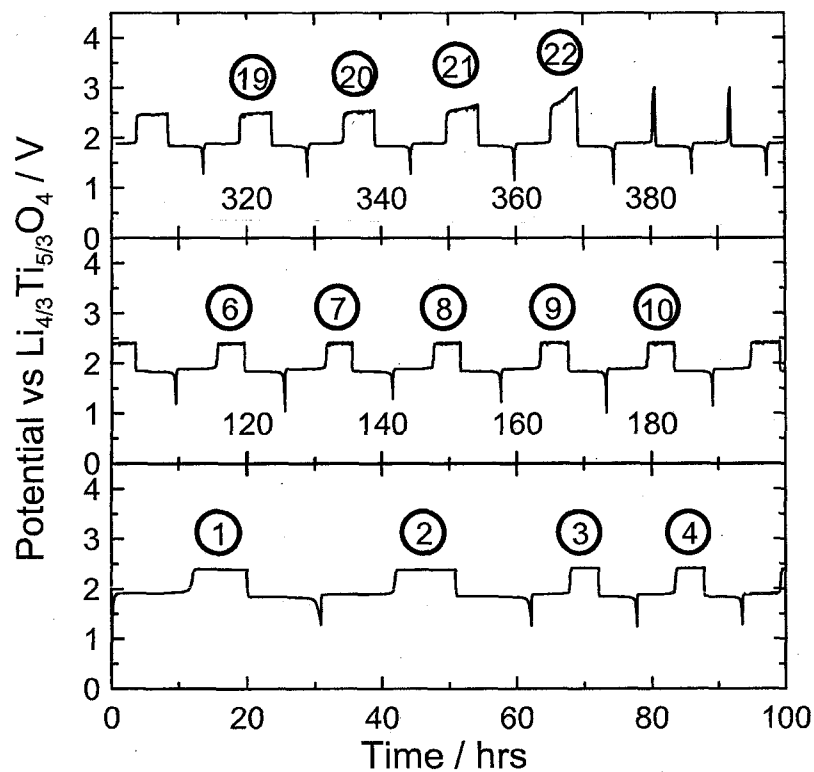


Figure 4.28 Cycling data for a $\text{LiFePO}_4/\text{Li}_{4/3}\text{Ti}_{5/3}\text{O}_4$ cell containing triphenylamine with cycle numbers shown.

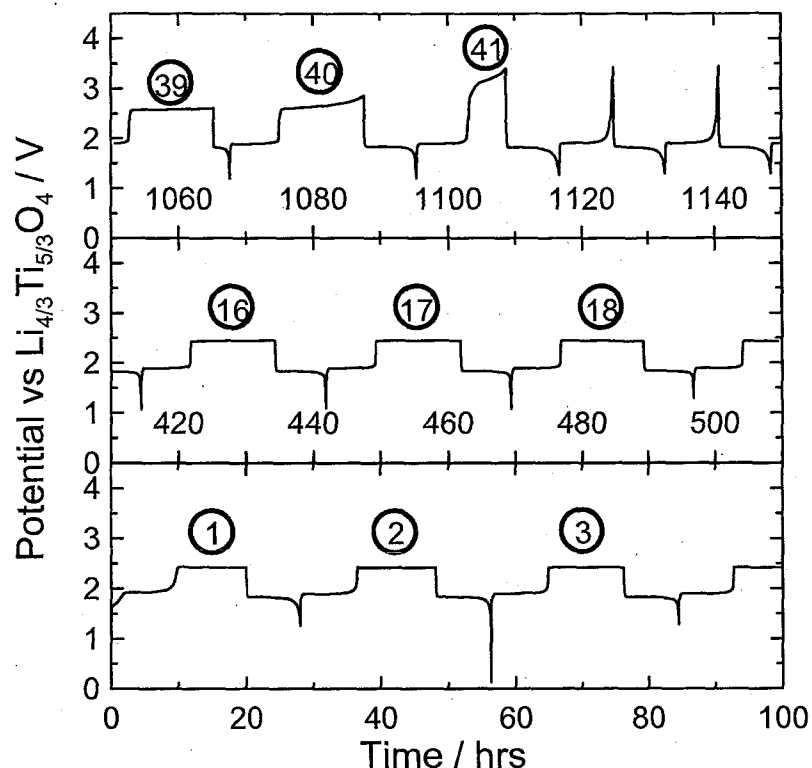


Figure 4.29 Cycling data for a $\text{LiFePO}_4/\text{Li}_{4/3}\text{Ti}_{5/3}\text{O}_4$ cell containing tris(4-bromophenyl)amine with cycle numbers shown.

The shapes of the CVs in Figure 4.26 are worthy of study. The molecules tris(4-bromophenyl)amine and tris(2,4-dibromophenyl)amine show a much more reversible CV than does triphenylamine itself. The oxidative and reductive peaks are very similar in size and shape for the Br-containing molecules, unlike for the molecule triphenylamine. Triphenylamine shows an oxidative peak that is significantly larger than the reductive peak, indicating that there is some portion of the oxidized shuttle molecules that are not being reduced during the experiment. Also, for triphenylamine, the first 2 cycles are shown so that the differences between them can be seen. The first cycle starts at around 3.3 V and the potential was swept up to 4.5 V then down to 2.9 V. During the down sweep, there are actually 2 peaks seen, one at 3.7 V and another smaller one at 3.6 V.

Then, during the second cycle, there is an extra, small oxidative peak at 3.7 V that was not present in the first scan. This unusual behaviour is attributed to the formation of the dimer, tetraphenylbenzidine (TPB). Figure 4.30 shows the reaction scheme for the dimerization of TPA [120].

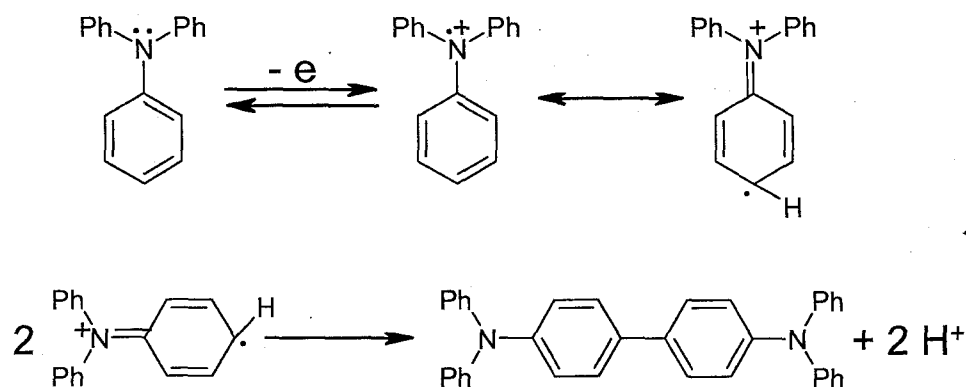


Figure 4.30 Reaction mechanism showing the dimerization of triphenylamine to tetraphenylbenzidine.

The molecule TPB has two separate, one electron oxidation processes that occur at potentials slightly below the oxidation potential of triphenylamine [120]. This explains the appearance of the CV of triphenylamine. The two reductive peaks are the two reduction processes of TPB generated by the first oxidation of TPA in the cell. The extra peak in the second oxidative scan is the first electron oxidation of TPB. The second electron oxidation of TPB is obscured by the larger oxidation peak from TPA in the cell. Resonance structures show that the radical can be delocalized from the central N to the ring carbons in the ortho and para positions. Figure 4.31 shows the calculated electron density for the LUMO(S^+) of TPA, which shows where the removed electron is localized. The ortho positions are somewhat protected from reaction by the presence of the other rings, so dimerization occurs at the para position. The presence of a bromine at the para

position prevents the formation of the dimer because the para position is blocked. The addition of groups in the para position of the aromatic rings has been previously shown to prevent the dimerization of TPA [123].

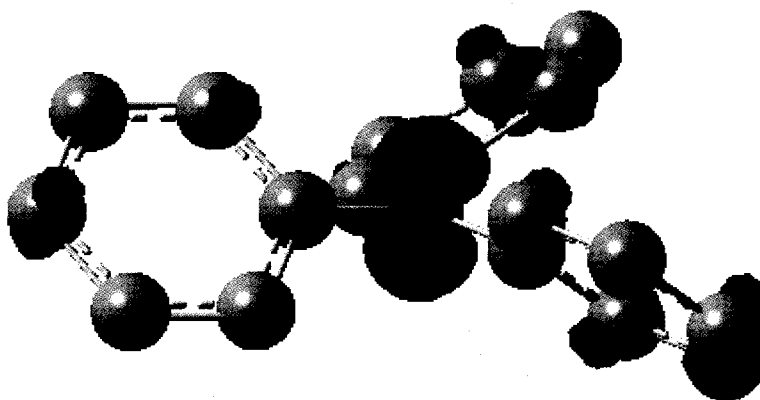


Figure 4.31 Calculated electron density of the LUMO(S¹) for triphenylamine. The electron density is heaviest on the central nitrogen, but can also be seen on the aromatic rings at the ortho and para positions.

The triphenylamine class of molecules has been shown to be successful as redox shuttles for overcharge protection in lithium-ion batteries. The oxidation of triphenylamine results in the formation of the dimer, tetraphenylbenzidine, through an electrochemical-chemical-electrochemical (ECE) mechanism. The addition of bromine to the molecule has several effects; the electronegativity of the bromine results in a higher oxidation potential; when placed at the para position of each ring, the bromine prevents the dimerization of triphenylamine, making the molecule more stable as a redox shuttle; and the addition of bromine results in poorer solubility of the molecule in the alkyl carbonate solvents used in lithium-ion batteries. These properties make triphenylamines an interesting class to study, but of limited use as shuttles in actual lithium-ion batteries.

4.5. Direct Comparison of Select Shuttles

The three classes of molecules that have been shown to be successful for protecting LiFePO_4 cells during overcharge are, the molecule 2,5-di-*t*-butyl-1,4-dimethoxybenzene (DDB), molecules based on phenothiazine, such as 10-methylphenothiazine (MPT) and molecules based on 2,2,6,6-tetramethylpiperidine-1-oxyl (TEMPO), such as TEMPO and 4-cyano-TEMPO. These molecules were examined using lithium-ion coin cells, three-electrode cyclic voltammetry and four-electrode cyclic voltammetry. Three-electrode cyclic voltammetry was used to measure the diffusion coefficients and the stability of the shuttle molecules at high and low potentials. The transport of electrons through the solid-electrolyte interface on the negative electrode to the oxidized shuttle molecule was examined using the four-electrode cell for electrolytes containing both LiPF_6 and LiBOB salts. The rate of charge transfer to the oxidized TEMPO and MPT molecules is significantly reduced on glassy carbon below 1.7 V (vs Li/Li^+) in electrolytes containing LiBOB, but not in electrolytes containing LiPF_6 . Charge transfer to oxidized DDB seems facile at all potentials above 0.2 V in both LiPF_6 and LiBOB electrolytes.

Cyclic voltammetry (CV) experiments were performed in the manner described in Chapter 2. It was possible to use the CV cells with either three or four electrodes simultaneously. When four electrodes were desired, the second working electrode was operated on a separate charger channel (in potentiodynamic mode) using the same reference and counter electrode.

The redox potential of each of the three molecules was determined by cyclic voltammetry. Figure 4.32 shows the CVs of the three molecules. There are a few

differences between the three molecules. The molecule DDB has a higher redox potential (just above 3.9 V vs Li/Li^+), than TEMPO at 3.5 V and MPT at 3.55 V. Also, the molecules DDB and MPT show a second oxidation at about 4.5 V and 4.3 V, respectively, while TEMPO shows no second oxidation in the range scanned. The second oxidation of DDB is irreversible, which means that any molecules that are eventually doubly oxidized are no longer capable of providing overcharge protection within the cell.

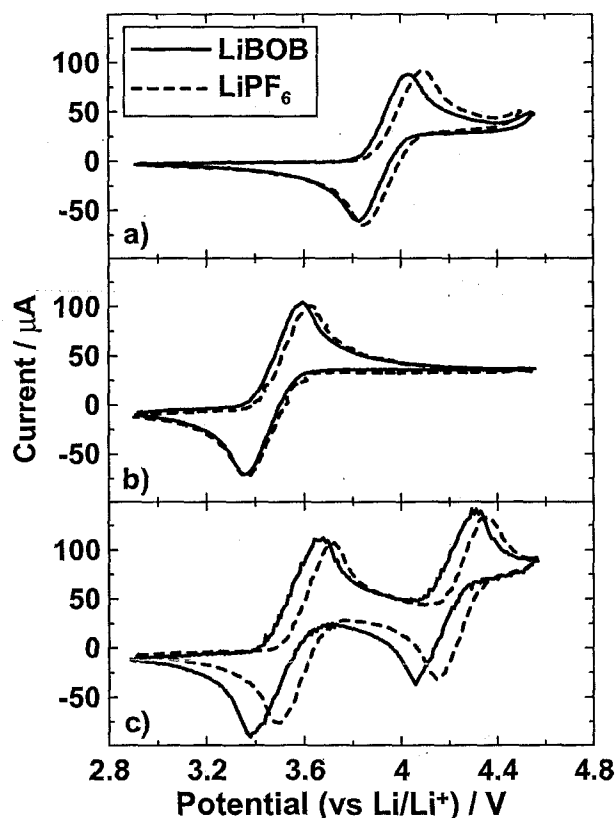


Figure 4.32 Figure 2. Cyclic voltammograms for a) 2,5-di-*tert*-butyl-1,4-dimethoxybenzene (DDB) b) 2,2,6,6-tetramethylpiperidine-1-oxyl (TEMPO) and c) 10-methylphenothiazine (MPT) in both LiPF_6 and LiBOB-based electrolytes.

Even at potentials below the second oxidation potential of the molecule, there will be a small amount of doubly oxidized species being formed. This means that molecules

with a reversible second oxidation, like MPT, or no second oxidation, like TEMPO, would be preferred as shuttle molecules within cells. Also, Figure 4.32 shows that in LiPF₆-based electrolytes, the measured oxidation potentials are slightly higher than in LiBOB-based electrolytes. This is a good example of how the electrolyte can have an effect on the electrochemistry taking place.

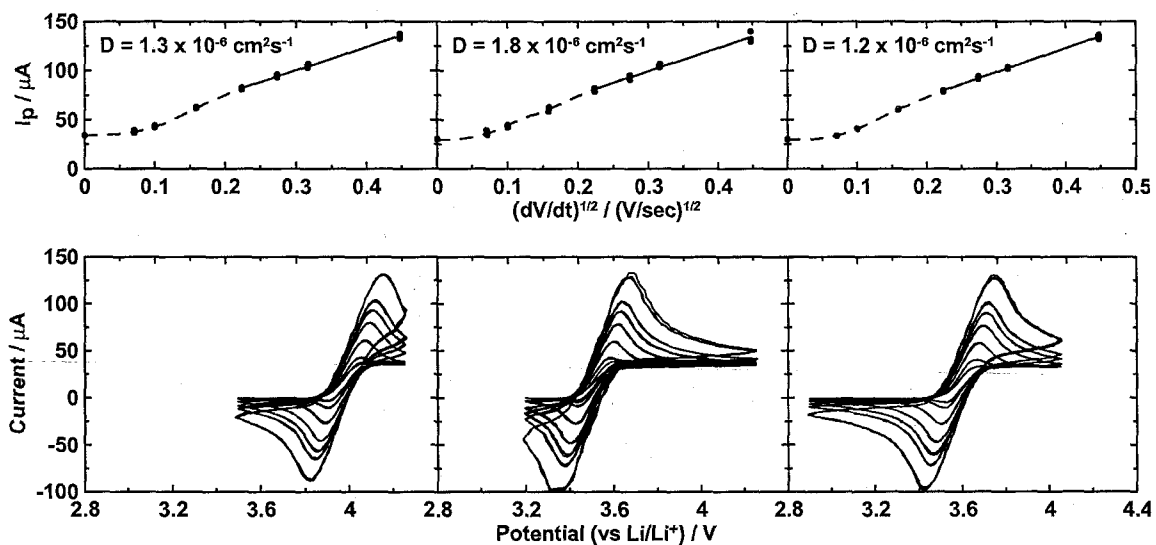


Figure 4.33 Figure 3. Determination of diffusion constants for the molecules 2,5-di-*tert*-butyl-1,4-dimethoxybenzene (left), 2,2,6,6-tetramethylpiperidine-1-oxyl (centre), and 10-methylphenothiazine (right).

The peak currents, I_p , during anodic scans at different sweep rates were used to extract the diffusion coefficient, D , of the shuttle molecules using the Randles-Sevcik equation:

$$I_p = (2.687 \times 10^5 \text{ C mol}^{-1} \text{ V}^{-1/2}) A D^{1/2} C \nu^{1/2} \quad (4-5)$$

where A is the electrode area (cm^2), C is the shuttle concentration (mol/cm^3), ν is the potential scan rate (V/sec), I_p is in units of amperes and D is in units of cm^2/sec . The other values described in equation 2-3 were combined into a single constant, with the

temperature assumed to be 25°C and the number of electrons involved being 1. The sweep rates used to calculate D were 500, 250, 100, 75, 50, 25 and 10 mV/sec.

Figure 4.33 shows the results of CV experiments used to determine the diffusion constants of the three molecules. The diffusion constant is an important property of redox shuttles because it is one of the factors that determines the maximum current capable of being carried by the shuttle [91]. The diffusion constants for the three molecules are $1.3 \times 10^{-6} \text{ cm}^2\text{s}^{-1}$ for DDB, $1.8 \times 10^{-6} \text{ cm}^2\text{s}^{-1}$ for TEMPO and $1.2 \times 10^{-6} \text{ cm}^2\text{s}^{-1}$ for MPT. The similarity in diffusion constant for the three molecules means that none of these molecules is superior to the others in this respect.

Figure 4.33 shows a constant current near the highest potentials scanned at the lower sweep rates in both the upward and downward scans for all three molecules rather than the expected $t^{-1/2}$ decay. This is indicative of a continuous shuttle current between the working and counter electrode. The path length between the working electrode and the counter electrode was approximately 5 mm, and this was apparently not long enough to approximate the semi-infinite conditions needed for equation 4-5. Thus, the use of equation 4-1 can only be justified at the highest sweep rates. The slopes in Figure 4.33 have been calculated from the data points at the four highest sweep rates, and the best fit to those points is shown by the solid line. The dashed line is a schematic that shows that the peak current does not extrapolate to zero under these measurement conditions. However, the presence of this background shuttle current effectively adds an offset to the values of I_p and hence the lines in Figure 4.33 do not intercept at the y-axis at $I_p = 0$. Since it is the slopes from Figure 4.33 that are used to calculate the diffusion coefficients, which are not affected by this offset, the diffusion currents reported are reliable.

Each of the three molecules was cycled in a CV cell in LiBOB-based electrolytes and LiPF₆-based electrolytes to a variety of lower cutoffs. This was to determine the effect of low potential on each molecule. In coin cells with graphite negative electrodes, the potential of the graphite electrode is near that of lithium, so it is important to check the stability of the shuttle molecules at low potentials. Figure 4.34 shows the results of such an experiment for the shuttle MPT. Figure 4.34 shows that in LiBOB-containing electrolyte, at potentials around 0.9 V vs Li/Li⁺, the oxidation current from the shuttle at high potentials begins to decrease, and at 0.4 V, there is no further oxidative current. All three molecules show similar results to that of MPT, with the effect being less pronounced for DDB than for either TEMPO or MPT. In LiPF₆-based electrolytes, the oxidation current is slightly reduced at very low potentials, but it is never stopped, as is the case with LiBOB-based electrolytes. This is not due to any permanent destruction of the shuttle molecules within the cell. This is known because cells that were cycled to a lower cutoff of 0.2 V and showing no subsequent oxidation could be returned to normal operation after a few cycles with the lower cutoff set to 3 V. This reduction in oxidation current is therefore attributed to the buildup of a resistive layer on the surface of the electrode that is stripped off when the electrode is at higher potentials.

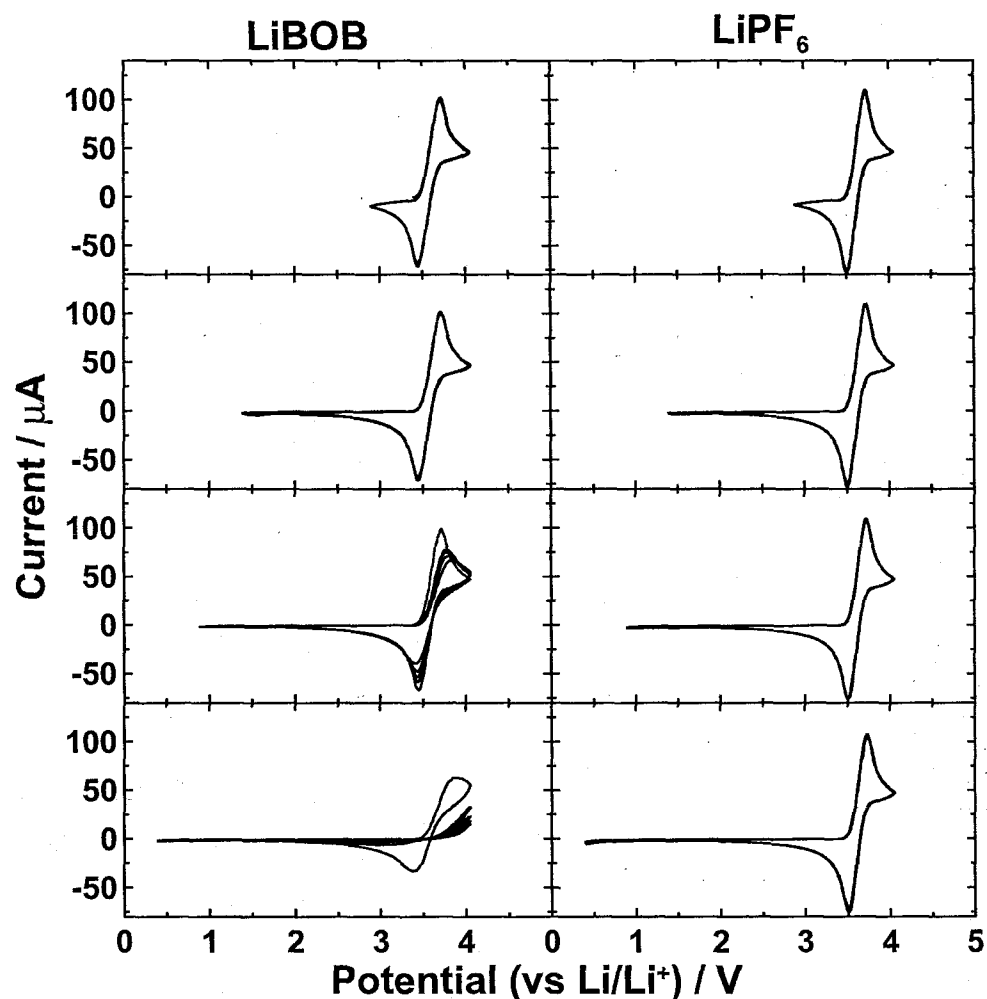


Figure 4.34 Figure 4. Cyclic voltammograms of 10-methylphenothiazine in LiBOB and LiPF₆-containing electrolytes to a variety of lower cutoff potentials.

Given that a single electrode in a normally operated lithium-ion cell does not change its potentials over the entire range of 0.2 V to 4.0 V, how close can these CV experiments mimic lithium-ion cell experiments? In lithium-ion coin cells, one electrode is the negative electrode and during normal cell operation it is below the potential of the positive electrode. During overcharge, the positive electrode is the site of oxidation and the negative electrode is the site of reduction. In CV experiments, one working electrode is swept in potential so it acts as both the site of oxidation and reduction. To more

closely approximate the conditions in a lithium-ion coin cell, the CV cell was modified to incorporate a second working electrode. Figure 4.35 shows the resulting electrode geometry and how shuttling occurs in such cells. One electrode becomes a 'positive' electrode and is the site of oxidation of shuttle molecules in the cell, the other working electrode is the 'negative' electrode. The shuttling process then occurs between these two electrodes, as it would inside a lithium-ion coin cell.

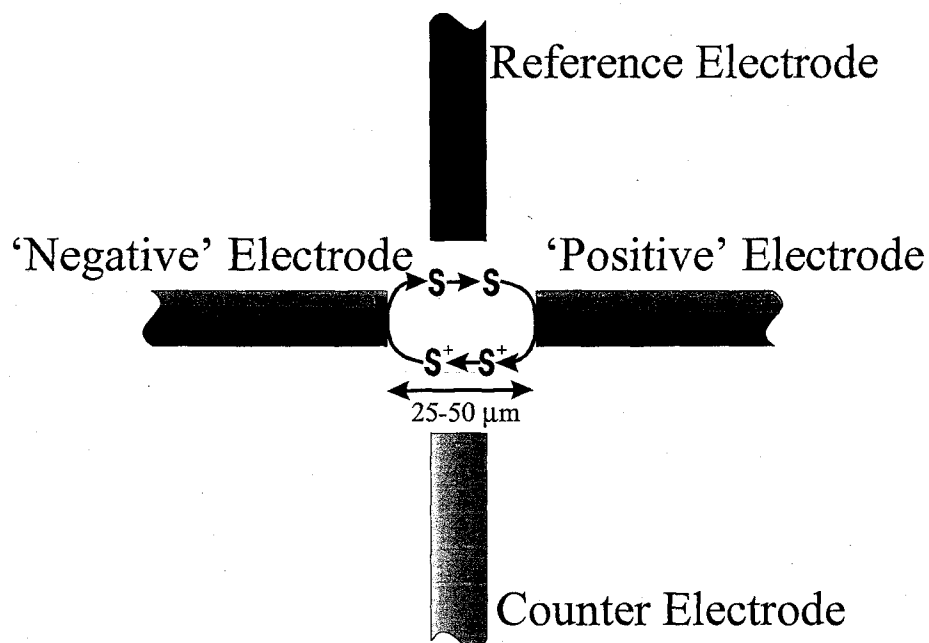


Figure 4.35 Figure 5. Electrode setup for 4-electrode cyclic voltammetry experiments.

The spacing of the two working electrodes in the cell of Figure 4.35 is adjusted by eye and then estimated from the diffusion constant of the shuttle molecule and the amount of time it takes for a reductive current to register at the negative electrode after the positive electrode begins to oxidize the shuttle. The spacing between the electrodes is on the order of 25 to 50 μm , which is similar to that in lithium-ion coin cells.

Typical experiments using the 4-electrode cell involved holding the positive electrode at a potential just above that required to oxidize the shuttle molecule, 4.0 V for the molecule DDB, which has a redox potential of 3.92 V, and the negative electrode is then cycled through a series of CV experiments with the lower cutoff potential periodically being stepped down. It is known that there is reduction of impurities in the LiBOB salt at 1.7 V and SEI formation in LiPF₆ based electrolytes around 0.8 V [17], which can be probed. In this experiment, the negative electrode is able to form surface layers from the reduction products of the electrolyte while being bathed in a constant flow of oxidized shuttle molecules from the positive electrode.

Figure 4.36 shows the results of 4-electrode CV experiments for DDB, TEMPO and MPT in both LiBOB and LiPF₆ based electrolytes. As the lower cutoff is swept down for the molecule DDB, the reduction current is decreased. This is believed to be due to a thickening of the SEI layer on the electrode surface at lower potentials. These results clearly show that charge transfer to the oxidized shuttle molecule can take place through the electronically insulating SEI layer. It is our opinion that this occurs by electron tunnelling to a final state (the oxidized shuttle molecule) that is significantly lower in energy than the final state represented by the reaction of the same electrons with Li⁺ ions and solvent molecules. Thus, even though the buildup of the SEI has stopped because the electron tunnelling rate to Li⁺ and solvent molecules in the electrolyte has become near zero due to SEI thickening, tunnelling of electrons to the oxidized shuttle molecule can still occur.

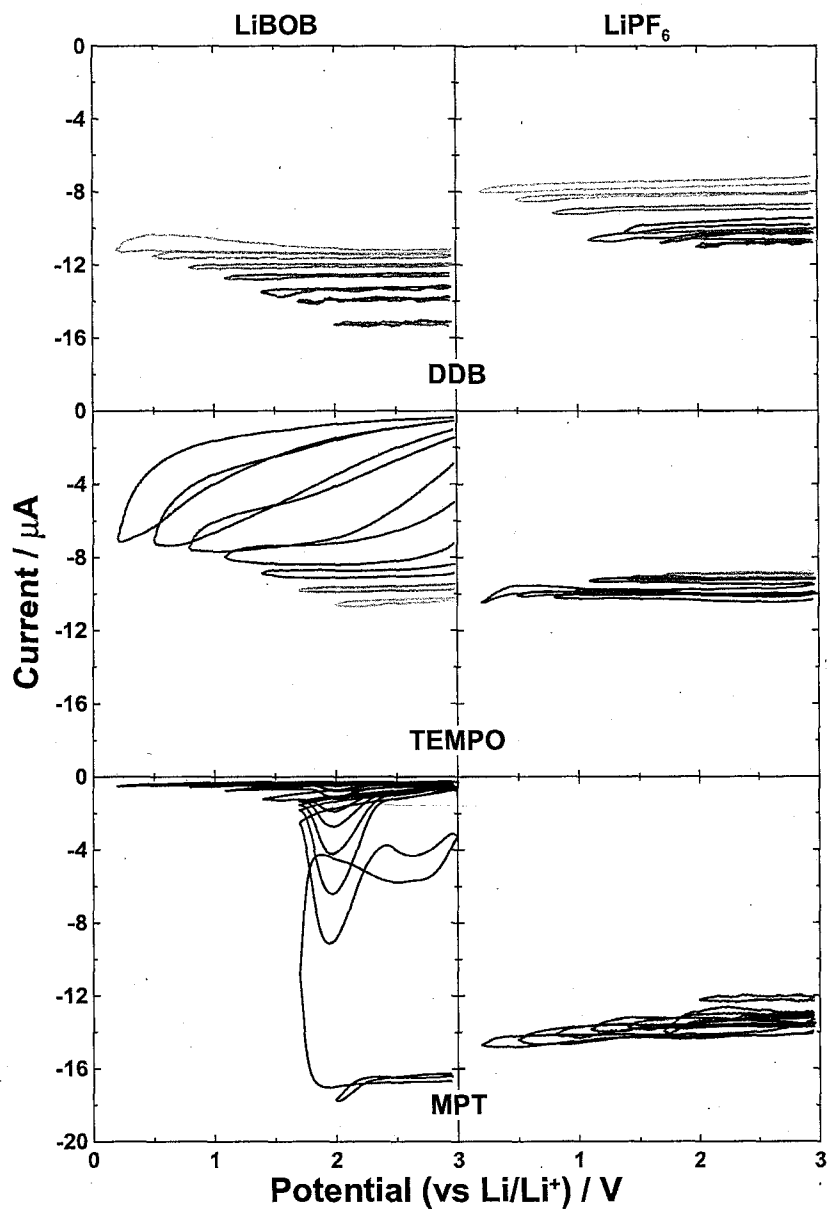


Figure 4.36 Figure 7. Results from a series of 4-electrode cyclic voltammetry experiments with the molecules 2,5-di-*t*-butyl-1,4-dimethoxybenzene, 2,2,6,6-tetramethylpiperidine-1-oxyl, and 10-methylphenothiazine, in both LiBOB (left) and LiPF₆ (right) based electrolytes.

The molecule TEMPO shows different results in 4-electrode CV experiments depending on the electrolyte salt used. In LiBOB-containing electrolytes, when the lower cutoff is reduced below about 1.5 V, the current measured at the negative electrode is reduced and varies strongly with potential. It is known that LiBOB-containing

electrolyte has irreversible reduction at around 1.7 V [17]. The presence of these reduction products is apparently interfering with the charge transfer to the oxidized TEMPO shuttle molecule in some way. The results in Figure 4.36 suggest that Li-ion cells with $\text{Li}_{4/3}\text{Ti}_{5/3}\text{O}_4$ negative electrodes will function normally with TEMPO shuttles in LiBOB-containing electrolyte, but will not when graphite negative electrode are used, which has been shown to be the case [124].

Figure 4.36 also shows that the molecule MPT shows unusual results in LiBOB based electrolyte. Below about 1.7V, there is a reaction that prevents any further reduction at the negative electrode. Presumably, there is a surface film formed from the reduction products of LiBOB, possibly MPT and possibly electrolyte components that prevents charge transfer. In LiPF_6 -based electrolytes, the film that is formed does not present a barrier to charge transfer and the reduction of the oxidized shuttle molecules occurs at all potentials scanned in the test. Studies of the MPT shuttle in lithium-ion coin cells [125] have shown that normal operation was observed with $\text{Li}_{4/3}\text{Ti}_{5/3}\text{O}_4$ negative electrodes in both LiBOB and LiPF_6 electrolytes, but that cells with graphite electrodes only showed stable shuttle effects when LiPF_6 electrolyte was used, in agreement with Figure 4.36.

The results in Figure 4.36 and from lithium-ion coin cell testing are summarized in Table 4-6. In those cases where the negative electrode current in Figure 4.36 is well-behaved at all potentials (LiPF_6 with all shuttles as well as LiBOB with DDB), lithium-ion coin cells showed a stable long-lived shuttle effect. In cases where the negative electrode current in Figure 4.36 showed anomalies at low potentials, lithium-ion coin cells did not show a stable long-lived shuttle effect. The exception to this is TEMPO.

Coin cells containing TEMPO in LiPF₆-based electrolytes did not cycle at all, and in LiBOB-based electrolytes, the cells would cycle only when a partially precharged negative electrode was used. This result is important because it highlights the importance of doing tests on real cells and not just CV studies.

Table 4-6 Summary of coin cell results for the shuttles DDB, TEMPO and MPT with either Li_{4/3}Ti_{5/3}O₄ or graphite negative electrodes and either LiBOB or LiPF₆ based electrolytes.

Shuttle Molecule	Negative Electrode	Electrolyte	# 100% overcharge cycles sustained at C/10	Anomalies observed in Figure 7 below 1.7 V
DDB	Li _{4/3} Ti _{5/3} O ₄	LiPF ₆	348	No
DDB	Li _{4/3} Ti _{5/3} O ₄	LiBOB	363	No
DDB	graphite	LiPF ₆	334	No
DDB	graphite	LiBOB	312	No
MPT	Li _{4/3} Ti _{5/3} O ₄	LiPF ₆	162	No
MPT	Li _{4/3} Ti _{5/3} O ₄	LiBOB	156	Yes
MPT	graphite	LiPF ₆	56	No
MPT	graphite	LiBOB	13	Yes
TEMPO	Li _{4/3} Ti _{5/3} O ₄	LiPF ₆	0	No
TEMPO	Li _{4/3} Ti _{5/3} O ₄	LiBOB	124	Yes
TEMPO	graphite	LiPF ₆	0	No
TEMPO	graphite	LiBOB	15	Yes

In Figure 4.36, the molecule DDB shows a shuttle current which is relatively invariant with respect to the lower cutoff potential. DDB would be expected to function normally in cells with Li_{4/3}Ti_{5/3}O₄ or graphite negative electrodes. This is indeed the case, where the molecule DDB has been shown to provide the largest number of cycles of overcharge protection of any molecule studied.

Coin cells containing MPT or TEMPO both show poorer cyclability in the cells with graphite negative electrodes than in cells with Li_{4/3}Ti_{5/3}O₄ negative electrodes. This,

presumably, is due to the reduction potential of the shuttle molecules being near or above 0 V, meaning that there could be a noticeable amount of reduction products present when the cell with an MCMB negative electrode is fully charged. The presence of these products could severely affect the ability of the shuttle molecules to protect the cell. The choice of electrolyte salt appears to have an effect on the length of overcharge protection, as well. For TEMPO, with LiPF_6 as the salt, there was no shuttling seen and the cells were only protected against overcharge with LiBOB as the salt. With MPT as the shuttle molecule, the coin cell data show slightly better results with LiPF_6 -containing electrolytes. It would appear that the choice of salt is important when selecting a shuttle molecule, but that one salt is not necessarily the best for all shuttles. The discrepancy between coin cell results and four-electrode CV results for the case of TEMPO reinforces the necessity of full cell testing for the determination of which molecules make good shuttle molecules.

These three molecules DDB, TEMPO and MPT have been shown to provide excellent overcharge protection in lithium-ion cells. Further testing of these molecules, by cyclic voltammetry and four-electrode cyclic voltammetry, has shown that these three molecules have different characteristics. The molecule DDB has shown to provide stable protection for hundreds of cycles and is the most stable of the three molecules at low potentials, but its stability is very sensitive to potentials above 4.0 V. The molecules MPT and TEMPO are both shown to be more resistant to potentials above their oxidation potentials, but they are also less stable at low potentials, which might prevent their use in cells with graphite negative electrodes. Understanding the specific strengths and

weaknesses of each shuttle molecule is necessary to decide which molecule to use in a specific cell.

Chapter 5. High Potential Shuttles

There is demand in industry for redox shuttle molecules that have oxidation potentials above 4.2 V. Shuttles with these potentials would find use in lithium-ion batteries with a wider range of positive electrode materials, not just in cells with LiFePO_4 positive electrodes. It has been a challenge to find molecules that have both a suitable potential for higher potential materials and that show lengthy overcharge protection in lithium-ion cells. As mentioned previously, electron withdrawing groups can be used to raise the potential of a molecule. Presented here are the results from some fluorinated shuttle molecules that have high oxidation potentials.

5.1. Fluorinated Naphthalenes

The search of highly fluorinated aromatic molecules turned up two interesting shuttle candidates. The molecules octafluoronaphthalene (OFN) and 2-methoxyheptafluoronaphthalene (HFN) are both highly fluorinated, which should result in high oxidation potentials, and their aromaticity allows for increased stability of the radical cation formed upon oxidation.

Figure 5.1 shows the cycling of 0.1 M OFN in a $\text{LiFePO}_4/\text{MCMB}$ cell. The shuttling is occurring at a high potential, above 4.5 V, but the number of cycles of 100% overcharge are relatively few. However, for several cycles after the full overcharge protection is lost, there remains at least some shuttling in each cycle. As seen in previous shuttle experiments, when a shuttle molecule fails within a cell, the overcharge protection fades in a matter of a few cycles. In this case, there is a significant amount of shuttling

seen for many cycles. This, combined with the fact that the shuttling potential is so close to the upper cutoff voltage of the experiments, suggests that perhaps the shuttle is not dead, but merely unable to fully operate within the experimental boundaries.

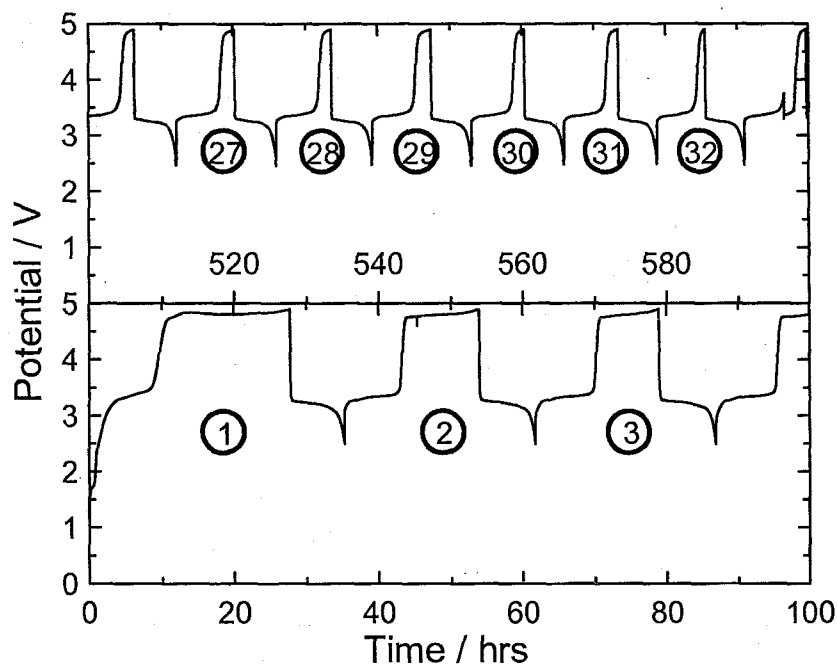


Figure 5.1 Coin cell data for a cell containing 0.1 M OFN in an electrolyte composed of 0.5 M LiBOB in PC:DMC:EC:DEC. The cell was charged at C/10 rate for 20 hours then discharged at C/10 rate.

Additional tests were performed on new cells where the overcharge per cycle was limited to 20% and the upper voltage cutoff was raised from 4.9 V to 5.0 V in an attempt to maximize the amount of shuttling seen. Since the shuttle plateau is upward sloping, the 20% overcharge limit was selected to try and prevent the upper potential cutoff from being reached. Figure 5.2 and Figure 5.3 show the results for OFN cycled under these conditions in a $\text{LiFePO}_4/\text{MCMB}$ cell. The shuttling occurs for over 60 cycles before beginning to taper off. Figure 5.4 and Figure 5.5 show the results for HFN in similar

tests where the cells cycle for over 30 cycles before the overcharge protection begins to fade.

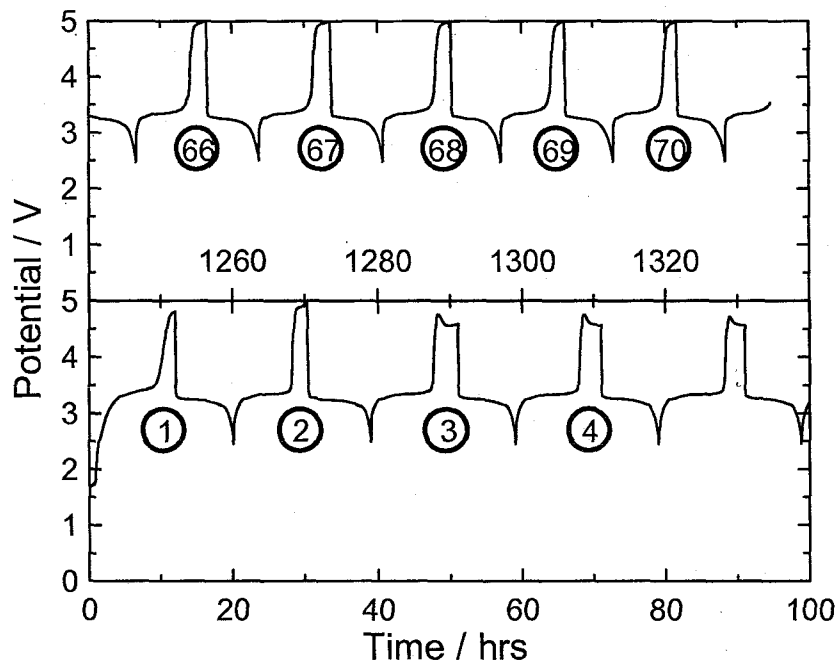


Figure 5.2 Coin cell data for a cell containing 0.1 M OFN in an electrolyte composed of 0.5 M LiBOB in PC:DMC:EC:DEC. The cell was charged at C/10 rate for 12 hours then discharged at C/10 rate.

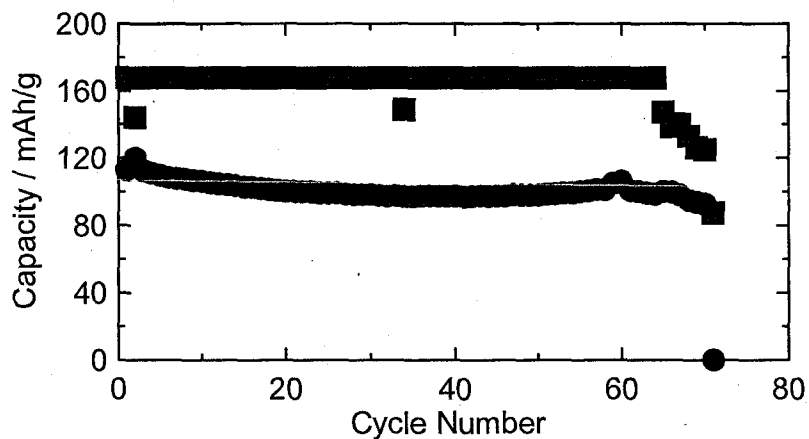


Figure 5.3 Charge (■) and discharge (●) capacities for a cell containing 0.1 M OFN in an electrolyte composed of 0.5 M LiBOB in PC:DMC:EC:DEC. The cell was charged at C/10 rate for 12 hours then discharged at C/10 rate.

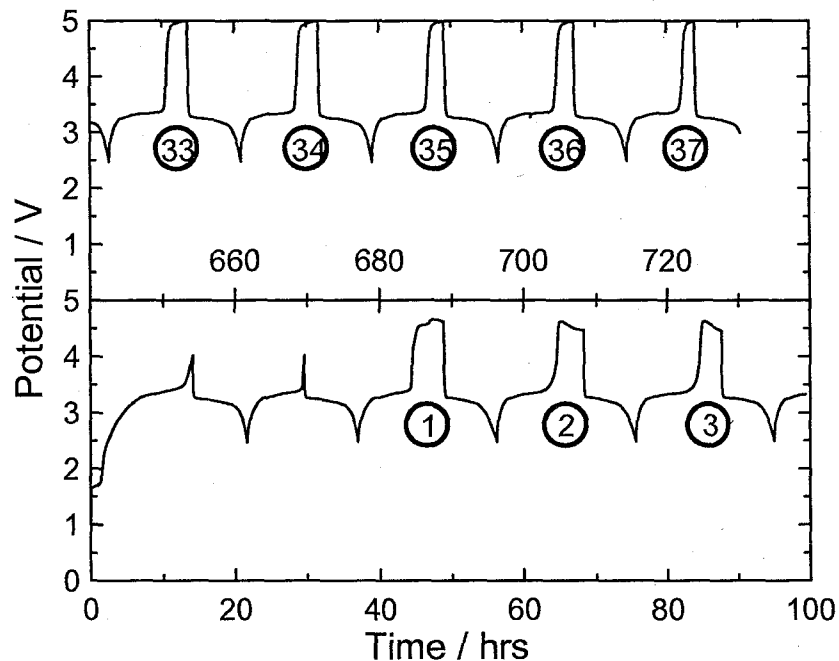


Figure 5.4 Coin cell data for cells containing 0.1 M HFN in an electrolyte composed of 0.5 M LiBOB in PC:DMC:EC:DEC. The cell was charged at C/10 rate for 12 hours then discharged at C/10 rate.

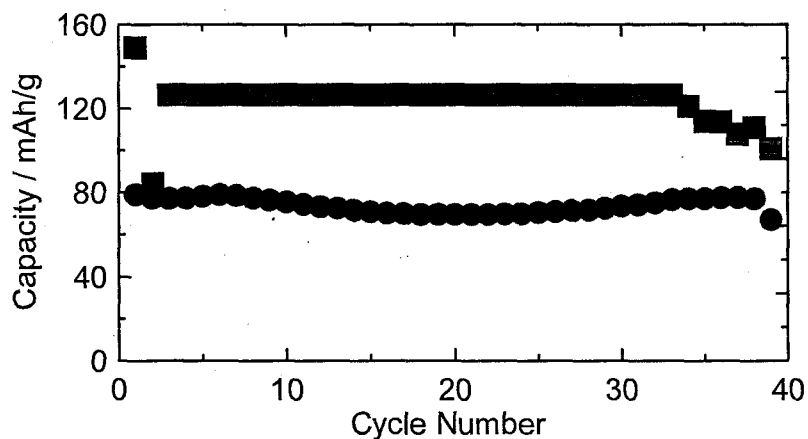


Figure 5.5 Charge (■) and discharge (●) capacities for a cell containing 0.1 M HFN in an electrolyte composed of 0.5 M LiBOB in PC:DMC:EC:DEC. The cell was charged at C/10 rate for 12 hours then discharged at C/10 rate.

The molecules OFN and HFN are molecules that have high shuttling potentials.

The limits of the electrolyte used in the coin cells requires the electrode potentials to stay

below 5 V. While it is of interest to look at these molecules since they are shuttles with very high oxidation potentials, it is doubtful that they could ever be used in manufactured cells since they shuttle at potentials that are well beyond the optimal 0.3 V above the positive electrode potential.

5.2. Substituted Benzenes

The molecule 2,5-di-*t*-butyl-1,4-dimethoxybenzene (DDB) has been previously shown to be a stable redox shuttle for use in lithium ion cells containing LiFePO_4 as the positive electrode material. DDB is a good shuttle molecule for these cells because it is a stable molecule in the voltage range the cell will be cycled through and it has a redox potential at 3.9 V vs Li/Li^+ . Both of these are important characteristics because the shuttle needs to provide protection for a large number of cycles and the shuttle needs to have a reversible oxidation that occurs at a potential that is slightly higher than the potential of the positive electrode at the end of charge to prevent significant self discharge. DDB, however, is unsuitable for use in lithium ion cells containing higher potential positive electrodes, such as LiCoO_2 or $\text{Li}[\text{Ni}_{1/3}\text{Mn}_{1/3}\text{Co}_{1/3}]\text{O}_2$, due its oxidation potential being lower than the potential of these materials at end of charge. For these positive electrode materials, a different molecule with a higher reversible oxidation potential is needed.

Rather than looking for completely new molecules in the search for successful shuttles, another strategy is to try and modify the potential of molecules that are already known to be stable. The molecule 2,5-di-*t*-butyl-1,4-dimethoxybenzene has been proven

to be a very stable shuttle molecule, so if the molecule could be altered to increase the oxidation potential without losing any of the stability its structure provides, perhaps a new, high potential molecule could be found. An example of such a molecule is 2,5-di-*t*-butyl-1,4-bis(2,2,2-trifluoroethoxy)benzene (DBFB). DBFB was synthesized at 3M Co. specifically for testing as a redox shuttle [126]. This molecule is shown here to be a stable redox shuttle with a redox potential of 4.25 V, which is more suitable for use with a variety of positive electrodes. Experiments using Li/LiCoO₂ and Li/Li[Ni_{1/3}Mn_{1/3}Co_{1/3}]O₂ cells show that this molecule can work with high energy density positive electrodes as well as in full cells containing LiFePO₄ positive electrodes and Li, MCMB or Li_{4/3}Ti_{5/3}O₄ negative electrodes.

DBFB was tested in LiFePO₄/Li, LiCoO₂/Li and Li[Ni_{1/3}Mn_{1/3}Co_{1/3}]O₂/Li half cells as well as in LiFePO₄/graphite and LiFePO₄/Li_{4/3}Ti_{5/3}O₄ lithium-ion coin cells. The maximum solubility of DBFB was determined to be 0.14 M at room temperature. Cells were charged using various currents corresponding to a normal recharge in 10 hours (C/10-rate) and cells were charged to 200% of their normal charge capacity or until a specified upper cut-off potential was reached, whichever occurred first.

Figure 5.6 shows the structures of DDB and DBFB. The structure of DDB has been found to provide an unusually high degree of stability to the radical-cation formed by one electron oxidation as evidenced from its unsurpassed shuttling performance in LiFePO₄ cells. The presence of the sterically bulky *t*-butyl groups provides protection for the ring, where the radical and positive charge are located. Also, the symmetry of the molecule helps to stabilize the molecule by more evenly delocalizing the unpaired electron and positive charge around the ring. The structure of DBFB is very similar to

that of DDB. The methoxy groups in DDB are replaced with the more electron withdrawing 2,2,2-trifluoroethoxy groups in DBFB. Because of this, one would expect DBFB to have a higher oxidation potential than that of DDB, as is the case.

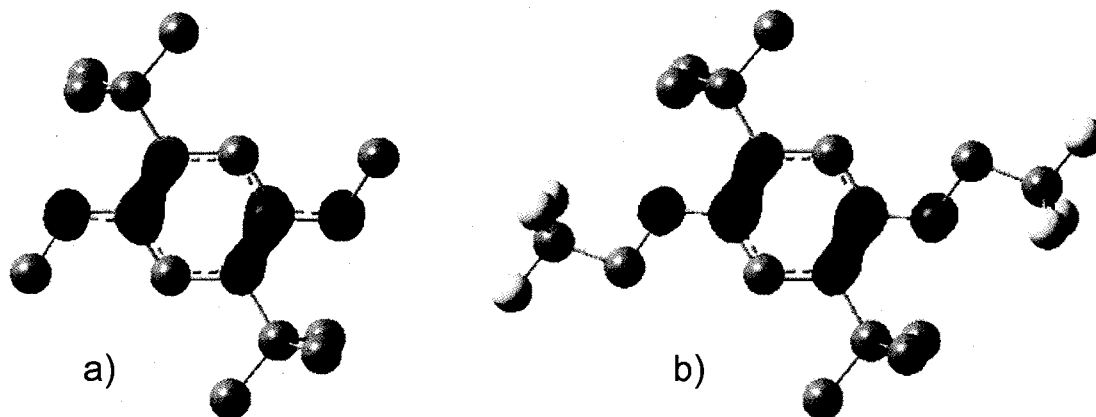


Figure 5.6: Structure and electron density of the LUMO(S⁺) of a) 2,5-di-*t*-butyl-1,4-dimethoxybenzene (DDB) and b) 2,5-di-*t*-butyl-1,4-bis(2,2,2-trifluoroethoxy)benzene (DBFB)

Figure 5.7a shows cyclic voltammetry data for DDB and DBFB between 2.9 V and 4.6 V vs Li/Li⁺ for DDB and between 2.9 V and 4.9 V for DBFB. The reason for the different upper cutoffs is that both molecules have an irreversible second oxidation and going above these potentials results in a large current corresponding to the decomposition of the radical cation formed from the oxidation of the molecules. DDB has an oxidation potential of 3.96 V vs Li/Li⁺ and DBFB has an oxidation potential of 4.25 V. Figure 5.7b shows the CV data for the two molecules with a lower cutoff of 0.2 V vs Li/Li⁺. Figure 5.7b shows that both molecules are reductively stable at low potentials, at least on the time frame of the CV experiments. The similarities in CV data and structures between these two molecules suggests that that DBFB should show high stability in coin cell testing. When the low potential region is blown up, the molecule DBFB shows a larger

reduction current than DDB. This might suggest that DBFB would be less stable in cells that use a graphite negative electrode.

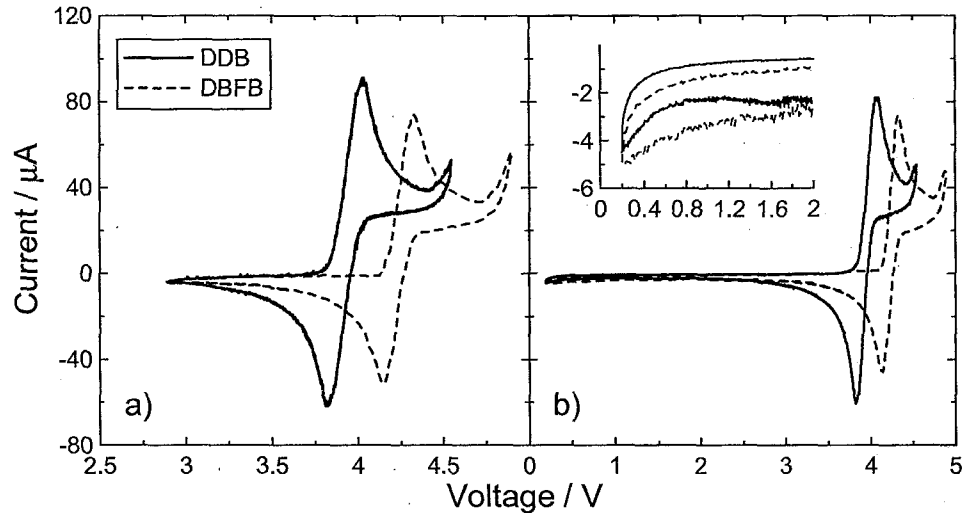


Figure 5.7: Cyclic voltammetry data for DDB and DBFB at a concentration of 0.1 M in a electrolyte composed of 0.5 M LiPF_6 in PC:DMC:EC:DEC. A sweep rate of 100 mV/sec was used. The upper cutoffs used were 4.6 V vs Li/Li^+ for DDB and 4.9 V for DBFB. The lower cutoffs used were 2.9 V vs Li/Li^+ in a) and 0.2 V in b). The insert shows an expanded view of the low potential region.

Figure 5.8 shows 2400, 2500 and 4800 hours worth of coin cell results for DBFB in $\text{LiFePO}_4/\text{Li}$, $\text{LiFePO}_4/\text{MCMB}$ and $\text{LiFePO}_4/\text{Li}_4\text{Ti}_5\text{O}_{12}$ coin cells, respectively. Figure 5.9 shows 1400 and 1100 hours, respectively, worth of coin cell results for half cells containing LiCoO_2 or $\text{Li}[\text{Ni}_{1/3}\text{Mn}_{1/3}\text{Co}_{1/3}]\text{O}_2$ electrodes and 0.1 M shuttle. The coin cells were charged at a constant C/10 rate for 20 hours before being discharged at C/10 rate. Table 5-1 summarizes the results from these coin cell experiments. In all five types of cells, the shuttling is seen for hundreds of hours worth of cycling.

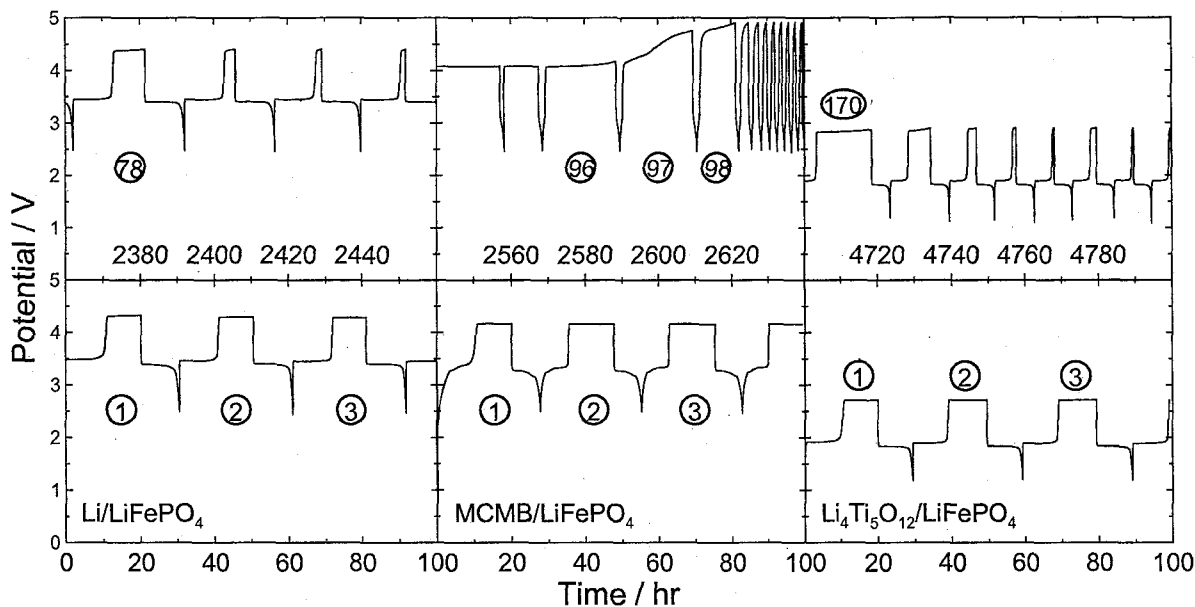


Figure 5.8: Coin cell data for cells containing 0.1 M DBFB in an electrolyte composed of 0.5 M LiPF_6 in PC:DMC:EC:DEC. The cells are; $\text{LiFePO}_4/\text{Li}$, $\text{LiFePO}_4/\text{MCMB}$ and $\text{LiFePO}_4/\text{Li}_{4/3}\text{Ti}_{5/3}\text{O}_4$. Cells were charged at $C/10$ rate for 20 hours then discharged at $C/10$ rate.

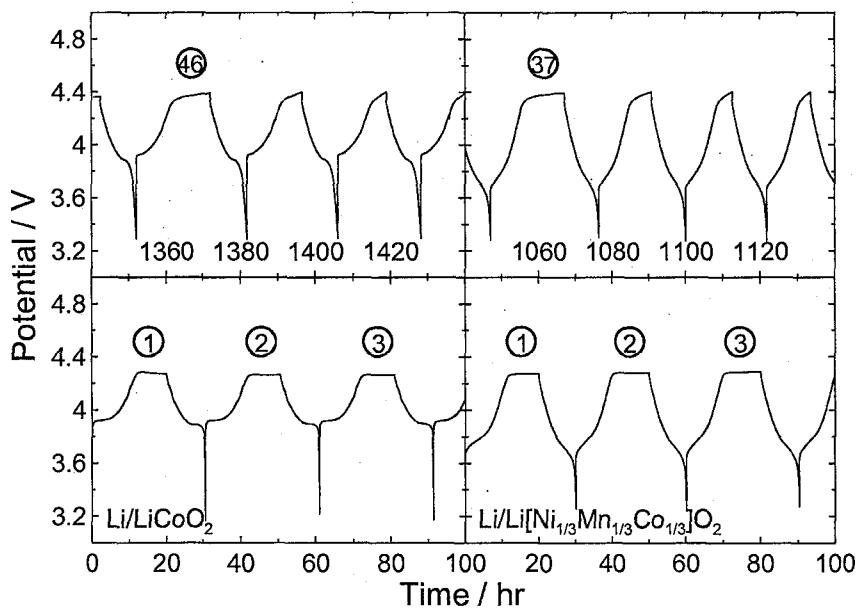


Figure 5.9: Coin cell data for cells containing 0.1 M DBFB in an electrolyte composed of 0.5 M LiPF_6 in PC:DMC:EC:DEC. The cells are LiCoO_2/Li and $\text{Li}[\text{Ni}_{1/3}\text{Mn}_{1/3}\text{Co}_{1/3}]\text{O}_2/\text{Li}$. Cells were charged at $C/10$ rate for 20 hours then discharged at $C/10$ rate.

Table 5-1 Summary of coin cell results for the molecule DBFB.

Negative electrode material	Positive electrode material	No. of 100% overcharge cycles
Li	LiFePO ₄	78
MCMB	LiFePO ₄	98
Li _{4/3} Ti _{5/3} O ₄	LiFePO ₄	170
Li	LiCoO ₂	46
Li	Li[Ni _{1/3} Mn _{1/3} Co _{1/3}]O ₂	37

Figure 5.10 shows the discharge capacities for 100 cycles for cells containing DBFB. Cells with MCMB as the negative electrode have the most rapid capacity fade, while the cell with Li_{4/3}Ti_{5/3}O₄ shows less fade and the cell with Li as the negative electrode shows no capacity fade after 100 cycles. This difference is most likely caused by a reaction between the shuttle the lithium atoms in the negative electrode. Since the lithium in MCMB has a higher chemical potential, it is more reactive than lithium in Li_{4/3}Ti_{5/3}O₄. During the formation of the SEI, an amount of lithium is consumed to form the reductive products needed to stabilize the negative electrode at low potentials. This SEI layer grows as the negative electrode goes to lower potentials. During cycling, if there is any degradation of the SEI, it must be rebuilt, which consumes more Li within the cell. Cells with MCMB or Li_{4/3}Ti_{5/3}O₄ negative electrodes contain all their starting lithium within the LiFePO₄ positive electrode, so as any amount of Li is consumed, the cell capacity drops. Cells with a Li negative electrode contain a large excess of Li, so when Li is consumed within the cell, this excess Li prevents the measured cell capacity from fading. For comparison, 100 cycles of a MCMB/LiFePO₄ cell are shown for a cell that contained no shuttle molecule to show that this fade is not an expected occurrence in

all cells. Also, it should be noted that if the molecule were reductively unstable, the number of cycles seen in cells with Li or MCMB negative electrodes would be significantly smaller than cells with $\text{Li}_{4/3}\text{Ti}_{5/3}\text{O}_4$ negative electrodes. This demonstrates that DBFB is likely not as reductively stable down to lithium potential as DDB.

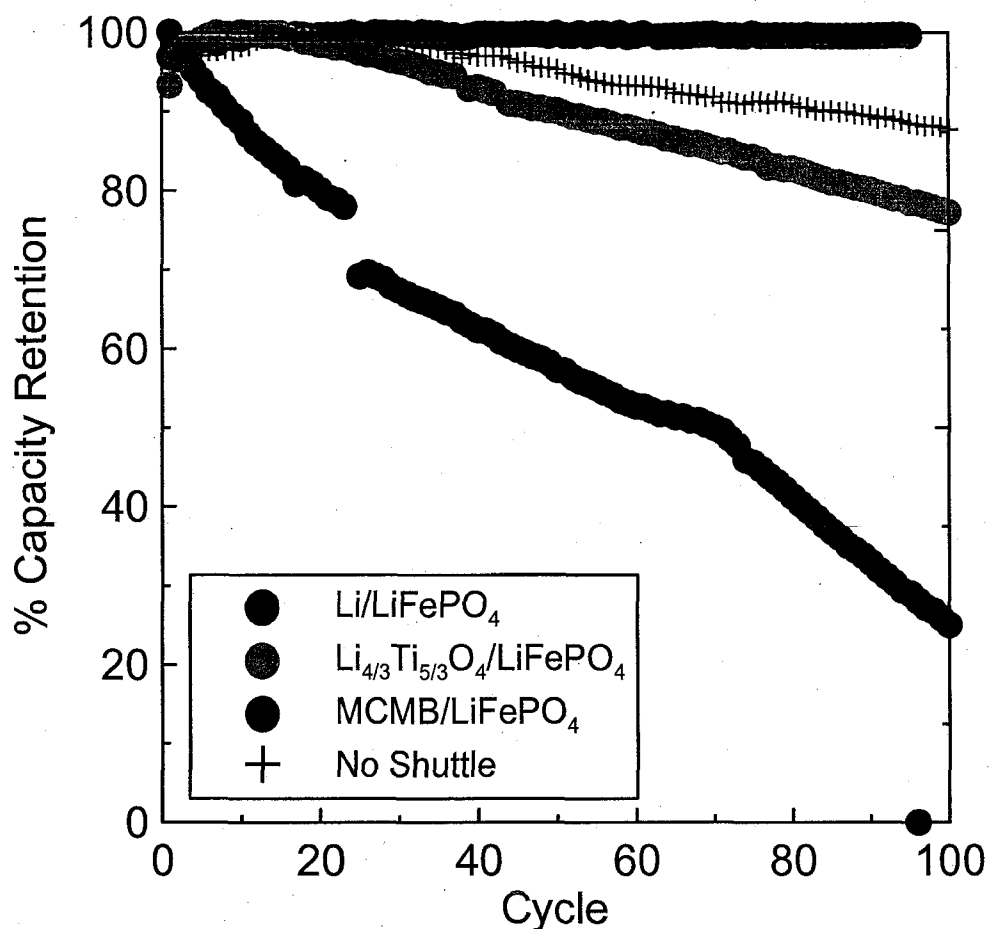


Figure 5.10: Discharge capacities for coin cells containing 0.1 M DBFB in an electrolyte composed of 0.5 M LiPF_6 in PC:DMC:EC:DEC. The cells are; Li/LiFePO₄, MCMB/LiFePO₄ and $\text{Li}_{4/3}\text{Ti}_{5/3}\text{O}_4/\text{LiFePO}_4$. Cells were cycled at C/10 rate. A MCMB/LiFePO₄ coin cell that contained no shuttle is also included for comparison sake.

The molecule 2,5-di-*t*-butyl-1,4-bis(2,2,2-trifluoroethoxy)benzene is one of the most stable shuttle molecules that we have tested that has a redox potential suitable for use in LiCoO_2 and $\text{Li}[\text{Ni}_{1/3}\text{Mn}_{1/3}\text{Co}_{1/3}]\text{O}_2$ -containing lithium-ion cells. The oxidation

potential of this shuttle molecule is 4.25 V vs Li/Li⁺ and it has been shown to provide overcharge protection for a large number of cycles with 100% overcharge each cycle for various cell chemistries.

Chapter 6. Computational Studies

It is not always possible to perform experiments on each and every molecule that can be dreamed up. A large limitation is whether or not molecules are commercially available or easily synthesized. Lack of commercial availability or lack of synthetic knowledge should not limit the ability to screen new molecules for their performance as redox shuttles. An excellent way to screen large numbers of molecules is to use computational methods to evaluate various properties of molecules. Some results obtained from the Gaussian03 computational package are shown in this chapter.

Gaussian is a computational chemistry software program initially released in 1970 by John Pople and his research group at Carnegie-Mellon University as Gaussian 70. It has been continuously updated since then. The name originates from Pople's use of Gaussian orbitals to speed up calculations for Hartree-Fock calculations [127]. The version of the program used for the work presented in this thesis was Gaussian 03 which was released in 2003. Recently, a newer version has been released as Gaussian09. The Gaussian package can perform molecular mechanics calculations, semi-empirical calculations and density functional theory (DFT) calculations, among others. The computational work presented in this thesis was done using DFT, which uses functionals to determine the electronic structure of many-electron systems. All calculations were performed on optimized structures.

Geometry optimization is the process of finding the arrangement of nuclei for which the potential energy is a minimum. Figure 6.1 shows the general shape of the total energy as it relates to the distance between two nuclei. At short range, the interactions between the nuclei repel one another, and at longer ranges, the nuclei attract one another.

The lowest energy is at the equilibrium bond length (r_e), where the derivative of the potential energy curve is zero. The geometry optimization procedure involves using an initial guess for the geometry and then calculating the gradient of the potential energy with respect to each of the nuclear coordinates. The gradient represents the force acting upon each atom. These energy gradients are then used to obtain a new geometry that is likely to be closer to the equilibrium geometry. This process is repeated until the energy gradients approach zero, indicating that an equilibrium geometry has been found.

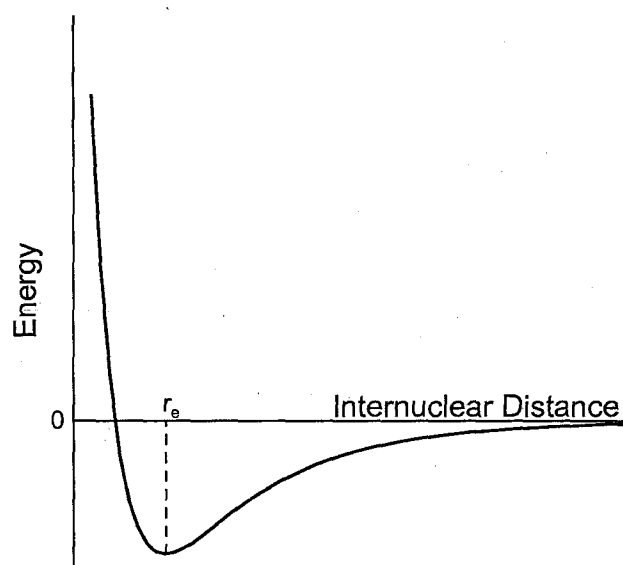


Figure 6.1 Potential energy curve showing the energy as a function of internuclear distance.

One way to display the electron density of a molecule is to choose a particular value of the electron density and show all points in space where the density has the chosen value. This value is known as the isovalue and is given in units of electron/Bohr³, where 1 Bohr = 0.529 Å. This surface provides a three-dimensional picture of the electron distribution and is not intended to mean that the electron cloud has a sharp, well defined edge. The choice of isovalue can have an effect on the data presented.

The 0.002 isovalue surface typically includes around 98% of the electron density and can be used to define the size and shape of the electron cloud [128]. It is a useful surface for mapping properties that affect intermolecular interactions. Higher isovalue surfaces are less diffuse and are more localized to the nuclei and are useful for investigating bonding interactions inside a molecule. Figures in this thesis are shown using an isovalue of 0.08 electrons/Bohr³.

The Gaussian computational package has been used in a large number of fields in Chemistry. There have been numerous reported applications in the field of lithium-ion batteries. A few such uses will be summarized here. The oxidation potentials of solvents for use in lithium-ion batteries at the positive electrode have been examined [129]. The solvents used in lithium-ion batteries must have very large windows of electrochemical stability to accommodate the potentials of the electrodes in the cell. For the same reason, the reduction of solvents is also of interest at the negative electrode [130]. The reaction pathways of solvents used in lithium-ion batteries are of interest and have also been studied [131] as well as the decomposition of the salt LiPF₆ and the stability of the decomposition product PF₅ [132]. In many of these cases, solvent effects are quite significant and should not be overlooked when drawing conclusions from calculated results. These are just a few examples of some of the applications of the Gaussian computational package in the field of lithium-ion batteries to demonstrate that there are numerous successes in using it and that it is a valid tool in this research field.

As stated in the Introduction, the calculations presented in this chapter were performed by Dr. Richard Wang and are included here to compare to the experimental results.

6.1. Method

The most important properties for determining the suitability of a molecule as a redox shuttle are its oxidation potential and stability. In two recent papers [133,134], Wang and Dahn demonstrated how the oxidation potential and stability of a shuttle molecule can be predicted by calculations based on density functional theory using the Gaussian03 computational package [135].

The standard oxidation potential E^0 , in V, of a neutral species S corresponds to the negative change in the standard free energies of formation G^0 , in eV, between the species S and its cation S^+ , divided by the electron charge e . To get values relative to the Li/Li⁺ redox couple, the negative change in the standard free energies between a Li atom in Li metal and a Li cation in electrolyte, or 1.46 V is subtracted [136] to give the following formula [133]:

$$E^0(S) = \frac{-[G^0(S) - G^0(S^+)]}{e} - 1.46V \quad (6-1)$$

The standard free energy of a molecule is approximately obtained using the B3LYP [137,138] density functional theory model and a 6-31G(d, p) basis set combined with the polarizable continuum model (PCM) to include the solvent effects. In an earlier paper, the oxidation potentials of seventeen molecules used as shuttle additives in Li-ion cells were calculated and compared with experiment [133]. The root mean square deviation between the calculated and measured oxidation potentials of these seventeen molecules was shown to be 0.15 V with the maximum deviation being 0.25 V.

One way to estimate shuttle stability is to analyze the possible reactions in which an oxidized shuttle radical may participate. This would be a very lengthy process and would require knowledge of all the possible reactions that could occur in the system over

a range of potentials. A simpler way, described by Wang and Dahn [134], was to choose the ethyl radical, ER, as a "reactivity detector". The calculated binding energy between the oxidized shuttle radical S^+ and the ER, $E_b(ER)$, is defined as:

$$E_b(ER) = \max\{E_t(S^+) + E_t(ER) - E_t(ER_S^+)\} \quad (6-2)$$

where $E_t(S^+)$, $E_t(ER)$ and $E_t(ER_S^+)$ are the total energies of the oxidized shuttle (S^+), the ethyl radical (ER) and the adduct of the ER and S^+ (ER_S^+), respectively.

The maximum value of $E_b(ER)$ can be used as the reactivity index of an oxidized shuttle taking into account a variety of configurations. In the calculations, the ethyl radical is positioned next to the various nuclei in a molecule and the binding interaction between the ethyl radical and that nucleus is calculated. Initially, ions were selected to be used as reactivity detectors. The electrolyte contains ions such as Li^+ or PF_6^- , so they were originally chosen, however the calculated binding energies did not match up with experimental results. The ethyl radical, which is a small and neutrally charged, is thought to more closely mimic possible reactions with other organic molecules and since it is also a radical, it should show strong binding energies with other radicals present in the electrolyte, such as the oxidized shuttle molecule. The ethyl radical was determined to be the reactivity detector that best matched experimental results.

In general, a larger $E_b(ER)$ indicates that the oxidized shuttle radical is more reactive and therefore less stable. Previously, the calculated ethyl radical binding energies of nineteen selected oxidized shuttle molecules show approximately the correct trend with respect to their experimental stability [134]. Among the nineteen selected shuttle molecules, there are three experimentally stable shuttles: 2,5-di-*t*-butyl-1,4-dimethoxybenzene, 3-chloro-10-ethylphenothiazine and 10-methylphenothiazine, each of

which provided protection for over one hundred cycles of 100% overcharge. These molecules had calculated binding energies ($E_b(\text{ER})$) of, less than 1.73 eV. On the other hand, the remaining sixteen shuttle molecules provided overcharge protection for only a few cycles except for one molecule that provided protection for 33 cycles. These molecules had calculated binding energies, $E_b(\text{ER})$, larger than 1.73 eV. Therefore, it was proposed that $E_b(\text{ER})$ could be used as a tool to predict the stability of a redox shuttle molecule: a redox shuttle molecule is assumed to be stable, probably stable, probably unstable and unstable if its $E_b(\text{ER})$ value is smaller than 1.65 eV, between 1.65 and 1.75 eV, between 1.75 and 1.85 eV, and larger than 1.85 eV, respectively.

6.2. Motivation

One of the most successful shuttle molecules for LiFePO_4 based cells is 2,5-di-*t*-butyl-1,4-dimethoxybenzene (DDB). After the success of this molecule as a shuttle, additional similar molecules were purchased for testing. These were comprised of methoxy and *t*-butyl substituted benzenes that were commercially available. These molecules all showed very poor results as shuttles [139]. It was believed that the only successful molecule from this class of molecules was DDB, which had already been found and patented. Later, after a publication by Feng et al. [140], another molecule, 4-*t*-butyl-1,2-dimethoxybenzene that they synthesized, was proposed to be a successful shuttle molecule. In order to not miss out on any additional molecules in this group, a survey of 43 molecules was carried out.

The 43 molecules chosen were chosen based on the following structure characteristics; starting with benzene, each molecule has between 1 and 3 *t*-butyl groups;

and between 0 and 5 methoxy groups. The substituent groups are then in placed in various positions around the benzene ring with the only restriction being that the bulky *t*-butyl groups would not be on adjacent carbons.

The calculated properties of these 43 molecules as redox shuttles are summarized in Table 6-1, where E_{ox} in V is the oxidation potential, $E_b(ER)$ in eV is the binding energy of the oxidized shuttle molecule with the ethyl radical, defined by Equation 6-2 and used as a reactivity index.

Table 6-1 Calculated properties of 43 molecules as redox shuttles: E_{ox} - the oxidation potential vs Li/Li^+ ; $E_b(ER)$ - the maximum binding energy of the molecule with the ethyl radical, which is a reactivity index.

No.	Shuttle	E_{ox}/V	$E_b(ER)/eV$
1	T-----	4.99	2.61
2	TM-----	4.36	2.29
3	T-M----	4.36	2.19
4	T--M---	4.25	2.11
5	TMM----	3.89	1.96
6	TM-M---	3.97	2.30
7	TM--M--	3.81	1.87
8	TM---M	4.23	2.56
9	T-MM---	3.9	1.86
10	T-M-M--	4.40	2.74
11	TMMM---	4.08	2.15
12	TMM-M-	3.55	1.71
13	TMM--M	3.64	1.91
14	TM-MM-	3.58	1.42
15	TM-M-M	3.98	2.48
16	T-MMM-	3.61	1.76
17	TMMMM-	3.56	1.59
18	TMMM-M	3.44	2.10
19	TMM-MM	3.32	1.49
20	TMMMMM	3.47	1.99
21	T-T----	5.03	2.38
22	TMT----	4.48	2.39
23	T-TM---	4.29	1.82
24	T-T-M-	4.52	2.2
25	TMTM---	4.24	2.29
26	TMT-M-	4.08	1.96
27	T-TMM-	3.88	1.63
28	T-TM-M	3.96	1.82
29	TMTMM-	3.73	2.08
30	TMTM-M	4.00	2.17
31	T-TMMM	4.05	1.8
32	TMTMMM	4.13	2.08
33	T--T---	4.83	2.17
34	TM-T---	4.34	2.03
35	TMMT---	4.36	2.01
36	TM-TM-	3.88	1.44
37	TM-T-M	4.45	2.69
38	TMMTM-	3.88	1.94
39	TMMTMM	3.87	1.84
40	T-T-T-	5.10	2.14
41	TMT-T-	4.51	2.02
42	TMTMT-	4.37	2.02
43	TMTMTM	4.29	1.97

6.3. Nomenclature

Since there are a large number of molecules discussed in this section, a simple shorthand is used to describe the substitution pattern on the ring. Figure 6.2 shows an

example of the nomenclature system used. For each of the 43 molecules in this group, a code of six consecutive symbols is used to express the substitution pattern. The i^{th} symbol corresponds to the substituent bonded on the i^{th} ring carbon, C(i), with 'T', 'M' and '-' representing *t*-butyl, methoxy and a hydrogen atom, respectively. Since each molecule has at least one *t*-butyl group, atom C(1) on the aromatic ring always bonds to a *t*-butyl group. Therefore, 2,5-di-*t*-butyl-1,4-dimethoxybenzene, is denoted as TM-TM- under this naming scheme. In addition, each molecule is given a number from 1 to 43 corresponding to its place in Table 1 to make it easier for the reader to find the corresponding data.

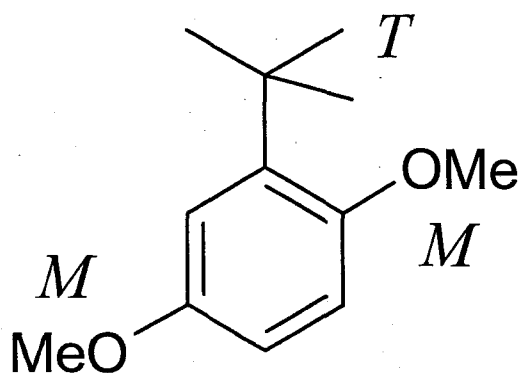


Figure 6.2 Explanation of the naming scheme used to describe the molecules in this paper. The symbol TM--M- represents this molecule, where 'T', 'M' and '-' stand for *t*-butyl, methoxy and hydrogen bonded on a ring carbon atom, respectively. The name for this molecule would be 2-*t*-butyl-1,4-dimethoxybenzene.

6.4. Results

To understand the trends of the calculated redox properties of these 43 molecules, it is necessary to know how an individual *t*-butyl or methoxy group bonded on the aromatic ring impacts the redox properties of benzene and the consequence of interactions between these groups. Figure 6.3 shows the effects of an individual *t*-butyl or methoxy group on the electron density of benzene. The calculated $E_b(\text{ER})$ values for different atom sites are given for benzene, T-----, M----- with an in-plane methoxy group and M----- with an out-of-plane methoxy group. The electron densities of the LUMOs of the oxidized shuttle radicals for the latter three molecules are also shown in Figure 6.3 at an isovalue of $0.08/\text{Bohr}^3$.

On a neutral shuttle molecule S, there are two electrons in the highest occupied molecular orbital, HOMO(S), with paired spins. Upon oxidation, one of them, say β -HOMO - the spin-down HOMO, is extracted, thus the shuttle molecule S is oxidized to the radical cation S^+ . The former α -HOMO - the spin-up HOMO, is still occupied and becomes the singly occupied molecular orbital of the radical cation S^+ , SOMO(S^+), while the unoccupied former β -HOMO becomes the lowest unoccupied molecular orbital of the radical cation S^+ , LUMO(S^+). The orbital energy of the LUMO(S^+) is lowered through interactions with the electrolyte to be close to that of the HOMO(S). In other words, a shuttle radical tends to associate with other species in the electrolyte and attract electron charge into its LUMO(S^+). Therefore the LUMO(S^+) is the most important orbital, although not the only orbital, that governs the reactivity of an oxidized shuttle radical.

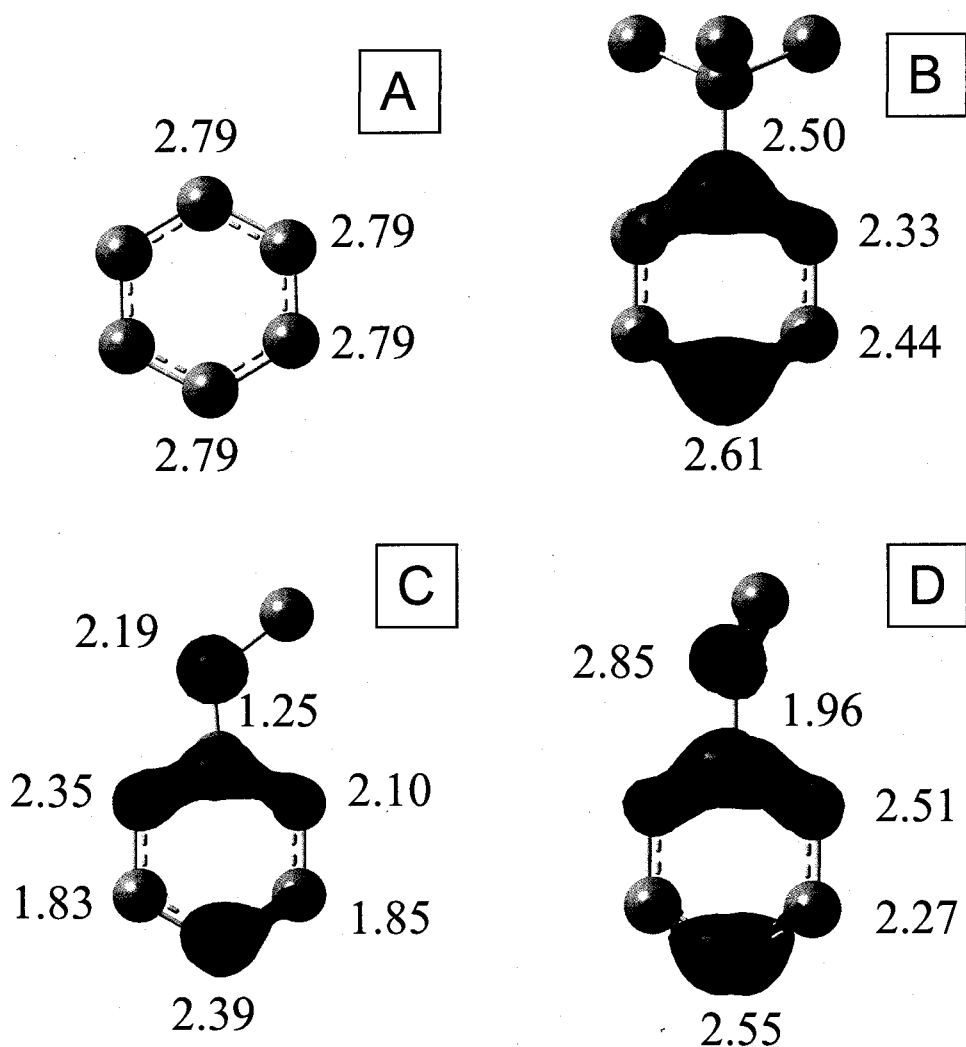


Figure 6.3 The effects of single *t*-butyl or methoxy substituent on oxidation potentials and reactivity. A. Benzene with $E_{\text{ox}} = 5.24\text{V}$; B. T----- with $E_{\text{ox}} = 4.99\text{V}$; C. M----- with a methoxy in the plane of the aromatic ring with $E_{\text{ox}} = 4.44\text{V}$ and D. M----- with a methoxy out of plane with the aromatic ring with $E_{\text{ox}} = 4.98\text{V}$. For B, C and D, their LUMO(S^+) are drawn at an isovalue of 0.08. The numbers by the atoms are the $E_b(\text{ER})$ values, in eV, at the corresponding site.

The atomistic values of $E_b(\text{ER})$ were calculated and are shown in Figure 6.3 for the atoms on the oxidized shuttle molecules. Taking benzene as the reference, for which E_{ox} is equal to 5.24 V and $E_b(\text{ER})$ is equal to 2.79 eV on each ring carbon atom, the

consequence of substituting a *t*-butyl group is to lower E_{ox} by 0.25 V to 4.99 V and reduce the reactivity on all ring carbon atoms, especially on the ortho ring carbon atoms neighbouring the *t*-butyl group where the $E_b(ER)$ is lowered to 2.33 eV. This stabilizing effect is due to the steric protection afforded by the *t*-butyl group.

The case of a methoxy substituted benzene is more complicated. The orientation of the O-C bond in a methoxy group relative to the plane of the aromatic ring may change depending on its interactions with the neighbouring substituents. Figure 6.3 shows two cases: an in-plane methoxy substituted benzene and an out-of-plane methoxy substituted benzene. For a methoxy substituted benzene, the in-plane methoxy substituted structure is the ground state due to the strong π -interaction between the lone pair on the oxygen atom and the π -orbitals on the ring carbon atoms. The individual ethyl radical binding energies calculated for each atom in electrolyte are 0.16 eV to 0.66 eV lower for the in-plane isomer, when compared to the out-of-plane methoxy substituted benzene. Compared to benzene, the addition of an in-plane methoxy group lowers the oxidation potential by 0.80 V to 4.44 V. Figure 6.3 shows that the reactivity of the ring carbon atoms is lowest at the carbon bonded to the methoxy group and at the meta positions. The highest reactivity ring positions are the ortho and para positions. This follows the pattern of increased electron density in the ring seen through drawing resonance structures of the molecule. The methoxy group donates electron density to the ring at the ortho and para positions. This increased electron density results in an increased affinity for the ethyl radical at these sites. Because of its higher energy, the out-of-plane methoxy exists only in configurations where steric groups reside on both sides of the methoxy group and prevent the in-plane configuration. Compared with benzene, the out-of-plane

methoxy group lowers oxidation potential by only 0.26 V to 4.98 V and reduces $E_b(\text{ER})$ on the neighbouring carbon atoms by only 0.28 eV. Having an $E_b(\text{ER})$ of 2.85 eV, the oxygen atom of the out-plane methoxy substituted benzene becomes extremely reactive. However, as mentioned above, the out-of plane methoxy group appears only in certain configurations and, therefore, the steric protection from the *t*-butyl groups on both sides provides an effective shielding for the oxygen atom on an out-of-plane methoxy group.

6.5. Discussion

Figure 6.4a shows the value of E_{ox} and $E_b(\text{ER})$ from Table 6-1 as they relate to the number of *t*-butyl groups on the molecule. There is no significant relationship between the number of *t*-butyl groups and either E_{ox} or $E_b(\text{ER})$. This was to be expected since the presence of alkyl groups has little effect on the π electrons in the molecule. Figure 6.4b shows the values of E_{ox} and $E_b(\text{ER})$ as they relate to the number of methoxy groups on each molecule. It can be seen that there is a general trend that more methoxy groups results in slightly lower oxidation potentials and slightly more stable molecules. The effect of methoxy groups on the oxidation potential of these molecules has been attributed to the electron donating effect of the group [140]. More electron density in the ring results in a lower oxidation potential.

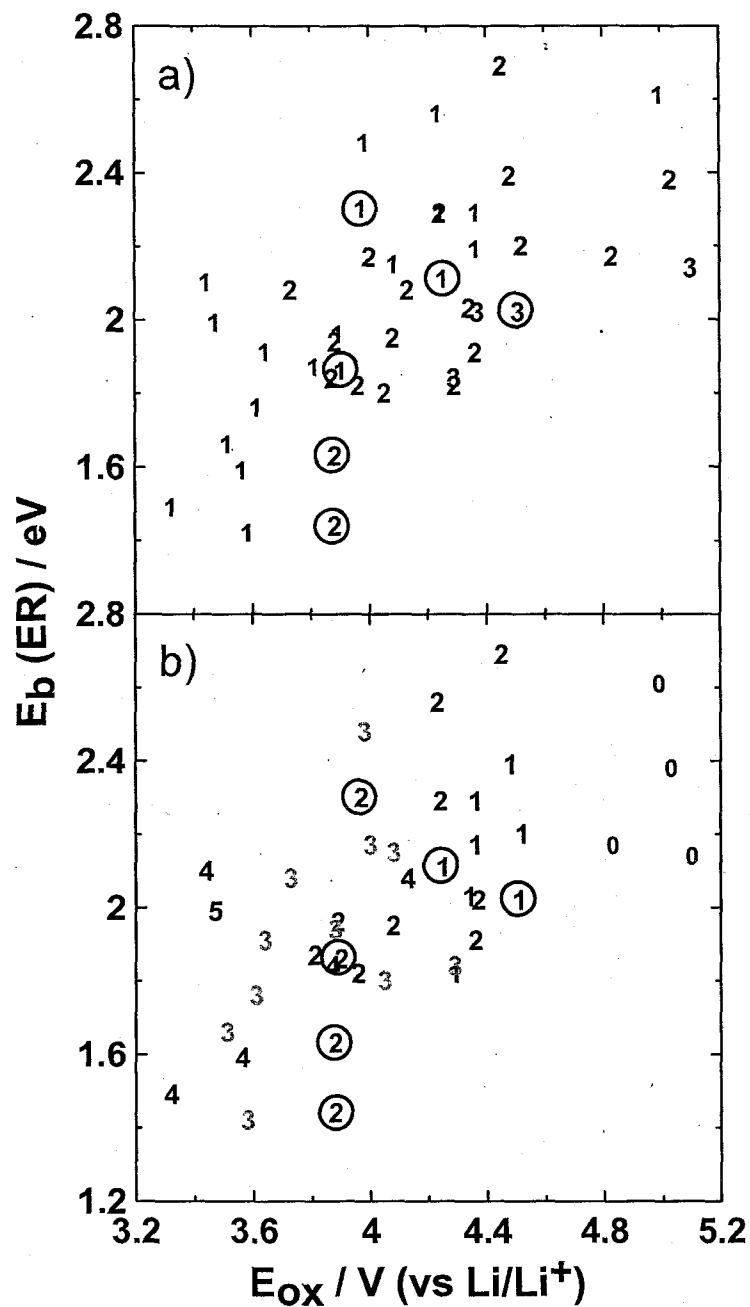


Figure 6.4 $E_b(ER)$ in eV vs E_{ox} in V for all 43 molecules with the number of methoxy groups indicated in the upper panel, or the number of *t*-butyl groups in the lower panel. Circles represent molecules that were also experimentally tested.

The effect of the methoxy groups on the value of $E_b(ER)$ is more complicated. For example, in Figure 6.4b, the molecules with two methoxy groups have a range of

values of $E_b(\text{ER})$ for the most active site that ranges from 1.44 eV to 2.69 eV, which spans the range of stability from stable to unstable. Figure 6.5 shows the values of E_{ox} and $E_b(\text{ER})$ only for the molecules that have exactly two methoxy groups. The symbols O, M and P represent the ortho, meta and para substitution patterns for the two methoxy groups on each molecule. From this figure, some of the structure-activity relationship can be seen. The molecules with ortho and para substitution patterns are more stable than all but one of the molecules with the meta substitution pattern. It is therefore assumed that the ability of the molecule to adopt a quinone-like resonance structure has a stabilizing effect on the radical cation of the molecule.

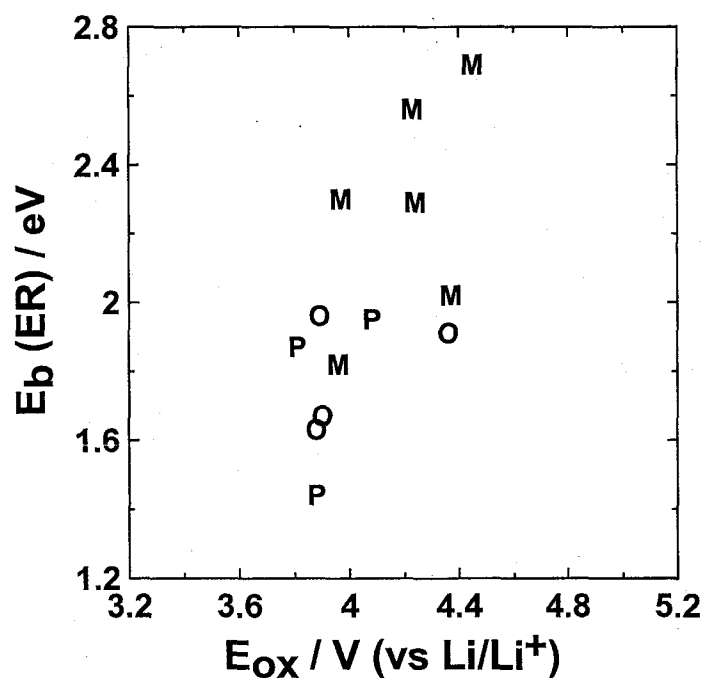


Figure 6.5 $E_b(\text{ER})$ in eV vs E_{ox} in V for the molecules containing exactly two methoxy groups. The symbols O, M and P represent the substitution pattern of the methoxy groups as *ortho*, *meta* and *para*, respectively.

The purpose of carrying out this analysis is to deepen the understanding of the redox properties of this kind of molecule and, more importantly, to search for possible shuttle additives for lithium-ion cells. A shuttle additive for lithium-ion cells should be stable and provide overcharge protection that lasts many cycles and its oxidation potential should be in a specified range. Computationally searching for shuttle additives, we can choose $E_b(\text{ER}) < 1.73 \text{ eV}$ as the criteria for shuttle stability, based on previous computational/experimental work. The oxidation potential of shuttle molecules proposed for use in LiFePO_4 based Li-ion cells should be in the range of 3.8 – 3.9 V, and those for LiMn_2O_4 based lithium-ion cells should be in the range of 4.4 – 4.5 V. Considering the computational error in oxidation potentials of about 0.15 V [133], the calculated oxidation potential of shuttle molecule used for LiFePO_4 based Li-ion cells should be in the range of 3.65 – 4.05 V, and those for LiMn_2O_4 based Li-ion cells should be in the range of 4.25 – 4.65 V.

Looking at Table 6-1, only two molecules other than 2,5-di-*t*-butyl-1,4-dimethoxybenzene fulfill the computational criteria for both stability and oxidation potential. They are molecule #9 or T-MM-- with $E_b(\text{ER}) = 1.86 \text{ eV}$ and $E_{\text{ox}} = 3.90 \text{ V}$ and molecule #27 or T-TMM- with $E_b(\text{ER}) = 1.63 \text{ eV}$ and $E_{\text{ox}} = 3.88 \text{ V}$. Therefore, molecule #9 is computationally expected to be unstable, while molecule #27 becomes the only possible, stable shuttle molecule in this group with its oxidation potential in the desired range. Whether these computational predictions are correct or not should be judged by experimental results.

6.6. Experimental

The molecules 2,5-di-*t*-butyl-1,4-dimethoxybenzene (#36), 4-*t*-butylmethoxybenzene (#4), and 2,4,6-tri-*t*-butylmethoxybenzene (#41) were obtained from Sigma Aldrich Chemical Co. The chemicals were used as-received. The molecule 4-*t*-butyl-1,2-dimethoxybenzene (#9) was synthesized at 3M as reported previously [141]. The molecules 2-*t*-butyl-1,4-dimethoxybenzene (#6) and 3,5-di-*t*-butyl-1,2-dimethoxybenzene (#27) were synthesized at 3M in a manner similar to that reported previously for the molecule 4-*t*-butyl-1,2-dimethoxybenzene (#9) [141]. The products were determined to be greater than 99% pure by GC and the identity of the products was confirmed by GC-MS.

Table 6-2 summarizes the results from the coin cell testing. These six molecules were chosen because they were either commercially available or were able to be synthesized in-house for testing. The experimentally determined oxidation potential for the shuttle molecules is taken as the potential at which shuttling begins in a cell. Often, the shuttling plateau is not flat, but rather it is sloping or it occurs in multiple steps. In these cases, the oxidation potential is taken as the onset of the first plateau after full charge, which is attributed to the shuttling process.

Table 6-2 Comparison of calculated and experimental results for the six molecules that were tested. Calculated results include the oxidation potential (E_{ox}) and the ethyl radical binding energy ($E_b(ER)$). Experimental results include the oxidation potential (E_{ox}) and the number of cycles of 100% overcharge protection provided by the shuttle molecule in graphite/LiFePO₄ and Li_{4/3}Ti_{5/3}O₄/LiFePO₄ coin cells.

Molecule		E_{ox} / V		$E_b(ER) / eV$	# Cycles	
		Calc.	Expt.		MCMB	LiTiO
4	T--M--	4.25	4.17	2.11	1	4
7	TM--M-	3.81	3.87	1.87	6	30
9	T-MM--	3.90	4.07	1.86	7	11
27	T-TMM-	3.88	4.05	1.63	27	70
36	TM-TM-	3.88	3.86	1.44	173	363
41	TMT-T-	4.51	4.38	2.02	1	3

Several coin cells were made for each shuttle molecule, and not every cell made provides exactly the same number of cycles of overcharge protection. Because of this, we take the maximum number of cycles for any particular molecule as the number of cycles reported. Figure 6.6 shows 100 hours of cycling for each of the six shuttle molecules tested in coin cells. The cycling data shows the last few cycles of shuttling for each molecule in MCMB/LiFePO₄ cells along with the cycle numbers. In all cases reported here, the number of cycles is greater for cells containing a Li_{4/3}Ti_{5/3}O₄ negative electrode than for cells containing a graphite negative electrode. The result of using a titanate negative electrode is that the voltage range that the cell experiences is much smaller than when graphite electrodes are used, so there is less possibility for reductive processes to degrade the shuttle molecules in the electrolyte.

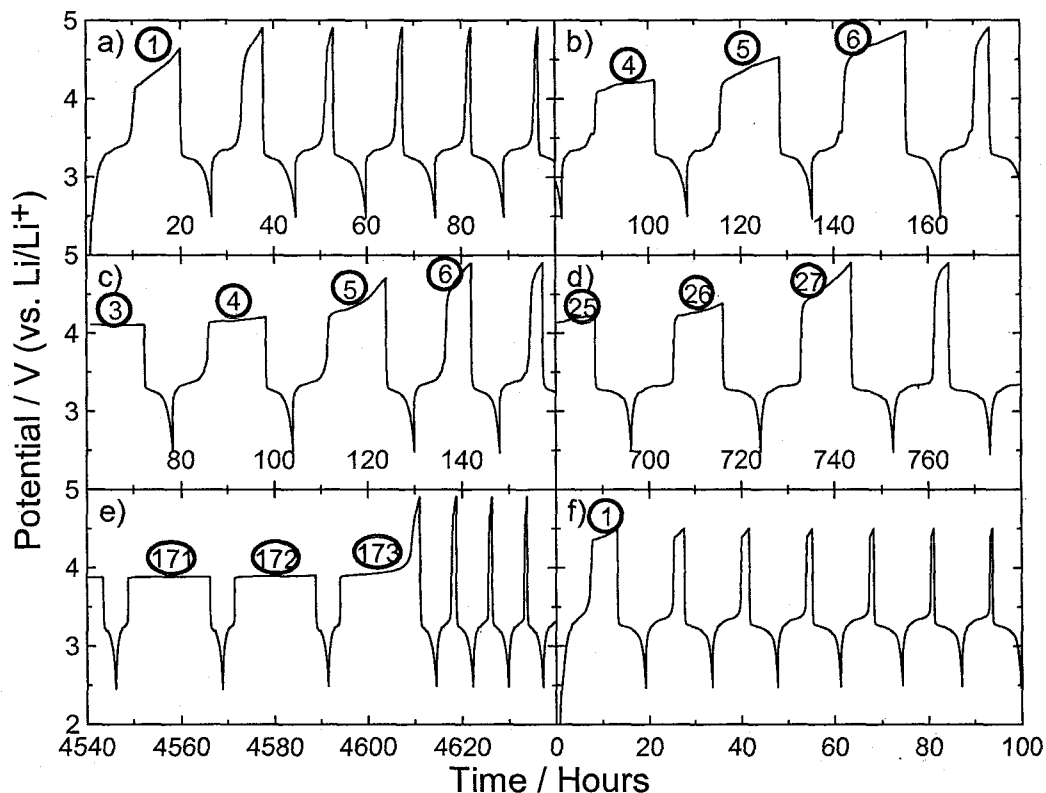


Figure 6.6 100 hours of cycling data for the following molecules: a) #4, T--M--; b) #7, TM--M-; c) #9, T-MM--; d) #27, T-TMM-; e) #36, TM-TM-; f) #41, TMT-T-. The cells were MCMB/LiFePO₄ Li-ion cells with 0.1M shuttle in the electrolyte. The numbers over the shuttling plateaus indicate the cycle number.

Figure 6.7 shows the number of cycles of overcharge protection as a function of $E_b(\text{ER})$ for the six molecules tested for both MCMB/LiFePO₄ and Li_{4/3}Ti_{5/3}O₄/LiFePO₄ types of coin cells. Figure 6.7 shows that the shuttle lifetime generally improves as $E_b(\text{ER})$ decreases. The experimental oxidation potentials are within 0.2 V of the calculated values in all cases as shown in Table 6-2 and in the cases of molecules #4, #7 and #36, the values are less than 0.1 V different. Also, there is a general agreement between the number of cycles of overcharge protection and the values of $E_b(\text{ER})$ for the molecules in Table 6-2. The two molecules with the longest period of overcharge

protection, #36 and #27, are also the two molecules with the lowest $E_b(\text{ER})$ values. Similarly, the two molecules with the fewest number of cycles of overcharge protection, #41 and #4, are the molecules with the highest values of $E_b(\text{ER})$. The coin cells we test contain the shuttle molecules at a concentration of 0.1 M and each cell contains a similar volume of electrolyte. Since, the electrodes areas are constant at 1.3 cm^2 , using the number of cycles of 100% overcharge as a measure of shuttle longevity yields results that are reasonably comparable.

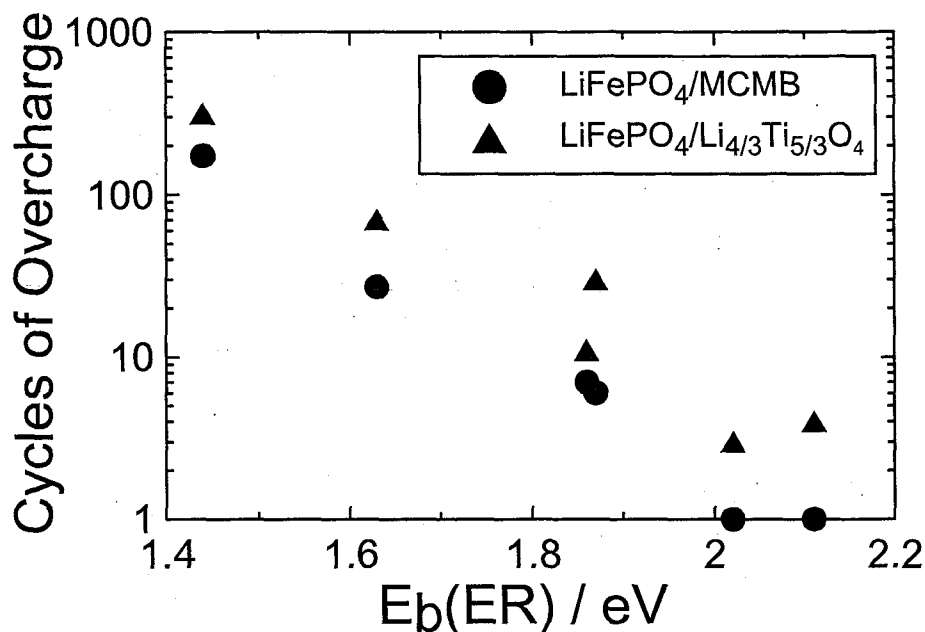


Figure 6.7 Number of cycles of 100% overcharge on a log scale as a function of $E_b(\text{ER})$ for the six molecules tested in coin cells. Both $\text{MCMB}/\text{LiFePO}_4$ and $\text{Li}_{4/3}\text{Ti}_{5/3}\text{O}_4/\text{LiFePO}_4$ cell data are shown. The grey data points are for molecule #9.

6.7. Conclusions

Both the oxidation potential and the stability of *t*-butyl and methoxy substituted benzene molecules agree well with the calculated results. Therefore, these methods for theoretically screening molecules as shuttles can be used to narrow the field of molecules so that more effort can be directed towards molecules of greater promise. It is worth noting, however, that the calculated results have some associated error. The calculated values of the oxidation potentials of the molecules agree well, to within 0.2 V of the experimental results for all of the molecules tested in coin cells. The coin cell results agree with the calculated results in that the two molecules with the lowest $E_b(\text{ER})$ values are the most stable and the two with the highest $E_b(\text{ER})$ values are the least stable, but the order of increasing stability does not strictly follow the order of decreasing $E_b(\text{ER})$ values. Based on the results presented here, it seems highly probable that 2,5-di-*t*-butyl-1,4-dimethoxybenzene (#36) is the most stable shuttle molecule suitable for LiFePO_4 -based cells of the 43 molecules considered here.

The claim from Feng et al. was shown here to be misleading. The cells used in their experiments were unusual, in that they contained a very large excess volume of electrolyte. The result of this is that even as the shuttle was decomposing, the sheer quantity of it present within the cell resulted in an increased number of cycles of overcharge protection. When tested using the same concentration of shuttle and same volume of electrolyte as other shuttle molecules presented in this thesis, the results for the molecule presented by Feng et al. are significantly poorer in comparison than claimed. This should help to demonstrate the need for consistent testing procedures when comparing the results of one shuttle molecule to another.

Chapter 7. Conclusions

7.1. Conclusions

The use of redox shuttles has the potential to make lithium-ion batteries safer and more accessible to consumers. The choice of which shuttle molecule to use in a battery is highly affected by the battery system itself. The positive electrode material determines the oxidation potential of the shuttle molecule. To minimize the self discharge current from the shuttle process, the oxidation potential of the shuttle should be 0.3 V above the potential of the positive electrode. Also, as has been shown, the choice of the negative electrode is important. Many molecules have been shown to provide fewer cycles of overcharge protection in cells using graphite negative electrodes than in cells with higher potential $\text{Li}_{4/3}\text{Ti}_{5/3}\text{O}_4$ negative electrodes. This is most likely due to reductive decomposition at the negative electrode. In order to be most successful, a shuttle molecule must possess the right oxidation potential and also show a highly reversible oxidation. Both of these properties must be met for a molecule to be considered to be of use in a battery.

This thesis has summarized many of the noteworthy molecules discovered, as well as discussed the properties of interest for such molecules and the techniques used to study them. These techniques include standard coin cell construction as well as modified coin cells, such as the three-electrode cells described in Chapter 2. The use of coin cells represent the best method for determining the duration of overcharge protection that a molecule can provide. This is done by counting the number of cycles of 100% overcharge protection provided by the shuttle molecule. Coin cells give results that most closely match those determined from studies on full sized batteries.

Coin cells are not the only useful method for characterizing shuttle molecules. Large volume electrochemical measurements, such as cyclic voltammetry, can be useful for determining other important properties. During these measurements, there is direct control of the electrode potentials, not just the potential difference between two electrodes, as there is with coin cells. This allows for the determination of properties such as diffusion coefficients and the accurate measurement of oxidation/reduction potentials.

The results of DFT calculations have also been shown to correlate well with the measured stability and oxidation potentials of molecules. While not always exact, these calculations have been shown to predict trends in data very well. It is therefore possible to use these calculations to guide experiment and predict which molecules would be most promising, and thus worthy of experimental effort.

Of the molecules studied there are two broad groups, molecules suitable for use with lower potential positive electrodes and molecules suitable for use with higher potential positive electrodes. From the list of lower potential shuttle molecules, 2,5-di-*t*-butyl-1,4-dimethoxybenzene has been shown to provide the largest number of cycles of overcharge protection. It is however, sensitive to decomposition through double oxidation. Other molecules showing large numbers of cycles of overcharge protection include a variety of substituted phenothiazines and TEMPOs. These two classes of molecules both show a higher degree of tolerance to higher potentials, but less stability at the lower potentials than are present in cells using graphite negative electrodes.

The higher potential shuttle molecules are desirable for lithium-ion battery systems aiming for high energy density, since the energy within a cell is the product of

the capacity and the working voltage. A higher potential positive electrode should allow for a higher energy density. Finding shuttles for high potential positive electrodes is very challenging since the molecule must be stable over the entire range of potentials within the cell. As shown with DDB and DBFB, the addition of more electron withdrawing –CH₂CF₃ groups can raise the oxidation potential of the molecule, but it has a similar effect on the reduction potential as well. DBFB is not as reductively stable at lithium potential as DDB is.

Of all of the molecules presented in this thesis, the molecule DDB is arguably the most successful shuttle molecule for LiFePO₄ based cells. To determine if DDB would be of use in full scale cells, DDB was tested in 18650 sized cylindrical cells. These were standard, commercial-sized cells custom-made at E-One Moli Energy in Maple Ridge, BC, containing 0.15 M DDB in an electrolyte comprised of 0.75 M LiPF₆ in EC:DEC with proprietary electrolyte additives. The purpose of testing DDB in full-sized cells was to ensure that the shuttle could operate in practical lithium-ion cells. Figure 7.1 shows the cycling data for an 18650 cell containing DDB.

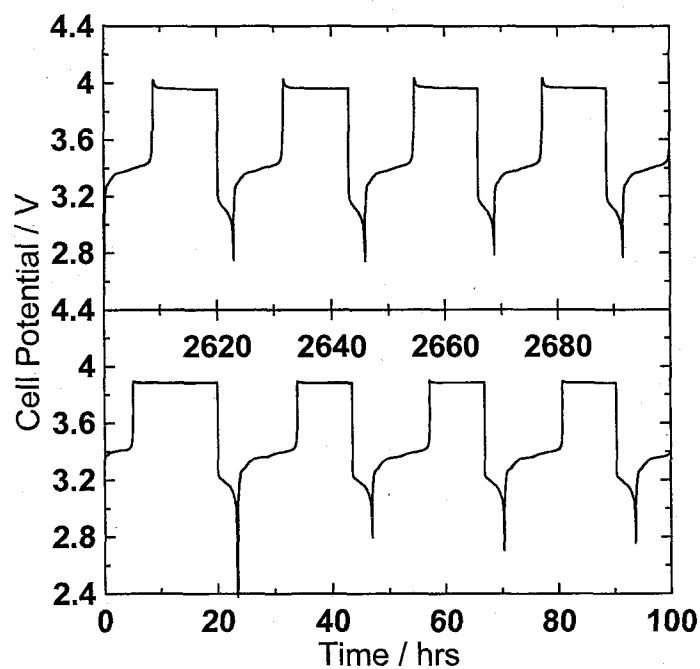


Figure 7.1 Cycling data for a LiFePO_4 /graphite 18650 cell containing the shuttle DDB.

This cell was charged for 20 hours at $C/10$ rate, and then discharged at three times this current, to speed up the length of each full cycle. Since the shuttle was only in operation during the overcharge portion of the cycle, the increased discharge current would not have had an effect on the results. With the exception of higher currents, the cycling results look identical to coin cell results. Another cell was cycled at similar rates, but without going into overcharge. Figure 7.2 shows the charge and discharge capacities from this cell.

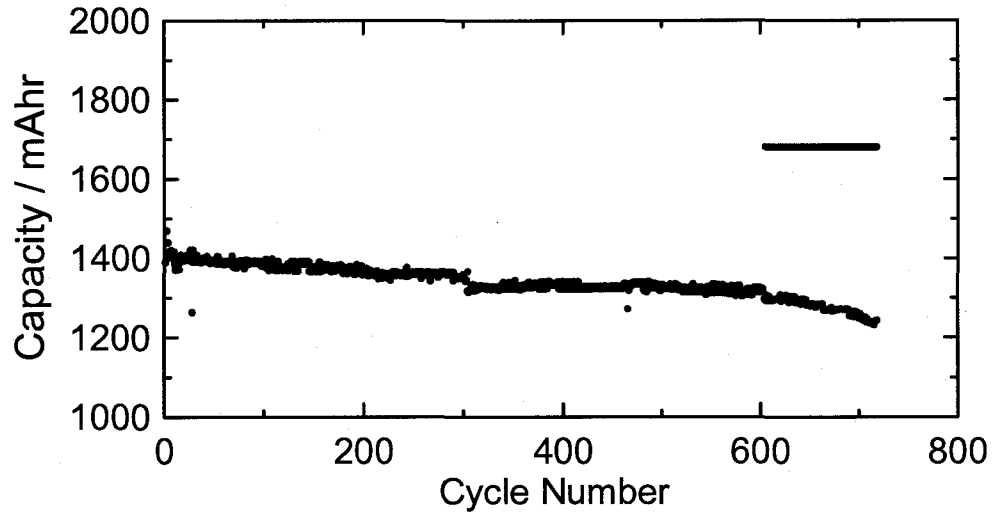


Figure 7.2 Charge(●) and discharge(●) capacities for an 18650 cell containing DDB. The cell was cycled for 600 cycles with no overcharging, then for another 120 cycles with 20% overcharging per cycle.

This cell was cycled for 600 cycles and showed excellent cycling. During cycles with no shuttling, the charge and discharge capacities overlap and cannot be distinguished from one another in the figure. After the 600 cycles, to make sure that the shuttle was still operational within the cell, the cell was exposed to 20% overcharge each cycle. Figure 7.2 shows that for the next 120 cycles, the shuttle was still present within the cell. During the regular operation of the cell, the shuttle was not degraded.

In addition to testing single cells, three-cell, series-connected packs were constructed from the 18650 cells. Figure 7.3 shows the cycling of a three-cell pack that was cycled with no overcharging.

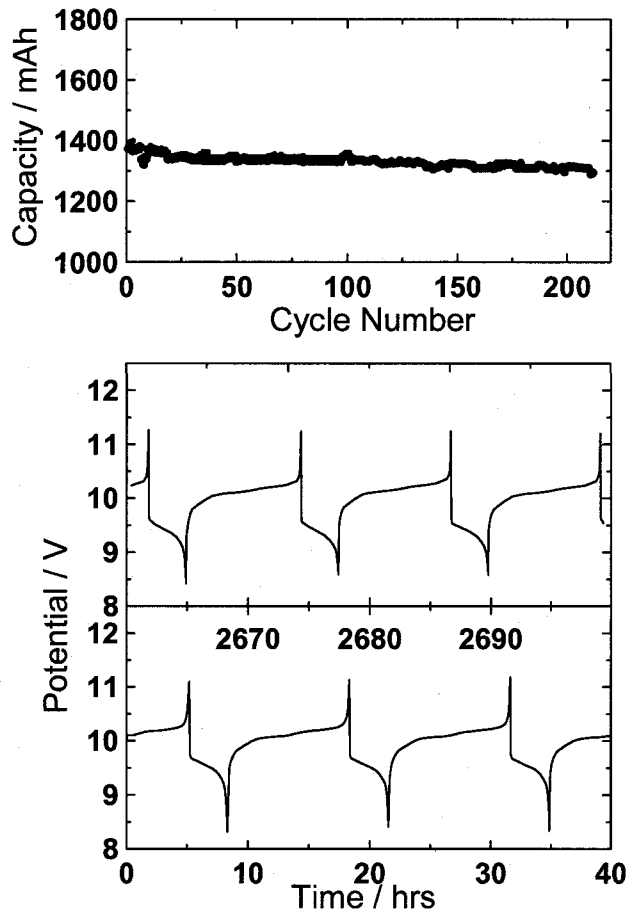


Figure 7.3 Cycling data with charge(●) and discharge(●) capacities for a 3 cell pack of 18650 cells in a series string. The three cells were of a similar capacity, so no overcharging occurs.

Some of the three-cell packs were constructed with one cell having a 330 Ω resistor connected in parallel to the cell, causing a slow continuous discharge. This resulted in that one cell taking longer to charge than the other two, so in order to fully charge the pack, the other two normal cells were forced into overcharge. Figure 7.4 shows the results from one of these packs that had a 330 Ω resistor.

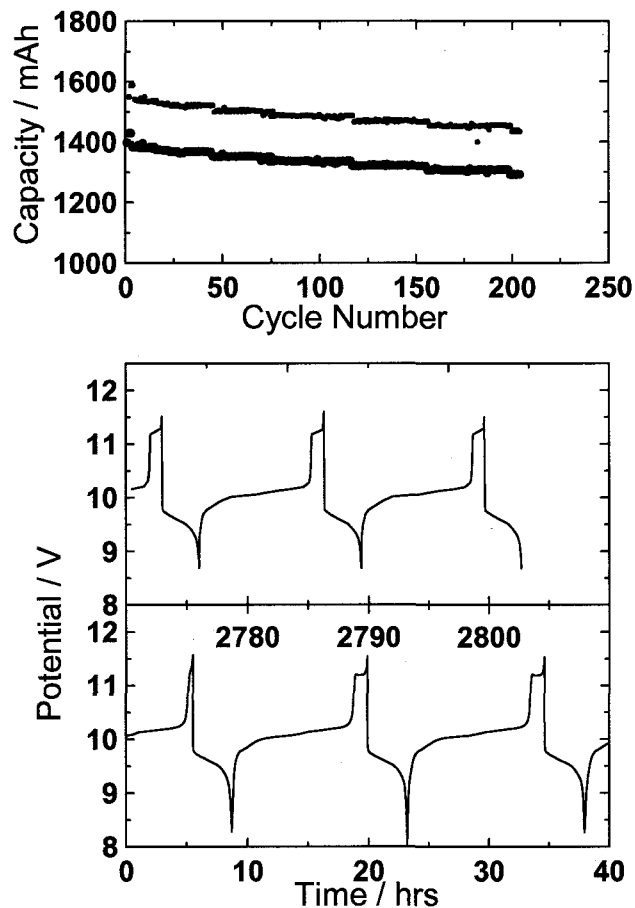


Figure 7.4 Cycling data with charge(●) and discharge(●) capacities for a 3 cell pack of 18650 cells in a series string. One of the cells was continually being discharged by a 330 Ω resistor.

With the data from these 18650 cells, the molecule DDB was shown to be successful in preventing overcharging in full-sized cells. DDB has been both patented and commercialized by 3M Co., which has been responsible for much of the funding of this research project. It is available as 3M product number L-19843. The high potential analogue, DBFB, is also being produced as an experimental product by 3M, product number L-20487.

One more important factor with regards to the commercial use of redox shuttle molecules is their solubility in electrolyte. To maximize the conductivity of the electrolyte, manufacturers use a salt concentration that is much higher than that used in the experiments presented here. The consequence of this is that as more salt is dissolved in the electrolyte, less of the shuttle can be dissolved. Figure 7.5 shows the measured solubility of the molecule DDB in a variety of electrolytes.

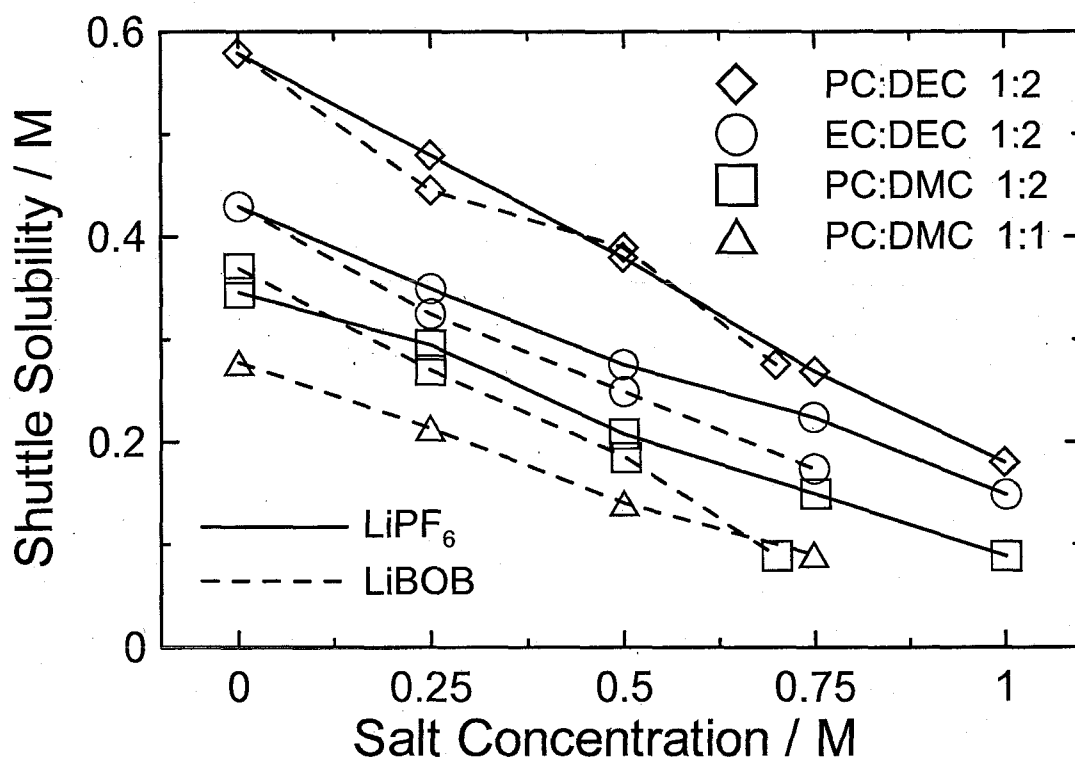


Figure 7.5 Solubility limits for DDB in electrolytes containing various concentrations of LiPF₆ or LiBOB in a variety of solvents.

There is a clear correlation between an increased salt concentration and a decreased shuttle solubility. The choice of solvents also plays a major role in the solubility. This is

just one more important factor to be taken into account when using redox shuttles as electrolyte additives in commercial cells.

The work presented in this thesis represents the largest volume of work published on redox shuttles. Chapters 4, 5 and 6 summarize the results from many experiments done on some of the more successful shuttle molecules. There were, however, many more molecules tested and corresponding results than have been shown. As shown in Figure 3.7, the molecules with the largest number of cycles of overcharge protection are among the least common. Most molecules offer little or no overcharge protection at all. Appendix A contains lists of the entire library of shuttle molecules tested, sorted first in order of increasing oxidation potential and then sorted by decreasing number of cycles of 100% overcharge protection. The most successful molecules from these lists have already been patented and some are being commercialized. The fact that there is sufficient of an interest to warrant the manufacture and sale of redox shuttles should be enough to convince the reader of the importance of this area of research and of the contribution the work presented in this thesis has made to the field.

7.2. Future Work

By no means is this thesis a comprehensive study of all aspects of redox shuttles in lithium-ion batteries. There are many areas of new research in addition to the continued search for new shuttle molecules. Several molecules have been found to be suitable for use in LiFePO_4 -based lithium-ion batteries, but there are fewer known to be of use with higher potential electrodes. This of course does not mean that searching for lower potential shuttles is no longer of interest. This thesis has shown that it is possible

to modify the oxidation potential of molecules by chemically modifying the molecule. So, finding stable, long lasting molecules with lower redox potentials and then modifying them to increase their redox potential is one way of coming up with new high potential shuttles.

One other avenue of future research is optimizing the use of shuttle molecules already discovered. This would mean trying to find an optimum electrolyte composition for the shuttle molecules that are known to perform well. Nearly all of the tests presented in this thesis were done in an electrolyte containing 0.5 M LiPF₆ or 0.5 M LiBOB as the electrolyte salt. LiPF₆ is the most commonly used electrolyte salt in lithium-ion batteries and LiBOB is a potential replacement for some applications. As has been shown in this thesis, some shuttles provide more protection when one salt is used over the other. However, these are not the only salts that could be used in lithium-ion batteries. Additional salts, such as lithium bistrifluoromethylsulfonylimide (LiTFSI) and lithium bisperfluoroethylsulfonylimide (LiBETI) could potentially provide longer overcharge protection, and they can also affect the oxidation potential of the shuttle itself. Finding the right salt, or blend of salts, could greatly increase the usefulness of redox shuttles in lithium-ion batteries.

Additionally, the choice of solvents used was not meant to imply that the best solvent choice for redox shuttles was a mix of PC:DMC:EC:DEC in the ratio of 1:2:1:2. These are all commonly used solvents in lithium-ion batteries, so this mix was chosen to represent a variety of solvents that are likely to be found in a battery. Just like with the salts, however, there are additional choices for solvents, such as ethyl methyl carbonate (EMC), diethyleneglycol dimethyl ether (diglyme), triethyleneglycol dimethyl ether

(triglyme), dimethyl ether or 1,3-dioxolane. A more recent field of study is the use of ionic liquids in lithium-ion battery electrolytes which could have a significant impact on the properties of redox shuttles in electrolytes containing them. These ionic liquids can contain a cation like cyclic quaternary ammonium cations, such as N-butyl-methyl pyrrolidinium, coupled with anions such as TFSI to form a molten salt that is liquid at room temperature. The use of such liquids could have significant impact on the electrochemistry of the electrolyte.

The use of electrolyte additives is also an area that could provide a significant impact on the overall usefulness of a redox shuttle. All of the components within an electrolyte are of importance for redox shuttles since they can all contribute to the formation of the surface layers on the electrodes or provide reaction pathways that could affect the lifetime of the shuttle molecules. There are a huge number of possible combinations of shuttle molecules with electrolyte additives, but it is probable that trends exist. It is likely that some additives are more beneficial for the shuttling procedure than others, so not every combination would need to be tested.

It has been explained in this thesis that the oxidation potential of the shuttle molecule should be 0.3 V above the potential of the positive electrode. Another way to look at this is to consider the choice of the positive electrode materials to be limited by the availability of stable shuttle molecules with suitable oxidation potentials. Similarly, the negative electrode material and the reactions that occur at the surface of the negative electrode are of significant importance to determining the overall stability of a shuttle molecule. The only negative electrodes presented in this thesis were graphite and $\text{Li}_{4/3}\text{Ti}_{5/3}\text{O}_4$. Some data was also presented using half cells containing a lithium negative

electrode. It would be interesting to see some results for other negative electrode materials, such as silicon based electrodes and tin-transition metal alloy negative electrodes, both of which are high capacity electrodes that are currently being researched.

As presented in this thesis, calculations can yield results that match experiments very closely. The oxidation potentials and electron densities are already in excellent agreement with experiment, but there is still room to improve the calculations that predict the stability of shuttle molecules and how these predictions match up with the experimentally determined number of cycles of overcharge protection. As work in this area improves, calculations will be able to better guide the field of research in search of new shuttle molecules.

One final area for future work is the potential to turn shuttle molecules into organic electrodes. Since the shuttle molecules are known to undergo thousands of reversible oxidations and reductions, it could be possible to use these molecules to store charge as an electrode. This could be done by modifying them to form long, insoluble polymer chains that could be mixed with conductive carbon and a polymer binder to form an electrode. One example of this is the use of a poly-TEMPO-4-methacrylate to form the electrode of a 'radical battery'[142]. The use of organic molecules as electrodes is of interest since they have the potential to be more environmentally friendly and thermally stable than transition metal oxide electrodes.

REFERENCES

- [1] D. Fouchard and J. B. Taylor, *J. Power Sources*, **21**, 195 (1987).
- [2] J. Yamaki, S. Tobishima, K. Hayashi, K. Saito, Y. Nemoto and M. Arakawa, *J. Power Sources*, **74**, 219 (1998).
- [3] N. Goldenfield, *J. Power Sources*, **26**, 121 (1989).
- [4] K. Kanamura, S. Shiraishi, and Z. Takehara, *J. Electrochem Soc.*, **141**, L108 (1994).
- [5] P. Dan, E. Mengeritski, Y. Geronov, D. Aurbach, and I. Weisman, *J. Power Sources*, **54**, 143 (1995).
- [6] <http://www.sony.net/Fun/SH/1-24/h3.html> last accessed Last accessed on June 3, 2009.
- [7] <http://www.e-one.com.tw/english/product/products1.html> accessed on May 26, 2009.
- [8] W. R. MacKinnon, Ph. D. thesis, University of British Columbia (1979).
- [9] T. Zheng, Ph. D. thesis, Simon Fraser University (1996).
- [10] <http://www.sony.net/SonyInfo/News/Press/200502/05-006E/> Last accessed on June 3, 2009.
- [11] K. Xu, *J. Electrochem. Soc.*, **156**, A751 (2009).
- [12] D. Aurbach, L. Daroux, P. W. Faguy, and E. Yeager, *J. Electrochem. Soc.*, **134**, 1611 (1987).
- [13] E. Peled, *J. Electrochem. Soc.*, **126**, 2047 (1979).
- [14] R. Fong, U. von Sacken, and J. R. Dahn, *J. Electrochem. Soc.*, **137**, 2009 (1990).
- [15] D. Aurbach, Y. Ein-Eli, O. Chusid, Y. Carmeli, M. Babai, and H. Yamin, *J. Electrochem. Soc.*, **141**, 603 (1994).
- [16] E. Peled, D. Golodnitsky, and G. Ardel, *J. Electrochem. Soc.*, **144**, L208 (1997).
- [17] K. Xu, U. Lee, S. Zhang, and T. R. Jow, *J. Electrochem. Soc.*, **151**, A2106 (2004).
- [18] C. R. Yang, Y. Y. Wang, and C. C. Wan, *J. Power Sources*, **72**, 66 (1998).
- [19] K. Xu, G. V. Zhuang, J. L. Allen, U. Lee, S. S. Zhang, P. N. Ross, and T. R. Jow, *J. Phys. Chem. B*, **110**, 7708 (2006).
- [20] D. Aurbach, B. Markovsky, K. Gamolsky, E. Levi, and Y. Ein-Eli, *Electrochim. Acta*, **46**, 67 (1999).

- [21] D. Aurbach, *J. Power Sources*, **119**, 497 (2003).
- [22] A. Xiao, L. Yang, B. L. Lucht, S. H. Kang, and D. P. Abraham, *J. Electrochem. Soc.*, **156**, A318 (2009).
- [23] A. Naji, J. Ghanbaja, B. Humbert, P. Willmann, and D. Billaud, *J. Power Sources*, **63**, 33 (1996).
- [24] D. Aurbach, Y. Ein-Eli, B. Markovsky, A. Zaban, S. Luski, Y. Carmeli, and H. Yamin, *J. Electrochem. Soc.*, **142**, 2882 (1995).
- [25] K. Xu, S. S. Zhang, U. Lee, J. L. Allen, and T. R. Jow, *J. Power Sources*, **146**, 79 (2005).
- [26] A. N. Dey and B. P. Sullivan, *J. Electrochem. Soc.*, **117**, 222 (1970).
- [27] J. O. Besenhard and H. P. Fritz, *J. Electroanal. Chem.*, **53**, 329 (1974).
- [28] K. C. Lim, A. M. Lackner, P. O. Braatz, W. H. Smith, J. D. Margerum, and H. S. Lim, in *Batteries for Portable Applications and Electric Vehicles*, Electrochemical Society, Pennington, NJ, 470,479 (1997).
- [29] D. Aurbach, B. Markovsky, A. Shechter, Y. Ein Eli, and H. Cohen, *J. Electrochem. Soc.*, **143**, 3809 (1996).
- [30] Y. Nishi, *J. Power Sources*, **100**, 101 (2001).
- [31] A. Jansen, A. Kahaian, K. Kepler, P. Nelson, K. Amine, D. Wees, D. Vissers, and M. Thackeray, *J. Power Sources*, **81**, 902 (1999).
- [32] T. Ohzuku, A. Ueda, and N. Yamamoto, *J. Electrochem. Soc.*, **142**, 1431 (1995).
- [33] S. Bourderau, T. Brousse, and D. M. Schleich, *J. Power Sources*, **81-82**, 233 (1999).
- [34] H. Jung, M. Park, Y-G. Yoon, G-B. Kim, and S-K. Joo, *J. Power Sources*, **115**, 346 (2003).
- [35] S. Ohara, J. Suzuki, K. Sekine and T. Takamura, *J. Power Sources*, **136**, 303 (2004).
- [36] L. Y. Beaulieu, S. D. Beattie, and J. R. Dahn, *J. Electrochem. Soc.*, **150**, A419 (2003).
- [37] J. Li, H. Li, Z. Wang, L. Chen, and X. Huang, *J. Power Source*, **107**, 1 (2002).
- [38] B. Veeraraghavan, A. Durairajan, B. Haran, B. Popov, and R. Guidotti, *J. Electrochem. Soc.*, **149**, A675 (2002)
- [39] <http://www.sony.net/SonyInfo/News/Press/200502/05-006E/> Last accessed on June 3, 2009.
- [40] K. M. Abraham, *J. Power Sources*, **7**, 1 (1981).
- [41] J. N. Reimers and J. R. Dahn, *J. Electrochem. Soc.*, **141**, 2091 (1992).

- [42] K. Mizushima, P. C. Jones, P. J. Wiseman, and J. B. Goodenough, *Mater. Res. Bull.*, **15**, 783 (1980).
- [43] C. Delmas, *Mater. Sci. Eng.*, **B3**, 97 (1989).
- [44] Z. Chen and J. R. Dahn, *Electrochim. Acta*, **49**, 1079 (2004)
- [45] M. Richard, Ph. D. thesis, Dalhousie University (1998).
- [46] L.-F. Wang, C.-C. Ou, K. A. Striebel, and J-S. Chen, *J. Electrochem. Soc.*, **150**, A905 (2003).
- [47] A. K. Padhi, K. S. Nanjundaswamy, and J. B. Goodenough, *J. Electrochem. Soc.*, **144**, 1188 (1997).
- [48] A. S. Andersson, J. O. Thomas, B. Kalska, and L. Haggstrom, *Electrochem. Solid-State Lett.*, **3**, 66 (2000).
- [49] J. Jiang and J. R. Dahn, *Electrochem. Commun.*, **6**, 39 (2004).
- [50] J. Molenda, A. Stoklosa, and T. Bak, *Solid State Ionics*, **36**, 53 (1989).
- [51] N. Ravet, S. Besner, M. Simoneau, A. Vallee, and A. Armand, Can. Pat., 2,307,119.
- [52] Z. Chen and J. R. Dahn, *J. Electrochem. Soc.*, **149**, A1184 (2002).
- [53] S. Y. Chung, J. T. Bloking and Y. M. Chiang, *Nature Materials*, **1**, 123 (2002).
- [54] P. Subramanya Herle, B. Ellis, N. Coombs, and L. F. Nazar, *Nature Materials*, **3**, 147 (2004).
- [55] T. Nakamura, Y. Miwa, M. Tabuchi, and Y. Yamada, *J. Electrochem. Soc.*, **153**, A1108 (2006).
- [56] P. P. Prosini, M. Carewska, S. Scaccia, P. Wisniewski, and M. Pasquali, *Electrochim. Acta*, **48**, 4205 (2003).
- [57] S. E. Sloop, J. K. Pugh, S. Wang, J. B. Kerr, and K. Kinoshita, *Electrochem. Solid-State Lett.*, **4**, A42 (2001).
- [58] A. D. Holding, D. Pletcher, and R. V. H. Jones, *Electrochim. Acta*, **34**, 1529 (1989).
- [59] K. Xu, S. Zhang, T. R. Jow, W. Xu, and C. A. Angell, *Electrochem. Solid-State Lett.*, **5**, A26 (2002).
- [60] W. Xu and C. A. Angell, *Electrochem. Solid-State Lett.*, **4**, E1 (2001).
- [61] K. Xu, S. Zhang, B. A. Poese, and T. R. Jow, *Electrochem. Solid-State Lett.*, **5**, A259 (2002).
- [62] K. Xu, S. Zhang, and T. R. Jow, *Electrochem. Solid-State Lett.*, **6**, A117 (2003).
- [63] T. Ohzuku, Y. Iwakoshi, and K. Sawai, *J. Electrochem. Soc.*, **140**, 2490 (1993).

- [64] D. P. Wilkinson and J. R. Dahn, US Patent 5 130 211 (1993).
- [65] D. Guyomard and J. M. Tarascon, *J. Electrochem. Soc.*, **140**, 3071 (1993).
- [66] D. Guyomard and J. M. Tarascon, *US Patent 5 192 629* (1993).
- [67] D. Aurbach, A. Zaban, A. Schechter, Y. Ein-Eli, E. Zinigrad, and B. Markovsky, *J. Electrochem. Soc.*, **142**, 2873 (1995).
- [68] P. W. Atkins, *Physical Chemistry*, 5th Ed., Freeman, New York (1994).
- [69] S. S. Zhang, *J. Power Sources*, **162**, 1379 (2006).
- [70] M. C. Smart, B. L. Lucht, and B. V. Ratnakumar, *J. Electrochem. Soc.*, **155**, A557 (2008).
- [71] W. Li, B. L. Lucht, M. C. Smart, and B. V. Ratnakumar, *J. Electrochem. Soc.*, **155**, A648 (2008).
- [72] M. Herstedt, H. Rensmo, H. Siegbahn, and K. Edstrom, *Electrochim. Acta*, **49**, 2351 (2004).
- [73] N. S. Choi, K. H. Yew, K. Y. Lee, M. Sung, H. Kim, and S. S. Kim, *J. Power Sources*, **161**, 1254 (2006).
- [74] L. Xiao, X. Ai, Y. Cao, and H. Yang, *Electrochim. Acta*, **49**, 4189 (2004).
- [75] X. M. Feng, X. P. Ai, and H. X. Yang, *J. App. Electrochem.*, **34**, 1199 (2004).
- [76] H. Maleki, G. Deng, A. Anani, and J. Howard, *J. Electrochem. Soc.*, **146**, 3224 (1999).
- [77] M. Richard and J. Dahn, *J. Power Sources*, **83**, 71 (1999).
- [78] S. Zhang, K. Xu, and T. Jow, *J. Power Sources*, **138**, 226 (2004)
- [79] D. D. MacNeil and J. R. Dahn, *J. Phys. Chem. A*, **105**, 4430 (2001)
- [80] R. A. Leising, M. J. Palazzo, E. S. Takeuchi, and K. J. Takeuchi, *J. Electrochem. Soc.*, **148**, A838 (2001)
- [81] P. G. Balakrishnan, R. Ramesh, and T. P. Kumar, *J. Power Sources*, **155**, 401 (2006)
- [82] K. Abraham and D. Pasquariello, US Patent 4 857 423 (1989).
- [83] M. Adachi, *US Patent 5 763 119* (1998).
- [84] M. Adachi, K. Tanaka, and K. Sekai, *J. Electrochem. Soc.*, **146**, 1256 (1999).
- [85] J. Chen, C. Buhmester, and J. R. Dahn, *Electrochem. Solid-State Lett.*, **8**, A59 (2005).
- [86] T. J. Richardson, Presentation given at the 22nd International Battery Seminar and Exhibit, March 14-17, 2005.

- [87] G. Chen and T. Richardson, *Electrochem. Solid-State Lett.*, **7**, A23 (2004).
- [88] K. Thomas-Alyea, J. Newman, G. Chen, and T. Richardson, *J. Electrochem. Soc.*, **151**, A509 (2004).
- [89] A. J. Bard and L. R. Faulkner, *Electrochemical Methods: Fundamentals and Applications*, 2nd Ed., John Wiley & Sons, Inc., New York (2001).
- [90] L. M. Moshurchak, C. Buhrmester, and J. R. Dahn, *J. Electrochem. Soc.*, **152**, A1279 (2005).
- [91] S. Narayanan, S. Surampudi, A. Attia, and C. Bankston, *J. Electrochem. Soc.*, **138**, 2224 (1991).
- [92] D. C. Giancoli, *Physics*, 3rd Ed., Prentice Hall, Englewood Cliffs (1991).
- [93] J. R. Dahn, J. Jiang, L. M. Moshurchak, M. D. Fleischauer, C. Buhrmester, and L. J. Krause, *J. Electrochem. Soc.*, **152**, A1283 (2005).
- [94] T. Hatchard, D. MacNeil, D. Stevens, L. Christensen, and J. Dahn, *Electrochem. Solid-State Lett.*, **3**, 305 (2000)
- [95] C. Buhrmester, J. Chen, L.M. Moshurchak, J. Jiang, R.L. Wang, and J.R. Dahn. *J. Electrochem. Soc.*, **152**, A2390 (2005).
- [96] X. Feng, X. Ai, and H. Yang, *J. App. Electrochem.*, **34**, 1199 (2004).
- [97] L. Appelbaum, M. Oron, and M. Michman, *Electrochem. Soc. Proc.*, **14**, 5 (2001).
- [98] K. M. Abraham, D. M. Pasquariello, and E. B. Willstaedt, *J. Electrochem. Soc.*, **137**, 1856 (1990).
- [99] M. N. Golovin, D. P. Wilkinson, J. T. Dudley, D. Holonko, and S. Woo, *J. Electrochem. Soc.*, **139**, 5 (1992)
- [100] M. J. Lain and R. J. Neat, U.S. Pat. 6,387,571 (2002)
- [101] S. T. Myung and H. T. Chung, *J. Power Sources*, **84**, 32 (1999).
- [102] K. Shima, M. Ue, and J. Yamaki, *Electrochemistry*, **71**,1231 (2003).
- [103] A. Zweig, W. G. Hodgson, and W. H. Jura, *J. Am. Chem. Soc.*, **86**, 4124 (1964).
- [104] C. C. Zeng and J. Y. Becker, *J. Org. Chem.*, **69**, 1053 (2004).
- [105] H. Svith, H. Jensen, J. Almstedt, P. Andersson, T. Lundback, K. Daasbjerg, and M. Jonsson, *J. Phys. Chem. A*, **108**, 4805 (2004).
- [106] J. T. Johnston, T. Tipton, D. A. Stone, C. Erickson, and S. L. Trabue, *Langmuir*, **289**, 7 (1991).
- [107] R. L. Wang, L. M. Moshurchak, W. M. Lamanna, M. Bulinski, and J. R. Dahn, *J. Electrochem. Soc.*, **155**, A66 (2008).

- [108] N. Kubota and Y. Takeuchi, Unexamined Japanese Patent Application, Japanese Kokai Tokkyo Koho JP 2000235867 (2000).
- [109] K. Nakahara, J. Iriyama, S. Iwasa, M. Suguro, and M. Sato, Unexamined Japanese Patent Application, Japanese Kokai Tokkyo Koho JP 2005228712 (2005).
- [110] Y. V. Mikhaylik, U.S. Pat. Appl. Publ. US 2005147886 (2005).
- [111] Y. V. Mikhaylik, U.S. Pat. Appl. Publ. US 2005147891 (2005).
- [112] H. Nishide, S. Iwasa, Y.-J. Pu, T. Suga, K. Nakahara, and M. Satoh, *Electrochim. Acta*, **50**, 827 (2004).
- [113] K. Nakahara, S. Iwasa, M. Satoh, Y. Morioka, J. Iriyama, M. Suguro, and E. Hasegawa, *Chem. Phys. Lett.*, **359**, 351 (2002).
- [114] H. Nishide, S. Iwasa, and Y.-J. Pu, *Electrochim. Acta*, **50**, 827 (2004).
- [115] K. Chabita and P. C. Mandal, *Indian J. Chem. A*, **41A**, 2231 (2002).
- [116] E. S. Takeuchi, H. Gan, M. Palazzo, R. A. Leising, and S. M. David, *J. Electrochem. Soc.*, **144**, 1944 (1997).
- [117] F. Tran-Van, M. Provencher, Y. Choquette, and D. Delabouglise, *Electrochim. Acta*, **44**, 2789 (1999).
- [118] D. Sun, S. V. Rosokha, and J. K. Kocji, *J. Am. Chem. Soc.*, **126**, 1388 (2004).
- [119] N. Zimova, I. Nemeč, M. Ehlova, and K. Waisser, *Collect. Czech. Chem. Commun.*, **55**, 63 (1990).
- [120] E. T. Seo, R. F. Nelson, J. M. Fritsch, L. S. Marcoux, D. W. Leedy, and R. N. Adams, *J. Amer. Chem. Soc.*, **88**, 3498 (1966).
- [121] M. Oyama, K. Nozaki, and S. Okazaki, *Anal. Chem.*, **63**, 1387 (1991).
- [122] W. Schmidt and E. Steckhan, *Chem. Ber.*, **113**, 577 (1980).
- [123] R. F. Nelson and R. N. Adams, *J. Amer. Chem. Soc.*, **90**, 3925 (1967).
- [124] C. Buhrmester, L. M. Moshurchak, R. L. Wang, and J. R. Dahn, *J. Electrochem. Soc.*, **153**, A288 (2006).
- [125] C. Buhrmester, L. M. Moshurchak, R. L. Wang, and J. R. Dahn, *J. Electrochem. Soc.*, **153**, A1800 (2006).
- [126] L. M. Moshurchak, W. M. Lamanna, M. Bulinski, R. L. Wang, R. G. Garsuch, J. Jiang, D. Magnuson, M. Triemert, and J. R. Dahn, *J. Electrochem. Soc.*, **156**, A309 (2009).
- [127] W. J. Hehre, R. F. Stewart, and J. A. Pople, *J. Chem. Phys.*, **51**, 2657 (1969).
- [128] R. F. Hout and W. J. Hehre, *J. Am. Chem. Soc.*, **105**, 3728 (1989).
- [129] X. Zhang, J. K. Pugh, and P. N. Ross, *J. Electrochem. Soc.*, **148**, E183 (2001).

- [130] K. Tasaki, *J. Phys. Chem. B*, **109**, 2920 (2005).
- [131] L. Xing, C. Wang, W. Li, M. Xu, X. Meng, and S. Zhao, *J. Phys. Chem. B*, **113**, 5181 (2009).
- [132] K. Tasaki, K. Kanda, S. Nakamura, and M. Ue, *J. Electrochem. Soc.*, **150**, A1628 (2003).
- [133] R. L. Wang, C. Buhrmester, and J. R. Dahn, *J. Electrochem. Soc.*, **153**, A445 (2006).
- [134] R. L. Wang and J. R. Dahn, *J. Electrochem. Soc.*, **153**, A1922 (2006).
- [135] M. J. Frisch, G. W. Trucks, H. B. Schlegel, G. E. Scuseria, M. A. Robb, J. R. Cheeseman, J. A. Montgomery, Jr., T. Vreven, K. N. Kudin, J. C. Burant, J. M. Millam, S. S. Iyengar, J. Tomasi, V. Barone, B. Mennucci, M. Cossi, G. Scalmani, N. Rega, G. A. Petersson, H. Nakatsuji, M. Hada, M. Ehara, K. Toyota, R. Fukuda, J. Hasegawa, M. Ishida, T. Nakajima, Y. Honda, O. Kitao, H. Nakai, M. Klene, X. Li, J. E. Knox, H. P. Hratchian, J. B. Cross, V. Bakken, C. Adamo, J. Jaramillo, R. Gomperts, R. E. Stratmann, O. Yazyev, A. J. Austin, R. Cammi, C. Pomelli, J. W. Ochterski, P. Y. Ayala, K. Morokuma, G. A. Voth, P. Salvador, J. J. Dannenberg, V. G. Zakrzewski, S. Dapprich, A. D. Daniels, M. C. Strain, O. Farkas, D. K. Malick, A. D. Rabuck, K. Raghavachari, J. B. Foresman, J. V. Ortiz, Q. Cui, A. G. Baboul, S. Clifford, J. Cioslowski, B. B. Stefanov, G. Liu, A. Liashenko, P. Piskorz, I. Komaromi, R. L. Martin, D. J. Fox, T. Keith, M. A. Al-Laham, C. Y. Peng, A. Nanayakkara, M. Challacombe, P. M. W. Gill, B. Johnson, W. Chen, M. W. Wong, C. Gonzalez, and J. A. Pople, Gaussian, Inc., Wallingford, CT (2004).
- [136] J. M. Vollmer, L. A. Curtiss, D. R. Vissers, and K. Amine, *J. Electrochem. Soc.*, **151**, L178 (2004).
- [137] A. D. Becke, *J. Chem. Phys.*, **98**, 5648 (1993).
- [138] C. Lee, W. Yang, and R. G. Parr, *Phys. Rev. B*, **37**, 785 (1988).
- [139] C. Buhrmester, J. Chen, L. Moshurchak, J. W. Jiang, R. L. Wang, and J. R. Dahn, *J. Electrochem. Soc.*, **152**, A2390 (2005).
- [140] J. K. Feng, X. P. Ai, Y. L. Cao, and H. X. Yang, *Electrochem. Comm.*, **9**, 25 (2007).
- [141] L. M. Moshurchak, M. Bulinski, W. M. Lamanna, R. L. Wang, and J. R. Dahn, *Electrochem. Comm.*, **9**, 1497 (2007).
- [142] K. Nakahara, J. Iriyama, S. Iwasa, M. Suguro, M. Satoh, and E. Cairns, *J. Power Sources*, **163**, 1110 (2007).

Appendix A List of Shuttle Molecules Sorted by Oxidation Potential

The table in this appendix lists the name, structure, shuttle potential and the number of cycles of overcharge protection for every shuttle molecule tested during the work on this thesis. They are arranged by order of increasing oxidation potentials.

The shuttle potentials reported are all taken from coin cell data as the potential of the potential plateau during overcharge at C/10 rate. Where multiple numbers are listed, they represent molecules with more than one oxidation potential. The number of cycles of overcharge protection represents the maximum number of cycles seen for each molecule from cells with LiFePO_4 positive electrodes, either MCMB or $\text{Li}_{4/3}\text{Ti}_{5/3}\text{O}_4$ negative electrodes and either LiPF_6 or LiBOB as the electrolyte salt. The molecules were tested in all four types of cells, but only the maximum number is represented in the table.

Molecules with --- in the Shuttle Potential column prevented the cells from charging at all, and as such, no experimental data is presented.

Many of the molecules presented here are not discussed in the body of this thesis and are only shown here to summarize the work done.

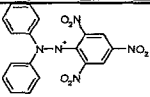
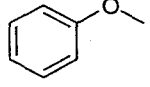
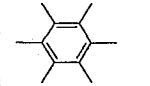
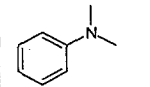
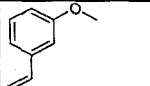
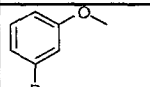
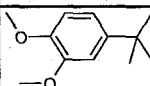
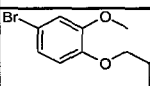
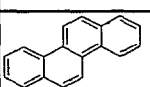
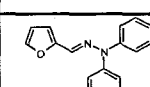
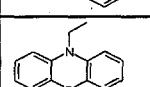
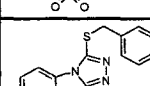
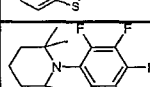
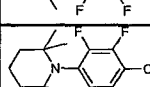
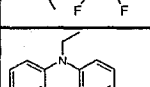
Name	Structure	Shuttle Potential vs Li/Li ⁺ / V	Cycles of Overcharge Protection
4-picoline-N-oxide		3.29	1
2,4,6-trimethoxy-1,3,5-triazine		3.4, 4.2	7
10-acethylphenoxazine		3.45	14
TEMPO		3.45	124
4-methoxy-TEMPO		3.45	133
10-ethylphenothiazine		3.47	150
10-methylphenothiazine		3.47	156
10-isopropylphenothiazine		3.5	163
N,N'-bis(3-methyl-3H-benzooxazol-2-ylidene)hydroxazine		3.5, 4.6	1
3-chloro-10-ethylphenothiazine		3.53	146
4-methylsulfonyloxy-TEMPO		3.56	35
4-hydroxy-TEMPO benzoate		3.58	86
cycloheptatriene		3.6	5
tris(4-methylphenyl)amine		3.6	8
2,4,6-trifluoromethyl-1,3,5-triazine		3.6, 4.1, 4.7	3

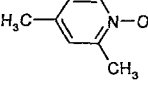
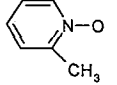
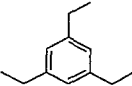
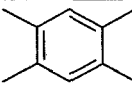
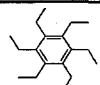
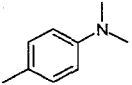
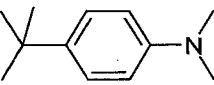
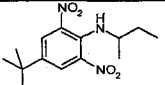
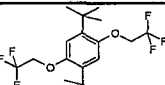
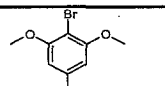
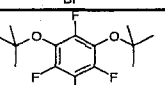
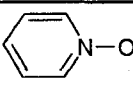
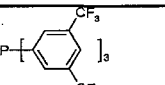
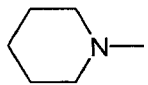
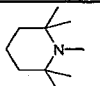
Name	Structure	Shuttle Potential vs Li/Li ⁺ / V	Cycles of Overcharge Protection
N ¹ -benzylidene-N,N-diphenylhydrazine		3.6, 4.6	3
4-cyano-TEMPO		3.61	158
3-(trifluoromethylsulfonyl)phenothiazine		3.66	17
4-carboxy-TEMPO		3.66	5
triphenylamine		3.67	22
4-oxo-TEMPO		3.67	33
3-cyano-PROXYL		3.69	158
N,2,2,6,6-pentamethyl-4-oxopiperidine		3.7	1
1,3-di- <i>t</i> -butyl-2-methoxy-5-methylbenzene		3.7, 4.2	3
2-chloro-10-(cyanoethyl)phenothiazine		3.71	1
9-methylcarbazole		3.78	1
N,N,2,4,6-pentamethylaniline		3.8	3
2,6-diisopropyl-N,N-dimethylaniline		3.8	1
2,5-bis(chloromethyl)-1,4-dimethoxybenzene		3.8, 4.2	1
1,3,5-trimethoxybenzene		3.8, 4.5, 4.8	1

Name	Structure	Shuttle Potential vs Li/Li ⁺ / V	Cycles of Overcharge Protection
2,5-dimethyl-1,4-dimethoxybenzene		3.85	13
10-acetylphenothiazine		3.88	114
2,5-di- <i>t</i> -butyl-1,4-di(triisopropylsiloxy)benzene		3.9	1
4-allyl-1,2-dimethoxybenzene		3.9	2
3-methyl-1,2-benzenediol		3.9	1
pyrene		3.9	2
2,4-dichloro-6-methoxy-1,3,5-triazine		3.9	1
1,4-dimethoxybenzene		3.9, 4.1	1
2,5-di- <i>t</i> -butyl-1,4-diethoxybenzene		3.9, 4.3	48
2,5-di- <i>t</i> -butyl-1,4-dimethoxybenzene		3.92	363
tris-(<i>p</i> -bromophenyl) amine		3.92	41
1-triphenylphosphoranylidene-2-propanone		3.94	1
1,4-diethoxybenzene		3.95	2
tetrakis(pentafluorophenyl)boron lithium ethyletherate		3.95	1
2-ethynylanisole		4.0	2

Name	Structure	Shuttle Potential vs Li/Li ⁺ / V	Cycles of Overcharge Protection
4-[(2-ethyl)hexyl]oxy]anisole		4.0	1
1-(3-(2,4-cyclopentadien-1-ylidene)-1-butenyl)-4-methoxybenzene		4.0	2
1-(ethoxycarbonyloxy)imino)methyl-4-methoxybenzene		4.0	1
3-amino-N-dodecyl-4-methoxybenzulfonamide		4.0	1
1,4-dimethoxy-2,3,5-trimethylbenzene		4.0	3
2- <i>t</i> -butyl-1,4-dimethoxybenzene		4.0	30
anthracene		4.0	3
triphenylphosphine oxide		4.0	1
trimesitylborane		4.0	3
N-methylpyrrolidine		4.0	1
4-ethynylanisole		4.0, 4.3	1
1,2-dimethoxybenzene		4.0, 4.4	2
N'-(1-(4-chlorophenyl)ethylidene)-N-(4-(3,4-dimethoxyphenyl)thiazol-2-yl)-N-phenylhydrazinic		4.0, 4.6	5
2-ethoxyanisole		4.0, 4.7	2
phenoxathiin		4.03	1

Name	Structure	Shuttle Potential vs Li/Li ⁺ / V	Cycles of Overcharge Protection
2,3-dimethoxytoluene		4.05	3
1-cyclopropyl-2-methoxybenzene		4.1	1
3,4-dimethoxytoluene		4.1	15
2,3,5,6-tetramethyl-1,4-dimethoxybenzene		4.1	16
3,5-di- <i>t</i> -butyl-1,2-dimethoxybenzene		4.1	10
4-bromo-1,2-dimethoxybenzene		4.1	3
2-bromo-1,3-dimethoxybenzene		4.1	6
4-fluoro-1,2-dimethoxybenzene		4.1	18
hexadecyloxy-4-methoxybenzene		4.1	0
2,6-di- <i>t</i> -butyl-1,4-benzoquinone		4.1	9
benzofurazan		4.1	1
benzothiazole		4.1	3
5-methyl-2-(2-(2-nitrophenyl)vinyl)benzothiazole		4.1, 4.5	2
D,L- α -tocopherol acetate		4.1, 4.6	2
4- <i>t</i> -butyl-1-methoxybenzene		4.15	4

Name	Structure	Shuttle Potential vs Li/Li ⁺ / V	Cycles of Overcharge Protection
1,1-diphenyl-2-picrylhydrazine		4.15	52
anisole		4.18	33
hexamethylbenzene		4.2	7
N,N-dimethylaniline		4.2	1
3-ethynylanisole		4.2	1
3-bromoanisole		4.2	2
4- <i>t</i> -butyl-1,2-dimethoxybenzene		4.2	9
1-(benzyloxy)-4-bromo-2-methoxybenzene		4.2	5
chrysene		4.2	1
N ² -furan-2-ylmethylene-N,N-diphenylhydrazine		4.2	5
10-ethylphenothiazine-5,5-dioxide		4.2	5
3-((4- <i>t</i> -butylbenzyl)thio)-(1,2,4)triazolo (3,4-B)(1,3)benzothiazole		4.2, 4.6	5
N-pentafluorophenyl-2,2,6,6-tetramethylpiperidine		4.2, 4.6	4
N-(4-trifluoromethyl-2,3,5,6-tetrafluorophenyl)-2,2,6,6-tetramethylpiperidine		4.2, 4.7	3
10-ethyl-3-nitrophenothiazine-5-oxide		4.21	1

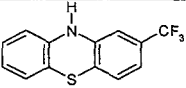
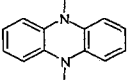
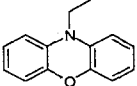
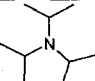
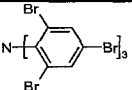
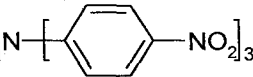
Name	Structure	Shuttle Potential vs Li/Li ⁺ / V	Cycles of Overcharge Protection
2,4-dimethylpyridine-N-oxide		4.24	1
2-picoline-N-oxide		4.26	1
1,3,5-triethylbenzene		4.3	1
1,2,4,5-tetramethylbenzene		4.3	1
hexaethylbenzene		4.3	1
N,N-dimethyl- <i>p</i> -toluidine		4.3	1
4- <i>t</i> -butyl-N,N-dimethylaniline		4.3	4
butralin		4.3	4
2,5-di- <i>t</i> -butyl-1,4-bis(2,2,2-trifluoroethoxy)benzene		4.3	170
2,4-dibromo-1,3-dimethoxybenzene		4.3	2
1,2,4,5-tetrafluoro-3,6-di- <i>t</i> -butoxybenzene		4.3	8
pyridine-N-oxide		4.3	1
tris[3,5-bis-(trifluoromethyl)-phenyl]phosphine		4.3	1
N-methylpiperidine		4.3	1
N,2,2,6,6-pentamethylpiperidine		4.3	1

Name	Structure	Shuttle Potential vs Li/Li ⁺ / V	Cycles of Overcharge Protection
3-picoline-N-oxide		4.33	1
4- <i>t</i> -butylpyridine-N-oxide		4.34	1
2-bromoanisole		4.35	12
2,4-di- <i>t</i> -butylphenyl-L3-acetamido-4-methoxybenzene sulfonate		4.35	4
1,3,5- <i>t</i> -butyl-2-methoxybenzene		4.37	3
4-bromoanisole		4.37	1
thiantrene		4.37	2
10-(trifluoroacetyl)phenothiazine		4.39	5
4- <i>t</i> -butyl-2,6-diaminoanisole		4.4	1
3- <i>t</i> -butyl-4-methoxybenzaldehyde		4.44	2
tris(2,4-dibromophenyl)amine		4.47	2
1,2-dimethoxy-4-nitrobenzene		4.5	2
4-bromo-N,N-dimethylaniline		4.6	3
1,2,4,5-tetrafluoro-3,6-dimethoxybenzene		4.6	4
1,2,4,5-tetrafluoro-3,6-diethoxybenzene		4.6	25

Name	Structure	Shuttle Potential vs Li/Li ⁺ / V	Cycles of Overcharge Protection
2-methoxy heptafluorofluoronaphthalene		4.6	37
2,4,6-tris(2-pyridyl)-1,3,5-triazine		4.6	1
2,5-dichloroanisole		4.61	1
2-bromo-4-fluoroanisole		4.68	1
3- <i>t</i> -butyl-4-methoxybenzonitrile		4.68	1
dimethyl-4-methoxyphthalate		4.7	6
dimethyl-5-methoxy isophthalate		4.7	4
1,2,3,4-tetrabromo-5,6-dimethoxybenzene		4.7	1
2-(ethylthio)benzothiazole		4.7	9
diisopropyl-3-pentylamine		4.7	1
tris(pentafluorophenyl)phosphine		4.7	2
diphenyl(pentafluorophenyl) phosphine		4.7	3
tris(pentafluorophenyl)borane		4.7	1
lithium tetraphenylborate (tris)1,2-dimethoxyethane		4.7	1
2,2,6,6-tetramethylcyclohexanone		4.75	2

Name	Structure	Shuttle Potential vs Li/Li ⁺ / V	Cycles of Overcharge Protection
2,4,6-trichloroanisole		4.79	6
benzene		4.8	2
2,5-di- <i>t</i> -butyl-1,4-bis(trimethylsilyl)benzene		4.8	1
1,2,4,5-tetrabromo-3,6-dimethoxybenzene		4.8	1
2,5-di- <i>t</i> -butyl-1,4-bis(hexafluoropropyl)benzene		4.8	6
octafluoronaphthalene		4.8	70
4-aminofurazan-3-carbonitrile		4.8	3
tris(4-fluorophenyl)phosphine		4.8	5
bis(pentafluorophenyl)phenylphosphine		4.8	2
2,4,6-tribromoanisole		4.82	1
4-methoxypyridine-N-oxide		4.85	1
[bis((trifluoromethyl)sulfonyl)methyl]benzene		4.9	2
2,2'-dithiobis(benzothiazole)		4.9	4
5- <i>t</i> -butyl-1,3-dinitro-2-methoxybenzene		4.91	2
furazan-N2-oxide-3,4-dicarboxylic acid diethyl ester		5.2	5

Name	Structure	Shuttle Potential vs Li/Li ⁺ / V	Cycles of Overcharge Protection
4,6,8-trimethylazulene		5.28	3
tris(2,3,5,6-tetrafluoro-3-(trifluoromethyl)phenyl)amine		5.3	1
2,4,6-tri- <i>t</i> -butyl- <i>N</i> -methylaniline		---	0
<i>N,N,N',N'</i> -tetramethyl- <i>p</i> -phenylenediamine		---	0
octamethylbenzene-1,4-diamine		---	0
1,4-bis(dimethylamino)-2,3,5,6-tetramethylbenzene		---	0
3-methoxybenzylbromide		---	0
3-methoxycatechol		---	0
2- <i>t</i> -butyl-4,6-dinitro-5-methylanisole		---	0
galvinoxyl		---	0
4-chloropyridine- <i>N</i> -oxide		---	0
hexamethylenetetramine		---	0
2,4,6-triallyloxy-1,3,5-triazine		---	0
triallyl-1,3,5-triazine-2,4,6-trione		---	0
phenothiazine		---	0

Name	Structure	Shuttle Potential vs Li/Li ⁺ / V	Cycles of Overcharge Protection
2-(trifluoromethyl) phenothiazine		---	0
5,10-dimethylphenazine		---	0
10-ethylphenoxazine		---	0
triisopropylamine		---	0
tris(2,4,6-tribromophenyl)amine		---	0
tris(4-nitrophenyl)amine		---	0

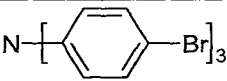
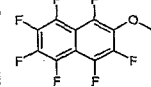
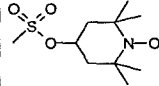
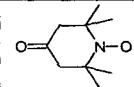
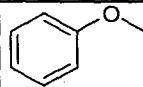
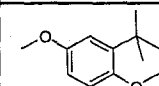
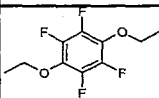
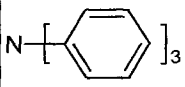
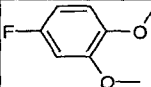
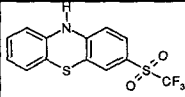
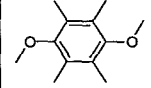
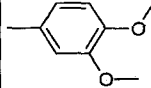
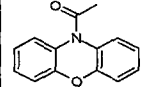
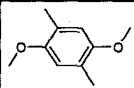
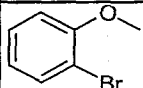
Appendix B List of Shuttle Molecules Sorted by Length of Overcharge Protection

This table is similar to that in Appendix A in that it lists the name, structure, shuttle potential and the number of cycles of overcharge protection for every shuttle molecule tested during the work on this thesis. They are arranged by order of decreasing number of cycles of overcharge protection.

The shuttle potentials reported are all taken from coin cell data as the potential of the potential plateau during overcharge at C/10 rate. Where multiple numbers are listed, they represent molecules with more than one oxidation potential. The number of cycles of overcharge protection represents the maximum number of cycles seen for each molecule from cells with LiFePO_4 positive electrodes, either MCMB or $\text{Li}_{4/3}\text{Ti}_{5/3}\text{O}_4$ negative electrodes and either LiPF_6 or LiBOB as the electrolyte salt. The molecules were tested in all four types of cells, but only the maximum number is represented in the table.

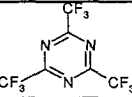
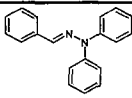
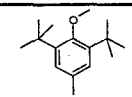
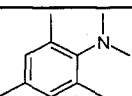
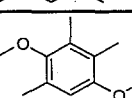
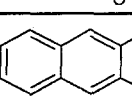
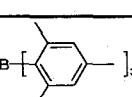
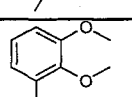
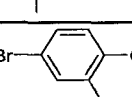
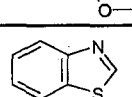
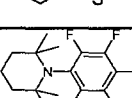
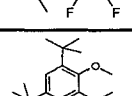
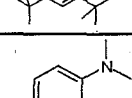
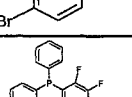
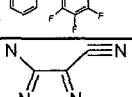
Molecules with --- in the Shuttle Potential column prevented the cells from charging at all, and as such, no experimental data is presented.

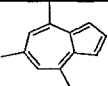
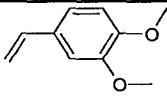
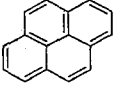
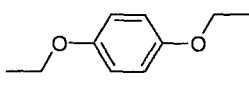
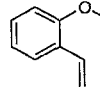
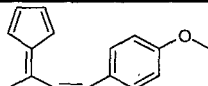
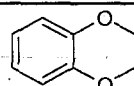
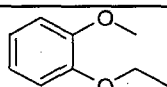
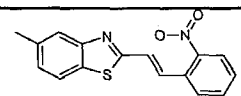
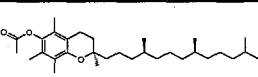
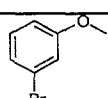
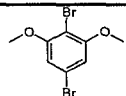
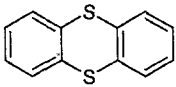
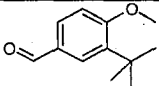
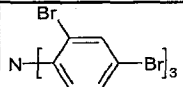
Name	Structure	Shuttle Potential vs Li/Li ⁺ / V	Cycles of Overcharge Protection
2,5-di- <i>t</i> -butyl-1,4-dimethoxybenzene		3.92	363
2,5-di- <i>t</i> -butyl-1,4-bis(2,2,2-trifluoroethoxy)benzene		4.3	170
10-isopropylphenothiazine		3.5	163
4-cyano-TEMPO		3.61	158
3-cyano-PROXYL		3.69	158
10-methylphenothiazine		3.47	156
10-ethylphenothiazine		3.47	150
3-chloro-10-ethylphenothiazine		3.53	146
4-methoxy-TEMPO		3.45	133
TEMPO		3.45	124
10-acetylphenothiazine		3.88	114
4-hydroxy-TEMPO benzoate		3.58	86
octafluoronaphthalene		4.8	70
1,1-diphenyl-2-picrylhydrazine		4.15	52
2,5-di- <i>t</i> -butyl-1,4-diethoxybenzene		3.9, 4.3	48

Name	Structure	Shuttle Potential vs Li/Li ⁺ / V	Cycles of Overcharge Protection
tris-(<i>p</i> -bromophenyl) amine		3.92	41
2-methoxy heptafluorofluoronaphthalene		4.6	37
4-methylsulfonyloxy-TEMPO		3.56	35
4-oxo-TEMPO		3.67	33
anisole		4.18	33
2- <i>t</i> -butyl-1,4-dimethoxybenzene		4.0	30
1,2,4,5-tetrafluoro-3,6-diethoxybenzene		4.6	25
triphenylamine		3.67	22
4-fluoro-1,2-dimethoxybenzene		4.1	18
3-(trifluoromethylsulfonyl) phenothiazine		3.66	17
2,3,5,6-tetramethyl-1,4-dimethoxybenzene		4.1	16
3,4-dimethoxytoluene		4.1	15
10-acetylphenoxazine		3.45	14
2,5-dimethyl-1,4-dimethoxybenzene		3.85	13
2-bromoanisole		4.35	12

Name	Structure	Shuttle Potential vs Li/Li ⁺ / V	Cycles of Overcharge Protection
3,5-di- <i>t</i> -butyl-1,2-dimethoxybenzene		4.1	10
2,6-di- <i>t</i> -butyl-1,4-benzoquinone		4.1	9
4- <i>t</i> -butyl-1,2-dimethoxybenzene		4.2	9
2-(ethylthio)benzothiazole		4.7	9
tris(4-methylphenyl)amine		3.6	8
1,2,4,5-tetrafluoro-3,6-di- <i>t</i> -butoxybenzene		4.3	8
2,4,6-trimethoxy-1,3,5-triazine		3.4, 4.2	7
hexamethylbenzene		4.2	7
2-bromo-1,3-dimethoxybenzene		4.1	6
dimethyl-4-methoxyphthalate		4.7	6
2,4,6-trichloroanisole		4.79	6
2,5-di- <i>t</i> -butyl-1,4-bis(hexafluoropropyl)benzene		4.8	6
cycloheptatriene		3.6	5
4-carboxy-TEMPO		3.66	5
N'-(1-(4-chlorophenyl)ethylidene)-N-(4-(3,4-dimethoxyphenyl)thiazol-2-yl)-N-phenylhydrazinic		4.0, 4.6	5

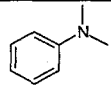
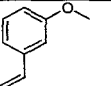
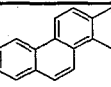
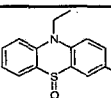
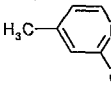
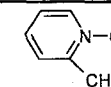
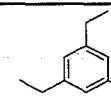
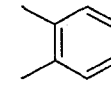
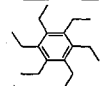
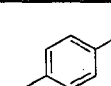
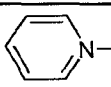
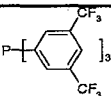
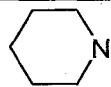
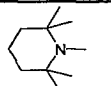
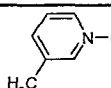
Name	Structure	Shuttle Potential vs Li/Li ⁺ / V	Cycles of Overcharge Protection
1-(benzyloxy)-4-bromo-2-methoxybenzene		4.2	5
N ² -furan-2-ylmethylene-N,N-diphenylhydrazine		4.2	5
10-ethylphenothiazine-5,5-dioxide		4.2	5
3-((4- <i>t</i> -butylbenzyl)thio)-(1,2,4)triazolo (3,4-B)(1,3)benzothiazole		4.2, 4.6	5
10-(trifluoroacetyl)phenothiazine		4.39	5
tris(4-fluorophenyl)phosphine		4.8	5
furazan-N2-oxide-3,4-dicarboxylic acid diethyl ester		5.2	5
4- <i>t</i> -butyl-1-methoxybenzene		4.15	4
N-pentafluorophenyl-2,2,6,6-tetramethylpiperidine		4.2, 4.6	4
4- <i>t</i> -butyl-N,N-dimethylaniline		4.3	4
butralin		4.3	4
2,4-di- <i>t</i> -pentylphenyl-L3-acetamido-4-methoxybenzene sulfonate		4.35	4
1,2,4,5-tetrafluoro-3,6-dimethoxybenzene		4.6	4
dimethyl-5-methoxy isophthalate		4.7	4
2,2'-dithiobis(benzothiazole)		4.9	4

Name	Structure	Shuttle Potential vs Li/Li ⁺ / V	Cycles of Overcharge Protection
2,4,6-trifluoromethyl-1,3,5-triazine		3.6, 4.1, 4.7	3
N'-benzylidene-N,N-diphenylhydrazine		3.6, 4.6	3
1,3-di- <i>t</i> -butyl-2-methoxy-5-methylbenzene		3.7, 4.2	3
N,N,2,4,6-pentamethylaniline		3.8	3
1,4-dimethoxy-2,3,5-trimethylbenzene		4.0	3
anthracene		4.0	3
trimesitylborane		4.0	3
2,3-dimethoxytoluene		4.05	3
4-bromo-1,2-dimethoxybenzene		4.1	3
benzothiazole		4.1	3
N-(4-trifluoromethyl-2,3,5,6-tetrafluorophenyl)-2,2,6,6-tetramethylpiperidine		4.2, 4.7	3
1,3,5- <i>t</i> -butyl-2-methoxybenzene		4.37	3
4-bromo-N,N-dimethylaniline		4.6	3
diphenyl(pentafluorophenyl) phosphine		4.7	3
4-amino furazan-3-carbonitrile		4.8	3

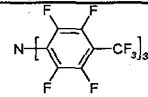
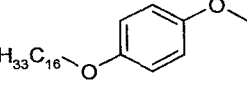
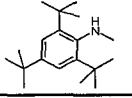
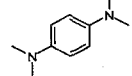
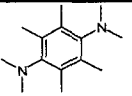
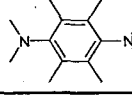
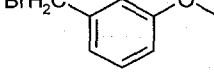
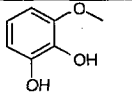
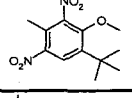
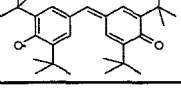
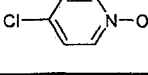
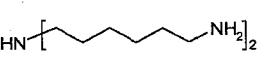
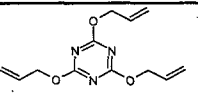
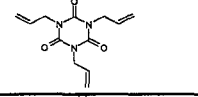
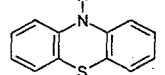
Name	Structure	Shuttle Potential vs Li/Li ⁺ / V	Cycles of Overcharge Protection
4,6,8-trimethylazulene		5.28	3
4-allyl-1,2-dimethoxybenzene		3.9	2
pyrene		3.9	2
1,4-diethoxybenzene		3.95	2
2-ethynylanisole		4.0	2
1-(3-(2,4-cyclopentadien-1-ylidene)-1-butenyl)-4-methoxybenzene		4.0	2
1,2-dimethoxybenzene		4.0, 4.4	2
2-ethoxyanisole		4.0, 4.7	2
5-methyl-2-(2-(2-nitrophenyl)vinyl)benzothiazole		4.1, 4.5	2
D,L-α-tocopherol acetate		4.1, 4.6	2
3-bromoanisole		4.2	2
2,4-dibromo-1,3-dimethoxybenzene		4.3	2
thianthrene		4.37	2
3- <i>t</i> -butyl-4-methoxybenzaldehyde		4.44	2
tris(2,4-dibromophenyl)amine		4.47	2

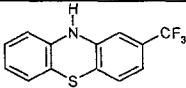
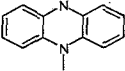
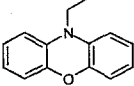
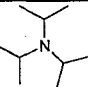
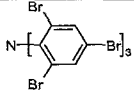
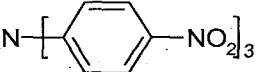
Name	Structure	Shuttle Potential vs Li/Li ⁺ / V	Cycles of Overcharge Protection
1,2-dimethoxy-4-nitrobenzene		4.5	2
tris(pentafluorophenyl)phosphine		4.7	2
2,2,6,6-tetramethylcyclohexanone		4.75	2
benzene		4.8	2
bis(pentafluorophenyl)phenylphosphine		4.8	2
[bis((trifluoromethyl)sulfonyl)methyl]benzene		4.9	2
5- <i>t</i> -butyl-1,3-dinitro-2-methoxybenzene		4.91	2
4-picoline-N-oxide		3.29	1
N,N'-bis(3-methyl-3H-benzooxazol-2-ylidene)hydroxazine		3.5, 4.6	1
N,2,2,6,6-pentamethyl-4-oxopiperidine		3.7	1
2-chloro-10-(cyanoethyl)phenothiazine		3.71	1
9-methylcarbazole		3.78	1
2,6-diisopropyl-N,N-dimethylaniline		3.8	1
2,5-bis(chloromethyl)-1,4-dimethoxybenzene		3.8, 4.2	1
1,3,5-trimethoxybenzene		3.8, 4.5, 4.8	1

Name	Structure	Shuttle Potential vs Li/Li ⁺ / V	Cycles of Overcharge Protection
2,5-di- <i>t</i> -butyl-1,4-di(triisopropylsiloxy)benzene		3.9	1
3-methyl-1,2-benzenediol		3.9	1
2,4-dichloro-6-methoxy-1,3,5-triazine		3.9	1
1,4-dimethoxybenzene		3.9, 4.1	1
1-triphenylphosphoranylidene-2-propanone		3.94	1
tetrakis(pentafluorophenyl)boron lithium ethyletherate		3.95	1
4-[(2-ethyl)hexyl]oxy]anisole		4.0	1
1-(ethoxycarbonyloxy)imino)methyl-4-methoxybenzene		4.0	1
3-amino-N-dodecyl-4-methoxybenzenesulfonamide		4.0	1
triphenylphosphine oxide		4.0	1
N-methylpyrrolidine		4.0	1
4-ethynylanisole		4.0, 4.3	1
phenoxathiin		4.03	1
1-cyclopropyl-2-methoxybenzene		4.1	1
benzofurazan		4.1	1

Name	Structure	Shuttle Potential vs Li/Li ⁺ / V	Cycles of Overcharge Protection
N,N-dimethylaniline		4.2	1
3-ethynylanisole		4.2	1
chrysene		4.2	1
10-ethyl-3-nitrophenothiazine-5-oxide		4.21	1
2,4-dimethylpyridine-N-oxide		4.24	1
2-picoline-N-oxide		4.26	1
1,3,5-triethylbenzene		4.3	1
1,2,4,5-tetramethylbenzene		4.3	1
hexaethylbenzene		4.3	1
N,N-dimethyl-p-toluidine		4.3	1
pyridine-N-oxide		4.3	1
tris[3,5-bis-(trifluoromethyl)-phenyl]phosphine		4.3	1
N-methylpiperidine		4.3	1
N,2,2,6,6-pentamethylpiperidine		4.3	1
3-picoline-N-oxide		4.33	1

Name	Structure	Shuttle Potential vs Li/Li ⁺ / V	Cycles of Overcharge Protection
4- <i>t</i> -butylpyridine-N-oxide		4.34	1
4-bromoanisole		4.37	1
4- <i>t</i> -butyl-2,6-diaminoanisole		4.4	1
2,4,6-tris(2-pyridyl)-1,3,5-triazine		4.6	1
2,5-dichloroanisole		4.61	1
2-bromo-4-fluoroanisole		4.68	1
3- <i>t</i> -butyl-4-methoxybenzotrile		4.68	1
1,2,3,4-tetrabromo-5,6-dimethoxybenzene		4.7	1
diisopropyl-3-pentylamine		4.7	1
tris(pentafluorophenyl)borane		4.7	1
lithium tetraphenylborate (tris)1,2-dimethoxyethane		4.7	1
2,5-di- <i>t</i> -butyl-1,4-bis(trimethylsilyl)benzene		4.8	1
1,2,4,5-tetrabromo-3,6-dimethoxybenzene		4.8	1
2,4,6-tribromoanisole		4.82	1
4-methoxypyridine-N-oxide		4.85	1

Name	Structure	Shuttle Potential vs Li/Li ⁺ / V	Cycles of Overcharge Protection
tris(2,3,5,6-tetrafluoro-3-(trifluoromethyl)phenyl)amine		5.3	1
hexadecyloxy-4-methoxybenzene		4.1	0
2,4,6-tri- <i>t</i> -butyl-N-methylaniline		---	0
N,N,N',N'-tetramethyl- <i>p</i> -phenylenediamine		---	0
octamethylbenzene-1,4-diamine		---	0
1,4-bis(dimethylamino)-2,3,5,6-tetramethylbenzene		---	0
3-methoxybenzylbromide		---	0
3-methoxycatechol		---	0
2- <i>t</i> -butyl-4,6-dinitro-5-methylanisole		---	0
galvinoxyl		---	0
4-chloropyridine-N-oxide		---	0
hexamethylenetetramine		---	0
2,4,6-triallyloxy-1,3,5-triazine		---	0
triallyl-1,3,5-triazine-2,4,6-trione		---	0
phenothiazine		---	0

Name	Structure	Shuttle Potential vs Li/Li ⁺ / V	Cycles of Overcharge Protection
2-(trifluoromethyl) phenothiazine		---	0
5,10-dimethylphenazine		---	0
10-ethylphenoxazine		---	0
triisopropylamine		---	0
tris(2,4,6-tribromophenyl)amine		---	0
tris(4-nitrophenyl)amine		---	0